Technische Universität München
Zentrum Mathematik

Vector Preisach Modeling of Magnetic Hysteresis

Kristina Löschner-Greenberg

Vollständiger Abdruck der von der Fakultät für Mathematik
der Technischen Universität München
zur Erlangung des akademischen Grades eines
Doktors der Naturwissenschaften (Dr. rer. nat.)
genehmigten Dissertation.

Vorsitzender:	Univ.-Prof. Dr. Bernd Simeon
Prüfer der Dissertation:	1. Univ.-Prof. Dr. Martin Brokate
	2. Lecturer Dr. Dmitrii Rachinskii, University College Cork, Irland
	3. Prof. Dr. Isaac D. Mayergoyz, University of Maryland, USA (schriftliche Beurteilung)

Die Dissertation wurde am 9.4.2008 bei der Technischen Universität München eingereicht und durch die Fakultät für Mathematik am 15.10.2008 angenommen.

Acknowledgements

This dissertation is the result of a Ph.D. project in the Corporate Sector Research and Advance Engineering of the Bosch Group. I would like to thank the company for presenting me with this interesting research opportunity and funding my work over the last three years.

My special thanks go to Prof. Martin Brokate for taking on the academic supervision of the dissertation and always being available for scientific discussion.

At Bosch, I would like to thank Dr. Volker Rischmüller for supervising this project. I am grateful to Dr. Oliver Rain and Dr. Thomas Fritzsche for taking the time to regularly discuss the progress of my work and for supporting me with questions regarding implementation and electromagnetic field simulation.

There are a number of other people that contributed to the successful completion of this dissertation: To my parents, I am extremely grateful for all of their support, both financial and moral, over the course of my studies. My mother-in-law Cheryl, with her strong sense of responsibility, is a wonderful role model as a woman in a leadership position. My co-Ph.D. students Katharina Straube, Arndt Kelleter and Nassar Albunni were fun to hang out with and great support in the tough phases bound to occur in the course of Ph.D. research. Katharina's presence, in particular, was invaluable during the challenging starting period. I very much enjoyed the technical as well as "world philosophic" discussions with Dr. Pavel Krejčí and owe him insight into some of the mathematical issues involved in partial differential equations with hysteresis.

Last, but most certainly not least, I want to thank my husband, Matt. He is one of the smartest people I know, yet patient, tolerant and humble. He is an amazing walking math reference and one of my role models for scientific research. I owe him deeply for all the encouragement and his confidence in me.

München, February 2008 Kristina Löschner-Greenberg

Abstract

The modeling of magnetic hysteresis in the context of electromagnetic field simulations is a challenging problem that has not yet been resolved to full satisfaction. This dissertation investigates a new vectorial hysteresis operator which represents an extension of the generally accepted scalar Preisach operator. A number of properties of the operator are mathematically shown. They turn out to be in good qualitative correspondence to basic characteristics of magnetic hysteresis. The results of first electromagnetic field simulations with the hysteresis operator reproduce the expected hysteresis effects and give insight in the field configurations forming due to hysteresis.

Zusammenfassung

Die Modellierung magnetischer Hysterese im Rahmen elektromagnetischer Feldsimulationen ist ein Problem, welches bisher noch nicht zur vollen Zufriedenheit gelöst werden konnte. Die vorliegende Dissertation untersucht einen neuen vektoriellen Hystereseoperator, der eine Erweiterung des allgemein anerkannten skalaren Preisach-Operators darstellt. Verschiedene Eigenschaften des Operators werden mathematisch hergeleitet. Sie zeigen eine gute qualitative Übereinstimmung mit grundlegenden Charakteristiken magnetischer Hysterese. Die Ergebnisse erster elektromagnetischer Feldsimulationen reproduzieren erwartete Hystereseeffekte und geben einen Einblick in die hysteresebedingten Feldkonfigurationen.

Contents

Introduction

Magnetic hysteresis is a topic of wide relevance in the design of electromagnetic components. In some applications, such as magnetic recording, hysteresis is specifically used as the basic functioning principle of the device. In other cases, such as magnetic valves or sensors, it represents an unwanted effect with negative impact on the device operation. The demand for better and more powerful yet economically competitive products gives rise to the need for adequate models that allow for more accurate computer simulation early on in the product development cycle. Even though much research has been done on the modeling of magnetic hysteresis, it remains a challenging subject which has not yet been resolved to full satisfaction. This dissertation investigates a new promising vector hysteresis operator and presents first simulations of electromagnetic devices with hysteresis modeled in terms of this operator.

Physically, hysteresis is a micromagnetic phenomenon. It results from the presence of magnetic dipol moments at the atomic level, which are induced both by the motion of electrons about the atomic nucleus and from the spin of each electron about its own axis [**55**]. Depending on the substance, an atom may or may not have a permanent magnetic moment. In any case, in magnetic materials, an ambient magnetic field $\boldsymbol{H}$ interacts with the electron motion and results in magnetic moments. The magnetization vector $\boldsymbol{M}$ is defined as the average of the magnetic moments over small volumes.* When subjected to a varying magnetic field, the magnetic moments arrange themselves in equilibrium states which may depend not only on the present field $\boldsymbol{H}$ but also on the preceeding magnetization state. As a consequence, such a material can exhibit a different magnetization $\boldsymbol{M}$ at the same current magnetic field $\boldsymbol{H}$, owing to a differing anterior variation of $\boldsymbol{H}$. This is the memory effect known as *magnetic hysteresis*. Figure 0.1 shows a typical uniaxial hysteresis curve measured for a ferromagnetic material.

Its microscopic nature makes the modeling of magnetic hysteresis a challenging subject. Micromagnetic modeling, which is an active field of current research, aims at reproducing the correct magnetization patterns at the microscopic level [**32**]. However, the scale of micromagnetic modeling is significantly smaller than the modeling scale in the electromagnetic field simulation of real life electromagnetic components like magnetic valves or electric drives. Due to computational limits, it is not

*This averaging process must, in fact, be applied to all fields involved in Maxwell's equations to obtain their macroscopic formulation as introduced in Chapter 3. This is because microscopically, the fields are the result of localized charges [**40**].

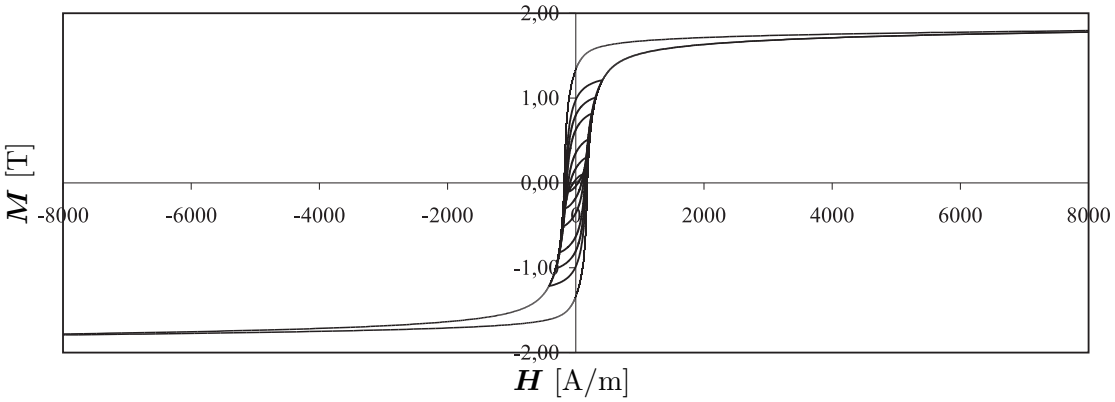

FIGURE 0.1. Hysteresis curve of a ferromagnetic material, measured uniaxially.

feasible at the present time to consider the micromagnetic models in the framework of the macroscopic Maxwell's equations for such applications.

Macroscopic hysteresis models aim at giving a good representation of the hysteretic behaviour of a material at the macroscopic level. In the past decades, scalar hysteresis models have been investigated intensively [**43, 51, 67, 16, 44, 22**]. They model the scalar dependence of the magnetization $\boldsymbol{M}$ on the magnetic field $\boldsymbol{H}$ observed under uniaxial input, like the curve shown in Figure 0.1. Here, the scalar Preisach model [**58, 51**] has been particularly successful. It consists of a set of relay operators with simple input-output behaviour, whose states represent the hysteresis memory. The output arises as a superposition of the relays subject to a weighting function. This weighting function can be parametrized to fit a given hysteresis by providing a full set of first order reversal curves [**51, 16**]. One reason for the extraordinary success of the Preisach model is undoubtedly its clear mathematical structure, which makes its memory evolution transparent and permits efficient representation of the internal memory state. It renders the model accessible for extensions adapting its properties, like the moving model or Preisach models with accommodation or rate-dependence [**51, 22**]. There is even a physical interpretation of the model by associating the relays with the magnetic moments and the position of each relay with the interaction field that a magnetic moment experiences from the surrounding magnetic moments in the material (see e.g. [**73**]).

Since hysteresis by nature is a vector valued process, a scalar representation is often not sufficient. In applications like electromagnetic field simulation, one requires a model that is able to reflect the fully vectorial character of the magnetization processes. The Stoner-Wohlfarth model [**64**] has been available for a long time and was successfully used in the field of magnetic recording, but it can only represent symmetric hysteresis loops and is computationally involved. Thus, when Mayergoyz published his vector Preisach model [**50, 51**], which is a generalization of the scalar Preisach operator and enables arbitrary vectorial input paths, it quickly enjoyed great popularity in the engineering community (e.g. [**1, 4, 27, 9, 60**]). Mayergoyz'

idea was to construct a hysteresis operator in $\mathbb{R}^n$ by overlaying scalar Preisach operators in each vectorial direction. This vectorization concept is, in fact, independent of the scalar hysteresis operator employed.

In this dissertation, we investigate a new vector Preisach model of hysteresis, which was recently introduced by Della Torre, Pinzaglia and Cardelli [**24, 25**]. It constitutes an interesting new approach to vector Preisach modeling by extending the notion of the relay to n dimensions, then adopting the weighted relay superposition in complete analogy to the scalar formulation. The operator might represent a promising new method in the vectorial modeling of magnetic hysteresis, because it intrinsically reproduces some of the properties observed in the hysteresis of magnetic materials, as we will show in this dissertation. For example, under rotating input, it gives the typical shape of the hysteresis loss curves obtained in measurements for real magnetic materials. It shows a realistic saturation behaviour where the magnetization is fully aligned with the magnetic field in the isotropic model, and has an inherent reversible component. Another appeal lies in the fact that the physical interpretation of the scalar Preisach operator in terms of magnetic moments and interaction fields carries over directly to this vector model [**24**].

The published work on this new vector Preisach operator consists of a sequence of articles by Della Torre, Cardelli and Pinzaglia [**24, 25, 17, 18**]. They introduce the hysteresis model for general relay shapes and discuss extensions like the moving model or the DOK model. They computer implement the operator and deduce from numerical experiments some of the properties that are mathematically proven in this dissertation, e.g. the congruency of vectorial loops or the shifted circular magnetization path for rotating input in the isotropic model. The hysteretic energy is discussed for rectangular input paths and is concluded to be dissipative.

Our goal here is to present a rigorous, extensive mathematical investigation of this new hysteresis model. We give a formal mathematical definition of the operator, focussing on spherical relays, and introduce a geometric representation of its memory evolution. We examine its properties such as isotropy, saturation, congruency and periodic behaviour, lag and dissipation, and show that it reduces to a scalar Preisach operator with reversible component for uniaxial input. Further, we examine its infinitesimal properties to show that its output is always continuous and give a formula for the right-hand derivative of the output to exhibit how its evolution depends on the input variation. In view of hysteresis loss computations for general paths, we suggest a possible hysteresis potential. Finally, we are the first to present electromagnetic field simulations with hysteresis modeled in terms of this new vector Preisach operator. We have simulated three two-dimensional model problems. The first one constitutes a simple magnetic ring core enclosing a conductor. Here, it is possible to compute the solution analytically and thereby verify the obtained simulation results. The second model represents a simple position sensor, which we had built and measured in the laboratory. In our simulations, we reproduce the hysteresis effect in the position signal observed in the measurements and numerically compute the hysteretic field distribution in the material. Our final model is that of a simple magnetic valve. In practice, materials that show too much hysteresis

are known to hamper the rapid switching of such a valve, forcing the industrial manufacturer to use more expensive materials with better magnetic characteristics. We simulate the effect of hysteresis on the switching times and numerically confirm an empirical result on how to decrease the hysteresis lag by a simple modification of the valve geometry. The simulation results render it possible to analyze the origin of this behavioural change by giving insight into the field configurations.

This dissertation is structured as follows: In Chapter 1, we summarize the mathematical background deployed in the course of this work. Aside from introducing basic definitions and notation, the chapter contains some theory regarding the differentiation and integration of vector valued functions, such as differentiation under the integral sign, the notion of bounded variation, Riemann-Stieltjes integrals and change of coordinates. Also, we briefly discuss the isometries of $\mathbb{R}^n$, and give some estimates for later reference. In Chapter 2, the vector Preisach operator and its properties are discussed. We start by giving a general mathematical introduction to hysteresis operators. We then formally define and examine the vector relay operator. The remainder of the chapter focuses on the vector Preisach operator and presents our results regarding its properties. Chapter 3 addresses electromagnetic field simulation with hysteresis. After giving a short overview of Maxwell's equations and formulating the numerical problem with hysteresis, our implementation of the vector Preisach operator is described. Finally, we present the electromagnetic field problems which we have simulated.

CHAPTER 1

Mathematical Tools

In this chapter, we have collected the mathematical tools used in the course of this thesis. This includes basic definitions and notation, some theory of differentiation and integration, an overview of the isometries of $\mathbb{R}^n$ and some estimates.

1.1. Basic definitions and notation

We denote the set of real numbers by $\mathbb{R}$, and the set $\{r \in \mathbb{R} \mid r > 0\}$ of positive real numbers by $\mathbb{R}_+$. For any integer n, the space $\mathbb{R}^n$ consists of all real n-vectors $\boldsymbol{x} = (x_1, \ldots, x_n)$. $\mathbb{R}^n$ forms a Euclidean space with the inner product

$$\boldsymbol{x} \cdot \boldsymbol{y} = \sum_{i=1}^{n} x_i y_i,$$

where $\boldsymbol{x} = (x_1, \ldots, x_n)$, $\boldsymbol{y} = (y_1, \ldots, y_n) \in \mathbb{R}^n$, and a Banach space with the corresponding norm

$$\|\boldsymbol{x}\| = (\boldsymbol{x} \cdot \boldsymbol{x})^{\frac{1}{2}}.$$

For $\boldsymbol{y} \in \mathbb{R}^n$ and $r \in \mathbb{R}_+$, we denote the n-dimensional open ball of radius r centered at $\boldsymbol{y}$ by

$$B_{\boldsymbol{y},r} := \{\boldsymbol{x} \in \mathbb{R}^n \mid \|\boldsymbol{x} - \boldsymbol{y}\| < r\},$$

and its boundary by $\partial B_{\boldsymbol{y},r}$. The volume of $B_{\boldsymbol{y},r}$ is given by [**35**]

$$V_B^{(n)}(r) = \frac{\pi^{n/2}}{\Gamma(\frac{n}{2}+1)} r^n.$$

The cone of height R centered at $\boldsymbol{y} \in \mathbb{R}^n$ is defined by

$$\mathcal{C}_{\boldsymbol{y},R} := \{(\boldsymbol{x}, r) \in \mathbb{R}^n \times [0, R] \mid \|\boldsymbol{x} - \boldsymbol{y}\| < r\} \subset \mathbb{R}^n \times \mathbb{R}_+, \tag{1.1}$$

and its volume is [**35**]

$$V_{\mathcal{C}}^{(n)}(R) = \frac{R}{n+1} V_B^{(n)}(R). \tag{1.2}$$

For $R = \infty$, we write

$$\mathcal{C}_{\boldsymbol{y}} := \{(\boldsymbol{x}, r) \in \mathbb{R}^n \times \mathbb{R}_+ \mid \|\boldsymbol{y} - \boldsymbol{x}\| < r\}.$$

We denote the set of all maps from X into Y by $Map(X; Y)$. The *graph* of a map $\boldsymbol{f} \in Map(X, Y)$ is the set $\{(\boldsymbol{x}, \boldsymbol{y}) \in X \times Y \mid \boldsymbol{y} = \boldsymbol{f}(\boldsymbol{x})\}$. The space of continuous functions from X to Y is denoted $C(X; Y)$, and the space of right-continuous functions $C_r(X; Y)$. For a function $\boldsymbol{f} \in Map([0, T], \mathbb{R}^n) : t \mapsto \boldsymbol{f}(t)$, we write

$$\lim_{t \to \tau -} \boldsymbol{f}(t) \quad \text{and} \quad \lim_{t \to \tau +} \boldsymbol{f}(t)$$

for the left and right hand limits at $\tau \in (0,T)$, respectively.

For the derivative of a function of one variable, we use the standard notation $\boldsymbol{f}'(t)$ or $\partial_t \boldsymbol{f}$. The one-sided derivatives are given by

$$\partial_{t+}\boldsymbol{f}(t) = \lim_{h\to 0+} \frac{\boldsymbol{f}(t+h)-\boldsymbol{f}(t)}{h} \quad \text{and} \quad \partial_{t-}\boldsymbol{f}(t) = \lim_{h\to 0-} \frac{\boldsymbol{f}(t+h)-\boldsymbol{f}(t)}{h}.$$

A function is called *continuously differentiable on the closed interval* $[t_1,t_2]$ if the derivative exists and is continuous everywhere in (t_1,t_2) and the left and right hand derivatives exist and are continuous in $[t_1,t_2)$ and $(t_1,t_2]$, respectively. In the case of a multivariate function $\boldsymbol{\varphi}:\mathbb{R}^n\to\mathbb{R}^m$, $\boldsymbol{y}=(y_1,\dots,y_n)\mapsto\boldsymbol{\varphi}(\boldsymbol{y})$, we write $\partial_{y_i}\boldsymbol{\varphi}(\boldsymbol{y})$ to denote the partial derivative $\frac{\partial\boldsymbol{\varphi}(\boldsymbol{y})}{\partial y_i}$, and $\partial_{\boldsymbol{y}}\boldsymbol{\varphi}(\boldsymbol{y})$ for the Jacobian matrix $\frac{\partial\boldsymbol{\varphi}(\boldsymbol{y})}{\partial\boldsymbol{y}}$.

A function $\boldsymbol{f}:\mathbb{R}^n\to\mathbb{R}^n$ is called *monotonic* on $\Omega\subseteq\mathbb{R}^n$ if and only if

$$(\boldsymbol{f}(\boldsymbol{x})-\boldsymbol{f}(\boldsymbol{y}))\cdot(\boldsymbol{x}-\boldsymbol{y})\geq 0 \quad \text{for all } \boldsymbol{x},\boldsymbol{y}\in\Omega,$$

and *strictly monotonic* if the inequality holds strictly.

Further, the closure of a set X is denoted by $\overline{X}$ and its boundary by ∂X. Bold symbols indicate vector-valued variables and functions. All integrals are to be interpreted as Lebesgue integrals unless explicitly stated otherwise.

1.2. Differentiation and integration

1.2.1. Differentiation under the integral sign. In this dissertation, we consider an operator defined in terms of an integral. We will make use of the theorems on differentiation under the integral sign presented below. The first one is a multidimensional version of the Leibniz rule, which deals with constant integration bounds. The second theorem extends the result to function valued integration bounds. The subsequent theorems generalize these statements to the multivariate setting and consider additional factors that do not depend on the variable with respect to which we differentiate. The proofs extend those presented in [**31**, Chapter XIV] from two variables on boxes to the higher dimensional case on more general sets.

THEOREM 1.2.1 (Leibniz rule). *Let the function $f(x_1,\dots,x_n,y)$ be continuous on $U\times[c,d]$, where $U=[a_1,b_1]\times\cdots\times[a_n,b_n]\subset\mathbb{R}^n$.*

(a) *Then*

$$F(x_2,\dots,x_n,y) := \int_{a_1}^{b_1} f(x_1,\dots,x_n,y)\,\mathrm{d}x_1$$

is continuous on $[a_2,b_2]\times\cdots\times[a_n,b_n]\times[c,d]$.

(b) *Assume further that $\partial_y f(x_1,\dots,x_n,y)$ exists and is continuous in $U\times(c,d)$. Then $\partial_y F$ exists in all of $[a_2,b_2]\times\cdots\times[a_n,b_n]\times(c,d)$ and is given by*

$$\partial_y F(x_2,\dots,x_n,y) = \int_{a_1}^{b_1} \partial_y f(x_1,\dots,x_n,y)\,\mathrm{d}x_1.$$

PROOF. (a) Let $(x_2^0,\dots,x_n^0,y^0)\in U\times[c,d]$. Since $f(x_1,\dots,x_n,y)$ is uniformly continuous on $U\times[c,d]$, $f(x_1,x_2,\dots,x_n,y)$ converges to $f(x_1,x_2^0,\dots,x_n^0,y^0)$ uniformly

with respect to x_1 as $(x_2, \ldots, x_n, y) \to (x_2^0, \ldots, x_n^0, y^0)$. Therefore, limit and integral can be interchanged and we have

$$\lim_{(x_2,\ldots,x_n,y)\to(x_2^0,\ldots,x_n^0,y^0)} \int_{a_1}^{b_1} f(x_1, x_2, \ldots, x_n, y)\,\mathrm{d}x_1 = \int_{a_1}^{b_1} f(x_1, x_2^0, \ldots, x_n^0, y^0)\,\mathrm{d}x_1.$$

(b) Fix $(x_2, \ldots, x_n, y)$ and let Δy be an increment. By definition,

$$\begin{aligned}
\partial_y F(x_2, \ldots, x_n, y) &= \lim_{\Delta y\to 0} \frac{F(x_2, \ldots, x_n, y+\Delta y) - F(x_2, \ldots, x_n, y)}{\Delta y} \\
&= \lim_{\Delta y\to 0} \int_{a_1}^{b_1} \frac{f(x_1, x_2, \ldots, x_n, y+\Delta y) - f(x_1, x_2, \ldots, x_n, y)}{\Delta y}\,\mathrm{d}x_1 \\
&= \int_{a_1}^{b_1} \lim_{\Delta y\to 0} \frac{f(x_1, x_2, \ldots, x_n, y+\Delta y) - f(x_1, x_2, \ldots, x_n, y)}{\Delta y}\,\mathrm{d}x_1 \\
&= \int_{a_1}^{b_1} \partial_y f(x_1, x_2, \ldots, x_n, y)\,\mathrm{d}x_1.
\end{aligned}$$

To justify interchanging limit and integral, we will show that the integrand converges towards $f_y(x_1, x_2, \ldots, x_n, y)$ uniformly with respect to x_1. By the Mean Value Theorem, there exists $\theta \in (0,1)$ such that

$$\frac{f(x_1, x_2, \ldots, x_n, y+\Delta y) - f(x_1, x_2, \ldots, x_n, y)}{\Delta y} = f_y(x_1, x_2, \ldots, x_n, y+\theta\Delta y).$$

Since $f_y(x_1, x_2, \ldots, x_n, y)$ is uniformly continuous on $[a_1, b_1] \times \{x_2\} \times \cdots \times \{x_n\} \times [y, y+\bar{\delta}]$ for some $\bar{\delta} > 0$, for any $\varepsilon > 0$ there is a $\delta > 0$ such that $\Delta y < \delta$ implies

$$\left| \frac{f(x_1, x_2, \ldots, x_n, y^0+\Delta y) - f(x_1, x_2, \ldots, x_n, y^0)}{\Delta y} - f_y(x_1, x_2, \ldots, x_n, y^0) \right| < \varepsilon.$$

Thus the integrand is uniformly continuous with respect to x_1. □

THEOREM 1.2.2 (Function valued integration bounds). *Assume that the function $f(x_1, \ldots, x_n, y)$ is continuous on $U \times [c, d]$, where*

$$\begin{aligned}
U = \{(x_1, \ldots, x_n) \mid\ & x_1 \in [A(x_2, \ldots, x_n), B(x_2, \ldots, x_n)], \\
& x_i \in [a_i, b_i],\ i = 2, \ldots, n\} \subset \mathbb{R}^n
\end{aligned}$$

with continuous functions $A, B : \mathbb{R}^{n-1} \to \mathbb{R}$, $A < B$. Assume $\varphi(x_2, \ldots, x_n, y)$ and $\psi(x_2, \ldots, x_n, y)$ are continuous and, fixing $y \in [c, d]$, for $x_i \in [a_i, b_i]$, $i = 2, \ldots, n$, the graphs of $x_1 = \varphi(x_2, \ldots, x_n, y)$ and $x_1 = \psi(x_2, \ldots, x_n, y)$ are in U.

(a) *Then*

$$F(x_2, \ldots, x_n, y) := \int_{\varphi(x_2,\ldots,x_n,y)}^{\psi(x_2,\ldots,x_n,y)} f(x_1, \ldots, x_n, y)\,\mathrm{d}x_1$$

is continuous on $[a_2, b_2] \times \cdots \times [a_n, b_n] \times [c, d]$.

(b) *Assume further that* $\partial_y f(x_1, \dots, x_n, y)$ *exists and is continuous in* $U \times (c, d)$, *and* $\partial_y \varphi$ *and* $\partial_y \psi$ *exist a.e. in* $[a_2, b_2] \times \cdots \times [a_n, b_n] \times (c, d)$. *If* $\partial_y \varphi(x_2, \dots, x_n, y)$ *and* $\partial_y \psi(x_2, \dots, x_n, y)$ *exist at* $(x_2, \dots, x_n, y) \in [a_2, b_2] \times \cdots \times [a_n, b_n] \times (c, d)$, *then* $\partial_y F(x_2, \dots, x_n, y)$ *exists and is given by*

$$\begin{aligned}\partial_y F(x_2, \dots, x_n, y) = & \int_{\varphi(x_2,\dots,x_n,y)}^{\psi(x_2,\dots,x_n,y)} \partial_y f(x_1, \dots, x_n, y)\, \mathrm{d}x_1 \\ & + \partial_y \psi(x_2, \dots, x_n, y) f(\psi(x_2, \dots, x_n, y), x_2, \dots, y) \\ & - \partial_y \varphi(x_2, \dots, x_n, y) f(\varphi(x_2, \dots, x_n, y), x_2, \dots, y).\end{aligned}$$

PROOF. (a) Given $(x_2^0, \dots, x_n^0, y^0)$, write

$$\begin{aligned}F(x_2, \dots, x_n, y) = & \int_{\varphi(x_2^0,\dots,x_n^0,y^0)}^{\psi(x_2^0,\dots,x_n^0,y^0)} f(x_1, \dots, x_n, y)\, \mathrm{d}x_1 \\ & + \int_{\psi(x_2^0,\dots,x_n^0,y^0)}^{\psi(x_2,\dots,x_n,y)} f(x_1, \dots, x_n, y)\, \mathrm{d}x_1 \\ & - \int_{\varphi(x_2^0,\dots,x_n^0,y^0)}^{\varphi(x_2,\dots,x_n,y)} f(x_1, \dots, x_n, y)\, \mathrm{d}x_1.\end{aligned} \tag{1.3}$$

Setting $M = \max_{U \times [c,d]} |f(x_1, \dots, x_n, y)|$, the second term can be estimated by

$$\int_{\psi(x_2^0,\dots,x_n^0,y^0)}^{\psi(x_2,\dots,x_n,y)} f(x_1, \dots, x_n, y)\, \mathrm{d}x_1 \le M |\psi(x_2, \dots, x_n, y) - \psi(x_2^0, \dots, x_n^0, y^0)|,$$

which goes to 0 as $(x_2, \dots, x_n, y)$ approaches $(x_2^0, \dots, x_n^0, y^0)$. The same estimate can be used on the last term. For the first term, as U is a closed set, f is uniformly continuous on $U \times [c, d]$. With the same argument as in the proof of Theorem 1(a), we can exchange limit and integral and get

$$\lim_{(x_2,\dots,x_n,y) \to (x_2^0,\dots,x_n^0,y^0)} F(x_2, \dots, x_n, y) = F(x_2^0, \dots, x_n^0, y^0).$$

(b) Suppose that $\partial_y \varphi$ and $\partial_y \psi$ exist at the point $(x_2^0, \dots, x_n^0, y^0)$. To obtain the derivative of F with respect to y at $(x_2^0, \dots, x_n^0, y^0)$, write F as in Equation (1.3). The derivative of the first term can be shown to be

$$\int_{\varphi(x_2^0,\dots,x_n^0,y^0)}^{\psi(x_2^0,\dots,x_n^0,y^0)} \partial_y f(x_1, x_2^0, \dots, x_n^0, y^0)\, \mathrm{d}x_1$$

by copying the proof of Theorem 1.2.1(b) with $a_1 = \varphi(x_2^0, \dots, x_n^0, y^0)$ and $b_1 = \psi(x_2^0, \dots, x_n^0, y^0)$.

To differentiate the second term, we apply the definition of the derivative to the integral expression and, since $\partial_y\psi$ exists at $(x_2^0,\dots,x_n^0,y^0)$, obtain

$$\begin{aligned}&\lim_{\Delta y\to 0}\frac{1}{\Delta y}\int_{\psi(x_2^0,\dots,x_n^0,y^0)}^{\psi(x_2^0,\dots,x_n^0,y^0+\Delta y)} f(x_1,x_2^0\dots,x_n^0,y^0+\Delta y)\,\mathrm{d}x_1\\ =&\lim_{\Delta y\to 0}\frac{\psi(x_2^0,\dots,x_n^0,y^0+\Delta y)-\psi(x_2^0,\dots,x_n^0,y^0)}{\Delta y} f(\bar{x}_1,x_2^0\dots,x_n^0,y^0+\Delta y)\\ =&\partial_y\psi(x_2^0,\dots,x_n^0,y^0) f(\psi(x_2^0,\dots,x_n^0,y^0),x_2^0\dots,x_n^0,y^0).\end{aligned}$$

We have applied the Mean Value Theorem for integrals, so

$$\psi(x_2^0,\dots,x_n^0,y^0)\le\bar{x}_1\le\psi(x_2^0,\dots,x_n^0,y^0+\Delta y).$$

Differentiating the third term in the same way concludes the proof. □

We can now derive a statement on the derivative of functions of the form

$$F(y):=\int_{a_n}^{b_n}\cdots\int_{a_2}^{b_2}\int_{\varphi(x_2,\dots,x_n,y)}^{\psi(x_2,\dots,x_n,y)} f(x_1,\dots,x_n,y)\,\mathrm{d}x_1\,\mathrm{d}x_2\cdots\mathrm{d}x_n \tag{1.4}$$

by iteratively applying Theorems 1.2.1 and 1.2.2.

COROLLARY 1.2.3. *Suppose f satisfies the assumptions of Theorem 1.2.2(a).*

(a) *Then $F(y)$ in Equation (1.4) is continuous on $[c,d]$.*
(b) *With the additional assumptions of Theorem 1.2.2(b), $\partial_y F$ exists in (c,d) and is given by*

$$\begin{aligned}\partial_y F(y)=\int_{a_n}^{b_n}\cdots\int_{a_2}^{b_2}\Big[&\int_{\varphi(x_2,\dots,x_n,y)}^{\psi(x_2,\dots,x_n,y)}\partial_y f(x_1,\dots,x_n,y)\,\mathrm{d}x_1\\ &+\partial_y\psi(x_2,\dots,x_n,y)f(\psi(x_2,\dots,x_n,y),x_2,\dots,y)\\ &-\partial_y\varphi(x_2,\dots,x_n,y)f(\varphi(x_2,\dots,x_n,y),x_2,\dots,y)\Big]\,\mathrm{d}x_2\cdots\mathrm{d}x_n,\end{aligned}$$

assuming these integrals exist.

In analogy with Theorem 1.2.2(a), we now extend the continuity statement to the case that F in (1.4) is a multivariable function.

THEOREM 1.2.4 (Continuity for multivariable function). *Let $V\subset\mathbb{R}^m$ be an open bounded set, $m\ge 1$. Assume the function $f(x_1,\dots,x_n,\boldsymbol{y})$ is continuous on $U\times\overline{V}$, where U is given in Theorem 1.2.2. Assume $\varphi(x_2,\dots,x_n,\boldsymbol{y})$ and $\psi(x_2,\dots,x_n,\boldsymbol{y})$ are continuous, and for any $\boldsymbol{y}\in\overline{V}$ the graphs of $x_1=\varphi(x_2,\dots,x_n,\boldsymbol{y})$ and $x_1=\psi(x_2,\dots,x_n,\boldsymbol{y})$, $x_i\in[a_i,b_i]$, $i=2,\dots,n$, are in U.*

Then

$$F(x_2,\dots,x_n,\boldsymbol{y}):=\int_{\varphi(x_2,\dots,x_n,\boldsymbol{y})}^{\psi(x_2,\dots,x_n,\boldsymbol{y})} f(x_1,\dots,x_n,\boldsymbol{y})\,\mathrm{d}x_1$$

is continuous on $[a_2,b_2]\times\cdots\times[a_n,b_n]\times\overline{V}$.

PROOF. The proof of Theorem 1.2.2(a) can be copied verbatim, just replacing $y\in\mathbb{R}$ by $\boldsymbol{y}\in\mathbb{R}^m$ and $U\times[c,d]$ by $U\times\overline{V}$. □

By repeated application of Theorem 1.2.4, we get:

COROLLARY 1.2.5. *Let f satisfy the assumptions of Theorem 1.2.4. Then*

$$F(\boldsymbol{y}) := \int_{a_n}^{b_n} \cdots \int_{a_2}^{b_2} \int_{\varphi(x_2,\ldots,x_n,\boldsymbol{y})}^{\psi(x_2,\ldots,x_n,\boldsymbol{y})} f(x_1,\ldots,x_n,\boldsymbol{y})\,\mathrm{d}x_1\,\mathrm{d}x_2\cdots\mathrm{d}x_n$$

is continuous on $\overline{V}$.

We now consider the case that the integrand contains a $\boldsymbol{y}$-independent factor $\omega(x_1,\ldots,x_n)$.

THEOREM 1.2.6 (Continuity for $\boldsymbol{y}$-indepent factor). *Assume $\omega(x_1,\ldots,x_n)$ is absolutely integrable on U. Under the hypotheses of Theorem 1.2.4, the function*

$$F(\boldsymbol{y}) := \int_{a_n}^{b_n} \cdots \int_{a_2}^{b_2} \int_{\varphi(x_2,\ldots,x_n,\boldsymbol{y})}^{\psi(x_2,\ldots,x_n,\boldsymbol{y})} \omega(x_1,\ldots,x_n) f(x_1,\ldots,x_n,\boldsymbol{y})\,\mathrm{d}x_1\,\mathrm{d}x_2\cdots\mathrm{d}x_n$$

is continuous on $\overline{V}$.

PROOF. Let y^0 be given. In analogy to the proof of Theorem 1.2.2(a), write

$$\begin{aligned} F(\boldsymbol{y}) = & \int_{a_n}^{b_n} \cdots \int_{a_2}^{b_2} \int_{\varphi(x_2,\ldots,x_n,\boldsymbol{y}^0)}^{\psi(x_2,\ldots,x_n,\boldsymbol{y}^0)} \omega(x_1,\ldots,x_n) f(x_1,\ldots,x_n,\boldsymbol{y})\,\mathrm{d}x_1\,\mathrm{d}x_2\cdots\mathrm{d}x_n \\ & + \int_{a_n}^{b_n} \cdots \int_{a_2}^{b_2} \int_{\psi(x_2,\ldots,x_n,\boldsymbol{y}^0)}^{\psi(x_2,\ldots,x_n,\boldsymbol{y})} \omega(x_1,\ldots,x_n) f(x_1,\ldots,x_n,\boldsymbol{y})\,\mathrm{d}x_1\,\mathrm{d}x_2\cdots\mathrm{d}x_n \\ & - \int_{a_n}^{b_n} \cdots \int_{a_2}^{b_2} \int_{\varphi(x_2,\ldots,x_n,\boldsymbol{y}^0)}^{\varphi(x_2,\ldots,x_n,\boldsymbol{y})} \omega(x_1,\ldots,x_n) f(x_1,\ldots,x_n,\boldsymbol{y})\,\mathrm{d}x_1\,\mathrm{d}x_2\cdots\mathrm{d}x_n. \end{aligned} \tag{1.5}$$

Setting $M = \max_{U\times\overline{V}} |f(x_1,\ldots,x_n,\boldsymbol{y})|$, the second term can be bounded by

$$\begin{aligned} & \int_{a_n}^{b_n} \cdots \int_{a_2}^{b_2} \int_{\psi(x_2,\ldots,x_n,\boldsymbol{y}^0)}^{\psi(x_2,\ldots,x_n,\boldsymbol{y})} \omega(x_1,\ldots,x_n) f(x_1,\ldots,x_n,\boldsymbol{y})\,\mathrm{d}x_1\,\mathrm{d}x_2\cdots\mathrm{d}x_n \\ \le & M \left| \int_{a_n}^{b_n} \cdots \int_{a_2}^{b_2} \int_{\psi(x_2,\ldots,x_n,\boldsymbol{y}^0)}^{\psi(x_2,\ldots,x_n,\boldsymbol{y})} \omega(x_1,\ldots,x_n)\,\mathrm{d}x_1\,\mathrm{d}x_2\cdots\mathrm{d}x_n \right|, \end{aligned}$$

which goes to 0 as $y \to y_0$. Again, the same estimate can be used on the last term.

For the first term, since f is uniformly continuous on $U \times \overline{V}$, for any $\varepsilon > 0$ there is a $\delta > 0$ such that for $|\boldsymbol{y} - \boldsymbol{y}_0| < \delta$ we have

$$\begin{aligned} & \left| \int_{a_n}^{b_n} \cdots \int_{a_2}^{b_2} \int_{\varphi(x_2,\ldots,x_n,\boldsymbol{y}^0)}^{\psi(x_2,\ldots,x_n,\boldsymbol{y}^0)} \omega(x_1,\ldots,x_n) f(x_1,\ldots,x_n,\boldsymbol{y})\,\mathrm{d}x_1\,\mathrm{d}x_2\cdots\mathrm{d}x_n \right. \\ - & \left. \int_{a_n}^{b_n} \cdots \int_{a_2}^{b_2} \int_{\varphi(x_2,\ldots,x_n,\boldsymbol{y}^0)}^{\psi(x_2,\ldots,x_n,\boldsymbol{y}^0)} \omega(x_1,\ldots,x_n) f(x_1,\ldots,x_n,\boldsymbol{y}_0)\,\mathrm{d}x_1\,\mathrm{d}x_2\cdots\mathrm{d}x_n \right| \end{aligned}$$

$$\leq \int_{a_n}^{b_n} \cdots \int_{a_2}^{b_2} \int_{\varphi(x_2,\ldots,x_n,\boldsymbol{y}^0)}^{\psi(x_2,\ldots,x_n,\boldsymbol{y}^0)} |\omega(x_1,\ldots,x_n)||f(x_1,\ldots,x_n,\boldsymbol{y}) - f(x_1,\ldots,x_n,\boldsymbol{y}_0)| \, \mathrm{d}x_1 \, \mathrm{d}x_2 \cdots \mathrm{d}x_n$$

$$< \varepsilon \int_{a_n}^{b_n} \cdots \int_{a_2}^{b_2} \int_{\varphi(x_2,\ldots,x_n,\boldsymbol{y}^0)}^{\psi(x_2,\ldots,x_n,\boldsymbol{y}^0)} |\omega(x_1,\ldots,x_n)| \, \mathrm{d}x_1 \, \mathrm{d}x_2 \cdots \mathrm{d}x_n$$

Since the last integral is bounded from above by the integral of $|\omega|$ over U, this goes to 0 as $\varepsilon \to 0$. □

1.2.2. Exchanging differentiation and limit. The following statement is proved in [**31**, Nr. 436, Satz 8].

LEMMA 1.2.7. *Let the functions $f_m(x)$ be differentiable in the interval (c,d), and suppose the sequence of derivatives $f'_m(x)$ converges uniformly with respect to x in this interval. If the sequence $\{f_m(x)\}$ converges at least in one point $x \in [c,d]$, then the sequence converges in all of $[c,d]$. The convergence is uniform, and the limit function is differentiable and satisfies*

$$f'(x) = \lim_{m\to\infty} f'_m(x).$$

1.2.3. Change of variables in a Lebesgue integral. The subsequent theorems can be found, for example, in [**75**].

THEOREM 1.2.8. *Let Q be a non-singular linear transformation in $\mathbb{R}^n$, and let $J = |\det(Q)|$. Then, if $f(\boldsymbol{x})$ is Lebesgue integrable over $\mathbb{R}^n$, we have*

$$\int_{\mathbb{R}^n} f(\boldsymbol{x}) \, \mathrm{d}\boldsymbol{x} = \int_{\mathbb{R}^n} f(Q\boldsymbol{x}) J \, \mathrm{d}\boldsymbol{x}.$$

PROOF. See e.g. [**75**, Chapter 9, § 39, Theorem 2]. □

THEOREM 1.2.9. *Assume that the real function $\boldsymbol{\varphi}(\boldsymbol{x}) = (\varphi_1(\boldsymbol{x}),\ldots,\varphi_n(\boldsymbol{x}))$ is defined on the open set $V_1 \subset \mathbb{R}^n$, and that all partial derivatives $\partial_{x_j}\varphi_i(\boldsymbol{x})$ exist and are continuous in V_1. Let $V_2 = \boldsymbol{\varphi}(V_1)$ be the image of V_1 under $\boldsymbol{\varphi}$, and $J(\boldsymbol{x}) = |\det \partial_{\boldsymbol{x}}\boldsymbol{\varphi}(\boldsymbol{x})|$ be the Jacobian determinant of $\boldsymbol{\varphi}$.*

The function $f(\boldsymbol{y})$ is Lebesgue integrable over V_2 if and only if $f\left(\boldsymbol{\varphi}(\boldsymbol{x})\right) J(\boldsymbol{x})$ is Lebesgue integrable over V_1, and then

$$\int_{V_2} f(\boldsymbol{y}) \, \mathrm{d}\boldsymbol{y} = \int_{V_1} f\left(\boldsymbol{\varphi}(\boldsymbol{x})\right) J(\boldsymbol{x}) \, \mathrm{d}\boldsymbol{x}.$$

PROOF. See e.g. [**75**, Chapter 9, § 40, Theorem 1]. □

1.2.4. Bounded variation and Riemann-Stieltjes integrals. Given a function $\boldsymbol{u} : [0,T] \to \mathbb{R}^n$, let

$$\Gamma = \{t_0, \dots, t_M\}$$

be a *partition* of $[0,T]$, that is, a finite set of points t_k in $[0,T]$ satisfying $0 = t_0 < \dots < t_M = T$. With any partition Γ, we associate the sum

$$S(\boldsymbol{u};\Gamma) = \sum_{i=k}^{M} \|\boldsymbol{u}(t_k) - \boldsymbol{u}(t_{k-1})\|. \tag{1.6}$$

Denote by $\Psi(0,T)$ the set of all partitions of the interval $[0,T]$. We can define the *total variation*, or length, of $\boldsymbol{u}$ by

$$\operatorname*{Var}_{[0,T]}(\boldsymbol{u}) := \sup_{\Gamma\in\Psi(0,T)} S(\boldsymbol{u};\Gamma). \tag{1.7}$$

We say that $\boldsymbol{u}$ is of *bounded variation* if the total variation of $\boldsymbol{u}$ is finite.

LEMMA 1.2.10. *The function $\boldsymbol{u} = (u_1, \dots, u_n)$ is of bounded variation if and only if the component functions u_i are of bounded variation.*

PROOF. Straightforward. □

We now introduce the Riemann-Stieltjes integral. Let two functions $u, w : [0,T] \to \mathbb{R}$ be given, where w is of bounded variation and continuous from the right. Let $\Gamma = \{t_0, \dots, t_M\}$ be a partition of $[0,T]$, and τ_k an arbitrary point in the subinterval $[t_{k-1}, t_k]$. Consider the sum

$$R(u,w;\Gamma) = \sum_{k=1}^{M} u(\tau_k)[w(t_k) - w(t_{k-1})].$$

Suppose that as the partition is refined, i.e., $|\Gamma| := \max_{k=1,\dots,M}(t_k - t_{k-1}) \to 0$, the sum approaches a limit independent of the choice of the points t_k and τ_k. Recall [**72, 66, 70**] that this limit is then called the *Riemann-Stieltjes integral* of u with respect to w, written

$$\int_0^T u \,\mathrm{d}w = \lim_{|\Gamma|\to 0} R(u,w;\Gamma).$$

More generally, for vector-valued functions $\boldsymbol{u}, \boldsymbol{w} : [0,T] \to \mathbb{R}^n$, we can define the Riemann-Stieltjes integral

$$\int_0^T \boldsymbol{u} \cdot \mathrm{d}\boldsymbol{w} = \lim_{|\Gamma|\to 0} R(\boldsymbol{u},\boldsymbol{w};\Gamma)$$

of $\boldsymbol{u}$ with respect to $\boldsymbol{w}$ for the standard scalar product in $\mathbb{R}^n$ by the corresponding limit of sums*

$$R(\boldsymbol{u},\boldsymbol{w};\Gamma) = \sum_{k=1}^{M} \boldsymbol{u}(\tau_k) \cdot (\boldsymbol{w}(t_k) - \boldsymbol{w}(t_{k-1})).$$

For the proofs of the following standard statements on vector-valued Riemann-Stieltjes integrals, we refer e.g. to [**70**].

*This corresponds to definition (II) of the Riemann-Stieltjes integral in [**70**].

PROPOSITION 1.2.11. *Suppose* $\int_0^T \boldsymbol{u}_1 \cdot \mathrm{d}\boldsymbol{w}$ *and* $\int_0^T \boldsymbol{u}_2 \cdot \mathrm{d}\boldsymbol{w}$ *exists. Then for any scalars* λ_1 *and* λ_2*,*

$$\int_0^T (\lambda_1 \boldsymbol{u}_1 + \lambda_2 \boldsymbol{u}_2) \cdot \mathrm{d}\boldsymbol{w} = \lambda_1 \int_0^T \boldsymbol{u}_1 \cdot \mathrm{d}\boldsymbol{w} + \lambda_2 \int_0^T \boldsymbol{u}_2 \cdot \mathrm{d}\boldsymbol{w}$$

and the left-hand side integral exists. The corresponding statement holds for $\int_0^T \boldsymbol{u} \cdot \mathrm{d}\boldsymbol{w}_1$ *and* $\int_0^T \boldsymbol{u} \cdot \mathrm{d}\boldsymbol{w}_2$*.*

PROPOSITION 1.2.12. *If* $\int_0^T \boldsymbol{u} \cdot \mathrm{d}\boldsymbol{w}$ *exists, then for any* $0 < \tilde{t} < T$*, the equality*

$$\int_0^T \boldsymbol{u} \cdot \mathrm{d}\boldsymbol{w} = \int_0^{\tilde{t}} \boldsymbol{u} \cdot \mathrm{d}\boldsymbol{w} + \int_{\tilde{t}}^T \boldsymbol{u} \cdot \mathrm{d}\boldsymbol{w}$$

holds and both right-hand side integrals exist.

THEOREM 1.2.13 (Integration by parts). *If* $\int_0^T \boldsymbol{u} \cdot \mathrm{d}\boldsymbol{w}$ *exists, then so does* $\int_0^T \boldsymbol{w} \cdot \mathrm{d}\boldsymbol{u}$*, and their values are related by*

$$\int_0^T \boldsymbol{u} \cdot \mathrm{d}\boldsymbol{w} + \int_0^T \boldsymbol{w} \cdot \mathrm{d}\boldsymbol{u} = \boldsymbol{u}(T) \cdot \boldsymbol{w}(T) - \boldsymbol{u}(0) \cdot \boldsymbol{w}(0).$$

For later reference, we add the following statement:

LEMMA 1.2.14. *Let* $\boldsymbol{x} \in \mathbb{R}^n$*. Then*

$$\int_0^T \boldsymbol{x} \cdot \mathrm{d}\boldsymbol{w} = \boldsymbol{x} \cdot (\boldsymbol{w}(T) - \boldsymbol{w}(0)).$$

In particular, if $\boldsymbol{w}(T) = \boldsymbol{w}(0)$*, then this is equal to 0.*

PROOF. For any Γ,

$$R(\boldsymbol{x}, \boldsymbol{w}; \Gamma) = \boldsymbol{x} \cdot \sum_{k=1}^{M} (\boldsymbol{w}(t_k) - \boldsymbol{w}(t_{k-1})) = \boldsymbol{x} \cdot (\boldsymbol{w}(T) - \boldsymbol{w}(0)). \qquad \square$$

THEOREM 1.2.15 (Existence). *If* $\boldsymbol{u}$ *is continuous on* $[0, T]$ *and* $\boldsymbol{w}$ *is of bounded variation, then* $\int_0^T \boldsymbol{u} \cdot \mathrm{d}\boldsymbol{w}$ *exists.*

The last theorem is the vector valued version of the corresponding statement in [**39**, Stieltjes integral]:

THEOREM 1.2.16. *Suppose* $\boldsymbol{u}$ *is Riemann-integrable and there is an absolutely integrable function* $\boldsymbol{v}$ *on* $[0, T]$ *such that*

$$\boldsymbol{w}(t) = C + \int_0^t \boldsymbol{v}(\tau)\, \mathrm{d}\tau.$$

Then

$$\int_0^T \boldsymbol{u} \cdot \mathrm{d}\boldsymbol{w} = \int_0^T \boldsymbol{u}(t) \cdot \boldsymbol{v}(t)\, \mathrm{d}t. \tag{1.8}$$

In particular, (1.8) *holds if* $\boldsymbol{w}$ *has a bounded and Riemann-integrable derivative* $\boldsymbol{w}'$ *on* $[0, T]$*; in this case* $\boldsymbol{v} = \boldsymbol{w}'$*.*

1.2.5. Hyperspherical coordinates. Hyperspherical coordinates are the extension of spherical coordinates to $\mathbb{R}^n$. In terms of cartesian coordinates, the transformation is given by

$$\begin{aligned}
x_1 &= \rho \sin\theta_0 \sin\theta_1 \sin\theta_2 \cdots \sin\theta_{n-2},\\
x_2 &= \rho \cos\theta_0 \sin\theta_1 \sin\theta_2 \cdots \sin\theta_{n-2},\\
x_3 &= \rho \qquad \cos\theta_1 \sin\theta_2 \cdots \sin\theta_{n-2},\\
x_4 &= \rho \qquad\qquad \cos\theta_2 \cdots \sin\theta_{n-2},\\
&\vdots\\
x_n &= \rho \qquad\qquad\qquad\qquad \cos\theta_{n-2}
\end{aligned}$$

with $0 \le \rho$, $0 \le \theta_0 \le 2\pi$, and $0 \le \theta_i \le \pi$ for $i = 2, \dots, n-2$. The Jacobian determinant of the transformation is

$$\left| \det \frac{\partial(x_1, \dots, x_n)}{\partial(\rho, \theta_0, \dots, \theta_{n-2})} \right| = \rho^{n-1} \sin\theta_1 \sin^2\theta_2 \cdots \sin^{n-2}\theta_{n-2}.$$

Hyperspherical coordinates are useful in proving the following statements.

LEMMA 1.2.17. *Suppose* $\boldsymbol{x} = (x_1, \dots, x_n) \in \mathbb{R}^n$, $n \ge 2$, *and* $\tilde{R} \in \mathbb{R}$, $\tilde{R} > 0$. *The integrals*

(a) $$\int_{\|\boldsymbol{x}\| \le \tilde{R}} \frac{x_1^2 + \cdots + x_{j-1}^2 + x_{j+1}^2 + \cdots + x_n^2}{\|\boldsymbol{x}\|^3} \, \mathrm{d}\boldsymbol{x}, \qquad j = 1, \dots, n,$$

(b) $$\int_{\|\boldsymbol{x}\| \le \tilde{R}} \frac{x_i x_j}{\|\boldsymbol{x}\|^3} \, \mathrm{d}\boldsymbol{x}, \qquad i, j = 1, \dots, n,\ i \ne j,$$

exist.

PROOF. (a) Assume without loss of generality that $j = n$. Conducting a change of variables into hyperspherical coordinates, note that

$$\begin{aligned}
x_1^2 + x_2^2 &= \rho^2 \sin^2\theta_1 \sin^2\theta_2 \cdots \sin^2\theta_{n-2},\\
&\vdots\\
x_1^2 + \cdots + x_{n-1}^2 &= \rho^2 \sin^2\theta_{n-2},
\end{aligned}$$

and

$$\|\boldsymbol{x}\|^3 = \rho^3.$$

Thus, integral (a) is equal to

$$\int_0^{\tilde{R}} \int_0^{2\pi} \int_0^{\pi} \cdots \int_0^{\pi} \rho^{n-2} \sin\theta_1 \sin^2\theta_2 \cdots \sin^{n-3}\theta_{n-3} \sin^n\theta_{n-2} \, \mathrm{d}\theta_{n-2} \cdots \mathrm{d}\theta_1 \, \mathrm{d}\theta_0 \, \mathrm{d}\rho.$$

This is a bounded function on a bounded box and thus exists.

(b) Assume now, without loss of generality, that $i = n-1$ and $j = n$. By change of variables into hyperspherical coordinates, integral (b) is equal to

$$\int_0^{\tilde{R}} \int_0^{2\pi} \int_0^{\pi} \cdots \int_0^{\pi} \rho^{n-2} \sin\theta_1 \sin^2\theta_2 \cdots \sin^{n-3}\theta_{n-3} \sin^{n-2}\theta_{n-2} \cos\theta_{n-3} \cos\theta_{n-2} \sin\theta_{n-2} \, \mathrm{d}\theta_{n-2} \cdots \mathrm{d}\theta_1 \, \mathrm{d}\theta_0 \, \mathrm{d}\rho.$$

and therefore again exists. □

1.3. Isometries of $\mathbb{R}^n$

1.3.1. Rotations and reflections. The *orthogonal group* of degree n, $O(n)$, represents the symmetry group of the n-dimensional spheres with origin 0 in $\mathbb{R}^n$. It consists of the orthonormal $n \times n$-matrices,

$$O(n) := \{Q \in \mathbb{R}^{n\times n} \mid Q^T Q = \mathcal{I}d\},$$

and forms a group under matrix multiplication. It acts on the elements of $\mathbb{R}^n$ in the obvious way.

The elements of $O(n)$ are isometries of $\mathbb{R}^n$: For all $\boldsymbol{x}, \boldsymbol{y} \in \mathbb{R}^n$ and $Q \in O(n)$,

$$\|Q\boldsymbol{x} - Q\boldsymbol{y}\| = ((\boldsymbol{x}-\boldsymbol{y})^T Q^T Q(\boldsymbol{x}-\boldsymbol{y}))^{\frac{1}{2}} = \|\boldsymbol{x}-\boldsymbol{y}\|. \tag{1.9}$$

Any $Q \in O(n)$ has determinant ± 1, as

$$1 = \det(Q^T Q) = (\det Q)^2.$$

For $n \leq 3$, $O(n)$ can be visualized as the group of all rotations and reflections of $\mathbb{R}^n$ preserving the origin [**2**].

The subgroup of $O(n)$ preserving orientation is the group of rotations of $\mathbb{R}^n$ or *special orthogonal group* [**2**],

$$SO(n) := \{Q \in O(n) \mid \det Q = 1\}.$$

We will later make use of the following two lemmas.

LEMMA 1.3.1. *The following are equivalent:*

(a) $\boldsymbol{x}_1, \boldsymbol{x}_2 \in \mathbb{R}^n$ *satisfy* $\|\boldsymbol{x}_1\| = \|\boldsymbol{x}_2\|$.
(b) *There exists a* $Q \in O(n)$ *such that* $\boldsymbol{x}_1 = Q\boldsymbol{x}_2$.
(c) *There exists a* $Q \in SO(n)$ *such that* $\boldsymbol{x}_1 = Q\boldsymbol{x}_2$.

PROOF. "(a)⇒(b)" We show that this is true for $\|\boldsymbol{x}_1\| = \|\boldsymbol{x}_2\| = 1$. Note that $\boldsymbol{x}_i$, $i = 1, 2$, forms the orthonormal basis of a 1-dimensional subspace of $\mathbb{R}^n$, which can be extended to an orthonormal basis $\{\boldsymbol{x}_i, \boldsymbol{y}_{i,2}, \ldots, \boldsymbol{y}_{i,n}\}$ of $\mathbb{R}^n$. Define the matrix Q_i such that its columns are this basis, $Q_i = (\boldsymbol{x}_i, \boldsymbol{y}_{i,2}, \ldots, \boldsymbol{y}_{i,n})$. Then $Q_i^T Q_i = \mathcal{I}d$, so $Q_i \in O(n)$, and $\boldsymbol{x}_i = Q_i(1, 0, \ldots, 0)^T$ gives $\boldsymbol{x}_2 = Q\boldsymbol{x}_1$ with $Q = Q_2 Q_1^T \in O(n)$. For arbitrary $\boldsymbol{x}_1$, $\boldsymbol{x}_2$, use linearity.

"(a)⇒(c)" If $\det Q_i = -1$ in the preceeding construction, replace $\boldsymbol{y}_{i,n}$ by $-\boldsymbol{y}_{i,n}$ to obtain a corresponding $\tilde{Q}_i \in SO(n)$ and subsequently $Q = \tilde{Q}_2 \tilde{Q}_1^T \in SO(n)$.

"(b)⇒(a)", "(c)⇒(a)" See Equation (1.9). □

LEMMA 1.3.2. *Define the subgroup $O^1(n) \subset O(n)$ consisting of all matrices of the form*

$$Q = \begin{pmatrix} 1 & \boldsymbol{y}^T \\ 0 & \\ \vdots & \widetilde{Q} \\ 0 & \end{pmatrix}, \quad \boldsymbol{y} \in \mathbb{R}^{n-1},\ Q \in O(n).$$

Then $Q\boldsymbol{x} = \boldsymbol{x}$ for all $Q \in O^1(n)$ if and only if $\boldsymbol{x} = (\lambda, 0, \dots, 0)^T$, $\lambda \in \mathbb{R}$.

PROOF. Assume first that $\boldsymbol{x}$ satisfies $Q\boldsymbol{x} = \boldsymbol{x}$ for all $Q \in O^1(n)$. By the rules for computing determinants, $\det \widetilde{Q} = \det Q$, and thus $\widetilde{Q} \in O(n-1)$. Therefore, Lemma 1.3.1 implies that for any $\tilde{\boldsymbol{x}} \neq 0$ there exists a $\widetilde{Q} \in O(n-1)$ such that $\widetilde{Q}\tilde{\boldsymbol{x}} \neq \tilde{\boldsymbol{x}}$. Consequently, $\tilde{\boldsymbol{x}} = 0$. The converse is trivial. □

The action of $O(n)$ on $\mathbb{R}^n$ induces obvious actions on different sets of functions involving $\mathbb{R}^n$ in image or preimage which will come up later. Let $Q \in O(n)$. The actions are defined as follows:

$$\begin{aligned} &\boldsymbol{u} \in Map([0,T];\mathbb{R}^n): && (Q\boldsymbol{u})(t) = Q(\boldsymbol{u}(t)), \\ &\omega \in Map(\mathbb{R}^n \times \mathbb{R}_+;\mathbb{R}): && (Q\omega)(\boldsymbol{x}, r) = \omega(Q^{-1}\boldsymbol{x}, r), \\ &\boldsymbol{\xi} \in Map(\mathbb{R}^n \times \mathbb{R}_+;\partial B_{\mathbf{0},1}): && (Q\boldsymbol{\xi})_{(\boldsymbol{x},r)} = Q(\boldsymbol{\xi}_{(Q^{-1}\boldsymbol{x},r)}). \end{aligned}$$

1.3.2. Translations. The group of *translations* of $\mathbb{R}^n$ consists of all maps $T_{\boldsymbol{v}}$, $\boldsymbol{v} \in \mathbb{R}^n$, defined by

$$\begin{aligned} T_{\boldsymbol{v}}:\ &\mathbb{R}^n \to \mathbb{R}^n, \\ &\boldsymbol{x} \mapsto \boldsymbol{x} + \boldsymbol{v}, \end{aligned}$$

together with addition,

$$T_{\boldsymbol{v}_1} + T_{\boldsymbol{v}_2} = T_{\boldsymbol{v}_1 + \boldsymbol{v}_2}.$$

The inverse element is given by

$$T_{\boldsymbol{v}}^{-1} = T_{-\boldsymbol{v}}.$$

Obviously, the group is isomorphic to $\mathbb{R}^n$ under addition.

Similar to $O(n)$, the group of translations of $\mathbb{R}^n$ acts on the above mentioned function sets in the obvious way:

$$\begin{aligned} &\boldsymbol{u} \in Map([0,T];\mathbb{R}^n): && (T_{\boldsymbol{v}}\boldsymbol{u})(t) = T_{\boldsymbol{v}}(\boldsymbol{u}(t)), \\ &\omega \in Map(\mathbb{R}^n \times \mathbb{R}_+;\mathbb{R}): && (T_{\boldsymbol{v}}\omega)(\boldsymbol{x}, r) = \omega(T_{\boldsymbol{v}}^{-1}\boldsymbol{x}, r), \\ &\boldsymbol{\xi} \in Map(\mathbb{R}^n \times \mathbb{R}_+;\partial B_{\mathbf{0},1}): && (T_{\boldsymbol{v}}\boldsymbol{\xi})_{(\boldsymbol{x},r)} = \boldsymbol{\xi}_{(T_{\boldsymbol{v}}^{-1}\boldsymbol{x},r)}. \quad , \end{aligned}$$

where $\boldsymbol{v} \in \mathbb{R}^n$.

1.4. Some estimates

LEMMA 1.4.1. *Assume* $\boldsymbol{v}_1,\ \boldsymbol{v}_2 \in \mathbb{R}^n$ *and* $\|\boldsymbol{v}_1\|, \|\boldsymbol{v}_2\| \geq L > 0$. *Then*

$$\left\| \frac{\boldsymbol{v}_2}{\|\boldsymbol{v}_2\|} - \frac{\boldsymbol{v}_1}{\|\boldsymbol{v}_1\|} \right\| \leq \min\left(\frac{\|\boldsymbol{v}_2 - \boldsymbol{v}_1\|}{L}, 2 \right).$$

PROOF. Assume without loss of generality that $\|\boldsymbol{v}_1\| \geq \|\boldsymbol{v}_2\|$. Then

$$\begin{aligned}
\left\| \frac{\boldsymbol{v}_2}{\|\boldsymbol{v}_2\|} - \frac{\boldsymbol{v}_1}{\|\boldsymbol{v}_1\|} \right\|^2 &= \left(\frac{\boldsymbol{v}_2}{\|\boldsymbol{v}_2\|} - \frac{\boldsymbol{v}_1}{\|\boldsymbol{v}_1\|} \right) \cdot \left(\frac{\boldsymbol{v}_2}{\|\boldsymbol{v}_2\|} - \frac{\boldsymbol{v}_1}{\|\boldsymbol{v}_1\|} \right) \\
&= 1 - 2\frac{\boldsymbol{v}_1}{\|\boldsymbol{v}_1\|} \cdot \frac{\boldsymbol{v}_2}{\|\boldsymbol{v}_2\|} + 1 \\
&= \left(1 - \frac{\boldsymbol{v}_1}{\|\boldsymbol{v}_1\|} \cdot \frac{\boldsymbol{v}_2}{\|\boldsymbol{v}_2\|} \right)^2 + 1 - \left(\frac{\boldsymbol{v}_1}{\|\boldsymbol{v}_1\|} \cdot \frac{\boldsymbol{v}_2}{\|\boldsymbol{v}_2\|} \right)^2 \\
&\leq \left(\frac{\|\boldsymbol{v}_1\|}{\|\boldsymbol{v}_2\|} - \frac{\boldsymbol{v}_1}{\|\boldsymbol{v}_1\|} \cdot \frac{\boldsymbol{v}_2}{\|\boldsymbol{v}_2\|} \right)^2 + 1 - \left(\frac{\boldsymbol{v}_1}{\|\boldsymbol{v}_1\|} \cdot \frac{\boldsymbol{v}_2}{\|\boldsymbol{v}_2\|} \right)^2 \\
&= \left(\frac{\boldsymbol{v}_2}{\|\boldsymbol{v}_2\|} - \frac{\boldsymbol{v}_1}{\|\boldsymbol{v}_2\|} \right) \cdot \left(\frac{\boldsymbol{v}_2}{\|\boldsymbol{v}_2\|} - \frac{\boldsymbol{v}_1}{\|\boldsymbol{v}_2\|} \right) \\
&\leq \left(\frac{\|\boldsymbol{v}_2 - \boldsymbol{v}_1\|}{L} \right)^2.
\end{aligned}$$

In the first estimate we used $\frac{\|\boldsymbol{v}_1\|}{\|\boldsymbol{v}_2\|} \geq 1 \geq \frac{\boldsymbol{v}_1}{\|\boldsymbol{v}_1\|} \cdot \frac{\boldsymbol{v}_2}{\|\boldsymbol{v}_2\|}$. Upper bound 2 is clear by the triangle inequality. □

LEMMA 1.4.2. *Assume* $\boldsymbol{v}_1,\ \boldsymbol{v}_2 \in \mathbb{R}^n$ *and* $\|\boldsymbol{v}_2\| \geq L \geq \|\boldsymbol{v}_1\|$. *Then*

$$\|\boldsymbol{v}_2 - \boldsymbol{v}_1\| \geq \left\| \frac{L}{\|\boldsymbol{v}_2\|} \boldsymbol{v}_2 - \boldsymbol{v}_1 \right\|.$$

PROOF. Because both terms are nonnegative, it suffices to show that the difference of the squares of these terms is nonnegative. We make use of the identities

$$\begin{aligned}
\|\boldsymbol{v}_2 - \boldsymbol{v}_1\|^2 &= \left\| \left(\boldsymbol{v}_2 - \frac{\boldsymbol{v}_1 \cdot \boldsymbol{v}_2}{\boldsymbol{v}_2 \cdot \boldsymbol{v}_2} \boldsymbol{v}_2 \right) - \left(\boldsymbol{v}_1 - \frac{\boldsymbol{v}_1 \cdot \boldsymbol{v}_2}{\boldsymbol{v}_2 \cdot \boldsymbol{v}_2} \boldsymbol{v}_2 \right) \right\|^2 \\
\left\| \frac{L}{\|\boldsymbol{v}_2\|} \boldsymbol{v}_2 - \boldsymbol{v}_1 \right\|^2 &= \left\| \left(\frac{L}{\|\boldsymbol{v}_2\|} \boldsymbol{v}_2 - \frac{\boldsymbol{v}_1 \cdot \boldsymbol{v}_2}{\boldsymbol{v}_2 \cdot \boldsymbol{v}_2} \boldsymbol{v}_2 \right) - \left(\boldsymbol{v}_1 - \frac{\boldsymbol{v}_1 \cdot \boldsymbol{v}_2}{\boldsymbol{v}_2 \cdot \boldsymbol{v}_2} \boldsymbol{v}_2 \right) \right\|^2
\end{aligned}$$

Applying $\|\boldsymbol{v}\|^2 = \boldsymbol{v} \cdot \boldsymbol{v}$ and multiplying out both scalar products, the mixed terms are quickly shown to both be 0. We obtain

$$\begin{aligned}\|\boldsymbol{v}_2 - \boldsymbol{v}_1\|^2 - \left\| \frac{L}{\|\boldsymbol{v}_2\|}\boldsymbol{v}_2 - \boldsymbol{v}_1 \right\|^2 &= \left(\boldsymbol{v}_2 - \frac{\boldsymbol{v}_1 \cdot \boldsymbol{v}_2}{\boldsymbol{v}_2 \cdot \boldsymbol{v}_2}\boldsymbol{v}_2\right) \cdot \left(\boldsymbol{v}_2 - \frac{\boldsymbol{v}_1 \cdot \boldsymbol{v}_2}{\boldsymbol{v}_2 \cdot \boldsymbol{v}_2}\boldsymbol{v}_2\right) \\ &\quad - \left(\frac{L}{\|\boldsymbol{v}_2\|}\boldsymbol{v}_2 - \frac{\boldsymbol{v}_1 \cdot \boldsymbol{v}_2}{\boldsymbol{v}_2 \cdot \boldsymbol{v}_2}\boldsymbol{v}_2\right) \cdot \left(\frac{L}{\|\boldsymbol{v}_2\|}\boldsymbol{v}_2 - \frac{\boldsymbol{v}_1 \cdot \boldsymbol{v}_2}{\boldsymbol{v}_2 \cdot \boldsymbol{v}_2}\boldsymbol{v}_2\right) \\ &= \left(\|\boldsymbol{v}_2\| - \frac{\boldsymbol{v}_1 \cdot \boldsymbol{v}_2}{\|\boldsymbol{v}_2\|}\right)^2 - \left(L - \frac{\boldsymbol{v}_1 \cdot \boldsymbol{v}_2}{\|\boldsymbol{v}_2\|}\right)^2 \\ &\geq 0.\end{aligned}$$

The inequality holds because

$$0 \leq L - \|\boldsymbol{v}_1\| \frac{\boldsymbol{v}_1}{\|\boldsymbol{v}_1\|} \cdot \frac{\boldsymbol{v}_2}{\|\boldsymbol{v}_2\|} = L - \frac{\boldsymbol{v}_1 \cdot \boldsymbol{v}_2}{\|\boldsymbol{v}_2\|} \leq \|\boldsymbol{v}_2\| - \frac{\boldsymbol{v}_1 \cdot \boldsymbol{v}_2}{\|\boldsymbol{v}_2\|}. \qquad \square$$

CHAPTER 2

Vector Preisach Hysteresis Modeling

This chapter investigates the vector Preisach operator recently introduced by Della Torre, Pinzaglia and Cardelli [**24, 25**]. It starts with a short overview of the general mathematical notion of hysteresis, where we extend the definition of scalar hysteresis operators from [**16**] to the vectorial setting. Then, we present a formal definition of the vector relay operator, which forms the elementary memory of the new vector Preisach operator, and work out some of its properties. In the third section, we investigate the new vector Preisach operator in detail. We consider its fundamental properties such as isotropy, saturation, periodic and congruency behaviour, lag and dissipation. The subsequent section shows that it reduces to a scalar Preisach operator under uniaxial input. Finally, the last section focuses on various infinitesimal properties of the operator, namely output continuity, the output derivative and a possible hysteresis potential.

2.1. General hysteresis operators

From a mathematical perspective, the characterizing features of hysteresis are rate-independence and memory. In their book, Brokate and Sprekels [**16**] give a formal definition of scalar hysteresis operators, i.e. hysteresis operators mapping scalar functions to scalar functions. The definition relies on rate-independent functionals and extends readily to the vector-valued case. We will follow part of the exposition in [**16**] to obtain the corresponding definitions for vectorial hysteresis.

Note that in [**16**], a strong focus is put on the correspondence between input functions and input strings in the context of scalar hysteresis. This correspondence arises from rate-independence, due to which scalar input is uniquely determined by its local minima and maxima. These concepts do not carry over to the general vectorial setup, where there exists no equivalent definition of an arbitrary curve in $\mathbb{R}^n$ in terms of discrete data. The correspondence is also the reason why scalar hysteresis operators are implicitly well-defined in the presence of jump discontinuities [**16**], whereas here in the vectorial context we will only consider inputs in the space $C([0,T];\mathbb{R}^n)$ of continuous vector-valued functions.

2.1.1. Definition. Vectorial hysteresis can be represented by an operator $\boldsymbol{\mathcal{W}}$ mapping an input function $\boldsymbol{u} : [0,T] \to \mathbb{R}^n$ to an output function $\boldsymbol{w} : [0,T] \to \mathbb{R}^n$,

$$\boldsymbol{w}(t) = \boldsymbol{\mathcal{W}}[\boldsymbol{u}](t), \qquad t \in [0,T].$$

Definition 2.1.1 (rate-independent operator, admissible time transformation). The operator $\boldsymbol{\mathcal{W}}$ is called *rate-independent* if and only if

$$\boldsymbol{\mathcal{W}}[\boldsymbol{u} \circ \varphi] = \boldsymbol{\mathcal{W}}[\boldsymbol{u}] \circ \varphi$$

holds for all *admissible time transformations*, that is, all continuous non-decreasing functions $\varphi : [0,T] \to [0,T]$ satisfying $\varphi(0) = 0$ and $\varphi(T) = T$.

As remarked earlier, aside from rate-independence, the second characteristic of a hysteresis operator $\boldsymbol{\mathcal{W}}$ is its memory. This notion is represented by the *Volterra property*. Let $\boldsymbol{u}_t$ denote the *truncation of* $\boldsymbol{u}$ *at* t:

$$\boldsymbol{u}_t(\tau) := \begin{cases} \boldsymbol{u}(\tau) & \text{for } 0 \le \tau \le t, \\ \boldsymbol{u}(t) & \text{for } t < \tau \le T. \end{cases}$$

Definition 2.1.2 (Volterra property). We say that $\boldsymbol{\mathcal{W}}$ satisfies the Volterra property if and only if $\boldsymbol{u}_t = \overline{\boldsymbol{u}}_t$ implies $(\boldsymbol{\mathcal{W}}[\boldsymbol{u}])_t = (\boldsymbol{\mathcal{W}}[\overline{\boldsymbol{u}}])_t$ for all $\boldsymbol{u}, \overline{\boldsymbol{u}} \in C([0,T];\mathbb{R}^n)$ and $t \in [0,T]$.

In view of this property, the definition of hysteresis operators will be based on rate-independent functionals.

Definition 2.1.3 (Rate-independent functionals). A functional $\boldsymbol{\mathcal{H}} : C([0,T];\mathbb{R}^n) \to \mathbb{R}^n$ is called *rate-independent* if and only if

$$\boldsymbol{\mathcal{H}}[\boldsymbol{u} \circ \varphi] = \boldsymbol{\mathcal{H}}[\boldsymbol{u}]$$

holds for all $\boldsymbol{u} \in C([0,T];\mathbb{R}^n)$ and all admissible time transformations φ.

We now have everything necessary to define general hysteresis operators.

Definition 2.1.4 (Hysteresis operator). We call an operator $\boldsymbol{\mathcal{W}} : C([0,T];\mathbb{R}^n) \to Map([0,T];\mathbb{R}^n)$ a *hysteresis operator* if and only if there exists a rate-independent functional $\boldsymbol{\mathcal{H}}$ such that

$$\boldsymbol{\mathcal{W}}[\boldsymbol{u}](t) = \boldsymbol{\mathcal{H}}[\boldsymbol{u}_t] \qquad \text{for all } t \in [0,T] \text{ and all } \boldsymbol{u} \in C([0,T];\mathbb{R}^n).$$

From

$$\boldsymbol{\mathcal{W}}[\boldsymbol{u}](T) = \boldsymbol{\mathcal{H}}[\boldsymbol{u}_T] = \boldsymbol{\mathcal{H}}[\boldsymbol{u}] \qquad \text{for all } \boldsymbol{u} \in C([0,T];\mathbb{R}^n),$$

we see that each hysteresis operator determines its underlying rate-independent functional uniquely. In correspondence to [**16**], we call this the *generating functional* of $\boldsymbol{\mathcal{W}}$ and denote it by $\boldsymbol{\mathcal{W}}_f$, so

$$\boldsymbol{\mathcal{W}}_f[\boldsymbol{u}] = \boldsymbol{\mathcal{W}}[\boldsymbol{u}](T).$$

The vectorial definition of hysteresis operators allows us to draw the same conclusions as found for scalar hysteresis operators in [**16**]:

- If $\boldsymbol{u}$ is constant on a subinterval of $[0,T]$, then $\boldsymbol{\mathcal{W}}[\boldsymbol{u}]$ is also constant on that interval.
- $\boldsymbol{\mathcal{W}}$ is completely determined by the vectors $\boldsymbol{\mathcal{W}}[\boldsymbol{u}](T)$ for all $\boldsymbol{u} \in C([0,T];\mathbb{R}^n)$.

Proposition 2.1.5 (Characterization of hysteresis operators). *The operator* $\boldsymbol{\mathcal{W}} : C([0,T];\mathbb{R}^n) \to Map([0,T];\mathbb{R}^n)$ *is a hysteresis operator if and only if* $\boldsymbol{\mathcal{W}}$ *is rate-independent and satisfies the Volterra property.*

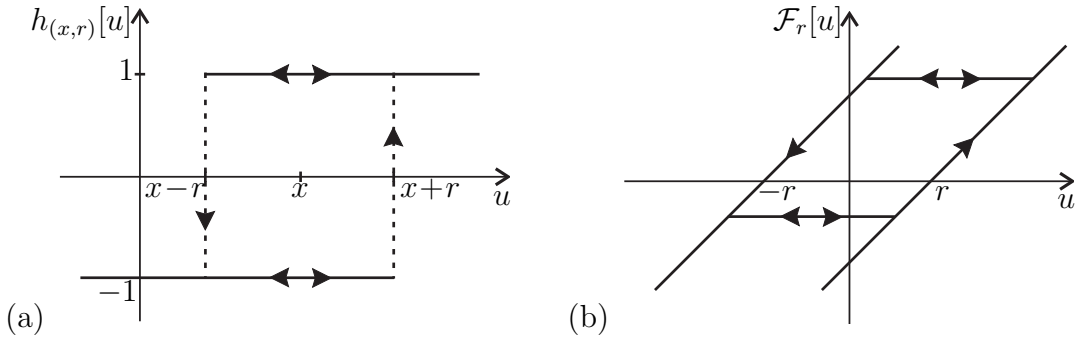

FIGURE 2.1. (a) Scalar relay operator $h_{(x,r)}$, (b) scalar play operator $\mathcal{F}_r$.

PROOF. To prove that a hysteresis operator is rate-independent and satisfies the Volterra property, just apply the definitions. For rate-independence, this gives

$$\boldsymbol{\mathcal{W}}[\boldsymbol{u}\circ\varphi](t)=\boldsymbol{\mathcal{W}}_f[(\boldsymbol{u}\circ\varphi)_t]=\boldsymbol{\mathcal{W}}_f[\boldsymbol{u}_{\varphi(t)}\circ\varphi]=\boldsymbol{\mathcal{W}}_f[\boldsymbol{u}_{\varphi(t)}]=\boldsymbol{\mathcal{W}}[\boldsymbol{u}](\varphi(t)),$$

as in Equation (2.22) in [**16**].

The converse follows in full analogy to the proof of Proposition 2.2.9 in [**16**]. □

2.1.2. Examples. In the following, some standard examples of hysteresis operators will be introduced for later reference.

EXAMPLE 2.1.6 (Scalar Relay Operator). The scalar relay operator [**58, 51, 16, 67, 22**] (Figure 2.1(a)), here denoted $h_{(x,r)}$, represents a delayed switch and is a very simple example of a scalar hysteresis operator. It is characterized by its mean value $x\in\mathbb{R}$ and radius $r\in\mathbb{R}_+$ and maps a function $u:\ [0,T]\to\mathbb{R}$ to a function $w:\ [0,T]\to\{-1,1\}$. The relay state will be undetermined if $u(0)\in(x-r,x+r)$, so it is necessary to provide an initial state $\xi\in\{-1,1\}$. The output function

$$w=h_{(x,r)}[u,\xi]$$

is defined as follows: If $u(t)$ is not in the open interval $(x-r,x+r)$, then $w(t)$ is 1 for $u(t)-x\geq r$ and -1 for $u(t)-x\leq -r$. If $u(t)$ is in the interval $(x-r,x+r)$, then $w(t)$ is "frozen" in the state it had when $u(t)$ last crossed one of the threshold values $x-r$ or $x+r$. Adopting the notation of [**67**] and setting

$$X_t:=\{\tau\in[0,t]\ \mid\ |u(\tau)-x|\geq r\},$$

this results in the formal definition

$$h_{(x,r)}[u,\xi](t)=\begin{cases}\frac{u(t)-x}{|u(t)-x|} & \text{if } |u(t)-x|\geq r,\\ h_{(x,r)}[u,\xi](\max X_t) & \text{if } |u(t)-x|<r \text{ and } X_t\neq\varnothing,\\ \xi & \text{otherwise.}\end{cases}\tag{2.1}$$

We have chosen this uncommon formulation of the definition to emphasize the correspondence to the later definition of the vector relay operator.

Visintin [**67**] gives a list of mathematical properties of the scalar relay operator.

EXAMPLE 2.1.7 (Scalar Play Operator). The play operator [**43, 16, 44**] (Figure 2.1(b)), denoted $\mathcal{F}_r$, reproduces the input-output relation of a mechanical play. It is characterized by its half-diameter $r \in \mathbb{R}_+$. For a piecewise monotone input function $u : [0,T] \to \mathbb{R}$ and a given initial state $a \in \mathbb{R}$, the output function $w \in Map([0,T];\mathbb{R})$,

$$w = \mathcal{F}_r[u,a],$$

is inductively defined by [**16**]

$$\begin{aligned} w(0) &= f_r(u(0),a), \\ w(t) &= f_r(u(t),w(t_i)), \quad \text{for } t_i < t \le t_{i+1}, \quad 0 \le i \le N-1. \end{aligned}$$

Here, $f_r : \mathbb{R} \times \mathbb{R} \to \mathbb{R}$ is given by

$$f_r(x,y) = \max\{x-r, \min\{x+r, y\}\}$$

and $\{t_0, \cdots, t_N\}$ is a partition of $[0,T]$ such that the function u is monotone on each of the subintervals $[t_i, t_{i+1}]$.

In fact, the play operator can be obtained as a linear superposition of scalar relays [**16**]:

$$\mathcal{F}_r[u](t) = \frac{1}{2}\int_{-\infty}^{\infty} h_{(x,r)}[u,\xi_{(x,r)}](t)\,\mathrm{d}x. \tag{2.2}$$

Here, $\xi_{(x,r)} \in \{-1,1\}$ specifies the initial value of relay $h_{(x,r)}$. The improper integral is interpreted as a principal value integral:

$$\int_{-\infty}^{\infty} h_{(x,r)}[u,\xi_{(x,r)}](t)\,\mathrm{d}x = \lim_{M\to\infty}\int_{-M}^{M} h_{(x,r)}[u,\xi_{(x,r)}](t)\,\mathrm{d}x.$$

EXAMPLE 2.1.8 (Scalar Preisach Operator). The *Preisach operator* $\mathcal{P}$ [**58, 51, 16**] arises as a linear weighted superposition of scalar relay operators $h_{(x,r)}$. The pairs (x,r) form the *Preisach half plane* $\mathbb{R} \times \mathbb{R}_+$. We write $\xi : \mathbb{R} \times \mathbb{R}_+ \to \{-1,1\}$ to denote the initial state, whose value at (x,r) is denoted $\xi_{(x,r)}$. For $u : [0,T] \to \mathbb{R}$, the scalar Preisach operator $\mathcal{P}$ with density function $\omega : \mathbb{R} \times \mathbb{R}_+ \to \mathbb{R}$ is given by

$$\mathcal{P}[u,\xi](t) := \int_{\mathbb{R}_+}\int_{\mathbb{R}} \omega(x,r) h_{(x,r)}[u,\xi_{(x,r)}]\,\mathrm{d}x\,\mathrm{d}r, \tag{2.3}$$

where $t \in [0,T]$.

The beauty of the scalar Preisach operator lies in its tangible mathematical structure, which allows to represent the memory evolution of the relays in a simple geometric way. For this, view $h_{(x,r)}[u,\xi_{(x,r)}](t)$ as a function in (x,r) mapping the Preisach half plane $\mathbb{R}\times\mathbb{R}_+$ to $\{-1,1\}$. Fixing ξ such that $\xi_{(x,r)} = 1$ where $x < 0$ and $\xi_{(x,r)} = -1$ where $x \ge 0$, it turns out that the attainable states can all be expressed in terms of a curve $x = \psi(r)$ separating the subdomain on which all relays take the state 1 from that with state -1 [**16, 51**]. Because of its shape it is often refered to as "staircase curve". It results from an input function u as follows: at any time t, all the relays $h_{(x,r)}$ such that $x \le u(t) - r$ take state 1, all those relays such that $x \ge u(t) + r$ take state -1. The remaining relays stay constant. Thus, the memory evolution can be represented in terms of the cone $\mathcal{C}_{u(t)} = \{(x,r) \mid |x - u(t)| < r\}$. As

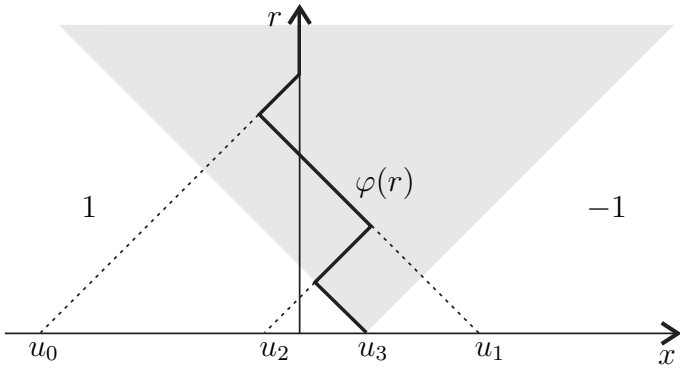

FIGURE 2.2. Memory evolution of the scalar Preisach operator: The staircase function $\psi(r)$ is the result of the piecewise linear input function interpolating $u(t_0) = u_0$, $u(t_1) = u_1$, $u(t_2) = u_2$, and $u(t_3) = u_3$ with $0 = t_0 < t_1 < t_2 < t_3 = T$. The cone $\mathcal{C}_{u(t_3)}$ is drawn shaded.

$u(t)$ increases and $\mathcal{C}_{u(t)}$ moves to the right, the relays leaving $\mathcal{C}_{u(t)}$ on the left switch to 1; conversely, as $u(t)$ decreases and $\mathcal{C}_{u(t)}$ moves to the left, the relays leaving $\mathcal{C}_{u(t)}$ on the right switch to -1. This is illustrated on an example in Figure 2.2.

The *set of Preisach memory curves* [**16**], that is, attainable staircase curves, is given by

$$\Psi_0 := \{\psi \mid \psi : \mathbb{R}_+ \to \mathbb{R}, |\psi(r) - \psi(\tilde{r})| \le |r - \tilde{r}| \text{ for all } r, \tilde{r} \ge 0, \\ \sup\{r \mid r \ge 0, \psi(r) \ne 0\} \le +\infty\}.$$

Given an initial memory state $\psi_{-1} \in \Psi_0$, the memory evolution can be represented in terms of memory curves and the play operator by

$$\psi(t)(r) = \mathcal{F}_r[u, \psi_{-1}(r)](t), \quad t \in [0, T].$$

With this, we can give an alternative formulation of the scalar Preisach operator $\mathcal{P}$ using the play operator $\mathcal{F}_r$, which is discussed in detail in [**16**]. It is a result of Equation (2.2) relating relay and play operator and holds advantages regarding the mathematical investigation of the Preisach operator because $\mathcal{F}_r$, unlike $h_{(x,r)}$, is continuous. In terms of the play operator, the scalar Preisach operator can be expressed as

$$\mathcal{P}[u](t) = \int_0^\infty q(r, \mathcal{F}_r[u](t))\,\mathrm{d}r \;+\; w_{00}, \tag{2.4}$$

where

$$q(r, s) = 2\int_0^s \omega(x, r)\,\mathrm{d}x,$$

$$w_{00} = \int_0^\infty \int_{-\infty}^0 \omega(x, r)\,\mathrm{d}x\,\mathrm{d}r - \int_0^\infty \int_0^\infty \omega(x, r)\,\mathrm{d}x\,\mathrm{d}r.$$

EXAMPLE 2.1.9 (Mayergoyz' vector Preisach model). This vector Preisach operator, independently suggested by Mayergoyz [**50**] and Damlamian and Visintin [**21**],

applies the scalar Preisach operator to construct a vectorial hysteresis operator $\boldsymbol{\mathcal{W}} : C([0,T];\mathbb{R}^n) \to C([0,T];\mathbb{R}^n)$. This is done by allocating a scalar Preisach operator $\mathcal{P}_{\boldsymbol{e}}$ for each vectorial direction $\boldsymbol{e} \in \partial B_{\mathbf{0},1}$. The input function $\boldsymbol{u}$ is projected onto each $\boldsymbol{e}$, the respective scalar Preisach operator $\mathcal{P}_{\boldsymbol{e}}$ is evaluated and all the outcomes are superposed:

$$\boldsymbol{\mathcal{W}}[\boldsymbol{u}](t) = \int_{\partial B_{\mathbf{0},1}} \mathcal{P}_{\boldsymbol{e}}[\boldsymbol{u}\cdot\boldsymbol{e}](t)\boldsymbol{e}\,\mathrm{d}\mu(\boldsymbol{e}),$$

where μ is the measure on the unit sphere $\partial B_{\mathbf{0},1}$ induced by parametrization in hyperspherical coordinates. The operator is investigated extensively for example in [**51, 36**].

2.2. Vector Relay Operator

We will now discuss the vector relay operator and its basic properties. This new vectorial generalization of the scalar relay operator (Example 2.1.6) was recently introduced by Della Torre, Pinzaglia and Cardelli [**24, 25**]. It constitutes the elementary memory of the vector Preisach operator discussed in the next section. The vector relay operator is conceptually related to the rotating model by Damlamian and Visintin [**21, 67**] through the idea of projecting the input function onto a convex set representing the relay, but the definition of the output differs.

In this section, we will present a formal definition of the vector relay operator. In particular, the definition exhibits the correspondence between scalar relay and vector relay. Then, we discuss the properties of the relay operator. This comprises basic facts like the semigroup property, normalization and behaviour subject to the isometries of $\mathbb{R}^n$. We will further give an affine bound on the operator output and show that it satisfies a dissipation property on cyclic inputs.

We have gathered a few additional facts which are of no immediate relevance in the framework of this dissertation in Appendix B.

2.2.1. Definition. The n-dimensional vector relay $\boldsymbol{h}_{(\boldsymbol{x},r)}$ associated with a tuple $(\boldsymbol{x},r) \in \mathbb{R}^n \times \mathbb{R}_+$ is represented by the open ball $B_{\boldsymbol{x},r}$. It maps a continuous input function $\boldsymbol{u} : [0,T] \to \mathbb{R}^n$ to an output function $\boldsymbol{w} : [0,T] \to \partial B_{\mathbf{0},1}$ taking values on the unit sphere. The output function $\boldsymbol{w} = \boldsymbol{h}_{(\boldsymbol{x},r)}[\boldsymbol{u}]$, which we will also refer to as *relay state*, is defined as follows: If $||\boldsymbol{u}(t) - \boldsymbol{x}|| \geq r$ then $\boldsymbol{w}(t)$ is the unit vector based at $\boldsymbol{x}$ pointing at $\boldsymbol{u}(t)$. As $\boldsymbol{u}$ enters the relay and $||\boldsymbol{u}(t) - \boldsymbol{x}|| < r$, the output "freezes" the moment $\boldsymbol{u}$ crosses the relay boundary and does not vary until $\boldsymbol{u}$ leaves the relay again. For an illustration, see Figure 2.3. Like for the scalar relay, an initial value $\boldsymbol{\xi} \in \partial B_{\mathbf{0},1}$ must be given, in case $\boldsymbol{u}(0)$ lies inside $B_{\boldsymbol{x},r}$ and thus leaves $\boldsymbol{w}(0)$ undetermined. Setting

$$X_t := \{\tau \in [0,t] \mid \|\boldsymbol{u}(\tau) - \boldsymbol{x}\| \geq r\},$$

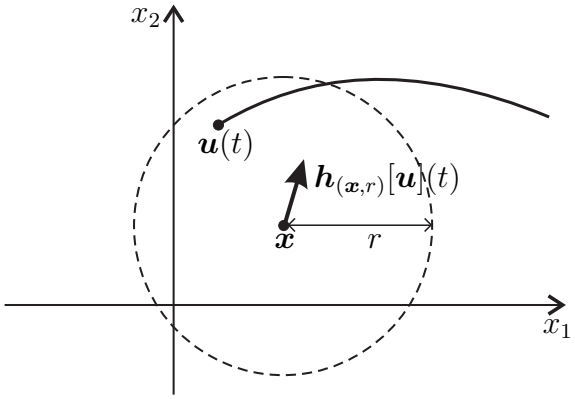

FIGURE 2.3. Vector relay operator $\boldsymbol{h}_{(\boldsymbol{x},r)}$.

this gives the formal definition

$$\boldsymbol{h}_{(\boldsymbol{x},r)}[\boldsymbol{u},\boldsymbol{\xi}](t) = \begin{cases} \frac{\boldsymbol{u}(t)-\boldsymbol{x}}{\|\boldsymbol{u}(t)-\boldsymbol{x}\|} & \text{if } \|\boldsymbol{u}(t)-\boldsymbol{x}\| \geq r, \\ \boldsymbol{h}_{(\boldsymbol{x},r)}[\boldsymbol{u},\boldsymbol{\xi}](\max X_t) & \text{if } \|\boldsymbol{u}(t)-\boldsymbol{x}\| < r \text{ and } X_t \neq \varnothing, \\ \boldsymbol{\xi} & \text{otherwise.} \end{cases} \tag{2.5}$$

Note that the definition of the vector relay operator $\boldsymbol{h}_{(\boldsymbol{x},r)}$, Equation (2.5), is the exact analogue of that of the scalar relay operator $h_{(x,r)}$, Equation (2.1).

For ease of notation, when $\boldsymbol{\xi}$ is clear from context, we will omit it and just write $\boldsymbol{h}_{(\boldsymbol{x},r)}[\boldsymbol{u}]$.

PROPOSITION 2.2.1. *The vector relay operator $\boldsymbol{h}_{(\boldsymbol{x},r)}$ is a hysteresis operator.*

PROOF. From Equation (2.5), $\boldsymbol{h}_{(\boldsymbol{x},r)}[\boldsymbol{u}](t) = \boldsymbol{h}_{(\boldsymbol{x},r)}[\boldsymbol{u}_t](T)$ follows immediately for any $t \in [0,T]$. It remains to show that the generating functional $\boldsymbol{h}_{(\boldsymbol{x},r),f}[\cdot] = \boldsymbol{h}_{(\boldsymbol{x},r)}[\cdot](T)$ is rate-independent, i.e. that $\boldsymbol{h}_{(\boldsymbol{x},r)}[\boldsymbol{u}](T) = \boldsymbol{h}_{(\boldsymbol{x},r)}[\boldsymbol{u}\circ\varphi](T)$ for all admissible time transformations φ. As $\boldsymbol{u}(T) = \boldsymbol{u}\circ\varphi(T)$, this is clear for $\boldsymbol{u}(T) \notin B_{\boldsymbol{x},r}$. If $\boldsymbol{u}(T) \in B_{\boldsymbol{x},r}$, then applying the definition in Equation (2.5) together with the fact that φ is continuous and non-decreasing gives

$$\begin{aligned} \boldsymbol{h}_{(\boldsymbol{x},r)}[\boldsymbol{u}](T) &= \frac{\boldsymbol{u}(\tau)-\boldsymbol{x}}{\|\boldsymbol{u}(\tau)-\boldsymbol{x}\|}, && \text{where } \tau = \max\{t\in[0,T] \mid \|\boldsymbol{u}(t)-\boldsymbol{x}\| \geq r\} \\ &= \frac{\boldsymbol{u}\circ\varphi(\overline{\tau})-\boldsymbol{x}}{\|\boldsymbol{u}\circ\varphi(\overline{\tau})-\boldsymbol{x}\|}, && \text{where } \overline{\tau} = \max\{t\in[0,T] \mid \|\boldsymbol{u}\circ\varphi(t)-\boldsymbol{x}\| \geq r\} \\ &= \boldsymbol{h}_{(\boldsymbol{x},r)}[\boldsymbol{u}\circ\varphi](T). \end{aligned}$$

□

2.2.2. Basic properties. The output function $\boldsymbol{w} = \boldsymbol{h}_{(\boldsymbol{x},r)}[\boldsymbol{u}]$ has jump discontinuities when $\boldsymbol{u}$ leaves the relay at another point than where it entered the relay. Since the relay represents an open set, $\boldsymbol{w}$ is a right-continuous function:

$$\boldsymbol{h}_{(\boldsymbol{x},r)} : C([0,T];\mathbb{R}^n) \times \partial B_{\mathbf{0},1} \to C_r([0,T];\partial B_{\mathbf{0},1}).$$

For $\tau \in [0,T]$, define the *shift* $\boldsymbol{u}^\tau$ of a function $\boldsymbol{u} : [0,T] \to \mathbb{R}^n$ by

$$\boldsymbol{u}^\tau(t) = \boldsymbol{u}(t+\tau), \quad t \in [0, T-\tau].$$

LEMMA 2.2.2 (Semigroup property). *For any $(\boldsymbol{x}, r) \in \mathbb{R}^n \times \mathbb{R}_+$, the vectorial relay operator $\boldsymbol{h}_{(\boldsymbol{x},r)}$ satisfies the semigroup property, that is, for any $t_1, t_2 \in [0,T]$ such that $t_1 \leq t_2$ the following holds true:*

$$\boldsymbol{h}_{(\boldsymbol{x},r)}[\boldsymbol{u}, \boldsymbol{\xi}](t_2) = \boldsymbol{h}_{(\boldsymbol{x},r)}[\boldsymbol{u}^{t_1}, \boldsymbol{h}_{(\boldsymbol{x},r)}[\boldsymbol{u}, \boldsymbol{\xi}](t_1)](t_2 - t_1).$$

PROOF. Straightforward. □

It is possible to associate the input-output behaviour of an arbitrary vector relay operator $\boldsymbol{h}_{(\boldsymbol{x},r)}$ to that of the *unit relay* $\boldsymbol{h}_{(\mathbf{0},1)}$, by subjecting the input funtion to the appropriate transformation. For any $(\boldsymbol{x}, r) \in \mathbb{R}^n \times \mathbb{R}_+$, this transformation is given by $\boldsymbol{\gamma}_{(\boldsymbol{x},r)} : C([0,T];\mathbb{R}^n) \to C([0,T];\mathbb{R}^n)$,

$$\boldsymbol{\gamma}_{(\boldsymbol{x},r)} \circ \boldsymbol{u}(t) := \frac{1}{r}(\boldsymbol{u}(t) - \boldsymbol{x}) \qquad \forall t \in [0,T].$$

LEMMA 2.2.3 (Normalization). *Let $\boldsymbol{u} \in C([0,T];\mathbb{R}^n)$ and $\boldsymbol{\xi} \in \partial B_{\mathbf{0},1}$. For any $(\boldsymbol{x}, r) \in \mathbb{R}^n \times \mathbb{R}_+$, the relay operator satisfies*

$$\boldsymbol{h}_{(\boldsymbol{x},r)}[\boldsymbol{u}, \boldsymbol{\xi}] = \boldsymbol{h}_{(\mathbf{0},1)}[\boldsymbol{\gamma}_{(\boldsymbol{x},r)} \circ \boldsymbol{u}, \boldsymbol{\xi}].$$

PROOF. By definition of $\boldsymbol{\gamma}_{(\boldsymbol{x},r)}$, $\boldsymbol{u}(t) \in B_{\boldsymbol{x},r}$ if and only if $\boldsymbol{\gamma}_{(\boldsymbol{x},r)} \circ \boldsymbol{u}(t) \in B_{\mathbf{0},1}$. With

$$\frac{\frac{1}{r}(\boldsymbol{u}(t) - \boldsymbol{x})}{\|\frac{1}{r}(\boldsymbol{u}(t) - \boldsymbol{x})\|} = \frac{\boldsymbol{u}(t) - \boldsymbol{x}}{\|\boldsymbol{u}(t) - \boldsymbol{x}\|},$$

the statement is quickly verified from the definition of $\boldsymbol{h}_{(\boldsymbol{x},r)}$. □

LEMMA 2.2.4 (Rotation and reflection). *For all $Q \in O(n)$, the relay operator satisfies*

$$Q\boldsymbol{h}_{(\boldsymbol{x},r)}[\boldsymbol{u}, \boldsymbol{\xi}] = \boldsymbol{h}_{(Q\boldsymbol{x},r)}[Q\boldsymbol{u}, Q\boldsymbol{\xi}].$$

PROOF. Equation (1.9) implies for any binary relation $* \in \{<, =, >\}$ that

$$\|Q\boldsymbol{u}(t) - Q\boldsymbol{x}\| * r \quad \text{if and only if} \quad \|\boldsymbol{u}(t) - \boldsymbol{x}\| * r. \tag{2.6}$$

Assume $\boldsymbol{u}(t)$ satisfies $\|\boldsymbol{u}(t) - \boldsymbol{x}\| \geq r$. Then

$$\boldsymbol{h}_{(Q\boldsymbol{x},r)}[Q\boldsymbol{u}, Q\boldsymbol{\xi}](t) = \frac{Q\boldsymbol{u}(t) - Q\boldsymbol{x}}{\|Q\boldsymbol{u}(t) - Q\boldsymbol{x}\|} = \frac{Q(\boldsymbol{u}(t) - \boldsymbol{x})}{\|\boldsymbol{u}(t) - \boldsymbol{x}\|} = Q\boldsymbol{h}_{(\boldsymbol{x},r)}[\boldsymbol{u}, \boldsymbol{\xi}](t).$$

Using (2.6) and (1.9) to show the statement for $\|\boldsymbol{u}(t) - \boldsymbol{x}\| < r$ is straightforward. □

LEMMA 2.2.5 (Translation). *For any translation $T_{\boldsymbol{v}}$, $\boldsymbol{v} \in \mathbb{R}^n$, the relay operator satisfies*

$$\boldsymbol{h}_{(\boldsymbol{x},r)}[\boldsymbol{u}, \boldsymbol{\xi}] = \boldsymbol{h}_{(T_{\boldsymbol{v}}\boldsymbol{x},r)}[T_{\boldsymbol{v}}\boldsymbol{u}, \boldsymbol{\xi}].$$

PROOF. Trivially, for any $* \in \{<, =, >\}$,

$$\|\boldsymbol{u}(t) - \boldsymbol{x}\| * r \quad \text{if and only if} \quad \|T_{\boldsymbol{v}}\boldsymbol{u}(t) - T_{\boldsymbol{v}}\boldsymbol{x}\| * r.$$

If $\|\boldsymbol{u}(t) - \boldsymbol{x}\| \geq r$, then

$$\boldsymbol{h}_{(\boldsymbol{x},r)}[\boldsymbol{u}, \boldsymbol{\xi}](t) = \frac{\boldsymbol{u}(t) - \boldsymbol{x}}{\|\boldsymbol{u}(t) - \boldsymbol{x}\|} = \frac{(\boldsymbol{u}(t) + \boldsymbol{v}) - (\boldsymbol{x} + \boldsymbol{v})}{\|(\boldsymbol{u}(t) + \boldsymbol{v}) - (\boldsymbol{x} + \boldsymbol{v})\|} = \boldsymbol{h}_{(T_{\boldsymbol{v}}\boldsymbol{x},r)}[T_{\boldsymbol{v}}\boldsymbol{u}, \boldsymbol{\xi}](t).$$

If $\|\boldsymbol{u}(t)-\boldsymbol{x}\|<r$, then either $\|\boldsymbol{u}(\tau)-\boldsymbol{x}\|<r$ for all $\tau\in[0,t]$ and

$$\boldsymbol{h}_{(\boldsymbol{x},r)}[\boldsymbol{u},\boldsymbol{\xi}](t)=\boldsymbol{\xi}=\boldsymbol{h}_{(T_{\boldsymbol{v}}\boldsymbol{x},r)}[T_{\boldsymbol{v}}\boldsymbol{u},\boldsymbol{\xi}](t),$$

or $\tilde{\tau}=\max\{\tau\mid\|\boldsymbol{u}(t)-\boldsymbol{x}\|=r\}=\max\{\tau\mid\|(\boldsymbol{u}(t)+\boldsymbol{v})-(\boldsymbol{x}+\boldsymbol{v})\|=r\}$ exists and

$$\boldsymbol{h}_{(\boldsymbol{x},r)}[\boldsymbol{u},\boldsymbol{\xi}](t)=\boldsymbol{h}_{(\boldsymbol{x},r)}[\boldsymbol{u},\boldsymbol{\xi}](\tilde{\tau})=\boldsymbol{h}_{(\boldsymbol{x}+\boldsymbol{v},r)}[\boldsymbol{u}+\boldsymbol{v},\boldsymbol{\xi}](\tilde{\tau})=\boldsymbol{h}_{(T_{\boldsymbol{v}}\boldsymbol{x},r)}[T_{\boldsymbol{v}}\boldsymbol{u},\boldsymbol{\xi}](t).\quad\square$$

2.2.3. Output variation and dissipation. We now show that even though the variation of $\boldsymbol{h}_{(\boldsymbol{x},r)}[\boldsymbol{u},\boldsymbol{\xi}]$ can be unbounded, it is affinely bounded by that of $\boldsymbol{u}$. Subsequently, we prove that $\boldsymbol{h}_{(\boldsymbol{x},r)}$ is dissipative on closed input loops, even though it does not need to be on arbitrary paths.

Let $\boldsymbol{u}\in C([0,T];\mathbb{R}^n)$ and $\boldsymbol{w}=\boldsymbol{h}_{(\boldsymbol{x},r)}[\boldsymbol{u},\boldsymbol{\xi}]$, $\boldsymbol{\xi}\in\partial B_{\mathbf{0},1}$. In the case of the scalar relay, $w=h_{(x;r)}[u]$ is of bounded variation for all $u\in C([0,T];\mathbb{R})$ [**67**]. This is not true in the vectorial case. To construct a counterexample, due to the subsequent lemma we need to look at functions $\boldsymbol{u}$ that are not of bounded variation themselves. For example, consider $u(t)=t\sin\frac{1}{t}$, $t\in[0,\pi]$, and define $\boldsymbol{u}\in C([0,\pi];\mathbb{R}^2)$ by

$$\boldsymbol{u}(t):=\begin{pmatrix}\sqrt{1-(u(t))^2}\\ u(t)\end{pmatrix}$$

to vary on the unit circle. Let $\boldsymbol{w}=\boldsymbol{h}_{(\mathbf{0},1)}[\boldsymbol{u},\boldsymbol{\xi}]$. As $\boldsymbol{u}\in\partial B_{\mathbf{0},1}$ for all $t\in[0,\pi]$, we have $\boldsymbol{w}=\boldsymbol{u}$. The total variation of a vectorial function is bounded from below by the total variations of its component functions, so $\operatorname*{Var}_{[0,\pi]}(\boldsymbol{w})\geq\operatorname*{Var}_{[0,\pi]}(u)=\infty$.

We have, however, that the variation of $\boldsymbol{w}$ is affinely bounded by that of $\boldsymbol{u}$:

LEMMA 2.2.6 (Affine bound on $\operatorname{Var}(\boldsymbol{h}_{(\boldsymbol{x},r)}[\boldsymbol{u},\boldsymbol{\xi}])$). *For any $\boldsymbol{u}\in C([0,T];\mathbb{R}^n)$ and $\boldsymbol{w}=\boldsymbol{h}_{(\boldsymbol{x},r)}[\boldsymbol{u},\boldsymbol{\xi}]$, $\boldsymbol{\xi}\in\partial B_{\mathbf{0},1}$,*

$$\operatorname*{Var}_{[0,T]}(\boldsymbol{w})\leq\frac{1}{r}\operatorname*{Var}_{[0,T]}(\boldsymbol{u})+2. \tag{2.7}$$

PROOF. First, we apply Lemma 2.2.3 to restate (2.7) in terms of the unit relay, so $\boldsymbol{w}=\boldsymbol{h}_{(\mathbf{0},1)}[\boldsymbol{\gamma}_{(\boldsymbol{x},r)}\circ\boldsymbol{u},\boldsymbol{\xi}]$. With(1.6) and (1.7), it is quickly verified that

$$\operatorname*{Var}_{[0,T]}(\boldsymbol{\gamma}_{(\boldsymbol{x},r)}\circ\boldsymbol{u})=\frac{1}{r}\operatorname*{Var}_{[0,T]}(\boldsymbol{u}).$$

As $\boldsymbol{\gamma}_{(\boldsymbol{x},r)}$ is a bijection of $C([0,T];\mathbb{R}^n)$, the statement of the Lemma is equivalent to: For any $\boldsymbol{u}\in C([0,T];\mathbb{R}^n)$ and $\boldsymbol{w}_0:=\boldsymbol{h}_{(\mathbf{0},1)}[\boldsymbol{u},\boldsymbol{\xi}]$, $\boldsymbol{\xi}\in\partial B_{\mathbf{0},1}$,

$$\operatorname*{Var}_{[0,T]}(\boldsymbol{w}_0)\leq\operatorname*{Var}_{[0,T]}(\boldsymbol{u})+2. \tag{2.8}$$

To show (2.8), we reformulate Equation (1.7) to be able to consider the jumps in $\boldsymbol{w}_0$ appropriately. For a given $\boldsymbol{u}$ and partition $\Gamma:=(t_1,\dots,t_M)\in\Psi([0,T])$, we construct a corresponding partition $\Gamma^{\boldsymbol{u}}:=(\tilde{t}_1,\dots,\tilde{t}_{\widetilde{M}})$ by adding additional elements to Γ. For each $i\in\{2,\dots,M\}$:

- If $\boldsymbol{u}(t_i)\in B_{\mathbf{0},1}$ and there exists some $\tau\in[t_{i-1},t_i)$ such that $\boldsymbol{u}(\tau)\notin B_{\mathbf{0},1}$, then add $\tau_i:=\max\{\tau\in[t_{i-1},t_i]\mid\boldsymbol{u}(\tau)\notin B_{\mathbf{0},1}\}$ to the partition, unless $\tau_i=t_{i-1}$.
- If $\boldsymbol{u}(t_{i-1})\in B_{\mathbf{0},1}$ and $\boldsymbol{u}(t_i)\notin B_{\mathbf{0},1}$, then there exists some $\tau_i\in(t_{i-1},t_i]$ such that $u(\tau_i)\in\partial B_{\mathbf{0},1}$. Add τ_i into the partition, unless $\tau_i=t_i$.

By the first rule, we have added the last point in time at which $\boldsymbol{u}$ on $\partial B_{\mathbf{0},1}$ and $\boldsymbol{w}$ took its current value at t_i. By the second rule, we ensure that any pair (t_{i-1}, t_i) in the partition lies fully inside $\overline{B_{\mathbf{0},1}}$ or fully outside $B_{\mathbf{0},1}$. The resulting partition $\Gamma^{\boldsymbol{u}}$ has at most $2M+1$ entries. Define the set consisting of all refined partitions $\Psi^{\boldsymbol{u}}([0,T]) := \{\Gamma^{\boldsymbol{u}} \mid \Gamma \in \Psi([0,T])\} \subset \Psi([0,T])$. Because $S(\boldsymbol{u};\Gamma) \leq S(\boldsymbol{u};\Gamma^{\boldsymbol{u}})$, we can rewrite definition (1.7) as

$$\operatorname{Var}(\boldsymbol{w}) = \sup_{\Psi^{\boldsymbol{u}}([0,T])} \sum_{j=1}^{\widetilde{M}} \|\boldsymbol{w}(\tilde{t}_i) - \boldsymbol{w}(\tilde{t}_{i-1})\|.$$

We will now prove Equation (2.8) by showing that for any partition $\Gamma^{\boldsymbol{u}} = (\tilde{t}_1, \ldots, \tilde{t}_{\widetilde{M}}) \in \Psi^{\boldsymbol{u}}([0,T])$, the corresponding sums satisfy

$$\sum_{j=1}^{\widetilde{M}} \|\boldsymbol{w}(\tilde{t}_i) - \boldsymbol{w}(\tilde{t}_{i-1})\| \leq \sum_{j=1}^{\widetilde{M}} \|\boldsymbol{u}(\tilde{t}_i) - \boldsymbol{u}(\tilde{t}_{i-1})\| + 2. \tag{2.9}$$

Assume first $\tilde{t}_{i-1}, \tilde{t}_i \notin B_{\mathbf{0},1}$. Then $\boldsymbol{w}(\tilde{t}_{i-1}) = \frac{\boldsymbol{u}(\tilde{t}_{i-1})}{\|\boldsymbol{u}(\tilde{t}_{i-1})\|}$ and $\boldsymbol{w}(\tilde{t}_i) = \frac{\boldsymbol{u}(\tilde{t}_i)}{\|\boldsymbol{u}(\tilde{t}_i)\|}$, so

$$\|\boldsymbol{w}(\tilde{t}_i) - \boldsymbol{w}(\tilde{t}_{i-1})\| \leq \|\boldsymbol{u}(\tilde{t}_i) - \boldsymbol{u}(\tilde{t}_{i-1})\|$$

holds by Lemma 1.4.1 with $L = 1$.

Now assume $\tilde{t}_{i-1}, \tilde{t}_i \in \overline{B_{\mathbf{0},1}}$. Then by construction of $\Psi^{\boldsymbol{u}}$, there exist $j_1, j_2 \in \mathbb{N}$, $j_1 \leq i-1 < i \leq j_2$, such that $\boldsymbol{u}(\tilde{t}_j) \in B_{\mathbf{0},1}$ and $\boldsymbol{w}(\tilde{t}_j) = \boldsymbol{w}(\tilde{t}_{j_1})$ for all j, $j_1 < j < j_2$, satisfying one of

- $\boldsymbol{u}(\tilde{t}_{j_1}), \boldsymbol{u}(\tilde{t}_{j_2}) \in \partial B_{\mathbf{0},1}$),
- $j_1 = 1$ and $\boldsymbol{u}(0) \in B_{\mathbf{0},1}$, or
- $j_2 = \widetilde{M}$ and $\boldsymbol{u}(T) \in B_{\mathbf{0},1}$.

In the first case, $\boldsymbol{w}(\tilde{t}_{j_1}) = \boldsymbol{u}(\tilde{t}_{j_1})$ and $\boldsymbol{w}(\tilde{t}_{j_2}) = \boldsymbol{u}(\tilde{t}_{j_2})$, and thus

$$\sum_{j=j_1+1}^{j_2} \|\boldsymbol{w}(\tilde{t}_j) - \boldsymbol{w}(\tilde{t}_{j-1})\| = \|\boldsymbol{u}(\tilde{t}_{j_2}) - \boldsymbol{u}(\tilde{t}_{j_1})\| \leq \sum_{j=j_1+1}^{j_2} \|\boldsymbol{u}(\tilde{t}_j) - \boldsymbol{u}(\tilde{t}_{j-1})\|$$

by the triangle inequality.

In the second case, $\boldsymbol{w}(\tilde{t}_{j_1}) = \boldsymbol{\xi}$ and $\boldsymbol{w}(\tilde{t}_{j_2}) = \boldsymbol{u}(\tilde{t}_{j_2})$. Thus, as both $\boldsymbol{u}(\tilde{t}_{j_2})$ and $\boldsymbol{\xi}$ are unit vectors,

$$\sum_{j=2}^{j_2} \|\boldsymbol{w}(\tilde{t}_j) - \boldsymbol{w}(\tilde{t}_{j-1})\| = \|\boldsymbol{u}(\tilde{t}_{j_2}) - \boldsymbol{\xi}\| \leq 2,$$

giving the constant term in (2.8).

In the third case, $\boldsymbol{w}(\tilde{t}_{j_1}) = \boldsymbol{w}(\tilde{t}_{j_2}) = \boldsymbol{u}(\tilde{t}_{j_1})$, so

$$0 = \sum_{j=j_1+1}^{\widetilde{M}} \|\boldsymbol{w}(\tilde{t}_j) - \boldsymbol{w}(\tilde{t}_{j-1})\| \leq \sum_{j=j_1+1}^{j_2} \|\boldsymbol{u}(\tilde{t}_j) - \boldsymbol{u}(\tilde{t}_{j-1})\|.$$

Thus, (2.9) holds, which finishes the proof of (2.8). □

COROLLARY 2.2.7. *If $\boldsymbol{u}$ is of bounded variation, then so is $\boldsymbol{w}$.*

Further, we can show that each relay satisfies a dissipation condition on closed paths that have the finite switching property. We say that a function $\boldsymbol{u} \in C([0,T];\mathbb{R}^n)$ satisfies the *finite switching property* if, for any $(\boldsymbol{x}, r)$, the set $\boldsymbol{u}([0,T]) \cap \partial B_{\boldsymbol{x},r}$ is finite. The input functions of interest to us (e.g. piecewise linear functions) all have the finite switching property. Related investigations were done in [**17**] considering an elliptic relay and rectangular sample paths. For simplicity, we confine the statement to piecewise differentiable inputs. Note that for $\boldsymbol{u}$ of bounded variation, the existence of integral (2.10) as Riemann-Stieltjes integral is guaranteed as a consequence of Corollary 2.2.7 and Theorem 1.2.15.

LEMMA 2.2.8 (Dissipation). *Assume $\boldsymbol{u} \in C([0,T];\mathbb{R}^n)$ is piecewise differentiable and has the finite switching property. Let $\boldsymbol{w} = \boldsymbol{h}_{(\boldsymbol{x},r)}[\boldsymbol{u}, \boldsymbol{\xi}]$. If $\boldsymbol{u}(0) = \boldsymbol{u}(T)$ and $\boldsymbol{w}(0) = \boldsymbol{w}(T)$, then $\boldsymbol{h}_{(\boldsymbol{x},r)}$ satisfies the dissipation property*

$$\int_0^T \boldsymbol{u} \cdot \mathrm{d}\boldsymbol{w} \geq 0. \tag{2.10}$$

PROOF. Set $\widetilde{\boldsymbol{u}} = \boldsymbol{u} - \boldsymbol{x}$. By Lemma 1.2.14,

$$\int_0^T \boldsymbol{u} \cdot \mathrm{d}\boldsymbol{w} = \int_0^T \boldsymbol{x} \cdot \mathrm{d}\boldsymbol{w} + \int_0^T \widetilde{\boldsymbol{u}} \cdot \mathrm{d}\boldsymbol{w} = \int_0^T \widetilde{\boldsymbol{u}} \cdot \mathrm{d}\boldsymbol{w}.$$

By the finite switching property, $\boldsymbol{u}$ intersects the relay boundary only finitely many times. For any interval $[t_1, t_2] \subseteq [0,T]$ on which $\|\boldsymbol{u}(t) - \boldsymbol{x}\| \geq r$, the relay output $\boldsymbol{w}(t) = \widetilde{\boldsymbol{u}}(t)/\|\widetilde{\boldsymbol{u}}(t)\|$ is continuous and piecewise differentiable. Verifying that $\widetilde{\boldsymbol{u}}^T \left[\partial(\widetilde{\boldsymbol{u}}/\|\widetilde{\boldsymbol{u}}\|)/\partial\widetilde{\boldsymbol{u}}\right] = 0$, we obtain

$$\int_{t_1}^{t_2} \widetilde{\boldsymbol{u}} \cdot \mathrm{d}\boldsymbol{w} = \int_{t_1}^{t_2} \widetilde{\boldsymbol{u}}(t) \cdot \boldsymbol{w}'(t)\,\mathrm{d}t = \int_{t_1}^{t_2} \widetilde{\boldsymbol{u}}(t)^T \left[\partial\boldsymbol{w}/\partial\widetilde{\boldsymbol{u}}\right] \widetilde{\boldsymbol{u}}'(t)\,\mathrm{d}t = 0.$$

As well, for any interval $[t_1, t_2] \subseteq [0,T]$ on which $\|\boldsymbol{u}(t) - \boldsymbol{x}\| < r$, $\boldsymbol{w}$ is constant and thus implies

$$\int_{t_1}^{t_2} \widetilde{\boldsymbol{u}} \cdot \mathrm{d}\boldsymbol{w} = 0.$$

The only case where a non-zero contribution to the integral is made is when $\widetilde{\boldsymbol{u}}$ touches the relay boundary and leaves the relay, i.e. $\|\boldsymbol{u}(t) - \boldsymbol{x}\| = r$ and $\|\boldsymbol{u}(t-\delta) - \boldsymbol{x}\| < r$ for some $\varepsilon > 0$ and all $0 < \delta < \varepsilon$. That contribution is

$$\widetilde{\boldsymbol{u}}(t) \cdot \left(\boldsymbol{w}(t) - \lim_{\tau \to t-} \boldsymbol{w}(\tau)\right) = \widetilde{\boldsymbol{u}}(t) \cdot \left(\frac{\widetilde{\boldsymbol{u}}(t)}{\|\widetilde{\boldsymbol{u}}(t)\|} - \lim_{\tau \to t-} \frac{\widetilde{\boldsymbol{u}}(\tau)}{\|\widetilde{\boldsymbol{u}}(\tau)\|}\right) \geq 0. \qquad \square$$

The proof exposes the significance of the closed loop assumption $\boldsymbol{u}(0) = \boldsymbol{u}(T)$ and $\boldsymbol{w}(0) = \boldsymbol{w}(T)$. If it is not satisfied, the term

$$\int_0^T \boldsymbol{x} \cdot \mathrm{d}\boldsymbol{w} = \boldsymbol{x} \cdot (\boldsymbol{w}(T) - \boldsymbol{w}(0))$$

may be negative and thus make the dissipation expression (2.10) negative.

2.3. Vector Preisach Operator

The scalar Preisach operator (Example 2.1.8) has been established in the modeling of scalar hysteresis for a long time. In the 1980s, the Mayergoyz vector Preisach model (Example 2.1.9) was proposed as a vectorial extension of the scalar operator. It remained the only dimension-independent vectorial generalization of the Preisach operator until recently, when in 2006 a new vector Preisach operator based on the vector relay operator $\boldsymbol{h}_{(\boldsymbol{x},r)}$ was introduced by Della Torre, Pinzaglia and Cardelli [**24**]. We will denote this operator by $\boldsymbol{\mathcal{P}}$. It represents the basis of all further investigations in this work.

After giving a formal definition of the vector Preisach operator $\boldsymbol{\mathcal{P}}$ and presenting a geometric visualization of its memory evolution in low dimension, the remainder of this chapter discusses its properties. We start with basic properties, in particular the action of rotations, reflections and translations on $\boldsymbol{\mathcal{P}}$. Then we investigate isotropy and anisotropy, state a sufficient isotropy condition and suggest a neutral memory state. We analyze saturation and find that, if the Preisach distribution is of bounded support, there is a saturation state with complete memory deletion, alignment of input and output in the isotropic case, asymptotic alignment in the anisotropic case, and an asymptotic output limit which is independent of the direction. Thus, the saturation behaviour of $\boldsymbol{\mathcal{P}}$ is found to be in good qualitative correspondence to that observed in magnetic hysteresis. We further show that periodic input results in periodic output, and, in particular, uniformly rotating input results in uniformly rotating output in $\mathbb{R}^2$. We prove that $\boldsymbol{\mathcal{P}}$ satisfies the congruency of vectorial loops property. Finally, we discuss the lag and dissipation behaviour. We show that $\boldsymbol{\mathcal{P}}$ satisfies the thermodynamic dissipation condition on closed input cycles, and we find the shape of lag angle and loss curves for uniformly rotating input to be in good agreement with those measured for magnetic materials.

2.3.1. Definition. The scalar Preisach operator arises as a weighted superposition of scalar relay operators $h_{(x,r)}$, Equation (2.3). The n-dimensional vector Preisach operator $\boldsymbol{\mathcal{P}} : C([0,T];\mathbb{R}^n) \times Map(\mathbb{R}^n \times \mathbb{R}_+; \partial B_{\mathbf{0},1}) \to Map([0,T];\mathbb{R}^n)$ is constructed in exact analogy as superposition of vector relays $\boldsymbol{h}_{(\boldsymbol{x},r)}$ with $(\boldsymbol{x},r) \in \mathbb{R}^n \times \mathbb{R}_+$. The initial states of the relays are given by a measurable function $\boldsymbol{\xi} : \mathbb{R}^n \times \mathbb{R}_+ \to \partial B_{\mathbf{0},1}$, the evaluation of $\boldsymbol{\xi}$ in a point $(\boldsymbol{x},r)$ is denoted $\boldsymbol{\xi}_{(\boldsymbol{x},r)}$. The vector Preisach operator $\boldsymbol{\mathcal{P}}$ is defined by

$$\boldsymbol{w}(t) = \boldsymbol{\mathcal{P}}[\boldsymbol{u},\boldsymbol{\xi}](t) := \int_0^\infty \int_{\mathbb{R}^n} \omega(\boldsymbol{x},r)\boldsymbol{h}_{(\boldsymbol{x},r)}[\boldsymbol{u},\boldsymbol{\xi}_{(\boldsymbol{x},r)}](t)\,\mathrm{d}\boldsymbol{x}\,\mathrm{d}r, \tag{2.11}$$

with a Lebesgue-integrable Preisach density function $\omega : \mathbb{R}^n \times \mathbb{R}_+ \to \mathbb{R}$.

Remark. A more general definition of $\boldsymbol{\mathcal{P}}$ is in terms of a finite Borel measure μ:

$$\boldsymbol{\mathcal{P}}[\boldsymbol{u},\boldsymbol{\xi}](t) := \int_{\mathbb{R}^n \times \mathbb{R}_+} \boldsymbol{h}_{(\boldsymbol{x},r)}[\boldsymbol{u},\boldsymbol{\xi}_{(\boldsymbol{x},r)}](t)\,\mathrm{d}\mu(\boldsymbol{x},r). \tag{2.12}$$

If μ is absolutely continuous with respect to the Lebesgue measure, then (2.12) is equivalent to (2.11) and $\omega(\boldsymbol{x},r)$ is the Radon-Nikodym derivative of μ. In this dissertation, we restrict our investigations to formulation (2.11).

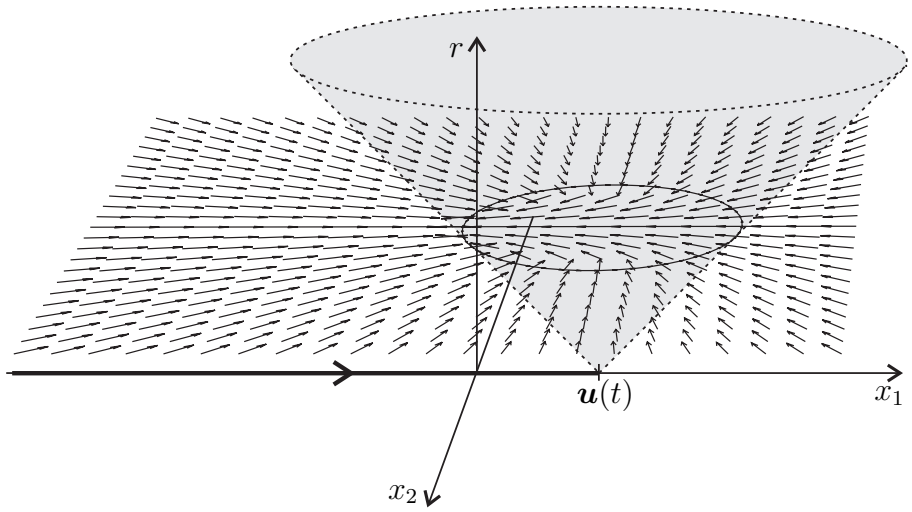

FIGURE 2.4. Geometric representation of the 2D vector Preisach operator.

REMARK. Note that, since $\boldsymbol{\mathcal{P}}$ is invariant under changes of ω on sets of measure 0, in all subsequent statements any assumption on ω will suffice to be satisfied for a function $\overline{\omega}$ such that

$$\omega = \overline{\omega} \quad \text{a.e. on } \mathbb{R}^n \times \mathbb{R}_+.$$

PROPOSITION 2.3.1. *The vector Preisach operator $\boldsymbol{\mathcal{P}}$ is a hysteresis operator.*

PROOF. As $\boldsymbol{\mathcal{P}}$ is a linear superposition of relays, the result follows immediately from Proposition 2.2.1. □

Figure 2.2 illustrated the geometric representation of the memory evolution of the scalar Preisach operator. It is also possible to visualize the memory evolution of the 2D vector Preisach operator. For this, note that by (2.5) at current input $\boldsymbol{u}(t)$, exactly those relays $\boldsymbol{h}_{(\boldsymbol{x},r)}$ are in a "frozen" state for which $\|\boldsymbol{u}(t) - \boldsymbol{x}\| < r$. Therefore, these relays form the cone $\mathcal{C}_{\boldsymbol{u}(t)}$, whose position varies with $\boldsymbol{u}(t)$. By (2.5), the relay states outside $\mathcal{C}_{\boldsymbol{u}(t)}$ are the unit vectors pointing at $\boldsymbol{u}(t)$. As $\boldsymbol{u}(t)$ varies, the relays on the boundary of $\mathcal{C}_{\boldsymbol{u}(t)}$ "freeze" in their current state as the cone moves and takes them in. They switch as they leave the cone. Fig. 2.4 shows the resulting geometric visualization with discrete relay states depicted in one plane $r =$ constant and $\boldsymbol{u}$ linearly increasing along the x_1-axis. Each vector represents the state $\boldsymbol{h}_{(\boldsymbol{x},r)}$ of the relay at its base point $(\boldsymbol{x}, r)$. The cone $\mathcal{C}_{\boldsymbol{u}(t)}$ is drawn shaded.

For $n = 3$, the same technique can be used to visualize the memory state for each hyperplane $r =$ constant in $\mathbb{R}^3$. The intersection of $\mathcal{C}_{\boldsymbol{u}(t)}$ with such a hyperplane forms the ball $B_{\boldsymbol{u}(t),r} \subset \mathbb{R}^3$.

2.3.2. Basic properties.

LEMMA 2.3.2 (Generalized semigroup property). *Given $t_1, t_2 \in [0, T]$, $t_1 \le t_2$, define $\boldsymbol{\xi}(t)$ by $\boldsymbol{\xi}_{(\boldsymbol{x},r)}(t) = \boldsymbol{h}_{(\boldsymbol{x},r)}[\boldsymbol{u}, \boldsymbol{\xi}_{(\boldsymbol{x},r)}](t)$. Then the following holds true:*

$$\boldsymbol{\mathcal{P}}[\boldsymbol{u}, \boldsymbol{\xi}](t_2) = \boldsymbol{\mathcal{P}}[\boldsymbol{u}^{t_1}, \boldsymbol{\xi}(t_1)](t_2 - t_1).$$

PROOF. By Lemma 2.2.2, at t_2 all the relay states are equal, so the statement follows. □

In Chapter 1 we have introduced the group of rotations and reflections of $\mathbb{R}^n$ about the origin, $O(n)$. We now investigate the behaviour of $\boldsymbol{\mathcal{P}}$ when these isometries are applied to the input function $\boldsymbol{u}$. As this involves transformations of ω, we will index $\boldsymbol{\mathcal{P}}$ with ω where necessary and write $\boldsymbol{\mathcal{P}}_\omega$. The following Lemma states that applying $Q \in O(n)$ to the output function $\boldsymbol{w} = \boldsymbol{\mathcal{P}}_\omega[\boldsymbol{u}]$ gives the same result as first applying Q to $\boldsymbol{u}$, ω and $\boldsymbol{\xi}$ and then evaluating $\boldsymbol{\mathcal{P}}$.

LEMMA 2.3.3 (Rotation and reflection). *For $Q \in O(n)$, the vector Preisach operator satisfies*

$$Q\boldsymbol{\mathcal{P}}_\omega[\boldsymbol{u}, \boldsymbol{\xi}] = \boldsymbol{\mathcal{P}}_{Q\omega}[Q\boldsymbol{u}, Q\boldsymbol{\xi}].$$

PROOF. Applying Lemma 2.2.4, we get

$$\begin{aligned}
Q\boldsymbol{\mathcal{P}}_\omega[\boldsymbol{u}, \boldsymbol{\xi}](t) &= \int_0^\infty \int_{\mathbb{R}^n} \omega(\boldsymbol{x}, r) Q\boldsymbol{h}_{(\boldsymbol{x},r)}[\boldsymbol{u}, \boldsymbol{\xi}_{(\boldsymbol{x},r)}](t)\, \mathrm{d}\boldsymbol{x}\, \mathrm{d}r \\
&= \int_0^\infty \int_{\mathbb{R}^n} \omega(\boldsymbol{x}, r) \boldsymbol{h}_{(Q\boldsymbol{x},r)}[Q\boldsymbol{u}, Q(\boldsymbol{\xi}_{(\boldsymbol{x},r)})](t)\, \mathrm{d}\boldsymbol{x}\, \mathrm{d}r \\
&= \int_0^\infty \int_{\mathbb{R}^n} \omega(Q^{-1}\boldsymbol{x}, r) \boldsymbol{h}_{(\boldsymbol{x},r)}[Q\boldsymbol{u}, Q(\boldsymbol{\xi}_{(Q^{-1}\boldsymbol{x},r)})](t)\, \mathrm{d}\boldsymbol{x}\, \mathrm{d}r \\
&= \int_0^\infty \int_{\mathbb{R}^n} Q\omega(\boldsymbol{x}, r) \boldsymbol{h}_{(\boldsymbol{x},r)}[Q\boldsymbol{u}, (Q\boldsymbol{\xi})_{(\boldsymbol{x},r)})](t)\, \mathrm{d}\boldsymbol{x}\, \mathrm{d}r.
\end{aligned}$$

The third equality is obtained by conducting a change of variables along Theorem 1.2.8 from $\boldsymbol{x}$ to $Q\boldsymbol{x}$ with Jacobian determinant $J = |\det Q| = 1$. □

The next lemma explores the translation invariance of $\boldsymbol{\mathcal{P}}$.

LEMMA 2.3.4 (Translation). *For any translation $T_{\boldsymbol{v}}$, $\boldsymbol{v} \in \mathbb{R}^n$,*

$$\boldsymbol{\mathcal{P}}_\omega[\boldsymbol{u}, \boldsymbol{\xi}](t) = \boldsymbol{\mathcal{P}}_{T_{\boldsymbol{v}}\omega}[T_{\boldsymbol{v}}\boldsymbol{u}, T_{\boldsymbol{v}}\boldsymbol{\xi}](t).$$

PROOF. Applying Lemma 2.2.5, we get

$$\begin{aligned}
\boldsymbol{\mathcal{P}}_\omega[\boldsymbol{u}, \boldsymbol{\xi}](t) &= \int_{\mathbb{R}^n \times \mathbb{R}_+} \omega(\boldsymbol{x}, r) \boldsymbol{h}_{(T_{\boldsymbol{v}}\boldsymbol{x},r)}[T_{\boldsymbol{v}}\boldsymbol{u}, \boldsymbol{\xi}_{(\boldsymbol{x},r)}](t)\, \mathrm{d}(\boldsymbol{x}, r) \\
&= \int_{\mathbb{R}^n \times \mathbb{R}_+} \omega(T_{-\boldsymbol{v}}\boldsymbol{x}, r) \boldsymbol{h}_{(\boldsymbol{x},r)}[\boldsymbol{u} + \boldsymbol{v}, \boldsymbol{\xi}_{(T_{-\boldsymbol{v}}\boldsymbol{x},r)}](t)\, \mathrm{d}(\boldsymbol{x}, r) \\
&= \boldsymbol{\mathcal{P}}_{T_{\boldsymbol{v}}\omega}[T_{\boldsymbol{v}}\boldsymbol{u}, T_{\boldsymbol{v}}\boldsymbol{\xi}](t).
\end{aligned}$$

In the second step, we have applied a change of variables along Theorem 1.2.9 with transformation $T_{-\boldsymbol{v}}$ and $J = |\det T_{-\boldsymbol{v}}| = 1$. □

2.3.3. Isotropy and neutral memory state. A vectorial hysteresis operator $\boldsymbol{\mathcal{W}}$ is called *isotropic* if its input-output behaviour is the same independent of the direction. Mathematically, this means that for any $\boldsymbol{u} \in C([0, T]; \mathbb{R}^n)$ and any isometry $Q \in O(n)$, $\boldsymbol{\mathcal{W}}$ satisfies

$$\boldsymbol{\mathcal{W}}[Q\boldsymbol{u}] = Q\boldsymbol{\mathcal{W}}[\boldsymbol{u}].$$

The vector Preisach operator $\boldsymbol{\mathcal{P}}$ does not only depend on $\boldsymbol{u}$, but also on the initial state $\boldsymbol{\xi}$. We thus need to extend the notion of isotropy to take the effect of $\boldsymbol{\xi}$ into consideration. We have

$$\boldsymbol{\mathcal{P}}[Q\boldsymbol{u}, \boldsymbol{\xi}](t) = \int_0^\infty \int_{\mathbb{R}^n} \omega(\boldsymbol{x}, r) \boldsymbol{h}_{(\boldsymbol{x},r)}[Q\boldsymbol{u}, \boldsymbol{\xi}_{(\boldsymbol{x},r)}](t) \, \mathrm{d}\boldsymbol{x} \, \mathrm{d}r \tag{2.13}$$

and, by Lemma 2.3.3,

$$Q\boldsymbol{\mathcal{P}}[\boldsymbol{u}, \boldsymbol{\xi}](t) = \int_0^\infty \int_{\mathbb{R}^n} Q\omega(\boldsymbol{x}, r) \boldsymbol{h}_{(\boldsymbol{x},r)}[Q\boldsymbol{u}, (Q\boldsymbol{\xi})_{(\boldsymbol{x},r)})](t) \, \mathrm{d}\boldsymbol{x} \, \mathrm{d}r. \tag{2.14}$$

Assume ω satisfies $\omega = Q\omega$. Then obviously $\boldsymbol{\xi}$ can cause these integrals to differ if for some $\boldsymbol{u}$ and t we have that $(Q\boldsymbol{\xi})_{(\boldsymbol{x},r)} \neq \boldsymbol{\xi}_{(\boldsymbol{x},r)}$ and $\boldsymbol{h}_{(\boldsymbol{x},r)}[Q\boldsymbol{u}, \boldsymbol{\xi}_{(\boldsymbol{x},r)}](t) = \boldsymbol{\xi}_{(\boldsymbol{x},r)}$ hold on some subset of $\mathbb{R}^n \times \mathbb{R}_+$ of non-zero measure. Thus, defining the set

$$\Xi = \{\boldsymbol{\xi} \mid \boldsymbol{\xi} = Q\boldsymbol{\xi} \text{ for all } Q \in O(n)\},$$

the natural definition of isotropy seems to be:

Definition 2.3.5 (Isotropy). We call the vector Preisach operator $\boldsymbol{\mathcal{P}}$ *isotropic* if and only if for any $\boldsymbol{u} \in C([0,T];\mathbb{R}^n)$ and any rotation $Q \in O(n)$, it satisfies

$$\boldsymbol{\mathcal{P}}[Q\boldsymbol{u}, \boldsymbol{\xi}] = Q\boldsymbol{\mathcal{P}}[\boldsymbol{u}, \boldsymbol{\xi}] \quad \text{for all } \boldsymbol{\xi} \in \Xi. \tag{2.15}$$

We have the following:

Lemma 2.3.6 (Sufficient isotropy condition). *If there exists a* $\tilde{\omega} : \mathbb{R}_+ \times \mathbb{R}_+ \to \mathbb{R}$ *such that* $\omega(\boldsymbol{x}, r) = \tilde{\omega}(||\boldsymbol{x}||, r)$*, then* $\boldsymbol{\mathcal{P}}$ *is isotropic.*

Proof. As

$$\omega(\boldsymbol{x}, r) = \tilde{\omega}(||\boldsymbol{x}||, r) = \tilde{\omega}(||Q^{-1}\boldsymbol{x}||, r) = \omega(Q^{-1}\boldsymbol{x}, r) = Q\omega(\boldsymbol{x}, r)$$

for any $Q \in O(n)$, this is obvious from comparing Equations (2.13) and (2.14). □

For ease of reference, we will call $\omega : \mathbb{R}^n \times \mathbb{R}_+ \to \mathbb{R}$ *isotropic* if and only if it satisfies the assumption of Lemma 2.3.6.

Lemma 2.3.7. *We have that* ω *is isotropic if and only if* $\omega(\boldsymbol{x}, r) = Q\omega(\boldsymbol{x}, r)$ *for all* $Q \in O(n)$.

Proof. Using Lemma 1.3.1, it is quickly shown that $\{Q\boldsymbol{x} \mid Q \in O(n)\} = \{\boldsymbol{y} \mid \|\boldsymbol{y}\| = \|\boldsymbol{x}\|\}$. Since $Q\omega(\boldsymbol{x}, r) = \omega(Q^{-1}\boldsymbol{x}, r)$, the statement follows. □

Remark (Visualization of isotropic ω). In other words, ω is isotropic exactly if it is invariant under rotation and reflection about the r-axis.

Remark (Anisotropy). In magnetism, many materials show anisotropic behaviour, i.e. their hysteresis differs with direction. However, under uniaxial input $\boldsymbol{u}(t) = u(t)\boldsymbol{e}$ with scalar function $u(t)$ and constant unit vector $\boldsymbol{e}$, the hysteresis of the uniaxially measured output $w(t) = \boldsymbol{\mathcal{P}}[\boldsymbol{u}](t) \cdot \boldsymbol{e}$ is always observed to be symmetric about 0, up to initial state effects. We can conclude that in general

$$\boldsymbol{\mathcal{P}}[-\boldsymbol{u}, \boldsymbol{\xi}](t) = -\boldsymbol{\mathcal{P}}[\boldsymbol{u}, \boldsymbol{\xi}](t) \quad \text{for all } \boldsymbol{\xi} \in \Xi$$

should hold in the modeling of magnetic hysteresis. It is quickly seen that this is satisfied if

$$\omega(\boldsymbol{x}, r) = \omega(-\boldsymbol{x}, r) \tag{2.16}$$

holds. Thus, we suggest using arbitrary ω satisfying (2.16) for the modeling of anisotropic magnetic hysteresis.

Another approach to represent anisotropy by means of this vector Preisach concept is to modify the relay definition. Della Torre, Pinzaglia, and Cardelli [**24, 25**] suggest an anisotropic vector Preisach operator by using general relay shapes, in particular elliptical relays, instead of the spherical $\boldsymbol{h}_{(\boldsymbol{x},r)}$. A relay is represented by an open bounded set $K \subset \mathbb{R}^n$ together with a point $\boldsymbol{x} \in K$, for example an ellipse and its center. They define the output state of this general relay $\widetilde{\boldsymbol{h}}_{(K,\boldsymbol{x})} : C([0,T];\mathbb{R}^n) \to Map([0,T];\mathbb{R}^n)$ as

$$\widetilde{\boldsymbol{h}}_{(K,\boldsymbol{x})}[\boldsymbol{u},\boldsymbol{\xi}](t) = \begin{cases} \frac{\boldsymbol{u}(t)-\boldsymbol{x}}{\|\boldsymbol{u}(t)-\boldsymbol{x}\|} & \text{if } \boldsymbol{u}(t) \notin K, \\ \widetilde{\boldsymbol{h}}_{(K,\boldsymbol{x})}[\boldsymbol{u},\boldsymbol{\xi}](\max X_t) & \text{if } \boldsymbol{u}(t) \in K \text{ and } X_t \neq \varnothing, \\ \boldsymbol{\xi} & \text{otherwise.} \end{cases} \tag{2.17}$$

Here, $X_t := \{\tau \in [0,t] \mid \boldsymbol{u}(\tau) \notin K\}$ and $\boldsymbol{\xi} \in \partial B_{\boldsymbol{0},1}$ is an initial state.

We suggest a similar idea, which does not require to distinguish a point in K. It uses projection onto convex sets as previously suggested by Damlamian and Visintin in their *rotating model* [**21, 67**], but defines the relay output in analogy to the vector relay $\boldsymbol{h}_{(\boldsymbol{x},r)}$ (2.5). For this, we replace the spherical relays by other families $\{K\}$ of open convex sets, for example ellipses, and generalize (2.5) to

$$\overline{\boldsymbol{h}}_K[\boldsymbol{u},\boldsymbol{\xi}](t) = \begin{cases} \frac{\boldsymbol{u}(t)-\operatorname{proj}_K \boldsymbol{u}(t)}{\|\boldsymbol{u}(t)-\operatorname{proj}_K \boldsymbol{u}(t)\|} & \text{if } \boldsymbol{u}(t) \notin K, \\ \overline{\boldsymbol{h}}_K[\boldsymbol{u},\boldsymbol{\xi}](\max X_t) & \text{if } \boldsymbol{u}(t) \in K \text{ and } X_t \neq \varnothing, \\ \boldsymbol{\xi} & \text{otherwise,} \end{cases} \tag{2.18}$$

with $X_t := \{\tau \in [0,t] \mid \boldsymbol{u}(\tau) \notin K\}$. Here, $\operatorname{proj}_K \boldsymbol{y}$ is the projection of $\boldsymbol{u}(t)$ onto K, that is, the point $\overline{\boldsymbol{y}} \in \overline{K}$ minimizing $\|\overline{\boldsymbol{y}} - \boldsymbol{y}\|$.

For both $\widetilde{\boldsymbol{h}}_{(K,\boldsymbol{x})}$ and $\overline{\boldsymbol{h}}_K$, the corresponding Preisach operator can be obtained as weighted superposition of all relays.

In view of the modeling of magnetic hysteresis, it would be desirable to compare the properties of the three approaches listed to those observed in measurements of anisotropic hysteretic materials. However, anisotropy shall not be in the focus of this dissertation.

Assume ω is isotropic. An interesting question that so far remains unaddressed is that of an appropriate *neutral memory state*, or, in the terminology of magnetic hysteresis, a "demagnetized state" of $\boldsymbol{\mathcal{P}}$. In the case of scalar hysteresis, such a neutral state ξ^0 is characterized by giving Preisach output 0 for input $u = 0$,

$$\mathcal{P}[0,\xi^0] = 0, \tag{2.19}$$

and symmetry with respect to input reflections,

$$\mathcal{P}[-u,\xi^0](t) = -\mathcal{P}[u,\xi^0](t) \tag{2.20}$$

for all $u \in C([0,T];\mathbb{R})$. It is quickly seen the scalar Preisach operator $\mathcal{P}$ meets these conditions for arbitrary ω only if $\xi_{(x,r)} = -\xi_{(-x,r)}$ a.e. The only staircase curve satisfying this condition is $\psi(r) \equiv 0$, so the neutral state is equal to [**51**]

$$\xi^0_{(x,r)} = \begin{cases} 1 & \text{if } x < 0, \\ -1 & \text{if } x \geq 0. \end{cases} \tag{2.21}$$

In the vectorial case, we seem to be looking for those $\boldsymbol{\xi}$ from Definition 2.3.5 that do not affect isotropy, that is, $\boldsymbol{\xi} \in \Xi$. If ω is isotropic, $\boldsymbol{\xi} \in \Xi$ immediately implies the vectorial counterparts of (2.19) and (2.20),

$$\boldsymbol{\mathcal{P}}[\mathbf{0}, \boldsymbol{\xi}] = \mathbf{0}$$

and

$$\boldsymbol{\mathcal{P}}[Q\boldsymbol{u}, \boldsymbol{\xi}] = Q\boldsymbol{\mathcal{P}}[\boldsymbol{u}, \boldsymbol{\xi}] \quad \text{for all } Q \in O(n).$$

It turns out that the elements of Ξ have a very specific form:

LEMMA 2.3.8. *A measurable $\boldsymbol{\xi} \in \mathrm{Map}(\mathbb{R}^n \times \mathbb{R}_+; \partial B_{\mathbf{0},1})$ is in Ξ if and only if, for some function $\alpha : \mathbb{R}_+ \to \{1,-1\}$, we have $\boldsymbol{\xi}_{(\boldsymbol{x},r)} = \alpha(\|\boldsymbol{x}\|)\dfrac{\boldsymbol{x}}{\|\boldsymbol{x}\|}$ for all $(\boldsymbol{x},r) \in \mathbb{R}^n \setminus \{\mathbf{0}\} \times \mathbb{R}_+$.*

PROOF. Assume first that $\boldsymbol{\xi} \in \Xi$. Let $\boldsymbol{x} = (\lambda, 0, \ldots, 0)^T$. Lemma 1.3.2 states that $Q\boldsymbol{x} = \boldsymbol{x}$ holds exactly for all $Q \in O^1(n)$. Because of $\boldsymbol{\xi} \in \Xi$, $Q\boldsymbol{x} = \boldsymbol{x}$ implies

$$\boldsymbol{\xi}_{(\boldsymbol{x},r)} = (Q\boldsymbol{\xi})_{(\boldsymbol{x},r)} = Q(\boldsymbol{\xi}_{(Q^{-1}\boldsymbol{x},r)}) = Q(\boldsymbol{\xi}_{(\boldsymbol{x},r)})$$

for all $Q \in O^1(n)$. Therefore,

$$\boldsymbol{\xi}_{(\boldsymbol{x},r)} = (\beta, 0, \ldots, 0)^T, \quad \beta = \pm 1.$$

For arbitrary $\boldsymbol{x} \neq \mathbf{0}$, by Lemma 1.3.1, there exists a $Q \in O(n)$ such that $\boldsymbol{x} = Q(\|\boldsymbol{x}\|, 0, \ldots, 0)^T$, so

$$\boldsymbol{\xi}_{(\boldsymbol{x},r)} = Q\boldsymbol{\xi}_{((\|\boldsymbol{x}\|,0,\ldots,0)^T,r)} = Q(\beta, 0, \ldots, 0)^T = \beta\frac{\boldsymbol{x}}{\|\boldsymbol{x}\|}.$$

Set $\alpha(\|\boldsymbol{x}\|) = \beta$.

Conversely, $\boldsymbol{\xi} = \alpha(\|\boldsymbol{x}\|)\boldsymbol{x}/\|\boldsymbol{x}\|$ is in Ξ because for all $Q \in O(n)$

$$(Q\boldsymbol{\xi})_{(\boldsymbol{x},r)} = Q\left(\alpha(\|\boldsymbol{x}\|)\frac{Q^{-1}\boldsymbol{x}}{\|Q^{-1}\boldsymbol{x}\|}\right) = \alpha(\|\boldsymbol{x}\|)\frac{\boldsymbol{x}}{\|\boldsymbol{x}\|} = \boldsymbol{\xi}_{(\boldsymbol{x},r)}. \qquad \square$$

The fact that all relays outside $\mathcal{C}_{\boldsymbol{u}(0)}$ at $\boldsymbol{u}(0) = \mathbf{0}$ are in this state and that it represents the vectorial analogue of (2.21) suggests that $\boldsymbol{\xi}^0$,

$$\boldsymbol{\xi}^0_{(\boldsymbol{x},r)} := -\frac{\boldsymbol{x}}{\|\boldsymbol{x}\|},$$

i.e. all relays pointing at $\mathbf{0}$, is the neutral initial state of $\boldsymbol{\mathcal{P}}$.

In fact, for $n = 2$ it can be shown that $\boldsymbol{\xi}^0$ results asymptotically from a "demagnetization" process via a rotating field of decreasing amplitude. Define $\tilde{\boldsymbol{u}}_k : [0,1] \to \mathbb{R}^2$ to be the spiral curve

$$\tilde{\boldsymbol{u}}_k(t) = R(1-t)\begin{pmatrix}\cos(2k\pi t)\\ \sin(2k\pi t)\end{pmatrix}$$

starting at $\tilde{\boldsymbol{u}}_k(0) = (R,0)$ and rotating with uniformly decreasing amplitude to $\tilde{\boldsymbol{u}}_k(1) = (0,0)$. Parameter $k \in \mathbb{N}$ equals the number of rotations of the spiral.

LEMMA 2.3.9. *For all $(\boldsymbol{x}, r) \in \mathbb{R}^n \times \mathbb{R}_+$ such that $r < R$ and $\boldsymbol{x} \neq 0$,*

$$\lim_{k\to\infty} \boldsymbol{h}_{(\boldsymbol{x},r)}[\tilde{\boldsymbol{u}}_k](1) = \boldsymbol{\xi}^0_{(\boldsymbol{x},r)}.$$

PROOF. Note that any ring $B_{\mathbf{0},d+\frac{R}{k}} \setminus B_{\mathbf{0},d}$ around 0 contains exacty one revolution of the spiral.

If $||\boldsymbol{x}|| \geq r$, the statement is obviously true as $(\boldsymbol{x}, r)$ is not in the freeze cone at $t = 1$. Assume $||\boldsymbol{x}|| < r < R$. For $d < r$, the circle $\partial B_{\mathbf{0},d}$ intersects the boundary of the relay $\partial B_{\boldsymbol{x},r}$ not at all for $d < r - ||\boldsymbol{x}||$, exactly once for $d = r - ||\boldsymbol{x}||$, and twice for $d > r - ||\boldsymbol{x}||$. Let P denote the intersection point for $d = r - ||\boldsymbol{x}||$. It is quickly geometrically verified that $(P - \boldsymbol{x})/\|P - \boldsymbol{x}\| = -\boldsymbol{x}/\|\boldsymbol{x}\|$. Let Q_k be the point at which $\tilde{\boldsymbol{u}}_k(t)$ last intersects $\partial B_{\boldsymbol{x},r}$. This implies that

$$\boldsymbol{h}_{(\boldsymbol{x},r)}[\tilde{\boldsymbol{u}}_k](t) \mid_{t=1} = \frac{Q_k - \boldsymbol{x}}{\|Q_k - \boldsymbol{x}\|}. \tag{2.22}$$

With the remark in the beginning and k large enough so $\frac{R}{k} < \|\boldsymbol{x}\|$, the point Q_k lies in the intersection of the ring $B_{\mathbf{0},r-||\boldsymbol{x}||+\frac{R}{k}} \setminus B_{\mathbf{0},r-||\boldsymbol{x}||}$ with $\partial B_{\boldsymbol{x},r}$. As $k \to \infty$, this intersection lies inside an arbitrarily small neighbourhood of P, so we have $Q_k \to P$. Then (2.22) results in the claim. □

This is the two-dimensional analogue of the standard uniaxial demagnetization process by an alternating field of decreasing amplitude, which results in ξ^0 [**51**].

2.3.4. Saturation. Suppose ω has bounded support, and let $\mathcal{K} := \{(\boldsymbol{x}, r) \mid ||\boldsymbol{x}|| + r \leq R\}$ be the minimal cone such that $\omega(\boldsymbol{x}, r) = 0$ a.e. outside $\mathcal{K}$. For any $\boldsymbol{u}(t)$ such that $||\boldsymbol{u}(t)|| > R$, the assumption $(\boldsymbol{x}, r) \in \mathcal{K}$ implies

$$r \leq R - \|\boldsymbol{x}\| \leq \|\boldsymbol{u}(t)\| - \|\boldsymbol{x}\| \leq \|\boldsymbol{u}(t) - \boldsymbol{x}\|.$$

Therefore,

$$\mathcal{C}_{\boldsymbol{u}(t)} \cap \mathcal{K} = \varnothing. \tag{2.23}$$

In other words, all hysteresis memory is erased:

LEMMA 2.3.10 (Memory deletion). *Assume $\boldsymbol{u}_1, \boldsymbol{u}_2 \in C([0,T];\mathbb{R}^n)$ satisfy $\boldsymbol{u}_1^t = \boldsymbol{u}_2^t$ for some $t \in [0,T]$. If $\|\boldsymbol{u}_1(t)\| \geq R$, then for arbitrary initial states $\boldsymbol{\xi}_1$, $\boldsymbol{\xi}_2$,*

$$\boldsymbol{\mathcal{P}}[\boldsymbol{u}_1, \boldsymbol{\xi}_1](\tau) = \boldsymbol{\mathcal{P}}[\boldsymbol{u}_2, \boldsymbol{\xi}_2](\tau) \quad \text{for all } t \leq \tau \leq T.$$

PROOF. For all $(\boldsymbol{x}, r) \in \mathcal{K}$, by (2.23) we have that

$$\boldsymbol{h}_{(\boldsymbol{x},r)}[\boldsymbol{u}_1, \boldsymbol{\xi}_1](t) = \frac{\boldsymbol{u}_1(t) - \boldsymbol{x}}{\|\boldsymbol{u}_1(t) - \boldsymbol{x}\|} = \boldsymbol{h}_{(\boldsymbol{x},r)}[\boldsymbol{u}_2, \boldsymbol{\xi}_2](t).$$

Thus, the semigroup property for vector relays at t results in

$$\boldsymbol{h}_{(\boldsymbol{x},r)}[\boldsymbol{u}_1, \boldsymbol{\xi}_1](\tau) = \boldsymbol{h}_{(\boldsymbol{x},r)}[\boldsymbol{u}_2, \boldsymbol{\xi}_2](\tau) \quad \text{for all } t \le \tau \le T$$

for all $(\boldsymbol{x}, r) \in \mathcal{K}$, and the statement follows. □

From the semigroup property of $\boldsymbol{\mathcal{P}}$, we obtain the following corollary:

COROLLARY 2.3.11. *If $\|\boldsymbol{u}(t)\| \ge R$, then for arbitrary initial states $\boldsymbol{\xi}$, $\overline{\boldsymbol{\xi}}$,*

$$\boldsymbol{\mathcal{P}}[\boldsymbol{u}, \boldsymbol{\xi}](\tau) = \boldsymbol{\mathcal{P}}[\boldsymbol{u}^t, \overline{\boldsymbol{\xi}}](\tau - t) \quad \text{for all } t \le \tau \le T.$$

In particular, $\boldsymbol{w}(t) = \boldsymbol{\mathcal{P}}[\boldsymbol{u}, \boldsymbol{\xi}](t)$ is fully determined by $\boldsymbol{u}(t)$.

In other words, there is a function $\boldsymbol{p} : \mathbb{R}^n \to \mathbb{R}^n$ such that $\boldsymbol{\mathcal{P}}[\boldsymbol{u}, \boldsymbol{\xi}](t) = \boldsymbol{p}(\boldsymbol{u}(t))$ for any initial state $\boldsymbol{\xi}$ if $\|\boldsymbol{u}(t)\| \ge R$. It is given by

$$\boldsymbol{p}(\boldsymbol{v}) = \int_{\mathcal{K}} \omega(\boldsymbol{x}, r) \frac{\boldsymbol{v} - \boldsymbol{x}}{\|\boldsymbol{v} - \boldsymbol{x}\|} \, \mathrm{d}(\boldsymbol{x}, r), \qquad \boldsymbol{v} \in \mathbb{R}^n.$$

That is, the hysteresis output for any $\boldsymbol{u}(t)$ satisfying $\|\boldsymbol{u}(t)\| \ge R$ is not multivalued. As a consequence of Lemma 2.3.10, the initial state and $\boldsymbol{u}$ in $[0, t)$ are completely deleted from the memory.

In addition, if ω is isotropic, then $\boldsymbol{u}(t)$ and $\boldsymbol{w}(t)$ are aligned:

LEMMA 2.3.12. *Assume ω is isotropic. If $\|\boldsymbol{u}(t)\| \ge R$, then there exists a $\lambda \in \mathbb{R}$, which depends on $\|\boldsymbol{u}(t)\|$, such that*

$$\boldsymbol{\mathcal{P}}[\boldsymbol{u}](t) = \lambda \boldsymbol{u}(t). \tag{2.24}$$

PROOF. Assume $\boldsymbol{u}(t) = (u(t), 0, \dots, 0)$. Lemma 1.3.2 states the group $O^1(n) \subset O(n)$ fixing $\boldsymbol{u}$. Since $\|\boldsymbol{u}(t)\| > R$, by Lemma 2.3.10 we can assume initial state $\boldsymbol{\xi}^0$. With $\omega(x, r) = Q\omega(x, r)$ for all $Q \in O^1(n)$, we have by Lemma 2.3.3

$$\boldsymbol{\mathcal{P}}[\boldsymbol{u}](t) = \boldsymbol{\mathcal{P}}[Q\boldsymbol{u}](t) = Q\boldsymbol{\mathcal{P}}[\boldsymbol{u}](t) \quad \text{for all } Q \in O^1(n). \tag{2.25}$$

Thus, $\boldsymbol{\mathcal{P}}[\boldsymbol{u}](t)$ must be equal to 0 in all but the first component,

$$\boldsymbol{\mathcal{P}}[\boldsymbol{u}](t) = (\lambda, 0, \dots, 0).$$

For an arbitrary $\boldsymbol{u}(t)$, there is a $Q \in O(n)$ such that $\boldsymbol{u}(t) = Q(\|\boldsymbol{u}(t)\|, 0, \dots, 0)$. As the second equality in (2.25) by Lemma 2.3.3 holds for all $Q \in O(n)$, there is a λ such that

$$\boldsymbol{\mathcal{P}}[\boldsymbol{u}](t) = Q(\lambda, 0, \dots, 0).$$ □

In general, independent of the symmetry properties of ω, the Preisach output $\boldsymbol{\mathcal{P}}[\boldsymbol{u}](t)$ asymptotically aligns with large $\boldsymbol{u}(t)$:

$$\lim_{\|\boldsymbol{v}\| \to \infty} \boldsymbol{p}(\boldsymbol{v}) = \lim_{\|\boldsymbol{v}\| \to \infty} \int_{\mathcal{K}} \omega(\boldsymbol{x}, r) \frac{\boldsymbol{v} - \boldsymbol{x}}{\|\boldsymbol{v} - \boldsymbol{x}\|} \, \mathrm{d}(\boldsymbol{x}, r) = \int_{\mathcal{K}} \omega(\boldsymbol{x}, r) \, \mathrm{d}(\boldsymbol{x}, r) \, \frac{\boldsymbol{v}}{\|\boldsymbol{v}\|}. \tag{2.26}$$

In any case, the relays inside $\mathcal{K}$ keep varying while $||\boldsymbol{u}(t)|| \ge R$. Thus, for large $\boldsymbol{u}(t)$, $\|\boldsymbol{\mathcal{P}}[\boldsymbol{u}](t)\|$ is not constant but varies. In this, the vector Preisach operator $\boldsymbol{\mathcal{P}}$

differs from the scalar Preisach operator, which gives constant output as soon as $|u(t)| > R_{\text{scal}}$, where $\mathcal{K}_{\text{scal}} := \{(x, r) \mid |x| + r \leq R_{\text{scal}}\} \subset \mathbb{R} \times \mathbb{R}_+$ is the minimal cone outside which $\omega(x, r) = 0$ a.e.

It is obvious from (2.26) that the saturation limit

$$\int_0^\infty \int_{\mathbb{R}^n} \omega(\boldsymbol{x}, r) \, \mathrm{d}\boldsymbol{x} \, \mathrm{d}r \tag{2.27}$$

that $\boldsymbol{p}(\boldsymbol{v})$ attains as $\|\boldsymbol{v}\| \to \infty$ is independent of the direction $\frac{\boldsymbol{v}}{\|\boldsymbol{v}\|}$.

Using that $\|\boldsymbol{h}_{(\boldsymbol{x},r)}[\boldsymbol{u}](t)\| = 1$, we can further derive the following bound on the Preisach output:

$$\|\boldsymbol{\mathcal{P}}[\boldsymbol{u}](t)\| \leq \int_0^\infty \int_{\mathbb{R}^n} \|\omega(\boldsymbol{x}, r)\boldsymbol{h}_{(\boldsymbol{x},r)}[\boldsymbol{u}](t)\| \, \mathrm{d}\boldsymbol{x} \, \mathrm{d}r \leq \int_0^\infty \int_{\mathbb{R}^n} |\omega(\boldsymbol{x}, r)| \, \mathrm{d}\boldsymbol{x} \, \mathrm{d}r.$$

Therefore, if $\omega \geq 0$, the saturation limit (2.27) represents an upper bound on $\|\boldsymbol{\mathcal{P}}[\boldsymbol{u}](t)\|$.

Example 2.3.13. We will illustrate the saturation behaviour for $n = 2$ and an isotropic linear ω defined by

$$\omega(\boldsymbol{x}, r) := \begin{cases} 1 - \|\boldsymbol{x}\| - r & \text{if } \|\boldsymbol{x}\| + r \leq 1, \\ 0 & \text{otherwise.} \end{cases}$$

Figure 2.5 shows scalar hysteresis curves computed with $\boldsymbol{\mathcal{P}}$ for uniaxial input. The curves merge into a single saturation curve at $R = 1$ and asymptotically approach their saturation limit

$$\int_0^\infty \int_{\mathbb{R}^2} \omega(\boldsymbol{x}, r) \, \mathrm{d}\boldsymbol{x} \, \mathrm{d}r = \frac{\pi}{12}.$$

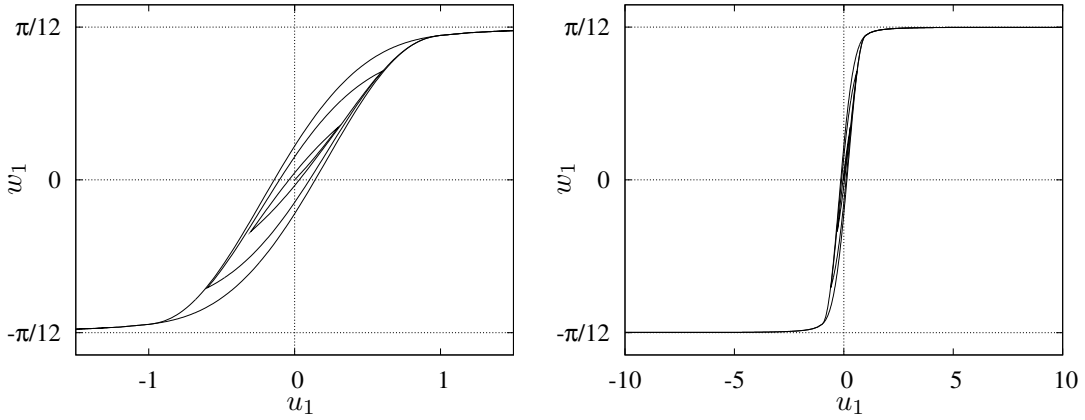

Figure 2.5. Uniaxial hysteresis curves of Example 2.3.13: enlarged on the interval $[-1.5, 1.5]$ (left), zoomed out to highlight the assymptotic behaviour (right).

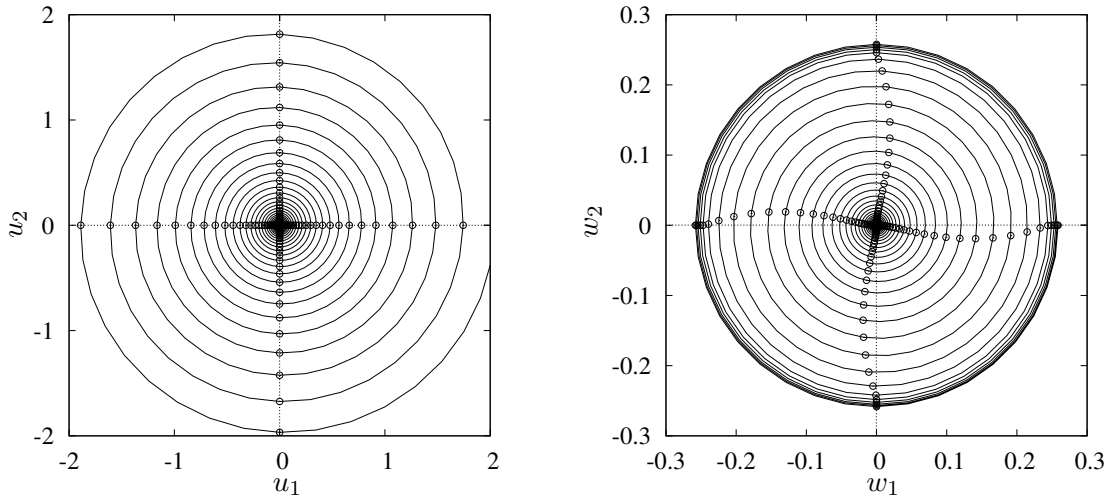

FIGURE 2.6. Input $\boldsymbol{u}$ (left) and output $\boldsymbol{w}$ (right) of Example 2.3.13: The input points marked for $\boldsymbol{u}$ along the horizontal and vertical axes correspond to the respective output points marked for $\boldsymbol{w}$.

Figure 2.6 shows $\boldsymbol{w}(t) = \boldsymbol{\mathcal{P}}[\boldsymbol{u}](t) = (w_1(t), w_2(t))$ for counter-clockwise rotating input $\boldsymbol{u}(t) = (u_1(t), u_2(t))$ of increasing amplitude. For $\|\boldsymbol{u}(t)\| < 1$, the marked points of $\boldsymbol{w}$ are tilted out of the axis on which the corresponding inputs lie and thus show the rotational lag effect due to hysteresis well. However, for $\|\boldsymbol{u}(t)\| \geq 1$, the points are aligned with the input as an effect of saturation.

The derived behaviour of $\boldsymbol{\mathcal{P}}$ agrees with that observed in measurements for hysteretic materials. In saturation, magnetic field $\boldsymbol{H}$ and $\boldsymbol{M}$ are aligned for the isotropic case [**22**], and align asymptotically for the anisotropic case [**57**]. In either case the saturation limit is independent of the direction [**10**]. Curves reported from measurements (e.g. [**74, 20, 41**]) show the merging of the uniaxial $\boldsymbol{M}(\boldsymbol{H})$ hysteresis loop into a single curve before zero slope, or slope μ_0 in the case of $\boldsymbol{B}(\boldsymbol{H})$ curves (cf. Chapter 3, Equation (3.6)), is attained. The latter property is related to the existence of a reversible component in $\boldsymbol{\mathcal{P}}$, which we explore in more detail in Section 2.4. The lack of a reversible contribution is one of the shortcomings of the classical scalar Preisach model frequently addressed by model extensions [**23, 22**].

REMARK (Distinction from Mayergoyz' vector Preisach model). If ω is isotropic and has bounded support $\mathcal{K}$, then $\boldsymbol{\mathcal{P}}$ is not equal to a Mayergoyz' vector Preisach model. This is seen comparing the output behaviour of both operators for large uniformly rotating input $\boldsymbol{u}$. For $\boldsymbol{\mathcal{P}}$, as shown in Lemma 2.3.12, the output $\boldsymbol{\mathcal{P}}[\boldsymbol{u}](t)$ aligns with $\boldsymbol{u}(t)$ as soon as $\|\boldsymbol{u}(t)\| > R$. For any Mayergoyz' vector Preisach model $\boldsymbol{\mathcal{W}}$, the output will always follow the input at a non-zero lag angle. This is demonstrated in [**51**, Chapter 3] for $n = 2$ in the proof of the "Rotational Symmetry Property", where it is derived that the tangent of the lag angle is positive.

2.3.5. Congruency and periodic behaviour. This section investigates the output congruency, lag and dissipation properties of $\boldsymbol{\mathcal{P}}$.

In the first set of lemmas, we will show that the Preisach output is periodic and satisfies the congruency of vectorial loops. That is, if after an arbitrary initial variation, two functions $\boldsymbol{u}_1$ and $\boldsymbol{u}_2$ are equal and periodic, then from the second cycle onwards the outputs are periodic and congruent. Here, congruency of two curves in $\mathbb{R}^n$ means that they are equal up to translation.

Then we will show that for isotropic ω, uniformly rotating input results in uniformly rotating output.

LEMMA 2.3.14 (Periodicity of $\boldsymbol{\mathcal{P}}$, congruency for differing initial states). *Suppose $\boldsymbol{u} \in C([0,T];\mathbb{R}^n)$ is periodic, i.e. there is a $\lambda < T$ such that $\boldsymbol{u}(t+\lambda) = \boldsymbol{u}(t)$ for any $t \in [0, T-\lambda]$. Then for any $\boldsymbol{\xi}_1, \boldsymbol{\xi}_2 : \mathbb{R}^n \times \mathbb{R}_+ \to \partial B_{\mathbf{0},1}$, the following holds:*

(a) *$\boldsymbol{\mathcal{P}}[\boldsymbol{u}, \boldsymbol{\xi}_1]$ is periodic with period λ on $[\lambda, T]$, i.e.*

$$\boldsymbol{\mathcal{P}}[\boldsymbol{u}, \boldsymbol{\xi}_1](t+\lambda) = \boldsymbol{\mathcal{P}}[\boldsymbol{u}, \boldsymbol{\xi}_1](t) \quad \text{for all } t:\ \lambda \le t \le T-\lambda.$$

(b) *There exists a $\boldsymbol{v} \in \mathbb{R}^n$ such that*

$$\boldsymbol{\mathcal{P}}[\boldsymbol{u}, \boldsymbol{\xi}_1](t) = \boldsymbol{\mathcal{P}}[\boldsymbol{u}, \boldsymbol{\xi}_2](t) + \boldsymbol{v} \quad \text{for all } t:\ \lambda \le t \le T.$$

PROOF. (a) It is quickly verified that $\boldsymbol{h}_{(\boldsymbol{x},r)}[\boldsymbol{u}, \boldsymbol{\xi}_1](t+\lambda) = \boldsymbol{h}_{(\boldsymbol{x},r)}[\boldsymbol{u}, \boldsymbol{\xi}_1](t)$ for $t \ge \lambda$ is satisfied by each relay. The periodicity carries over to $\boldsymbol{\mathcal{P}}$ in the obvious way.

(b) Clearly, $\boldsymbol{h}_{(\boldsymbol{x},r)}[\boldsymbol{u}, \boldsymbol{\xi}_1](t) = \boldsymbol{\xi}_1$ as well as $\boldsymbol{h}_{(\boldsymbol{x},r)}[\boldsymbol{u}, \boldsymbol{\xi}_2](t) = \boldsymbol{\xi}_2$ for all t if and only if $\|\boldsymbol{u}(t) - \boldsymbol{x}\| < r$ for all $t \in [0, \lambda)$. Otherwise, $\boldsymbol{h}_{(\boldsymbol{x},r)}[\boldsymbol{u}, \boldsymbol{\xi}_1](t) = \boldsymbol{h}_{(\boldsymbol{x},r)}[\boldsymbol{u}, \boldsymbol{\xi}_2](t)$ for any $t \in [\lambda, T]$. Therefore,

$$\boldsymbol{\mathcal{P}}[\boldsymbol{u}, \boldsymbol{\xi}_1](t) - \boldsymbol{\mathcal{P}}[\boldsymbol{u}, \boldsymbol{\xi}_2](t) = \int_{\{(\boldsymbol{x},r) \mid \|\boldsymbol{u}(t) - \boldsymbol{x}\| < r \,\forall t \in [0,\lambda)\}} \omega(\boldsymbol{x}, r)(\boldsymbol{\xi}_1 - \boldsymbol{\xi}_2)\, \mathrm{d}\boldsymbol{x}\, \mathrm{d}r =: \boldsymbol{v}$$

for all $t \in [\lambda, T]$. □

LEMMA 2.3.15 (Congruency of vectorial loops). *Suppose $\boldsymbol{u}_1, \boldsymbol{u}_2 \in C([0,T];\mathbb{R}^n)$ satisfy $\boldsymbol{u}_1(t) = \boldsymbol{u}_2(t)$ for all $t \in [t_0, T]$, $0 \le t_0 \le T$. Suppose further there exists a $\lambda > 0$ such that $\boldsymbol{u}_1$ and $\boldsymbol{u}_2$ are periodic on $[t_0, T]$, i.e. $\boldsymbol{u}_1(t+\lambda) = \boldsymbol{u}_1(t)$ for all $t \in [t_0, T-\lambda]$. Set $\boldsymbol{w}_1 = \boldsymbol{\mathcal{P}}[\boldsymbol{u}_1, \boldsymbol{\xi}_1]$ and $\boldsymbol{w}_2 = \boldsymbol{\mathcal{P}}[\boldsymbol{u}_2, \boldsymbol{\xi}_2]$, where $\boldsymbol{\xi}_1, \boldsymbol{\xi}_2 : \mathbb{R}^n \times \mathbb{R}_+ \to \partial B_{\mathbf{0},1}$. Then:*

(a) *$\boldsymbol{w}_1$ and $\boldsymbol{w}_2$ are periodic with period λ on $[t_0 + \lambda, T]$, i.e.*

$$\boldsymbol{w}_i(t+\lambda) = \boldsymbol{w}_i(t) \quad \text{for all } t:\ t_0 + \lambda \le t \le T - \lambda \text{ and } i = 1, 2.$$

(b) *There exists a $\boldsymbol{v} \in \mathbb{R}^n$ such that*

$$\boldsymbol{w}_1(t) = \boldsymbol{w}_2(t) + \boldsymbol{v} \quad \text{for all } t:\ t_0 + \lambda \le t \le T.$$

PROOF. Define $\boldsymbol{\xi}_i(t_0)$ as $\boldsymbol{\xi}_{i,(\boldsymbol{x},r)}(t_0) = \boldsymbol{h}_{(\boldsymbol{x},r)}[\boldsymbol{u}_i, \boldsymbol{\xi}_{i,(\boldsymbol{x},r)}]$. By the generalized semigroup property, Lemma 2.3.2, we have

$$\boldsymbol{\mathcal{P}}[\boldsymbol{u}_i, \boldsymbol{\xi}_i](t) = \boldsymbol{\mathcal{P}}[\boldsymbol{u}_i^{t_0}, \boldsymbol{\xi}_i(t_0)](t - t_0) \quad \text{for all } t \in [t_0, T],\ i = 1, 2.$$

As $\boldsymbol{u}_1^{t_0}$ and $\boldsymbol{u}_2^{t_0}$ are periodic on $[t_0, T]$ and $\boldsymbol{u}_1^{t_0} = \boldsymbol{u}_2^{t_0}$, statements (a) and (b) follow directly from Lemma 2.3.14 (a) and (b), respectively, for $\boldsymbol{\mathcal{P}}[\boldsymbol{u}_i^{t_0}, \boldsymbol{\xi}_i(t_0)](t - t_0)$. □

We see that the transient phase in the first period is a result of the deletion of differing relay states during this period. The congruency property of $\boldsymbol{\mathcal{P}}$ has been previously observed in computer simulations [**18**].

We now investigate the behaviour of $\boldsymbol{w} = \boldsymbol{\mathcal{P}}[\boldsymbol{u}]$ in the case $n = 2$ for uniformly rotating $\boldsymbol{u}$. Assume $\boldsymbol{u}$ rotates clockwise. Due to the rate-independence of $\boldsymbol{\mathcal{P}}$, it suffices to investigate $\boldsymbol{\mathcal{P}}[\boldsymbol{u}_{\mathrm{rot}}]$ for

$$\boldsymbol{u}_{\mathrm{rot}}(t) = Q(t)\boldsymbol{u}_0, \quad \boldsymbol{u}_0 \in \mathbb{R}^2, \quad t \in [0,T], \tag{2.28}$$

$$Q(t) := \begin{pmatrix} \cos t & \sin t \\ -\sin t & \cos t \end{pmatrix}.$$

The function $\boldsymbol{u}_{\mathrm{rot}}$ rotates uniformly about 0 at magnitude $\|\boldsymbol{u}_{\mathrm{rot}}(t)\| = \|\boldsymbol{u}_0\|$ and period 2π. Note that we have [**33**]

$$\{Q(t) \mid t \in [t_0, t_0 + 2\pi)\} = SO(2) \tag{2.29}$$

for arbitrary $t_0 \in \mathbb{R}$.

The statement of the following Lemma has been experimentally confirmed in [**25**].

LEMMA 2.3.16 (Uniformly rotating input). *Assume ω is isotropic. For all $t \geq 2\pi$, the curve $\boldsymbol{w} = \boldsymbol{\mathcal{P}}[\boldsymbol{u}_{\mathrm{rot}}, \boldsymbol{\xi}]$ describes a circle, i.e. there exist constant vectors $\boldsymbol{v}, \boldsymbol{w}_0 \in \mathbb{R}^2$ such that*

$$\boldsymbol{w}(t) = \boldsymbol{v} + Q(t)\boldsymbol{w}_0.$$

In particular, if $\boldsymbol{\xi}_{(\boldsymbol{x},r)} = \boldsymbol{\xi}^0_{(\boldsymbol{x},r)}$ for all $(\boldsymbol{x}, r)$ such that $\|\boldsymbol{x}\| < r - \|\boldsymbol{u}_0\|$, then $\boldsymbol{v} = 0$ and the circle is centered at 0.

For the proof of Lemma 2.3.16, we apply the following two lemmas:

LEMMA 2.3.17. *The following statements are equivalent:*

(a) $\|\boldsymbol{x}\| < r - \|\boldsymbol{u}_0\|$,
(b) $\|\boldsymbol{u}_{\mathrm{rot}}(t) - \boldsymbol{x}\| < r$ *for all* $t \in [t_0, t_0 + 2\pi)$.

PROOF. To show that (a) implies (b), assume $\|\boldsymbol{x}\| < r - \|\boldsymbol{u}_0\|$. Then

$$\|\boldsymbol{u}_{\mathrm{rot}}(t) - \boldsymbol{x}\| \leq \|Q(t)\boldsymbol{u}_0\| + \|\boldsymbol{x}\| \leq r.$$

To show the converse, assume $\|\boldsymbol{x}\| \geq r - \|\boldsymbol{u}_0\|$. By (2.29) and Lemma 1.3.1 there exists a $\tau \in [t_0, t_0 + 2\pi)$ such that $-\boldsymbol{x}/\|\boldsymbol{x}\| = Q(\tau)\boldsymbol{u}_0/\|\boldsymbol{u}_0\|$. Thus,

$$\|Q(\tau)\boldsymbol{u}_0 - \boldsymbol{x}\| = \left\| Q(\tau)\boldsymbol{u}_0 + \frac{\|\boldsymbol{x}\|}{\|\boldsymbol{u}_0\|} Q(\tau)\boldsymbol{u}_0 \right\| = \|\boldsymbol{x}\| + \|\boldsymbol{u}_0\| \geq r$$

negates (b). □

LEMMA 2.3.18. *If $\|\boldsymbol{x}\| \geq r - \|\boldsymbol{u}_0\|$, then*

$$\boldsymbol{h}_{(Q(t)\boldsymbol{x},r)}[\boldsymbol{u}_{\mathrm{rot}}](t) = Q(t)\boldsymbol{h}_{(\boldsymbol{x},r)}[\boldsymbol{u}_{\mathrm{rot}}](2\pi) \quad \text{for all } t \geq 2\pi.$$

PROOF. For any $t \geq 0$, we have

$$\|\boldsymbol{u}_{\mathrm{rot}}(t) - Q(t)\boldsymbol{x}\| = \|Q(t)\boldsymbol{u}_0 - Q(t)\boldsymbol{x}\| = \|\boldsymbol{u}_0 - \boldsymbol{x}\|. \tag{2.30}$$

To prove the statement of the lemma, we have to consider two cases: $\|\boldsymbol{u}(2\pi) - \boldsymbol{x}\| \geq r$ and $\|\boldsymbol{u}(2\pi) - \boldsymbol{x}\| < r$.

First, assume $\|\boldsymbol{u}(2\pi)-\boldsymbol{x}\| \geq r$. Then by Equation (2.30), $\|\boldsymbol{u}_{\mathrm{rot}}(t)-Q(t)\boldsymbol{x}\| \geq r$, and thus for $t \geq 2\pi$,

(2.31)
$$\boldsymbol{h}_{(Q(t)\boldsymbol{x},r)}[\boldsymbol{u}](t) = \frac{\boldsymbol{u}_{\mathrm{rot}}(t)-Q(t)\boldsymbol{x}}{\|\boldsymbol{u}_{\mathrm{rot}}(t)-Q(t)\boldsymbol{x}\|} = \frac{Q(t)(\boldsymbol{u}_{\mathrm{rot}}(2\pi)-\boldsymbol{x})}{\|\boldsymbol{u}_{\mathrm{rot}}(2\pi)-\boldsymbol{x}\|} = Q(t)\boldsymbol{h}_{(\boldsymbol{x},r)}[\boldsymbol{u}_{\mathrm{rot}}](2\pi).$$

Second, assume $\|\boldsymbol{u}_{\mathrm{rot}}(2\pi)-\boldsymbol{x}\| < r$. Set $\tau_t = \max\{\tau \in [0,t] \mid \|\boldsymbol{u}_{\mathrm{rot}}(t)-Q(t)\boldsymbol{x}\| \geq r\}$. Then because of Lemma 2.3.17, the assumption $\|\boldsymbol{x}\| \geq r - \|\boldsymbol{u}_0\|$ implies that τ_t exists for all $t \geq 2\pi$. By (2.30), we have that $t - \tau_t = 2\pi - \tau_{2\pi}$. Thus,

$$\boldsymbol{h}_{(Q(t)\boldsymbol{x},r)}[\boldsymbol{u}](t) = \frac{\boldsymbol{u}_{\mathrm{rot}}(\tau_t)-Q(t)\boldsymbol{x}}{\|\boldsymbol{u}_{\mathrm{rot}}(\tau_t)-Q(t)\boldsymbol{x}\|} = \frac{Q(t)(\boldsymbol{u}_{\mathrm{rot}}(\tau_{2\pi})-\boldsymbol{x})}{\|\boldsymbol{u}_{\mathrm{rot}}(\tau_{2\pi})-\boldsymbol{x}\|} = Q(t)\boldsymbol{h}_{(\boldsymbol{x},r)}[\boldsymbol{u}_{\mathrm{rot}}](2\pi).$$

□

Proof of Lemma 2.3.16. Lemma 2.3.17 implies that $\boldsymbol{h}_{(\boldsymbol{x},r)}[\boldsymbol{u}_{\mathrm{rot}}] = \boldsymbol{\xi}_{(\boldsymbol{x},r)}$ if and only if $\|\boldsymbol{x}\| < r - \|\boldsymbol{u}_0\|$. Otherwise, $\boldsymbol{h}_{(\boldsymbol{x},r)}[\boldsymbol{u}_{\mathrm{rot}}]$ is given by Lemma 2.3.18. Therefore, we have

$$\begin{aligned}\boldsymbol{w}(t) = &\int_{\|\boldsymbol{x}\|<r-\|\boldsymbol{u}_0\|} \omega(\boldsymbol{x},r)\boldsymbol{\xi}_{(\boldsymbol{x},r)}\,\mathrm{d}(\boldsymbol{x},r)\\ &+ Q(t)\int_{\|\boldsymbol{x}\|\geq r-\|\boldsymbol{u}_0\|} \omega(\boldsymbol{x},r)\boldsymbol{h}_{(\boldsymbol{x},r)}[\boldsymbol{u}_{\mathrm{rot}}](2\pi)\,\mathrm{d}(\boldsymbol{x},r).\end{aligned}$$

The first integral gives $\boldsymbol{v}$, the second integral $\boldsymbol{w}_0$.

To show the second statement, set $\boldsymbol{\xi}_{(\boldsymbol{x},r)} = \boldsymbol{\xi}^0_{(\boldsymbol{x},r)}$. By Lemma 1.3.1, $\boldsymbol{v} = 0$ if and only if $Q(t)\boldsymbol{v} = \boldsymbol{v}$ for all $t \in [0, 2\pi)$. This is quickly verified:

$$\begin{aligned}Q(t)\boldsymbol{v} &= -\int_0^\infty \int_{\mathbb{R}^n} \chi_{\|\boldsymbol{x}\|<r-\|\boldsymbol{u}_0\|}\omega(\boldsymbol{x},r)\frac{Q(t)\boldsymbol{x}}{\|\boldsymbol{x}\|}\,\mathrm{d}\boldsymbol{x}\,\mathrm{d}r\\ &= -\int_0^\infty \int_{\mathbb{R}^n} \chi_{\|Q(t)\boldsymbol{x}\|<r-\|\boldsymbol{u}_0\|}\omega(Q(t)\boldsymbol{x},r)\frac{Q(t)\boldsymbol{x}}{\|Q(t)\boldsymbol{x}\|}\,\mathrm{d}\boldsymbol{x}\,\mathrm{d}r\\ &= -\int_0^\infty \int_{\mathbb{R}^n} \chi_{\|\boldsymbol{x}\|<r-\|\boldsymbol{u}_0\|}\omega(\boldsymbol{x},r)\frac{\boldsymbol{x}}{\|\boldsymbol{x}\|}\,\mathrm{d}\boldsymbol{x}\,\mathrm{d}r\\ &= \boldsymbol{v}\end{aligned}$$

where the second equality uses $\|Q(t)\boldsymbol{x}\| = \|\boldsymbol{x}\|$ and that ω is isotropic, and χ is the characteristic function. For the third equality, a coordinate transformation along Lemma 1.2.8 is carried out. □

Note that the proof provides a formula for $\boldsymbol{v}$ and $\boldsymbol{w}_0$.

2.3.6. Lag angles and dissipation. Two questions that are closely related are those of the hysteretic lag between $\boldsymbol{u}$ and $\boldsymbol{\mathcal{P}}[\boldsymbol{u}]$ and the dissipative properties of $\boldsymbol{\mathcal{P}}$. In the following, we will investigate the lag for uniformly rotating input in $\mathbb{R}^2$ and dissipation under periodic input in general and uniformly rotating input in $\mathbb{R}^2$ in particular. On a few examples, we will demonstrate that in these properties, $\boldsymbol{\mathcal{P}}$ shows good qualitative correspondence to the behaviour of magnetic hysteresis observed in measurements.

Suppose $\boldsymbol{u} \in C([0,T];\mathbb{R}^2)$. The *lag angle* $\alpha_{\text{lag}}(t) = \measuredangle(\boldsymbol{u}(t), \boldsymbol{w}(t))$, that is, the oriented angle between $\boldsymbol{u}(t)$ and $\boldsymbol{w}(t) = \boldsymbol{\mathcal{P}}[\boldsymbol{u}](t)$, is given by

$$\cos\alpha_{\text{lag}}(t) = \frac{u_1(t)w_1(t) + u_2(t)w_2(t)}{\|\boldsymbol{u}(t)\|\|\boldsymbol{w}(t)\|}, \tag{2.32}$$

$$\sin\alpha_{\text{lag}}(t) = \frac{u_1(t)w_2(t) - u_2(t)w_1(t)}{\|\boldsymbol{u}(t)\|\|\boldsymbol{w}(t)\|}. \tag{2.33}$$

In simulations [**25**], it has been observed that the lag angle varies periodically for uniformly rotating input $\boldsymbol{u}_{\text{rot}}$, and is 0 for the isotropic model and sufficiently large input $\boldsymbol{u}(t)$. Mathematically, the first property is a consequence of Lemma 2.3.14, which states that $\boldsymbol{w} = \boldsymbol{\mathcal{P}}[\boldsymbol{u}_{\text{rot}}]$ is periodic with the same period as $\boldsymbol{u}_{\text{rot}}$. Regarding isotropic ω and neutral initial state, we can now add the mathematical proof for the second fact:

LEMMA 2.3.19 (Lag angle for uniformly rotating input). *Assume ω is isotropic. Let $\boldsymbol{w}(t) = \boldsymbol{\mathcal{P}}[\boldsymbol{u}_{\text{rot}}, \boldsymbol{\xi}^0](t)$. Then $\alpha_{\text{lag}}(t)$ is constant for all $t \geq 2\pi$ and equal to $\measuredangle(\boldsymbol{u}_0, \boldsymbol{w}_0)$, where $\boldsymbol{w}_0$ is as in Lemma 2.3.16.*

PROOF. Obviously, as by Lemma 2.3.16 we have $\boldsymbol{w} = Q(t)\boldsymbol{w}_0$,

$$\cos\alpha_{\text{lag}}(t) = \frac{\boldsymbol{u}_{\text{rot}}(t)\cdot\boldsymbol{w}(t)}{\|\boldsymbol{u}_{\text{rot}}(t)\|\|\boldsymbol{w}(t)\|} = \frac{(Q(t)\boldsymbol{u}_0)\cdot(Q(t)\boldsymbol{w}_0)}{\|\boldsymbol{u}_0\|\|\boldsymbol{w}_0\|} = \frac{\boldsymbol{u}_0\cdot\boldsymbol{w}_0}{\|\boldsymbol{u}_0\|\|\boldsymbol{w}_0\|}.$$

Defining the $(2,2)$-matrices $M(t) = (\boldsymbol{u}(t), \boldsymbol{w}(t))$, so $M(0) = (\boldsymbol{u}_0, \boldsymbol{w}_0)$, and using that $\det Q(t) = 1$ by (2.29), gives

$$\sin\alpha_{\text{lag}}(t) = \frac{\det M(t)}{\|\boldsymbol{u}_{\text{rot}}(t)\|\|\boldsymbol{w}(t)\|} = \frac{\det\left(Q(t)M(0)\right)}{\|\boldsymbol{u}_0\|\|\boldsymbol{w}_0\|} = \frac{\det M(0)}{\|\boldsymbol{u}_0\|\|\boldsymbol{w}_0\|}.$$

Therefore, $\alpha_{\text{lag}}(t) = \measuredangle(\boldsymbol{u}_0, \boldsymbol{w}_0)$ is constant. □

Thus, we can compute a curve $\alpha_{\text{lag}}(\|\boldsymbol{u}_0\|) = \measuredangle(\boldsymbol{u}_{\text{rot}}(t), \boldsymbol{w}(t))$ in dependence of the amplitude $\|\boldsymbol{u}_0\|$ at which $\boldsymbol{u}_{\text{rot}}$ rotates. If ω is isotropic and has bounded support $\mathcal{K}$, as introduced in Section 2.3.4, then the alignment of $\boldsymbol{u}_{\text{rot}}(t)$ and $\boldsymbol{w}(t)$ in saturation by Lemma 2.3.12 implies that

$$\alpha_{\text{lag}}(\|\boldsymbol{u}_0\|) = 0 \text{ for all } \|\boldsymbol{u}_0\| \geq R.$$

If in addition we have $\omega \geq 0$, then

$$0 \leq \alpha_{\text{lag}}(\|\boldsymbol{u}_0\|) \leq \pi, \tag{2.34}$$

that is, $\boldsymbol{w}(t)$ always lags behind $\boldsymbol{u}_{\text{rot}}(t)$. To outline why (2.34) is true, consider without loss of generality $\boldsymbol{u}_0 = (\|\boldsymbol{u}_0\|, 0)$ and $t = 4\pi$, so $\boldsymbol{u}_{\text{rot}}(4\pi) = \boldsymbol{u}_0$. Figure 2.7 illustrates the corresponding memory state in the plane $r = \text{const}$. For $\boldsymbol{x} = Q(t)(\|\boldsymbol{x}\|, 0)^T$, we have

$$\boldsymbol{h}_{(\boldsymbol{x},r)}[\boldsymbol{u}](4\pi) = \begin{cases} \boldsymbol{\xi}^0_{(\boldsymbol{x},r)} & \text{if } \|\boldsymbol{x}\| < r - \|\boldsymbol{u}_0\|, \\ Q(t)\boldsymbol{h}_{((\|\boldsymbol{x}\|,0)^T,r)}[\boldsymbol{u}_{\text{rot}}](2\pi) & \text{if } \|\boldsymbol{x}\| \geq r - \|\boldsymbol{u}_0\| \text{ and } \|\boldsymbol{x}-\boldsymbol{u}_0\| < r, \\ \frac{\boldsymbol{x}-\boldsymbol{u}_0}{\|\boldsymbol{x}-\boldsymbol{u}_0\|} & \text{if } \|\boldsymbol{x}\| \geq r - \|\boldsymbol{u}_0\| \text{ and } \|\boldsymbol{x}-\boldsymbol{u}_0\| \geq r. \end{cases}$$

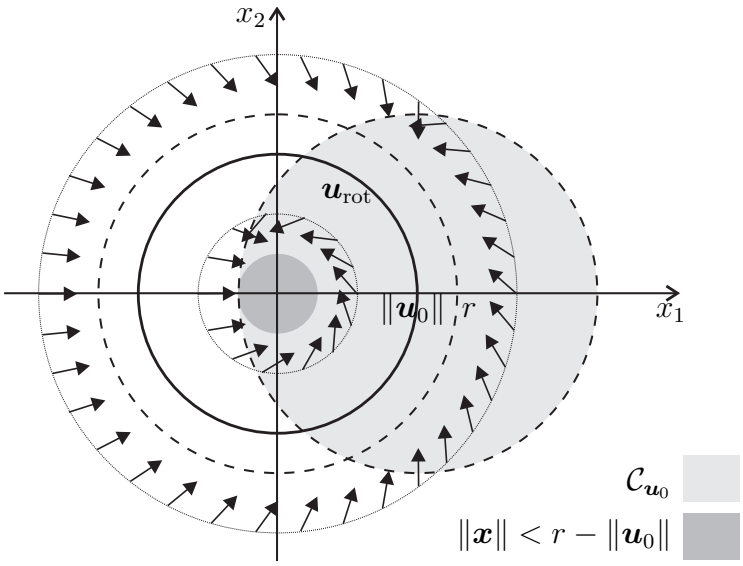

FIGURE 2.7. Memory state in the plane $\mathbb{R}^2 \times \{r\}$ at $t = 4\pi$ for $\boldsymbol{u}_{\mathrm{rot}}$ with $\boldsymbol{u}_0 = (\|\boldsymbol{u}_0\|, 0)$: The relay states are depicted along two circles $\|\boldsymbol{x}\| = \text{const}$. The freeze cone is drawn light shaded, the set $\|\boldsymbol{x}\| < r - \|\boldsymbol{u}_0\|$ dark shaded.

The relays such that $\|\boldsymbol{x}\| < r - \|\boldsymbol{u}_0\|$ contribute 0 to $\boldsymbol{\mathcal{P}}[\boldsymbol{u}_{\mathrm{rot}}]$, as discussed in the proof of Lemma 2.3.16. The relays satisfying $\|\boldsymbol{x}\| \geq r - \|\boldsymbol{u}_0\|$ and $\|\boldsymbol{x} - \boldsymbol{u}_0\| \geq r$ contribute $\lambda \boldsymbol{u}_0$, $\lambda \in \mathbb{R}$, because ω, relay states and domain are symmetric about the x_1-axis. For the remaining relays inside $\mathcal{C}_{\boldsymbol{u}_0}$, it is quickly verified geometrically that $\boldsymbol{h}_{((\|\boldsymbol{x}\|,0)^T,r)}[\boldsymbol{u}_{\mathrm{rot}}](2\pi)$ has a nonnegative second vector component. Since the freeze cone is symmetric about the x_1-axis, the integral over the relay states along any circle segment $\|\boldsymbol{x}\| = \text{const}$ inside the freeze cone gives

$$\int_{-\varphi(\|\boldsymbol{x}\|)}^{\varphi(\|\boldsymbol{x}\|)} Q(t) \boldsymbol{h}_{((\|\boldsymbol{x}\|,0)^T,r)}[\boldsymbol{u}_{\mathrm{rot}}](2\pi)\,\mathrm{d}t \;=\; 2\sin\varphi(\|\boldsymbol{x}\|)\, \boldsymbol{h}_{((\|\boldsymbol{x}\|,0)^T,r)}[\boldsymbol{u}_{\mathrm{rot}}](2\pi)$$

with some $\varphi(\|\boldsymbol{x}\|) \in [0, \pi]$, so $\sin\varphi(\|\boldsymbol{x}\|) \geq 0$. Therefore, if $\omega \geq 0$, these relays contribute a vector with nonnegative second component to $\boldsymbol{\mathcal{P}}[\boldsymbol{u}_{\mathrm{rot}}]$. Together with the other contributions, we obtain $\boldsymbol{w} = (w_1, w_2)^T$, $w_2 \geq 0$, and thus with Equation (2.33) that $\sin\alpha_{\mathrm{lag}}(4\pi) \geq 0$. This results in (2.34).

If ω is reasonable, it seems to be an inherent property of the vector Preisach operator $\boldsymbol{\mathcal{P}}$ that the resulting lag angle curves look like those observed for real magnetic materials [**10**],[**52**, Fig. 4]. Figure 2.8 shows a few lag angle curves computed for exemplary Preisach distributions.

REMARK (Distinction from the Mròz model). The vector Preisach operator $\boldsymbol{\mathcal{P}}$ is not equal to a Mròz model [**56, 14**]. This can be seen because for uniformly rotating input $\boldsymbol{u}_{\mathrm{rot}}$, the output of the Mròz model is aligned with the input (see e.g. [**15**, Example 5.1]), whereas $\boldsymbol{\mathcal{P}}$ results in a non-zero lag for small $\boldsymbol{u}(t)$, compare Figure 2.8.

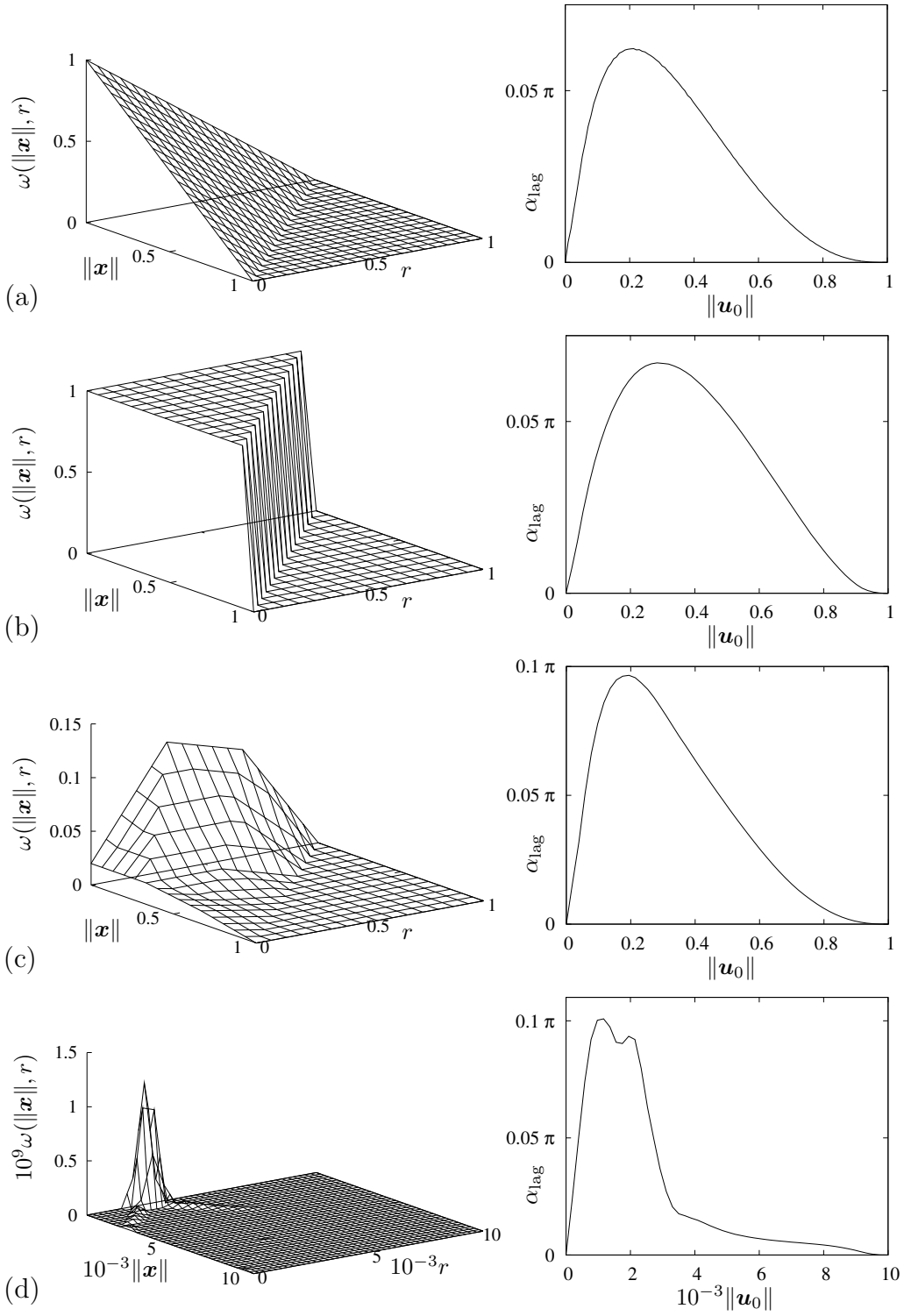

FIGURE 2.8. Different isotropic Preisach distributions ω (left) and the corresponding lag angle curves (right): (a) linear ω, (b) constant ω, (c) ω used in the applications in Sections 3.3 and 3.4, (d) ω of the armature material in the magnetic valve application in Section 3.5.

The remainder of this section shall address the question of hysteresis dissipation under periodic input. This is of interest regarding our ultimate goal in Chapter 3 to use $\boldsymbol{\mathcal{P}}$ to represent the hysteresis relationship between the physical quantities magnetic field $\boldsymbol{H}$, magnetization $\boldsymbol{M}$ and magnetic flux $\boldsymbol{B}$, given by (cf. Section 3.1)

$$\boldsymbol{B} = \mu_0 \boldsymbol{H} + \boldsymbol{M} \tag{2.35}$$

where μ_0 is the magnetic field constant, via

$$\boldsymbol{M} = \boldsymbol{\mathcal{P}}[\boldsymbol{H}]. \tag{2.36}$$

The energy injected in the time interval $[t_1, t_2]$ of a magnetization process is given by the integral [**5, 48**]

$$\int_{t_1}^{t_2} \boldsymbol{H} \cdot \mathrm{d}\boldsymbol{B}. \tag{2.37}$$

In a periodic process, the internal states at the beginning and the end of one period are equal. Thus, the energy dissipated in the course of each period equals the integral over that period. Say a period length is λ. To be consistent with the principles of thermodynamics, the dissipated energy must satisfy:

$$\int_{t}^{t+\lambda} \boldsymbol{H} \cdot \mathrm{d}\boldsymbol{B} \geq 0. \tag{2.38}$$

The following lemma rephrases (2.38) in terms of $\boldsymbol{H}$ and $\boldsymbol{M}$, that is, with (2.36), $\boldsymbol{H}$ and $\boldsymbol{\mathcal{P}}[\boldsymbol{H}]$.

LEMMA 2.3.20. *Assume $\boldsymbol{H}(t+\lambda) = \boldsymbol{H}(t)$ and $\boldsymbol{M}(t+\lambda) = \boldsymbol{M}(t)$. Then the following holds:*

$$\int_{t}^{t+\lambda} \boldsymbol{H} \cdot \mathrm{d}\boldsymbol{B} = \int_{t}^{t+\lambda} \boldsymbol{H} \cdot \mathrm{d}\boldsymbol{M}.$$

PROOF. Applying the material equation (2.35), the statements on the Riemann-Stieltjes integral in Section 1.2.4 and $\int_t^{t+\lambda} \boldsymbol{H} \cdot \mathrm{d}\boldsymbol{H} = 0$ give

$$\int_{t}^{t+\lambda} \boldsymbol{H} \cdot \mathrm{d}\boldsymbol{B} = -\int_{t}^{t+\lambda} (\mu_0 \boldsymbol{H} + \boldsymbol{M}) \cdot \mathrm{d}\boldsymbol{H} = -\int_{t}^{t+\lambda} \boldsymbol{M} \cdot \mathrm{d}\boldsymbol{H} = \int_{t}^{t+\lambda} \boldsymbol{H} \cdot \mathrm{d}\boldsymbol{M}.$$

□

With Lemma 2.3.20 and (2.36), the energy balance (2.38) is satisfied exactly if $\boldsymbol{\mathcal{P}}$ satisfies

$$\int_{t}^{t+\lambda} \boldsymbol{u} \cdot \mathrm{d}\boldsymbol{w} \geq 0 \tag{2.39}$$

for all $\boldsymbol{u}$ with period λ, $\boldsymbol{w} = \boldsymbol{\mathcal{P}}[\boldsymbol{u}]$ and $t \geq \lambda$.

The total loss of $\boldsymbol{\mathcal{P}}$ results as weighted superposition of the losses of the single relays $\boldsymbol{h}_{(\boldsymbol{x},r)}$. Therefore, the following proposition is an immediate consequence of Lemma 2.2.8.

PROPOSITION 2.3.21 (Dissipation). *If $\omega \geq 0$ and $\boldsymbol{u}$ is piecewise differentiable and has the finite switching property, then $\boldsymbol{\mathcal{P}}$ satisfies the energy balance* (2.39).

In particular, we again want to look at uniformly rotating input, $\boldsymbol{u}_{\mathrm{rot}}$. For this case, dissipation has been the subject of measurements early in the history of magnetism research and results in a typical curve shape [**3, 71, 10**]. If ω is isotropic, $\boldsymbol{w} = \boldsymbol{\mathcal{P}}[\boldsymbol{u}_{\mathrm{rot}}]$ is continuously differentiable and we have

$$\int_{t_1}^{t_2} \boldsymbol{u} \cdot \,\mathrm{d}\boldsymbol{w} = \int_{t_1}^{t_2} \boldsymbol{u}(t) \cdot \boldsymbol{w}'(t)\,\mathrm{d}t.$$

Thus, the dissipation rate is given by $\boldsymbol{u}(t) \cdot \boldsymbol{w}'(t)$.

LEMMA 2.3.22. *Assume ω is isotropic. Then for all $t > 2\pi$, the dissipation rate $\boldsymbol{u}_{\mathrm{rot}}(t) \cdot \boldsymbol{w}'(t)$ is constant.*

PROOF. Applying Lemma 2.3.16, for $t > 2\pi$ we have

$$\boldsymbol{u}_{\mathrm{rot}}(t) \cdot \boldsymbol{w}'(t) = Q(t)\boldsymbol{u}_0 \cdot \partial_t(\boldsymbol{v} + Q(t)\boldsymbol{w}_0) = \boldsymbol{u}_0^T Q(t)^T Q'(t)\boldsymbol{w}_0.$$

This is constant as

$$Q(t)^T Q'(t) = \begin{pmatrix} \cos t & -\sin t \\ \sin t & \cos t \end{pmatrix} \begin{pmatrix} -\sin t & \cos t \\ -\cos t & -\sin t \end{pmatrix} = \begin{pmatrix} 0 & 1 \\ -1 & 0 \end{pmatrix}. \qquad \square$$

Investigating the dissipation term (2.39) in dependence of $\|\boldsymbol{u}_0\|$, we obtain:

LEMMA 2.3.23. *For uniformly rotating input $\boldsymbol{u}_{\mathrm{rot}}$ and $\omega \geq 0$, the dissipation rate $\boldsymbol{u}_{\mathrm{rot}}(t) \cdot \boldsymbol{w}'(t)$ is nonnegative and 0 if $||\boldsymbol{u}_0|| = 0$ or $||\boldsymbol{u}_0|| \geq R$.*

PROOF. Nonnegativity is a consequence of Proposition 2.3.21 and Lemma 2.3.22. If $||\boldsymbol{u}_0|| = 0$, then $\boldsymbol{u}_{\mathrm{rot}} = 0$ and obviously $\int \boldsymbol{u}_{\mathrm{rot}} \cdot \,\mathrm{d}\boldsymbol{w} = 0$. If $||\boldsymbol{u}_0|| \geq R$, then the alignment of $\boldsymbol{u}_{\mathrm{rot}}(t)$ and $\boldsymbol{w}(t)$ implies $\boldsymbol{w}_0 = \lambda \boldsymbol{u}_0$ for some $\lambda \geq 0$. Plugging this into the computations in the preceeding proof gives $\boldsymbol{u}_{\mathrm{rot}}(t) \cdot \boldsymbol{w}'(t) = 0$. $\square$

In fact, using Lemma 2.3.22 and the computations in its proof, for $t \geq 2\pi$ we obtain an explicit formula for the hysteresis losses, namely

$$\int_t^{t+2\pi} \boldsymbol{u}_{\mathrm{rot}} \cdot \,\mathrm{d}\boldsymbol{w} = \int_t^{t+2\pi} \boldsymbol{u}_{\mathrm{rot}}(\tau) \cdot \boldsymbol{w}'(\tau)\,\mathrm{d}\tau = 2\pi \det(\boldsymbol{u}_0, \boldsymbol{w}_0).$$

Applying this formula, Figure 2.9 shows the resulting loss curves corresponding to the Preisach distributions and lag angles computed in Figure 2.8. We can see that for the more well-behaved ω's in (a), (b), and (c), the resulting loss curves ressemble those measured in [**3**], [**71**] and more recent work [**38**].

A more general approach to the question of the energy dissipated and the energy stored in the magnetic field will be presented later in Section 2.5.3, because the discussion of hysteresis potentials requires differentiation of $\boldsymbol{\mathcal{P}}[\boldsymbol{u}]$, which is the topic of Section 2.5.2.

2.4. Reduction from vector to scalar Preisach operator

In this section, we will show that under uniaxial input, the isotropic vector Preisach operator $\boldsymbol{\mathcal{P}}$ reduces to a scalar Preisach operator, at least after all effects due to the initial state have been erased. Mayergoyz [**49, 51**] discovered that the defining features of the scalar Preisach operator are the typical memory deletion

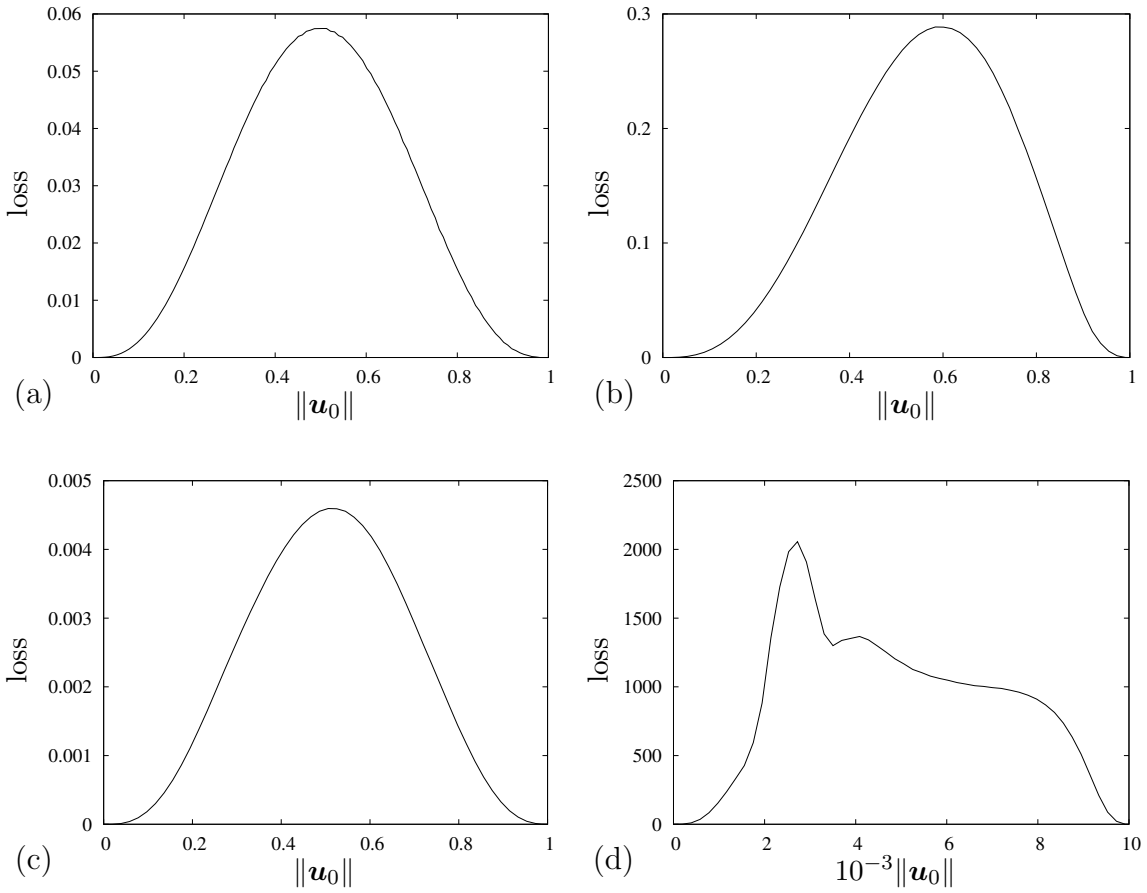

FIGURE 2.9. Loss curves corresponding to the respective Preisach distributions in Figure 2.8.

properties that he called the "congruency" and the "wiping out" property. Subsequently, Brokate [**12**] developed a formal mathematical characterization of scalar Preisach operators, on which the following discussion relies.

Brokate's characterization proceeds in two steps [**16**]: First, the notion of operators of Preisach type is introduced. These are exactly those hysteresis operators showing the typical memory deletion properties represented by Mayergoyz' congruency and wiping out properties. Second, the subclass of Preisach operators within this class is defined to be those operators whose output map results as integral of the relay states over the Preisach plane subject to a density function, as defined in Example 2.1.8, Equation (2.3). To show the reduction, we adopt these two steps, for each summarizing the theoretical background from [**16**] and following it up with our own exposition.

By *uniaxial input*, we mean input that varies along one vector direction only, that is,

$$\boldsymbol{u}(t) = u(t)\,\boldsymbol{e},$$

with $u : [0,T] \to \mathbb{R}$ and constant $\boldsymbol{e} \in \mathbb{R}^n$. Due to Lemma 2.3.3, without loss of generality we can assume this direction to be the first vector component, i.e.

$$\boldsymbol{u}(t) = (u(t), 0, \dots, 0)^T \in C([0,T]; \mathbb{R}^n). \tag{2.40}$$

We require that the Preisach distribution ω be of bounded support, that is, there exists an $R \in \mathbb{R}$ such that $\omega(\boldsymbol{x}, r) = 0$ a.e. outside $\mathcal{K}$, where

$$\mathcal{K} := \{(\boldsymbol{x}, r) \in \mathbb{R}_n \times \mathbb{R}_+ \mid \|\boldsymbol{x}\| + r \leq R\}.$$

This is a necessary prerequisite because initial states will, in general, impede the characteristic memory deletion. We guarantee all initial states to be erased from the significant part $\mathcal{K}$ of the memory of $\boldsymbol{\mathcal{P}}$ by assuming

$$u(0) \geq R. \tag{2.41}$$

In this way, any relay $\boldsymbol{h}_{(\boldsymbol{x},r)}$, $(\boldsymbol{x}, r) \in \mathcal{K}$, has "forgotten" its initial state $\boldsymbol{\xi}_{(\boldsymbol{x},r)}$.

Remark. In fact, instead of requiring ω to be of bounded support and condition (2.41), the subsequent argument will easily carry over to $t > t_0$ if $\boldsymbol{u}$ satisfies $\boldsymbol{u}(t) \in [\min_{\tau\in[0,t_0]} \boldsymbol{u}(\tau), \max_{\tau\in[0,t_0]} \boldsymbol{u}(\tau)]$ for all $t \in [t_0, T]$, though with an additional constant vector offset owing to the initial states remaining at t_0.

2.4.1. Scalar hysteresis operators of Preisach type. We already mentioned that for scalar hysteresis operators, it is a consequence of rate-independence that at any time, the output is completely determined by the local minima and maxima of the input function. This results in a bijective correspondence between real-valued mappings on the set of finite real strings and rate-independent functionals on the set of piecewise monotone functions, which form the generating functionals of scalar hysteresis operators. Migrating to strings simplifies the description of memory deletion processes and lies at the heart of the exposition in [**16**]. Thus, we give a brief introduction to this approach, which forms the basis for the definition and characterization of hysteresis operators of Preisach type. For details, refer to [**16**, Chapter 2.2]. We will adopt the notation from [**16**] as far as it applies.

Definition 2.4.1 (piecewise monotone function, monotonicity partition). A function $u : [0,T] \to \mathbb{R}$ is called *piecewise monotone* if there exists a partition $\Gamma = \{t_i\}_{0\leq i\leq N}$, $0 = t_0 < t_1 < \ldots < t_N = T$, such that u is monotone on all subintervals (t_i, t_{i+1}). We call Γ a *monotonicity partition*.

The set of all piecewise monotone functions on $[0,T]$ is denoted by

$$M_{pm}[0,T] = \{u \in Map([0,T]; \mathbb{R}) \mid u \text{ is piecewise monotone } \}.$$

The set of all continuous piecewise monotone functions is denoted by

$$C_{pm}[0,T] = M_{pm}[0,T] \cap C([0,T]; \mathbb{R}).$$

For any $u \in M_{pm}[0,T]$, the minimal monotonicity partition $t_0 = 0$, $t_{i+1} = \max\{t \in [t_i, T] \mid u \text{ is monotone on } [t_i, t]\}$ if $0 \leq t_i < T$, is called the *standard monotonicity partition* of u.

We write

$$S = \{(u_0, u_1, \dots, u_N) \mid N \in \mathbb{N}_0, u_i \in \mathbb{R}, 0 \le i \le N\},$$

for the set of all finite strings of real numbers, and

$$S_A = \{(u_0, u_1, \dots, u_N) \in S \mid N \ge 1, (u_{i+1} - u_i)(u_i - u_{i-1}) < 0,\ 1 < i < N-1\}.$$

for the set of alternating strings.

As described in [**16**], we can pass from piecewise monotone functions to strings via the *restriction operator* $\rho_A : M_{pm}[0,T] \to S_A$,

$$\rho_A[u] = (u(t_0), \dots, u(t_N)),$$

where $\{t_i\}_{0 \le i \le N}$ is the standard monotonicity partition of u. Conversely, we can pass from strings to piecewise monotone functions via the *prolongation operator* $\pi_A : S \to C_{pm}[0,T]$ by setting the function $u = \pi_A(u_0, \dots, u_N)$ to be the linear interpolation of the points $u(\frac{i}{N}T) = u_i$.

As shown in [**16**], for any scalar hysteresis operator $\mathcal{W}$ on $M_{pm}[0,T]$ there is an equivalent hysteresis operator $\tilde{\mathcal{W}} : S \to S$. For $s = (u_0, \dots, u_N) \in S$, it is given by

$$\tilde{\mathcal{W}}(s) = (\tilde{\mathcal{W}}_f(u_0), \tilde{\mathcal{W}}_f(u_0, u_1), \dots, \tilde{\mathcal{W}}_f(u_0, u_1, \dots, u_N))$$

with the map $\tilde{\mathcal{W}}_f : S \to \mathbb{R}$ defined in terms of the generating functional of $\mathcal{W}$ by

$$\tilde{\mathcal{W}}_f(s) = \mathcal{W}_f \circ \pi_A(s)(t).$$

Based on this correspondence, we no longer need to distinguish between functions and strings as input to scalar hysteresis operators and just write $\mathcal{W}[u]$ or $\mathcal{W}(s)$ for both depending on context.

Brokate's approach to the scalar Preisach operator is based on the representation of the Preisach memory in terms of the play operator and Preisach memory curves, which we introduced in Example 2.1.8. Define the mapping $\mathcal{F}_f : S \times \Psi_0 \to \Psi_0$ by

$$\mathcal{F}_f(s; \psi_{-1})(r) := \mathcal{F}_{r,f}(s; \psi_{-1}) \quad \text{for all } r \ge 0.$$

It formalizes the Preisach memory evolution described in Example 2.1.8. Operators of Preisach type are exactly those hysteresis operators that have a memory of this form:

Definition 2.4.2 (Hysteresis Operators of Preisach Type – [**16**], Def. 2.4.2). Suppose a mapping $Q : \Psi_0 \to \mathbb{R}$ and an initial state $\psi_{-1} \in \Psi_0$ are given. Then the hysteresis operator $\mathcal{W}$ given by the generating functional

$$\mathcal{W}_f(s; \psi_{-1}) := Q(\mathcal{F}_f(s; \psi_{-1})), \quad s \in S,$$

is called the *hysteresis operator of Preisach type associated with the output mapping Q and the initial memory state ψ_{-1}.*

Since this definition in essence is independent of the image of the output mapping Q, it extends to uniaxial vector-valued input by generalizing Q to be a map from Ψ_0 to $\mathbb{R}^n$.

The characterization of the class of hysteresis operators of Preisach type relies on its typical memory deletions, which can be described elegantly in terms of strings.

For this, we introduce orderings on S which are based on string deletions. Deletions are maps from S to S consisting of deleting entries from $s \in S$ subject to a given set of rules. We define the following deletion rules:

(1) *monotone deletion*:

$$(u_0, \dots, u_N) \mapsto (u_0, \dots, u_{i-1}, u_{i+1}, \dots, u_N), \quad \text{if } u_i \in [u_{i-1}, u_{i+1}]$$

(2) *Madelung deletion*:

$$(u_0, \dots, u_N) \mapsto (u_0, \dots, u_{i-1}, u_{i+2}, \dots, u_N),$$
$$\text{if } [u_i, u_{i+1}] \subset [u_{i-1}, u_{i+2}], \quad u_i \notin [u_{i-1}, u_{i+1}], \quad u_{i+1} \notin [u_i, u_{i+2}]$$
$$\text{for some } 1 \le i \le N-2$$

(3) *frontal deletion* (deletion rule (7.2) in [**16**]):

$$(u_0, \dots, u_N) \mapsto (u_1, \dots, u_N), \quad \text{if } u_0 \in [u_1, u_2]$$

(4) *initial state dependent deletion* (deletion rule (7.6) in [**16**]):
For any $\psi_{-1} \in \Psi_0$,

$$(u_0, \dots, u_N) \mapsto (u_1, \dots, u_N), \quad \text{if } R_M(u_0, \psi_{-1}) \le R_I(u_1, \psi_{-1}),$$

where

$$R_M(y; \psi_{-1}) := \inf \{r \in \mathbb{R} \mid r \ge 0, y + r = \psi_{-1}(r) \text{ or } y - r = \psi_{-1}(r)\},$$
$$R_I(y; \psi_{-1}) := \sup\{r \in \mathbb{R} \mid r \ge 0, y + r = \psi_{-1}(r) \text{ or } y - r = \psi_{-1}(r)\}$$

are discussed in more detail in [**16**].

Note that for the initial memory curve $\psi_{-1} \equiv 0$, the initial state dependent deletion rule (4) takes the form [**16**]

$$(u_0, \dots, u_N) \mapsto (u_1, \dots, u_N), \quad \text{if } |u_0| \le |u_1|. \tag{2.42}$$

We do not elaborate further on the exact definition of deletion rule (4) because it exclusively takes care of exactly those initial state deletion effects that we exclude by assumption (2.41).

Definition 2.4.3 (Orderings on S). A set of deletion rules induces an ordering $\le$ on S by defining that $s' \le s$ for $s', s \in S$ if and only if s' results from s by successive applications of deletion rules from this set. The *Preisach ordering* $\le_P$ is the ordering on S induced by deletion rules (1), (2), and (3). The ordering $\le_{\psi_{-1}}$ is the ordering induced by deletion rules (1), (2), (3), and (4).*

Thus, we have everything necessary for giving a formal definition of memory deletions of a scalar hysteresis operator.

Definition 2.4.4 (Forgetting – [**16**], Def. 2.7.1). Let $\le$ be an ordering on the set S of all strings. We say that a hysteresis operator $\mathcal{W}$ *forgets according to* $\le$, if $s' \le s$ implies that $\mathcal{W}_f(s) = \mathcal{W}_f(s')$.

With this, we are now ready to state the characterization.

*We denote the ordering $\le_\delta$ in [**16**] by $\le_{\psi_{-1}}$ for notational convenience.

THEOREM 2.4.5 (Characterization of scalar Operators of Preisach Type – [**16**], Theorem 2.7.7). *Let $\psi_{-1} \in \Psi_0$ be given such that*

$$|\psi_{-1}(r) - \psi_{-1}(\rho)| < |r - \rho|, \qquad \text{if } r \neq \rho.$$

If a hysteresis operator $\mathcal{W}$ forgets according to the ordering $\leq_{\psi_{-1}}$, then $\mathcal{W}$ is of Preisach type.

2.4.2. Reduction to a scalar hysteresis operator of Preisach type. We will show that the isotropic vector Preisach operator reduces to a scalar hysteresis operator of Preisach type for uniaxial input (2.40). The correspondence between a scalar function u and the associated string $(u_0, \dots, u_N)$ carries over to vector-valued uniaxial input $u\boldsymbol{e}$ in the obvious way. The reduction property is independent of the image of the output mapping Q associated with a hysteresis operator of Preisach type. The string corresponding to $\boldsymbol{u}$ in (2.40) is thus $s = \rho_A[u(t)]$ and the meaning of $\boldsymbol{\mathcal{W}}(s)$ is clear.

Theorem 2.4.5 has provided us with a simple criterion for identifying operators of Preisach type.

LEMMA 2.4.6. *Let $(\boldsymbol{x}, r) \in \mathbb{R}^n \times \mathbb{R}_+$. Under uniaxial input* (2.40)*, the vectorial relay operator $\boldsymbol{h}_{(\boldsymbol{x},r)}$ forgets according to the Preisach ordering.*

PROOF. The semigroup property, which $\boldsymbol{h}_{(\boldsymbol{x},r)}$ satisfies by Lemma 2.2.2, in terms of strings translates to

(2.43)
$$\boldsymbol{h}_{(\boldsymbol{x},r),f}((u_0, \dots, u_N), \boldsymbol{\xi}_{(\boldsymbol{x},r)}) = \boldsymbol{h}_{(\boldsymbol{x},r),f}((u_i, \dots, u_N), \boldsymbol{h}_{(\boldsymbol{x},r),f}((u_0, \dots, u_{i-1}), \boldsymbol{\xi}_{(\boldsymbol{x},r)}))$$

for any string $(u_0, \dots, u_N)$ and any $\boldsymbol{\xi}_{(\boldsymbol{x},r)} \in \partial B_{\boldsymbol{0},1}$.

We will first show that $\boldsymbol{h}_{(\boldsymbol{x},r)}$ forgets according to the monotone deletion rule: Because of (2.43), it suffices to show that $u_i \in [u_{i-1}, u_{i+1}]$ implies

$$\boldsymbol{h}_{(\boldsymbol{x},r),f}((u_{i-1}, u_i, u_{i+1}), \boldsymbol{\xi}) = \boldsymbol{h}_{(\boldsymbol{x},r),f}((u_{i-1}, u_{i+1}), \boldsymbol{\xi}).$$

If $(u_{i+1}, 0, \dots, 0)^T$ lies outside the relay, that is, $\|\boldsymbol{x} - (u_{i+1}, 0, \dots, 0)^T\| \geq r$, this is obviously true. If $\|\boldsymbol{x} - (u_{i+1}, 0, \dots, 0)^T\| < r$, assume first that $\|\boldsymbol{x} - (u_{i-1}, 0, \dots, 0)^T\| < r$. In this case, the entire line segment connecting these two point is inside the relay, so

$$\boldsymbol{h}_{(\boldsymbol{x},r),f}((u_{i-1}, u_i, u_{i+1}), \boldsymbol{\xi}) = \boldsymbol{h}_{(\boldsymbol{x},r),f}((u_{i-1}, u_{i+1}), \boldsymbol{\xi}) = \boldsymbol{\xi}.$$

For $\|\boldsymbol{x} - (u_{i-1}, 0, \dots, 0)^T\| \geq r$, on the other hand, there is exacty one $\tilde{u}$ such that $(\tilde{u}, 0, \dots, 0)^T = \lambda(u_{i-1}, 0, \dots, 0)^T + (1 - \lambda)(u_{i+1}, 0, \dots, 0)^T$, $\lambda \in [0, 1)$, and $\|(\tilde{u}, 0, \dots, 0)^T - \boldsymbol{x}\| = r$, and

$$\boldsymbol{h}_{(\boldsymbol{x},r),f}((u_{i-1}, u_i, u_{i+1}), \boldsymbol{\xi}) = \boldsymbol{h}_{(\boldsymbol{x},r),f}((u_{i-1}, u_{i+1}), \boldsymbol{\xi}) = \frac{1}{r}((\tilde{u}, 0, \dots, 0)^T - \boldsymbol{x}).$$

Now we will prove that $\boldsymbol{h}_{(\boldsymbol{x},r)}$ forgets according to the Madelung deletion rule: Assume the string $(\boldsymbol{u}_0, \dots, \boldsymbol{u}_N)$ allows a Madelung deletion at $i \in \{1, \dots, N-2\}$. By (2.43), it suffices to show that

$$\boldsymbol{h}_{(\boldsymbol{x},r),f}((u_{i-1}, u_i, u_{i+1}, u_{i+2}), \boldsymbol{\xi}) = \boldsymbol{h}_{(\boldsymbol{x},r),f}((u_{i-1}, u_{i+2}), \boldsymbol{\xi}). \tag{2.44}$$

If $\|\boldsymbol{u}_{i+2} - \boldsymbol{x}\| \geq r$, then (2.44) obviously holds. Assume $\|(u_{i+2}, 0, \dots, 0)^T - \boldsymbol{x}\| < r$. If $\|(u_{i-1}, 0, \dots, 0)^T - \boldsymbol{x}\| < r$, then $\boldsymbol{h}_{(\boldsymbol{x},r)}$ never leaves state $\boldsymbol{\xi}$ and (2.44) holds. If, on the other hand, $\|(u_{i-1}, 0, \dots, 0)^T - \boldsymbol{x}\| \geq r$, then like for the monotone deletion rule, there is exacty one $\tilde{u}$ such that $(\tilde{u}, 0, \dots, 0)^T = \lambda(u_{i-1}, 0, \dots, 0)^T + (1 - \lambda)(u_{i+2}, 0, \dots, 0)^T$, $\lambda \in [0, 1)$, and $\|(\tilde{u}, 0, \dots, 0)^T - \boldsymbol{x}\| = r$. As the input variations for both $(u_{i-1}, u_i, u_{i+1}, u_{i+2})$ and (u_{i-1}, u_{i+2}) take place on the entire line segment connecting $(u_{i-1}, 0, \dots, 0)^T$ and $(u_{i+2}, 0, \dots, 0)^T$, we have

$$\boldsymbol{h}_{(\boldsymbol{x},r),f}((u_{i-1}, u_i, u_{i+1}, u_{i+2}), \boldsymbol{\xi}) = \boldsymbol{h}_{(\boldsymbol{x},r),f}((u_{i-1}, u_{i+2}), \boldsymbol{\xi}) = \frac{1}{r}((\tilde{u}, 0, \dots, 0)^T - \boldsymbol{x}).$$

To show that $\boldsymbol{h}_{(\boldsymbol{x},r)}$ forgets according to the frontal deletion rule, i.e. by (2.43),

$$\boldsymbol{h}_{(\boldsymbol{x},r),f}((u_0, u_1, u_2), \boldsymbol{\xi}) = \boldsymbol{h}_{(\boldsymbol{x},r),f}((u_1, u_2), \boldsymbol{\xi}) \tag{2.45}$$

for $u_0 \in [u_1, u_2]$, the same argument as for the Madelung deletion rule works for the interval $[u_1, u_2]$. This concludes the proof. □

Since the memory of the Preisach operator consists entirely of relay operators, we immediately obtain:

COROLLARY 2.4.7. *Under uniaxial input the vector Preisach operator $\boldsymbol{\mathcal{P}}$ forgets according to the Preisach ordering.*

THEOREM 2.4.8 (Reduction to an operator of Preisach type). *Under uniaxial input satisfying* (2.41), *$\boldsymbol{\mathcal{P}}$ reduces to an operator of Preisach type with $\psi_{-1} \equiv 0$.*

PROOF. We show that $\boldsymbol{\mathcal{P}}$ forgets according to the initial state dependent deletion rule, which takes the form (2.42). Assume $|u_0| \leq |u_1|$. This implies $|u_1| \geq R$, and the formulation of Corollary 2.3.11 in terms of strings results in

$$\boldsymbol{\mathcal{P}}_f(u_0, \dots, u_N) = \boldsymbol{\mathcal{P}}_f(u_1, \dots, u_N).$$

Together with Corollary 2.4.7, $\boldsymbol{\mathcal{P}}$ therefore forgets according to the ordering $\leq_{\psi_{-1}}$ and satisfies Theorem 2.4.5. □

REMARK. Note that the discussed memory deletion properties of $\boldsymbol{\mathcal{P}}$ are independent of ω. They are satisfied for all vector Preisach operators, if ω is isotropic or not.

Assumption (2.41) is necessary because initial state effects will generally impede appropriate initial state dependent deletions. As counterexample, consider $\boldsymbol{\mathcal{P}}$ with neutral initial state $\boldsymbol{\xi}^0$. If there was a corresponding scalar Preisach operator, it would have to satisfy the symmetry condition (2.20). Therefore, its initial state would have to be ξ^0 and the corresponding memory curve $\psi_{-1} \equiv 0$. We can show that $\boldsymbol{h}_{(\boldsymbol{x},r)}$ does not satisfy the initial state dependent deletion (2.42), because with $u_0 = 0$ and $u_1 < R$ we have

$$\boldsymbol{h}_{(\boldsymbol{x},r),f}((u_0, -u_1, u_1), \boldsymbol{\xi}^0_{(\boldsymbol{x},r)}) \neq \boldsymbol{h}_{(\boldsymbol{x},r),f}((u_0, u_1), \boldsymbol{\xi}^0_{(\boldsymbol{x},r)}) \tag{2.46}$$

for almost all $(\boldsymbol{x}, r) \in \mathcal{K}$ such that

$$\|\boldsymbol{x}\| < r, \quad \|(u_1, 0, \dots, 0)^T - \boldsymbol{x}\| < r, \quad \text{and } \|(-u_1, 0, \dots, 0)^T - \boldsymbol{x}\| \geq r. \tag{2.47}$$

This is because for $(\boldsymbol{x}, r)$ satisfying (2.47),

$$\boldsymbol{h}_{(\boldsymbol{x},r),f}((u_0, u_1), \boldsymbol{\xi}^0_{(\boldsymbol{x},r)}) = \boldsymbol{\xi}^0_{(\boldsymbol{x},r)}.$$

On the other hand,

$$\boldsymbol{h}_{(\boldsymbol{x},r),f}((u_0, -u_1, u_1), \boldsymbol{\xi}^0_{(\boldsymbol{x},r)}) = \frac{(\tilde{u}, 0, \ldots, 0)^T - \boldsymbol{x}}{r}$$

where $\tilde{u} \in (-u_1, u_1)$ and $\|(\tilde{u}, 0, \ldots, 0)^T - \boldsymbol{x}\| = r$. Solving the latter equality for $\tilde{u}$, with $\boldsymbol{x} = (x_1, \ldots, x_n)$ we obtain

$$\boldsymbol{h}_{(\boldsymbol{x},r)}(0, -u_1, u_1) = \pm\frac{1}{r}\begin{pmatrix} \sqrt{r^2 - (x_2^2 + \cdots + x_n^2)} \\ x_2 \\ \vdots \\ x_n \end{pmatrix}, \tag{2.48}$$

so (2.46) is shown.

2.4.3. Scalar Preisach operators. This section briefly quotes the relevant definitions and the characterization theorem from [**16**].

Definition 2.4.9 (Preisach Operators – [**16**], Definition 2.4.6). Any hysteresis operator $\mathcal{P}$ of Preisach type that has an output mapping $Q : \Psi_0 \to \mathbb{R}$ of the form

$$Q(\psi) = \int_0^\infty q(r, \psi(r))\, \mathrm{d}\nu(r) + w_{00} \tag{2.49}$$

is called a *Preisach operator*. Here, ν denotes a regular σ-finite Borel measure on $\mathbb{R}_+$, $w_{00} \in \mathbb{R}$, and q is given by

$$q(r, s) = 2\int_0^s \omega(r, x)\, \mathrm{d}x \tag{2.50}$$

for a given function $\omega \in L^1_{loc}(\mathbb{R}_+ \times \mathbb{R}; \nu \otimes \lambda)$.

The space $L^1_{loc}(\mathbb{R}_+ \times \mathbb{R}; \nu \otimes \lambda)$ is the space of functions which are locally integrable with respect to the product measure $\nu \otimes \lambda$, see [**16**]. We only consider the case where ν is the Lebesgue measure and, by Theorem 2.4.8, $\psi_{-1} \equiv 0$. From the remarks in Example 2.1.8 is it clear that then (2.49) represents a scalar Preisach operator of the form (2.3) plus constant w_{00} with $\xi = \xi^0$ and ω as in (2.50).

Brokate states that the characterizing feature of scalar Preisach operators is the existence of a so-called shape function [**16**].

Definition 2.4.10 (shape function – [**16**], Definition 2.9.1). We say that a hysteresis operator $\mathcal{W}$ of Preisach type with initial state $\psi_{-1} \in \Psi_0$ has the *shape function* $\ell : \mathbb{R}^2 \to \mathbb{R}$, if

$$\mathcal{W}_f(s) = \mathcal{W}_f(v_0, \ldots, v_{N-1}) + \ell(v_{N-1}, v_N)$$

for all $s = (v_0, \ldots, v_N) \in \bar{S}(\psi_{-1})$, where

$$\bar{S}(\psi_{-1}) := \{(v_0, \ldots, v_N) \mid R_M(v_1; \psi_{-1}) \leq R_I(v_0; \psi_{-1}), v_{i+1} \in [v_{i-1}, v_i] \text{ for } 1 \leq i < N\}.$$

As a result of Theorem 2.4.8 we only need to consider initial state $\psi_{-1} \equiv 0$ in our investigations. Equation (2.42) implies that $\bar{S}(\psi_{-1})$ then takes the form

$$\bar{S}(0) = \{(v_0, \dots, v_N) \mid |v_1| \le |v_0|,\ v_{i+1} \in [v_{i-1}, v_i] \text{ for } 1 \le i < N\}.$$

In view of the subsequent theorem, define $S(\psi_{-1})$ to be the set containing all strings in S that are irreducible with respect to the ordering $\le_{\psi_{-1}}$.

THEOREM 2.4.11 (Characterization of scalar Preisach operators – [**16**], Theorem 2.9.4). *Let $\mathcal{W}$ be a hysteresis operator of Preisach type having the initial state $\psi_{-1} \in \Psi_0$ and a shape function $\ell \in C(\mathbb{R}^2) \cap C^2(\{(v_1, v_2) \mid v_1 \le v_2\})$. Consider the Preisach operator $\mathcal{P}$ defined by*

$$\mathcal{P}[v](t) := \int_0^\infty q(r, \mathcal{F}_r[v; \psi_{-1}(r)](t))\, \mathrm{d}r + q_0(v(t)),$$

where, for $r \ge 0$ and $s \in \mathbb{R}$,

$$q(r,s) := 2\int_0^s \tilde{\omega}(r,\sigma)\, \mathrm{d}\sigma, \quad \tilde{\omega}(r,s) := -\partial_{y_1 y_2}\ell(y_1, y_2)\,|_{y_1 = s-r, y_2 = s+r},$$

$$q_0(s) := \frac{1}{2}\int_0^s (\partial_{y_2} - \partial_{y_1})\ell(y_1, y_2)\,|_{y_1 = y_2 = \sigma}\ \mathrm{d}\sigma.$$

Then also $\mathcal{P}$ has the shape function ℓ, and the final value mappings $\mathcal{W}_f$ and $\mathcal{P}_f$ satisfy

$$\mathcal{W}_f(s) - \mathcal{P}_f(s) = \mathcal{W}_f(v_0) - \mathcal{P}_f(v_0), \quad \forall s = (v_0, \dots, v_N) \in S(\psi_{-1}),$$

i.e. $\mathcal{W}_f$ and $\mathcal{P}_f$ coincide except for effects due to initial states.

2.4.4. Reduction to a scalar Preisach operator. In this section, we will show that if $\boldsymbol{\mathcal{P}}$ has an isotropic Preisach density ω, then it has a shape function ℓ under uniaxial input. Assuming that ω is continuous, we will differentiate ℓ to obtain $\tilde{\omega}$.

So far, we have not discussed if the output is uniaxial at all. As a matter of fact, if $\boldsymbol{u}$ satisfies (2.40) and (2.41) and ω is isotropic, then $\boldsymbol{w} = \boldsymbol{\mathcal{P}}[\boldsymbol{u}]$ is of the form

$$\boldsymbol{w}(t) = (w(t), 0, \dots, 0)^T. \tag{2.51}$$

This is a consequence of Lemmas 2.3.3 and 1.3.2, which imply that

$$Q\boldsymbol{w}(t) = \boldsymbol{\mathcal{P}}_{Q\omega}[Q\boldsymbol{u}, Q\boldsymbol{\xi}] = \boldsymbol{\mathcal{P}}_{\omega}[\boldsymbol{u}, Q\boldsymbol{\xi}] = \boldsymbol{w} \quad \text{for all } Q \in O^1(n),$$

since all relays $\boldsymbol{h}_{(\boldsymbol{x},r)}$ lying in $\mathcal{K}$ have left their initial state $\boldsymbol{\xi}_{(\boldsymbol{x},r)}$.

We will show that $u(t)$ and $w(t)$ are related through a scalar Preisach operator, which we denote by $\mathcal{P}$,

$$w = \mathcal{P}[u].$$

For this, we present the shape function ℓ characterizing $\mathcal{P}$. We will use ℓ to derive an explicit representation of $\mathcal{P}$ by Theorem 2.4.11.

Before getting started, however, we must provide a few definitions needed in the subsequent computations. In the context of uniaxial input functions we will write $\mathcal{C}_y$ as short for the cone based at the input vector $(y, 0, \dots, 0)^T$, that is,

$$\mathcal{C}_y = \mathcal{C}_{(y,0,\dots,0)^T}.$$

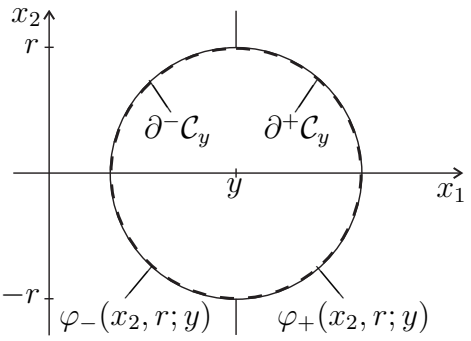

FIGURE 2.10. Illustration of φ_-, φ_+, $\partial^- C_y$ and $\partial^+ C_y$ for $n = 2$.

Define the functions

$$\varphi_-(x_2, \dots, x_n, r; y) := \begin{cases} y - \sqrt{r^2 - (x_2^2 + \cdots + x_n^2)}, & \text{if } x_2^2 + \cdots + x_n^2 < r^2, \\ y & \text{otherwise,} \end{cases}$$

$$\varphi_+(x_2, \dots, x_n, r; y) := \begin{cases} y + \sqrt{r^2 - (x_2^2 + \cdots + x_n^2)}, & \text{if } x_2^2 + \cdots + x_n^2 < r^2, \\ y & \text{otherwise.} \end{cases}$$

The boundary $\partial \mathcal{C}_y$ can be represented as disjoint union

$$\partial \mathcal{C}_y = \partial^- \mathcal{C}_y \cup \partial^+ \mathcal{C}_y$$

of the two halfshells

$$\partial^- \mathcal{C}_y := \{(x_1, \dots, x_n, r) \mid x_2^2 + \cdots + x_n^2 < r^2,\ x_1 = \varphi_-(x_2, \dots, x_n, r; y)\},$$
$$\partial^+ \mathcal{C}_y := \{(x_1, \dots, x_n, r) \mid x_2^2 + \cdots + x_n^2 < r^2,\ x_1 = \varphi_+(x_2, \dots, x_n, r; y)\}.$$

For an illustration, see Figure 2.10. It will be notationally advantageous to define

$$\partial^0 \mathcal{C}_y := \varnothing.$$

By (2.51), it suffices to look at the first vector component of the relay states and neglect the other dimensions, which cancel out. Define

$$f_{\text{out}}(x_1, \dots, x_n; y) := \frac{y - x_1}{\sqrt{(y - x_1)^2 + x_2^2 + \cdots + x_n^2}},$$

which represents the x_1-component of the state

$$\frac{(y, 0, \dots, 0)^T - \boldsymbol{x}}{\|(y, 0, \dots, 0)^T - \boldsymbol{x}\|}$$

of all relays outside the freeze cone $\mathcal{C}_y$. The function f_{out} is absolutely bounded by 1, and defined and continuously differentiable everywhere but at $(y, 0, \dots, 0)$, where it has a jump discontinuity. It varies in y, and where $\boldsymbol{x} \neq (y, 0, \dots, 0)^T$,

$$\partial_y f_{\text{out}}(\boldsymbol{x}; y) = \frac{x_2^2 + \cdots + x_n^2}{((x_1 - y)^2 + x_2^2 + \cdots + x_n^2)^{\frac{3}{2}}}. \tag{2.52}$$

The function

$$f_{\text{in}}(x_2,\dots,x_n,r) := \begin{cases} \sqrt{1-\frac{x_2^2+\cdots+x_n^2}{r^2}}, & \text{if } x_2^2+\cdots+x_n^2 \le r^2, \\ 0 & \text{otherwise,} \end{cases}$$

defines the first component of the relay states inside any $\mathcal{C}_y$ up to sign as derived in Equation (2.48), continuously extended with 0 to all of $\mathbb{R}^n \times \mathbb{R}_+$.

Let $\Pi_i : \mathbb{R}^n \times \mathbb{R}_+ \to \mathbb{R}^{n-1} \times \mathbb{R}_+$ be the projection map onto the orthogonal complement of the x_i-axis,

$$\Pi_i(x_1,\dots,x_n,r) = (x_1,\dots,x_{i-1},x_{i+1},\dots,x_n,r).$$

To project out multiple dimensions, define

$$\Pi_{i_1\dots i_m}(x_1,\dots,x_n,r) = \Pi_{i_1}\cdots\Pi_{i_m}(x_1,\dots,x_n,r), \quad i_j \in \{1,\dots,n\}.$$

Define the sign function

$$\operatorname{sign}(x) := \begin{cases} 1 & \text{if } x > 0, \\ 0 & \text{if } x = 0, \\ -1 & \text{if } x < 0. \end{cases}$$

LEMMA 2.4.12 (Shape function). *If ω is isotropic and of bounded support, then $\mathcal{P}$ satisfies*

$$\mathcal{P}(u_0,\dots,u_N) = \mathcal{P}(u_0,\dots,u_{N-1}) + \ell(u_{N-1},u_N) \tag{2.53}$$

for all strings $(u_0,\dots,u_N) \in \overline{S}(0)$ such that $|u_0| \ge R$. The shape function $\ell : \mathbb{R}^2 \to \mathbb{R}$ is given by

$$\begin{aligned} \ell(y_1,y_2) = &\int_{(\mathbb{R}_+\times\mathbb{R}^n)\setminus\mathcal{C}_{y_2}} \omega(\boldsymbol{x},r) f_{\text{out}}(\boldsymbol{x};y_2)\,\mathrm{d}(\boldsymbol{x},r) \\ &- \int_{(\mathbb{R}_+\times\mathbb{R}^n)\setminus\mathcal{C}_{y_1}} \omega(\boldsymbol{x},r) f_{\text{out}}(\boldsymbol{x};y_1)\,\mathrm{d}(\boldsymbol{x},r) \\ &+ \operatorname{sign}(y_1-y_2) \int_{(\mathcal{C}_{y_1}\setminus\mathcal{C}_{y_2})\cup(\mathcal{C}_{y_2}\setminus\mathcal{C}_{y_1})} \omega(\boldsymbol{x},r) f_{\text{in}}(x_2,\dots,x_n,r)\,\mathrm{d}(\boldsymbol{x},r). \end{aligned} \tag{2.54}$$

PROOF. It suffices to consider the subdomain $\mathcal{K}$ where $\omega(\boldsymbol{x},r) \neq 0$. We can easily derive the x_1-components of the relay states $\boldsymbol{h}_{(\boldsymbol{x},r),f}(u_0,\dots,u_i)$ by induction. For the string (u_0), by assumption $|u_0| \ge R$, we have that

$$\boldsymbol{h}_{(\boldsymbol{x},r),f}(u_0) = f_{\text{out}}(\boldsymbol{x};u_0) \quad \text{for all } (\boldsymbol{x},r) \in \mathcal{K}.$$

For the string $(u_0,\dots,u_i)$, $0 < i \le N$,

$$\boldsymbol{h}_{(\boldsymbol{x},r),f}(u_0,\dots,u_i) = \begin{cases} f_{\text{out}}(\boldsymbol{x};u_i) & \text{if } (\boldsymbol{x},r) \in \mathcal{K}\setminus\mathcal{C}_{u_i}, \\ \boldsymbol{h}_{(\boldsymbol{x},r),f}(u_0,\dots,u_{i-1}) & \text{if } (\boldsymbol{x},r) \in \mathcal{C}_{u_i}\cap\mathcal{C}_{u_{i-1}}, \\ -\operatorname{sign}(u_i-u_{i-1}) f_{\text{in}}(x_2,\dots,x_n,r) & \text{if } (\boldsymbol{x},r) \in \mathcal{C}_{u_i}\setminus\mathcal{C}_{u_{i-1}}. \end{cases}$$

At $N = 1$, Equation (2.54) is quickly confirmed for $\ell(u_0,u_1)$. Assume now $N \ge 2$. Split the integral $\boldsymbol{\mathcal{P}}_f(u_0,\dots,u_N)$ into a sum of integrals over the three subdomains $\mathcal{K}\setminus\mathcal{C}_{u_N}$, $\mathcal{C}_{u_N}\cap\mathcal{C}_{u_{N-1}}$, and $\mathcal{C}_{u_N}\setminus\mathcal{C}_{u_{N-1}}$, and the integral $\boldsymbol{\mathcal{P}}_f(u_0,\dots,u_{N-1})$

over the subdomains $\mathcal{K} \setminus \mathcal{C}_{u_{N-1}}$, $\mathcal{C}_{u_N} \cap \mathcal{C}_{u_{N-1}}$, and $\mathcal{C}_{u_{N-1}} \setminus \mathcal{C}_{u_N}$. By the assumption $u_N \in [u_{N-2}, u_{N-1}]$, we have $\mathcal{C}_{u_{N-1}} \setminus \mathcal{C}_{u_N} \subseteq \mathcal{C}_{u_{N-1}} \setminus \mathcal{C}_{u_{N-2}}$ and $\operatorname{sign}(u_{N-1} - u_{N-2}) = -\operatorname{sign}(u_N - u_{N-1})$. Therefore $\boldsymbol{h}_{(\boldsymbol{x},r),f}(u_0, \dots, u_i)$ on this subdomain is given by the last line in the preceeding formula. We then obtain Equation (2.54) for $\ell(u_{N-1}, u_N)$ by taking the difference of $\boldsymbol{\mathcal{P}}_f(u_0, \dots, u_N)$ and $\boldsymbol{\mathcal{P}}_f(u_0, \dots, u_{N-1})$. □

Obviously, the shape function satisfies

$$\ell(y_1, y_2) = -\ell(y_2, y_1) \text{ for all } y_1, y_2 \in \mathbb{R},$$

and, in particular, $\ell(y, y) = 0$ for all $y \in \mathbb{R}$, as it should [**16**].

In view of deriving $\tilde{\omega}$, the following lemma explicitly specifies the derivatives $\partial_{y_1}\ell(y_1, y_2)$, $\partial_{y_2}\ell(y_1, y_2)$ and $\partial_{y_1 y_2}\ell(y_1, y_2)$. In preparation, define the function

$$\begin{aligned}
&\vartheta(x_3, \dots, x_n, r, y_1, y_2) \\
&\quad := \begin{cases} \sqrt{r^2 - x_3^2 - \cdots - x_n^2 - \frac{1}{4}(y_1 - y_2)^2} & \text{if } r \geq \frac{|y_1 - y_2|}{2} \text{ and} \\ & x_3^2 + \cdots + x_n^2 \leq r^2 - \frac{1}{4}(y_1 - y_2)^2, \\ 0 & \text{otherwise.} \end{cases}
\end{aligned}$$

Set

$$\kappa = \operatorname{sign}(y_1 - y_2)$$

and

$$\tilde{\boldsymbol{x}} = (x_2, \dots, x_n).$$

LEMMA 2.4.13. *Assume that ω is isotropic, continuous and of bounded support $\mathcal{K}$, and that $y_1 \neq y_2$. Then the first partial derivatives $\partial_{y_1}\ell(y_1, y_2)$ and $\partial_{y_2}\ell(y_1, y_2)$ are continuous, and*

$$\begin{aligned}
\partial_{y_1}\ell(y_1, y_2) = &- \int_{\mathcal{K} \setminus \mathcal{C}_{y_1}} \omega(\boldsymbol{x}, r) \partial_{y_1} f_{\text{out}}(\boldsymbol{x}; y_1) \, \mathrm{d}(\boldsymbol{x}, r) \\
&- 2 \int_{\Pi_{x_1}(\partial^{-\kappa}\mathcal{C}_{y_1} \setminus \mathcal{C}_{y_2})} \omega(\varphi_{-\kappa}(\tilde{\boldsymbol{x}}, r; y_1), \tilde{\boldsymbol{x}}, r) f_{\text{in}}(\tilde{\boldsymbol{x}}) \, \mathrm{d}(\tilde{\boldsymbol{x}}, r), \\
\partial_{y_2}\ell(y_1, y_2) = &\int_{\mathcal{K} \setminus \mathcal{C}_{y_2}} \omega(\boldsymbol{x}, r) \partial_{y_2} f_{\text{out}}(\boldsymbol{x}; y_2) \, \mathrm{d}(\boldsymbol{x}, r) \\
&+ 2 \int_{\Pi_{x_1}(\partial^{\kappa}\mathcal{C}_{y_2} \setminus \mathcal{C}_{y_1})} \omega(\varphi_{\kappa}(\tilde{\boldsymbol{x}}, r; y_2), \tilde{\boldsymbol{x}}, r) f_{\text{in}}(\tilde{\boldsymbol{x}}) \, \mathrm{d}(\tilde{\boldsymbol{x}}, r), \\
\partial_{y_1 y_2}\ell(y_1, y_2) = &\ \kappa \frac{(y_1 - y_2)^2}{4} \int_{\Pi_{x_1 x_2}(\partial\mathcal{C}_{y_1} \cap \partial\mathcal{C}_{y_2})} \frac{1}{r \vartheta(x_3, \dots, x_n, r, y_1, y_2)} \\
&\Big[\omega\left(\tfrac{y_1 + y_2}{2}, -\vartheta(x_3, \dots, x_n, r, y_1, y_2), x_3, \dots, x_n, r\right) \\
&+ \omega\left(\tfrac{y_1 + y_2}{2}, \vartheta(x_3, \dots, x_n, r, y_1, y_2), x_3, \dots, x_n, r\right) \Big] \, \mathrm{d}x_3 \cdots \mathrm{d}x_n \, \mathrm{d}r.
\end{aligned}$$

We will proof Lemma 2.4.13 by a sequence of lemmas using differentiation under the integral sign as introduced in Section 1.2.1. The first lemma is an auxiliary result on uniform convergence.

LEMMA 2.4.14. *Let $\mathcal{K}$ be a compact set, and $\{F_n\}$ a bounded increasing sequence of continuous functions $F_n : \mathcal{K} \to \mathbb{R}$ converging pointwise to a function F. Then $F_n \to F$ uniformly.*

PROOF. We will show that for the sequence $\{f_n := F - F_n\} \to 0$ the convergence is uniform. Let $\epsilon > 0$ and $x \in \mathcal{K}$. There is an open neighbourhood U_x of x such that there exists $N \in \mathbb{N}$ satisfying

$$f_n(y) < \epsilon \quad \text{for all } y \in U_x \text{ and for all } n > N.$$

This is because f_N is continuous and $f_n(y) \leq f_N(y)$ for all $y \in \mathcal{K}$ and for all $n > N$, so $f_N(x) < \epsilon$ implies $f_n(y) \leq f_N(y) < \epsilon$ in some open neighbourhood of x. By compactness of $\mathcal{K}$, there exists a finite subcover $\{U_{x_i}\}$ of $\mathcal{K}$ with respect to ϵ. Setting $N = \max N_i$, we have that

$$f_n(y) < \epsilon \quad \text{for all } y \in \mathcal{K} \text{ and for all } n > N,$$

and thus uniform convergence. □

LEMMA 2.4.15. *Assume that ω is continuous and of bounded support $\mathcal{K}$. The function $F : \mathbb{R} \to \mathbb{R}$,*

$$F(y) := \int_{\mathcal{K}\setminus C(y)} \omega(\boldsymbol{x}, r) f_{\text{out}}(\boldsymbol{x}, y)\, \mathrm{d}(\boldsymbol{x}, r).$$

is continuous. Its derivative exists, is continuous and given by

(2.55)

$$\begin{aligned}\partial_y F(y) = &\int_{\mathcal{K}\setminus\mathcal{C}_y} \omega(\boldsymbol{x}, r)\partial_y f_{\text{out}}(\boldsymbol{x}, y)\, \mathrm{d}(\boldsymbol{x}, r) \\ &+ \int_{\Pi_1\mathcal{C}_y} \left(\omega(\varphi_-(\tilde{\boldsymbol{x}}, r; y), \tilde{\boldsymbol{x}}, r) + \omega(\varphi_+(\tilde{\boldsymbol{x}}, r; y), \tilde{\boldsymbol{x}}, r)\right) f_{\text{in}}(\tilde{\boldsymbol{x}}, r)\, \mathrm{d}(\tilde{\boldsymbol{x}}, r).\end{aligned}$$

PROOF. Assume without loss of generality $\omega \geq 0$. If this does not hold true, write $F(y)$ in terms of $\omega^+ = \max(\omega, 0)$ and $\omega^- = \max(-\omega, 0)$. Fix y_0. We will show the statements hold in y_0.

To apply Corollary 1.2.3 to $F(y)$, we replace $\mathcal{K}$ by the box $[0, R] \times [-R, R]^n$ containing it and parametrize the boundary of $\mathcal{C}_y$ in terms of the functions φ_- and φ_+, obtaining

$$F(y) = F_-(y) + F_+(y) \tag{2.56}$$

with

$$\begin{aligned}F_-(y) &:= \int_0^R \int_{-R}^R \cdots \int_{-R}^R \int_{-R}^{\varphi_-(x_2,\ldots,x_n,r,y)} \omega(\boldsymbol{x}, r) f_{\text{out}}(\boldsymbol{x}, r, y)\, \mathrm{d}x_1\, \mathrm{d}x_2 \cdots \mathrm{d}x_n\, \mathrm{d}r, \\ F_+(y) &:= \int_0^R \int_{-R}^R \cdots \int_{-R}^R \int_{\varphi_+(x_2,\ldots,x_n,r,y)}^R \omega(\boldsymbol{x}, r) f_{\text{out}}(\boldsymbol{x}, r, y)\, \mathrm{d}x_1\, \mathrm{d}x_2 \cdots \mathrm{d}x_n\, \mathrm{d}r.\end{aligned}$$

The function f_{out} has a jump discontinuity on the boundary of the integration domain at $(\boldsymbol{x}, r) = (y, 0, \ldots, 0, 0)$, resulting in an essential discontinuity for $\partial_y f_{\text{out}}$ with limit ∞ along some paths approaching this point. Because of this, Corollary 1.2.3 cannot be applied directly and we pass to a limit argument. Both $F_-(y)$ and $F_+(y)$

can be dealt with in the exactly same way, so we will only consider $F_-(y)$ from now on.

Define the sequence of functions

$$F_{-,m}(y) := \int_{\frac{1}{m}}^{R} \int_{-R}^{R} \cdots \int_{-R}^{R} \int_{-R}^{\varphi_-(x_2,\ldots,x_n,r,y)} \omega(\boldsymbol{x},r) f_{\text{out}}(\boldsymbol{x},r,y)\,\mathrm{d}x_1\,\mathrm{d}x_2 \cdots \mathrm{d}x_n\,\mathrm{d}r.$$

and a sequence of sets

$$U_m(y) := \{(\boldsymbol{x},r) \mid r \in [0,R],\ x_1 \in [-R,\ \varphi_-(x_1,\ldots,x_n,\tfrac{1}{2m},y)],\\ x_2,\ldots,x_n \in [-R,R]\}.$$

The sequences are chosen so that for all m, the discontinuity is excluded from the integral and ωf_{out} satisfies the assumptions of Corollary 1.2.3(a) on $U_m(y_0) \times \left[y_0 - \frac{1}{4m}, y_0 + \frac{1}{4m}\right]$. Thus $F_{-,m}(y)$ is continuous in y_0. Fixing any $a > 0$, by the same line of argument, $F_{-,m}(y)$ is continuous for all y in the interval $[y_0 - a, y_0 + a]$. Note that by assumption ωf_{out} is nonnegative on the integration domain, so the sequence $F_{-,m}(y)$ is increasing. Thus, by Lemma 2.4.14, $F_-(y)$ is the uniform limit of continuous functions on this interval, proving the continuity statement in y_0.

Further, ωf_{out} satisfies the assumptions of Corollary 1.2.3(b) in $U_m(y_0) \times (y_0 - \frac{1}{4m}, y_0 + \frac{1}{4m})$, and $\partial_y \varphi_- \equiv 1$. Therefore, $\partial_y F_{-,m}(y_0)$ exists and is given by

(2.57)

$$\partial_y F_{-,m}(y) := \int_{\frac{1}{m}}^{R} \int_{-R}^{R} \cdots \int_{-R}^{R} \Bigg[\int_{-R}^{\varphi_-(x_2,\ldots,x_n,r,y)} \omega(\boldsymbol{x},r) \partial_y f_{\text{out}}(\boldsymbol{x},r,y)\,\mathrm{d}x_1 \\ + \left[\omega(\boldsymbol{x},r) f_{\text{out}}(\boldsymbol{x},r)\right] \big|_{x_1=\varphi_-(\tilde{\boldsymbol{x}},r,y)} \Bigg] \mathrm{d}x_2 \cdots \mathrm{d}x_n\,\mathrm{d}r$$

evaluated at $y = y_0$.

To show that $\partial_y F_-(y) \,|_{y=y_0}$ exists and is equal to

$$\lim_{m\to\infty} \partial_y F_{-,m}(y) \,|_{y=y_0}, \tag{2.58}$$

we first show the existence of (2.58) and then apply Lemma 1.2.7 to exchange limit and differentiation.

For the second integrand in (2.57), the existence of the limit integral is clear by the monotone convergence theorem. For the first integrand with its discontinuity at $(\boldsymbol{x}, r) = (y, 0, \ldots, 0, 0)$, the limit integral exists as a consequence of Lemma 1.2.17, since ω is bounded.

To exchange limit and differentiation, define the pointwise limit

$$D(y) := \lim_{m\to\infty} \partial_y F_{-,m}(y).$$

As for any m and y, all functions involved are continuous on $U_m(y) \times \left[y - \frac{1}{4m}, y + \frac{1}{4m}\right]$, Corollary 1.2.3(a) gives the continuity of $\partial_y F_{-,m}(y)$ on $[y_0 - a, y_0 + a]$. As ω, f_{out} and $\partial_y f_{\text{out}}$ are nonnegative, the sequence $\partial_y F_{-,m}(y)$ is increasing, so by Lemma 2.4.14 it converges to $D(y)$ uniformly on $[y_0 - a, y_0 + a]$. Thus, we have the continuity of

$D(y)$ on this interval, and by Lemma 1.2.7 we can exchange limit and differentiation and get

$$\partial_y F_-(y) \mid_{y=y_0} = D(y_0).$$

Applying the same line of argument to $F_+(y)$, we obtain

$$\begin{aligned}\partial_y F(y) =& \partial_y F_-(y) + \partial_y F_+(y)\\ =& \int_0^R \int_{-R}^R \cdots \int_{-R}^R \Bigg[\int_{-R}^{\varphi_-(x_2,\dots,x_n,r,y)} \omega(\boldsymbol{x},r)\partial_y f_{\text{out}}(\boldsymbol{x},r,y)\,\mathrm{d}x_1\\ &+ [\omega(\boldsymbol{x},r)f_{\text{out}}(\boldsymbol{x},r)] \mid_{x_1=\varphi_-(\tilde{\boldsymbol{x}},r,y)}\\ &+ \int_{\varphi_+(x_2,\dots,x_n,r,y)}^{R} \omega(\boldsymbol{x},r)\partial_y f_{\text{out}}(\boldsymbol{x},r,y)\,\mathrm{d}x_1\\ &- [\omega(\boldsymbol{x},r)f_{\text{out}}(\boldsymbol{x},r)] \mid_{x_1=\varphi_+(\tilde{\boldsymbol{x}},r,y)} \Bigg] \mathrm{d}x_2 \cdots \mathrm{d}x_n\,\mathrm{d}r.\end{aligned}$$

For $(x_2,\dots,x_n) \notin \Pi_1\mathcal{C}_y$, the second and the fourth term cancel:

$$[\omega(\boldsymbol{x},r)f_{\text{out}}(\boldsymbol{x},r)] \mid_{x_1=\varphi_-(\tilde{\boldsymbol{x}},r,y)} - [\omega(\boldsymbol{x},r)f_{\text{out}}(\boldsymbol{x},r)] \mid_{x_1=\varphi_+(\tilde{\boldsymbol{x}},r,y)} = 0. \tag{2.59}$$

If $(x_2,\dots,x_n) \in \Pi_1\mathcal{C}_y$, on the other hand, then for $\alpha \in \{+,-\}$ we have

$$f_{\text{out}}(\varphi_\alpha(\tilde{\boldsymbol{x}},r,y),\tilde{\boldsymbol{x}},r) = -\alpha\sqrt{1-\tfrac{x_2^2+\cdots+x_n^2}{r^2}} = -\alpha\, f_{\text{in}}(\tilde{\boldsymbol{x}},r).$$

This concludes the proof. □

LEMMA 2.4.16. *The function*

$$G(y_1,y_2) := \int_{\mathcal{C}_{y_1}\setminus\mathcal{C}_{y_2}} \omega(\boldsymbol{x},r) f_{\text{in}}(\tilde{\boldsymbol{x}},r)\,\mathrm{d}(\boldsymbol{x},r).$$

is continuous. For $y_1 \neq y_2$, its derivatives are

$$\begin{aligned}\partial_{y_1} G(y_1,y_2) = \kappa\Bigg[&\int_{\Pi_1\mathcal{C}_{y_1}} \omega(\varphi_\kappa(\tilde{\boldsymbol{x}},r,y_1),\tilde{\boldsymbol{x}},r) f_{\text{in}}(\tilde{\boldsymbol{x}},r)\,\mathrm{d}(\tilde{\boldsymbol{x}},r)\\ &- \int_{\Pi_1(\partial^{-\kappa}\mathcal{C}_{y_1}\setminus\mathcal{C}_{y_2})} \omega(\varphi_{-\kappa}(\tilde{\boldsymbol{x}},r,y_1),\tilde{\boldsymbol{x}},r) f_{\text{in}}(\tilde{\boldsymbol{x}},r)\,\mathrm{d}(\tilde{\boldsymbol{x}},r)\Bigg]\end{aligned}$$

and

$$\partial_{y_2} G(y_1,y_2) = -\kappa \int_{\Pi_1(\partial^{\kappa}\mathcal{C}_{y_2}\cap\mathcal{C}_{y_1})} \omega(\varphi_\kappa(\tilde{\boldsymbol{x}},r,y_2),\tilde{\boldsymbol{x}},r) f_{\text{in}}(\tilde{\boldsymbol{x}},r)\,\mathrm{d}(\tilde{\boldsymbol{x}},r).$$

PROOF. Assume first $y_1 > y_2$. The approach is the same as in the preceeding proof, but as the integrand here is continuous everywhere and its derivative with respect to y_1 and y_2 is equal to 0, we can apply Corollary 1.2.3 directly. As first step, we again parametrize the boundaries of the integral. Define the continuous function

$$\varphi_\wr(\tilde{\boldsymbol{x}},r,y_1,y_2) := \begin{cases}\varphi_+(\tilde{\boldsymbol{x}},r,y_2), & \text{if } \varphi_+(\tilde{\boldsymbol{x}},r,y_2) \geq \varphi_-(\tilde{\boldsymbol{x}},r,y_1)\\ \varphi_-(\tilde{\boldsymbol{x}},r,y_1), & \text{otherwise.}\end{cases}$$

With this,

$$G(y_1,y_2)=\int_0^R\int_{-R}^R\cdots\int_{-R}^R\int_{\varphi_\wr(\tilde{\boldsymbol{x}},r,y_1,y_2)}^{\varphi_+(\tilde{\boldsymbol{x}},r,y_1)}\omega(\boldsymbol{x},r)f_{\mathrm{in}}(\tilde{\boldsymbol{x}},r)\,\mathrm{d}(\boldsymbol{x},r).$$

As $\varphi_\wr$ and φ_+ are continuous, G is continuous by Corollary 1.2.3(a).

To obtain the derivatives as stated, apply Corollary 1.2.3(b) and for $\partial_{y_1}G(y_1,y_2)$ cancel as in Equation (2.59). The derivatives of the functions involved are

$$\partial_{y_i}f_{\mathrm{in}}(\tilde{\boldsymbol{x}},r)=0,\quad i=1,2,$$
$$\partial_{y_1}\varphi_+(\tilde{\boldsymbol{x}},r,y_1)=1,\quad \partial_{y_2}\varphi_+(\tilde{\boldsymbol{x}},r,y_1)=0,$$
$$\partial_{y_1}\varphi_\wr(\tilde{\boldsymbol{x}},r,y_1,y_2)=\begin{cases}0, & \text{if } \varphi_+(\tilde{\boldsymbol{x}},r,y_2)\geq\varphi_-(\tilde{\boldsymbol{x}},r,y_1)\\ 1, & \text{otherwise,}\end{cases}$$
$$\partial_{y_2}\varphi_\wr(\tilde{\boldsymbol{x}},r,y_1,y_2)=\begin{cases}1, & \text{if } \varphi_+(\tilde{\boldsymbol{x}},r,y_2)\geq\varphi_-(\tilde{\boldsymbol{x}},r,y_1)\\ 0, & \text{otherwise.}\end{cases}$$

For $y_1<y_2$, define $\varphi_\wr$ by

$$\varphi_\wr(\tilde{\boldsymbol{x}},r,y_1,y_2):=\begin{cases}\varphi_-(\tilde{\boldsymbol{x}},r,y_2), & \text{if } \varphi_-(\tilde{\boldsymbol{x}},r,y_2)\geq\varphi_+(\tilde{\boldsymbol{x}},r,y_1),\\ \varphi_+(\tilde{\boldsymbol{x}},r,y_1), & \text{otherwise,}\end{cases}$$

so

$$G(y_1,y_2)=\int_0^R\int_{-R}^R\cdots\int_{-R}^R\int_{\varphi_-(\tilde{\boldsymbol{x}},r,y_1)}^{\varphi_\wr(\tilde{\boldsymbol{x}},r,y_1,y_2)}\omega(\boldsymbol{x},r)f_{\mathrm{in}}(\tilde{\boldsymbol{x}},r)\,\mathrm{d}(\boldsymbol{x},r).$$

Proceed as for $y_1>y_2$.

Regarding continuity at $y_1=y_2$, it is easily seen that

$$\lim_{y_1\to y_2+}G(y_1,y_2)=0=\lim_{y_1\to y_2-}G(y_1,y_2).\qquad\square$$

LEMMA 2.4.17. *Assume that ω is continuous and of bounded support $\mathcal{K}$, and $y_1\neq y_2$. Then $\partial_{y_1}G(y_1,y_2)$ and $\partial_{y_2}G(y_1,y_2)$ are continuous, and, if this integral exists,*

$$\begin{aligned}\partial_{y_1y_2}G(y_1,y_2)=&\kappa\frac{(y_1-y_2)^2}{8}\int_{\Pi_{12}(\partial\mathcal{C}_{y_1}\cap\partial\mathcal{C}_{y_2})}\frac{1}{r\vartheta(x_3,\dots,x_n,r,y_1,y_2)}\\&\Big[\omega\left(\tfrac{y_1+y_2}{2},-\vartheta(x_3,\dots,x_n,r,y_1,y_2),x_3,\dots,x_n,r\right)\\&+\omega\left(\tfrac{y_1+y_2}{2},\vartheta(x_3,\dots,x_n,r,y_1,y_2),x_3,\dots,x_n,r\right)\Big]\,\mathrm{d}x_3\cdots\mathrm{d}x_n\,\mathrm{d}r.\end{aligned}$$

PROOF. From the components of $\partial_{y_1}G$ and $\partial_{y_2}G$ in Lemma 2.4.16, define the functions

$$H_1(y_1,y_2):=\int_{\Pi_1\partial^\kappa\mathcal{C}_{y_1}}\omega(\varphi_{-\kappa}(\tilde{\boldsymbol{x}},r,y_1),\tilde{\boldsymbol{x}},r)\ f_{\mathrm{in}}(\tilde{\boldsymbol{x}},r)\,\mathrm{d}(\tilde{\boldsymbol{x}},r),$$
$$H_2(y_1,y_2):=\int_{\Pi_1(\partial^\kappa\mathcal{C}_{y_1}\setminus\mathcal{C}_{y_2})}\omega(\varphi_{-\kappa}(\tilde{\boldsymbol{x}},r;y_1),\tilde{\boldsymbol{x}},r)\ f_{\mathrm{in}}(\tilde{\boldsymbol{x}},r)\,\mathrm{d}(\tilde{\boldsymbol{x}},r),$$
$$H_3(y_1,y_2):=\int_{\Pi_1(\partial^{-\kappa}\mathcal{C}_{y_1}\cap\mathcal{C}_{y_2})}\omega(\varphi_{\kappa}(\tilde{\boldsymbol{x}},r,y_1),\tilde{\boldsymbol{x}},r)\quad f_{\mathrm{in}}(\tilde{\boldsymbol{x}},r)\,\mathrm{d}(\tilde{\boldsymbol{x}},r).$$

To show the continuity of $\partial_{y_1} G(y_1, y_2)$ and $\partial_{y_2} G(y_1, y_2)$, it suffices to show the continuity of H_1, H_2 and H_3.

As in the preceeding proofs, we parametrize the integrals on the box $[0, R] \times [-R, R]^n$. A point $(\boldsymbol{x}, r)$ is in $\partial^{-\kappa}\mathcal{C}_{y_1} \setminus \mathcal{C}_{y_2}$ if and only if

$$x_1 = \varphi_{-\kappa}(x_2, \dots, x_n, r, y_1), \tag{2.60}$$

$$r^2 \geq x_2^2 + \cdots + x_n^2, \tag{2.61}$$

$$r^2 \leq (x_1 - y_2)^2 + x_2^2 + \cdots + x_n^2. \tag{2.62}$$

The substitution of Equation (2.60) into (2.62) and evaluation of $\varphi_{-\kappa}$ assuming that $(x_2, \dots, x_n)$ satisfies (2.61) results in

$$0 \leq r^2 - x_2^2 - x_3^2 - \cdots - x_n^2 \leq \frac{1}{4}(y_1 - y_2)^2.$$

Together with (2.61), this gives us a parametrisation of $\Pi_1(\partial^{-\kappa}\mathcal{C}_{y_1} \setminus \mathcal{C}_{y_2})$ and, by reversing the right-hand inequality, of $\Pi_1(\partial^{-\kappa}\mathcal{C}_{y_1} \cap \mathcal{C}_{y_2})$. For $i = 3, \dots, n$, define

$$\vartheta_i(x_i, \dots, x_n, r) := \begin{cases} \sqrt{r^2 - x_i^2 - \cdots - x_n^2}, & \text{if } x_i^2 + \cdots + x_n^2 \leq r^2, \\ 0, & \text{otherwise.} \end{cases}$$

Then

$$H_1(y_1, y_2) = \int_0^R \int_{-r}^{r} \int_{-\vartheta_n(x_n,r)}^{\vartheta_n(x_n,r)} \cdots \int_{-\vartheta_4(x_4,\dots,x_n,r)}^{\vartheta_4(x_4,\dots,x_n,r)} \int_{-\vartheta_3(x_3,\dots,x_n,r)}^{\vartheta_3(x_3,\dots,x_n,r)} \omega(\varphi_\kappa(\tilde{\boldsymbol{x}}, r; y_1), \tilde{\boldsymbol{x}}, r) f_{\text{in}}(\tilde{\boldsymbol{x}}, r) \, \mathrm{d}x_2 \, \mathrm{d}x_3 \cdots \mathrm{d}x_{n-1} \, \mathrm{d}x_n \, \mathrm{d}r,$$

$$H_2(y_1, y_2) = \int_0^R \int_{-r}^{r} \int_{-\vartheta_n(x_n,r)}^{\vartheta_n(x_n,r)} \cdots \int_{-\vartheta_4(x_4,\dots,x_n,r)}^{\vartheta_4(x_4,\dots,x_n,r)} \left[\int_{-\vartheta_3(x_3,\dots,x_n,r)}^{-\vartheta(x_3,\dots,x_n,r,y_1,y_2)} + \int_{\vartheta(x_3,\dots,x_n,r,y_1,y_2)}^{\vartheta_3(x_3,\dots,x_n,r)} \right] \omega(\varphi_\kappa(\tilde{\boldsymbol{x}}, r; y_1), \tilde{\boldsymbol{x}}, r) f_{\text{in}}(\tilde{\boldsymbol{x}}, r) \, \mathrm{d}x_2 \, \mathrm{d}x_3 \cdots \mathrm{d}x_{n-1} \, \mathrm{d}x_n \, \mathrm{d}r,$$

$$H_3(y_1, y_2) = \int_0^R \int_{-r}^{r} \int_{-\vartheta_n(x_n,r)}^{\vartheta_n(x_n,r)} \cdots \int_{-\vartheta_4(x_4,\dots,x_n,r)}^{\vartheta_4(x_4,\dots,x_n,r)} \int_{-\vartheta(x_3,\dots,x_n,r,y_1,y_2)}^{\vartheta(x_3,\dots,x_n,r,y_1,y_2)} \omega(\varphi_\kappa(\tilde{\boldsymbol{x}}, r; y_1), \tilde{\boldsymbol{x}}, r) f_{\text{in}}(\tilde{\boldsymbol{x}}, r) \, \mathrm{d}x_2 \, \mathrm{d}x_3 \cdots \mathrm{d}x_{n-1} \, \mathrm{d}x_n \, \mathrm{d}r.$$

As $\omega(\varphi_\kappa(\tilde{\boldsymbol{x}}, r; y_1), \tilde{\boldsymbol{x}}, r)\, f_{\text{in}}(\tilde{\boldsymbol{x}}, r)$ is continuous in $[0, R] \times [-R, R]^n \times \mathbb{R}^2$, we get the continuity of $H_1(y_1, y_2)$, $H_2(y_1, y_2)$ and $H_3(y_1, y_2)$ from Corollary 1.2.5.

To find the double derivative $\partial_{y_1 y_2} G(y_1, y_2)$, note that

$$\partial_{y_1 y_2} G(y_1, y_2) = \partial_{y_2} H_2(y_1, y_2).$$

Since the integrand in $H_2(y_1, y_2)$ does not depend on y_2, by Corollary 1.2.3 the derivative will only consist of integrals over boundary components of the integration domain of H_2. The derivative of ϑ with respect to y_1 is

$$\partial_{y_1} \vartheta(x_3, \dots, x_n, r, y_1, y_2) = \begin{cases} -\frac{y_1 - y_2}{4\sqrt{r^2 - x_3^2 - \cdots - x_n^2 - \frac{1}{4}(y_1 - y_2)^2}}, & \text{if } r > \frac{|y_1 - y_2|}{2} \\ & \text{and } r^2 - x_3^2 - \cdots - x_n^2 - \frac{1}{4}(y_1 - y_2)^2 > 0, \\ 0, & \text{otherwise.} \end{cases}$$

It is not defined on $\partial\mathcal{C}_{y_1} \cap \partial\mathcal{C}_{y_2}$. The functions f_{in} and φ_κ evaluated at $x_2 = \pm\vartheta$ give

$$f_{\text{in}}(\tilde{\boldsymbol{x}}, r) \mid_{x_2=\pm\vartheta(x_3,\dots,x_n,r,y_1,y_2)} = \frac{|y_1 - y_2|}{2r},$$
$$\varphi_\kappa(\tilde{\boldsymbol{x}}, r; y_2) \mid_{x_2=\pm\vartheta(x_3,\dots,x_n,r,y_1,y_2)} = \frac{y_1 + y_2}{2}.$$

With this, taking in particular into account that $\partial_{y_1}\vartheta$ is 0 where

$$r^2 - x_3^2 - \cdots - x_n^2 - \tfrac{1}{4}(y_1 - y_2)^2 < 0,$$

we have

$$\begin{aligned}
\partial_{y_2} H_2(y_1, y_2) := \int_0^R \int_{-r}^{r} \int_{-\sqrt{r^2-x_n^2}}^{\sqrt{r^2-x_n^2}} \cdots \int_{-\sqrt{r^2-x_n^2-\cdots-x_4^2}}^{\sqrt{r^2-x_n^2-\cdots-x_4^2}} \quad & \partial_{y_2}\vartheta(x_3, \dots, x_n, r, y_1, y_2) \\
\Big[\omega(\varphi_\kappa(\tilde{\boldsymbol{x}}, r; y_1), \tilde{\boldsymbol{x}}, r) f_{\text{in}}(\tilde{\boldsymbol{x}}, r) \mid_{x_2=\vartheta(x_3,\dots,x_n,r,y_1,y_2)} + & \\
\omega(\varphi_\kappa(\tilde{\boldsymbol{x}}, r; y_1), \tilde{\boldsymbol{x}}, r) f_{\text{in}}(\tilde{\boldsymbol{x}}, r) \mid_{x_2=-\vartheta(x_3,\dots,x_n,r,y_1,y_2)}\Big] & \,\mathrm{d}x_3 \cdots \mathrm{d}x_{n-1}\,\mathrm{d}x_n\,\mathrm{d}r \\
= \kappa \frac{(y_1 - y_2)^2}{8} \int_{\frac{1}{2}|y_1-y_2|}^{R} \int_{-\sqrt{r^2-x_n^2-\frac{1}{4}(y_1-y_2)^2}}^{\sqrt{r^2-x_n^2-\frac{1}{4}(y_1-y_2)^2}} \cdots \int_{-\sqrt{r^2-x_n^2-\cdots-x_4^2-\frac{1}{4}(y_1-y_2)^2}}^{\sqrt{r^2-x_n^2-\cdots-x_4^2-\frac{1}{4}(y_1-y_2)^2}} & \\
\left(r\sqrt{r^2 - x_3^2 - \cdots - x_n^2 - \tfrac{1}{4}(y_1 - y_2)^2}\right)^{-1} & \\
\left[\omega\left(\tfrac{y_1+y_2}{2}, -x_2, \dots, x_n, r\right) + \omega\left(\tfrac{y_1+y_2}{2}, x_2, \dots, x_n, r\right)\right]_{x_2=\vartheta(x_3,\dots,x_n,r,y_1,y_2)} & \\
\mathrm{d}x_3 \cdots \mathrm{d}x_{n-1}\,\mathrm{d}x_n\,\mathrm{d}r. &
\end{aligned}$$

The integration domain is exactly the projection with respect to x_1 and x_2 of

$$\begin{aligned}
\partial\mathcal{C}_{y_1} \cap \partial\mathcal{C}_{y_2} = \Big\{ & x_1 = \tfrac{y_1+y_2}{2},\ x_2 = \pm\vartheta(x_3, \dots, x_n, r, y_1, y_2), \\
& r^2 - x_3^2 - \cdots - x_n^2 - \tfrac{1}{4}(y_1 - y_2)^2 \geq 0,\ r \geq \tfrac{|y_1-y_2|}{2}\Big\},
\end{aligned}$$

which concludes the proof. □

From Lemmas 2.4.15, 2.4.16 and 2.4.17 we can assemble the statements of Lemma 2.4.13:

Proof of Lemma 2.4.13. We have that

$$\ell(y_1, y_2) = F(y_2) - F(y_1) + \operatorname{sign}(y_1 - y_2)\left(G(y_1, y_2) + G(y_2, y_1)\right).$$

Assume $y_1 \neq y_2$. Then

$$\partial_{y_1}\ell(y_1, y_2) = -\partial_{y_1}F(y_1) + \operatorname{sign}(y_1 - y_2)\left(\partial_{y_1}G(y_1, y_2) + \partial_{y_1}G(y_2, y_1)\right).$$

Plugging in the derivatives of F and G from Lemmas 2.4.15 and 2.4.16 gives the statement of Lemma 2.4.13 after removing those terms that cancel out. At $y_1 = y_2$,

$$\lim_{y_1 \to y_2+} \partial_{y_1}\ell(y_1, y_2) = -\int_{\mathcal{K}\setminus C(y_1)} \omega(\boldsymbol{x}, r)\partial_{y_1} f_{\text{out}}(\boldsymbol{x}; y_1)\,\mathrm{d}(\boldsymbol{x}, r) = \lim_{y_1 \to y_2-} \partial_{y_1}\ell(y_1, y_2).$$

For $\partial_{y_1y_2}\ell(y_1, y_2)$, assume again $y_1 \neq y_2$, so by the symmetry of $G(y_1, y_2)$ with respect to y_1 and y_2

$$\partial_{y_1y_2}\ell(y_1, y_2) = \kappa\left(\partial_{y_1y_2}G(y_1, y_2) + \partial_{y_1y_2}G(y_2, y_1)\right) = 2\kappa\,\partial_{y_1y_2}G(y_1, y_2).$$

At $y_1 = y_2$,

$$\kappa\,\partial_{y_1y_2}G(y_1, y_2) = 0 = \partial_{y_1y_2}G(y_1, y_2). \qquad \square$$

From Lemma 2.4.13 together with Theorem 2.4.11, we can conclude the following:

THEOREM 2.4.18 (Reduction to a scalar Preisach operator). *Assume the vector Preisach operator $\boldsymbol{\mathcal{P}}$ has a continuous isotropic Preisach density ω of bounded support. Then for input satisfying Equations* (2.40) *and* (2.41)*, $\boldsymbol{\mathcal{P}}$ reduces to a scalar Preisach operator $\mathcal{P}$,*

$$\mathcal{P}[u](t) := \int_0^\infty \int_{\mathbb{R}} \tilde{\omega}(s, \rho) h_{(s,\rho)}[u](t)\,\mathrm{d}s\;\mathrm{d}\rho + q_0(u(t)),$$

with the Preisach density $\tilde{\omega}(s, \rho) : \mathbb{R} \times \mathbb{R}_+ \to \mathbb{R}$,

$$\tilde{\omega}(\rho, s) = 2\rho^2 \int_{\Pi_{12}(\partial\mathcal{C}_{s-\rho} \cap \partial\mathcal{C}_{s+\rho})} \frac{1}{r\sqrt{r^2 - x_3^2 - \cdots - x_n^2 - \rho^2}} \\ \omega\left(s, \sqrt{r^2 - x_3^2 - \cdots - x_n^2 - \rho^2}, \hat{\boldsymbol{x}}, r\right)\,\mathrm{d}(\hat{\boldsymbol{x}}, r),$$

where $\hat{\boldsymbol{x}} = (x_3, \ldots, x_n)$, and the reversible component

$$\begin{aligned} q_0(s) = &\int_0^s \int_{\mathcal{K}\setminus\mathcal{C}_\sigma} \omega(\boldsymbol{x}, r)\partial_y f_{\mathrm{out}}(\boldsymbol{x}; y)\,|_{y=\sigma}\;\mathrm{d}(\boldsymbol{x}, r)\,\mathrm{d}\sigma \\ = &\int_{\mathcal{K}\setminus\mathcal{C}_s} \omega(\boldsymbol{x}, r) f_{\mathrm{out}}(\boldsymbol{x}; s)\,\mathrm{d}(\boldsymbol{x}, r) - \int_{\mathcal{K}\setminus\mathcal{C}_0} \omega(\boldsymbol{x}, r) f_{\mathrm{out}}(\boldsymbol{x}; 0)\,\mathrm{d}(\boldsymbol{x}, r) \\ &- \int_0^s \int_{\Pi_1\mathcal{C}_0} \left(\omega(\varphi_-(\tilde{\boldsymbol{x}}, r; \sigma), \tilde{\boldsymbol{x}}, r) + \omega(\varphi_+(\tilde{\boldsymbol{x}}, r; \sigma), \tilde{\boldsymbol{x}}, r)\right) f_{\mathrm{in}}(\tilde{\boldsymbol{x}}, r)\,\mathrm{d}(\tilde{\boldsymbol{x}}, r)\,\mathrm{d}\sigma. \end{aligned}$$

PROOF. To get $\tilde{\omega}(s, \rho)$, plug $\partial_{y_1y_2}\ell(y_1, y_2)$ from Lemma 2.4.13 into the formula given in Theorem 2.4.11.

For $q_0(s)$, the first formula is quickly obtained in the same way. The second formula is obtained by applying Lemma 2.4.15 to transform the inner integral:

$$\begin{aligned} q_0(s) = &\int_0^s \partial_y F(y)\,|_{y=\sigma}\;\mathrm{d}\sigma \\ &- \int_0^s \int_{\Pi_1\mathcal{C}_\sigma} \left(\omega(\varphi_-(\tilde{\boldsymbol{x}}, r; \sigma), \tilde{\boldsymbol{x}}, r) + \omega(\varphi_+(\tilde{\boldsymbol{x}}, r; \sigma), \tilde{\boldsymbol{x}}, r)\right) f_{\mathrm{in}}(\tilde{\boldsymbol{x}}, r)\,\mathrm{d}(\tilde{\boldsymbol{x}}, r)\,\mathrm{d}\sigma \\ = &\; F(s) - F(0) \\ &- \int_0^s \int_{\Pi_1\mathcal{C}_\sigma} \left(\omega(\varphi_-(\tilde{\boldsymbol{x}}, r; \sigma), \tilde{\boldsymbol{x}}, r) + \omega(\varphi_+(\tilde{\boldsymbol{x}}, r; \sigma), \tilde{\boldsymbol{x}}, r)\right) f_{\mathrm{in}}(\tilde{\boldsymbol{x}}, r)\,\mathrm{d}(\tilde{\boldsymbol{x}}, r)\,\mathrm{d}\sigma. \end{aligned}$$

As the cones $\mathcal{C}_\sigma$ vary only along the x_1-axis, $\Pi_1\mathcal{C}_\sigma = \Pi_1\mathcal{C}_0$ for all $\sigma \in \mathbb{R}$. $\square$

The following example presents a pairing $\boldsymbol{\mathcal{P}}$ and $\mathcal{P}$ computed with the theorem.

EXAMPLE 2.4.19. Let $n = 2$ and ω be given by

$$\omega : \mathbb{R}^2 \times \mathbb{R}_+ \to \mathbb{R},$$
$$\omega(\boldsymbol{x}, r) := \begin{cases} 1 - \|\boldsymbol{x}\| - r & \text{if } \|\boldsymbol{x}\| + r \le 1, \\ 0 & \text{otherwise,} \end{cases}$$

displayed in Figure 2.11(a). The scalar first order reversal curves $(u(t), w(t))$ corresponding to this distribution are shown in Figure 2.11(b). By Theorem 2.4.18, the corresponding scalar Preisach operator has the Preisach distribution

$$\tilde{\omega}(\rho, s) = 2\rho^2 \int_\rho^1 \frac{1}{r\sqrt{r^2 - \rho^2}}\, \omega(s, \sqrt{r^2 - \rho^2}, r)\, \mathrm{d}r.$$

The integral converges in spite of the discontinuity of the integrand at $r = \rho$ because

$$\int_\rho^R \frac{1}{r\sqrt{r^2 - \rho^2}}\, \mathrm{d}r = \frac{1}{\rho} \arccos\left(\frac{\rho}{R}\right)$$

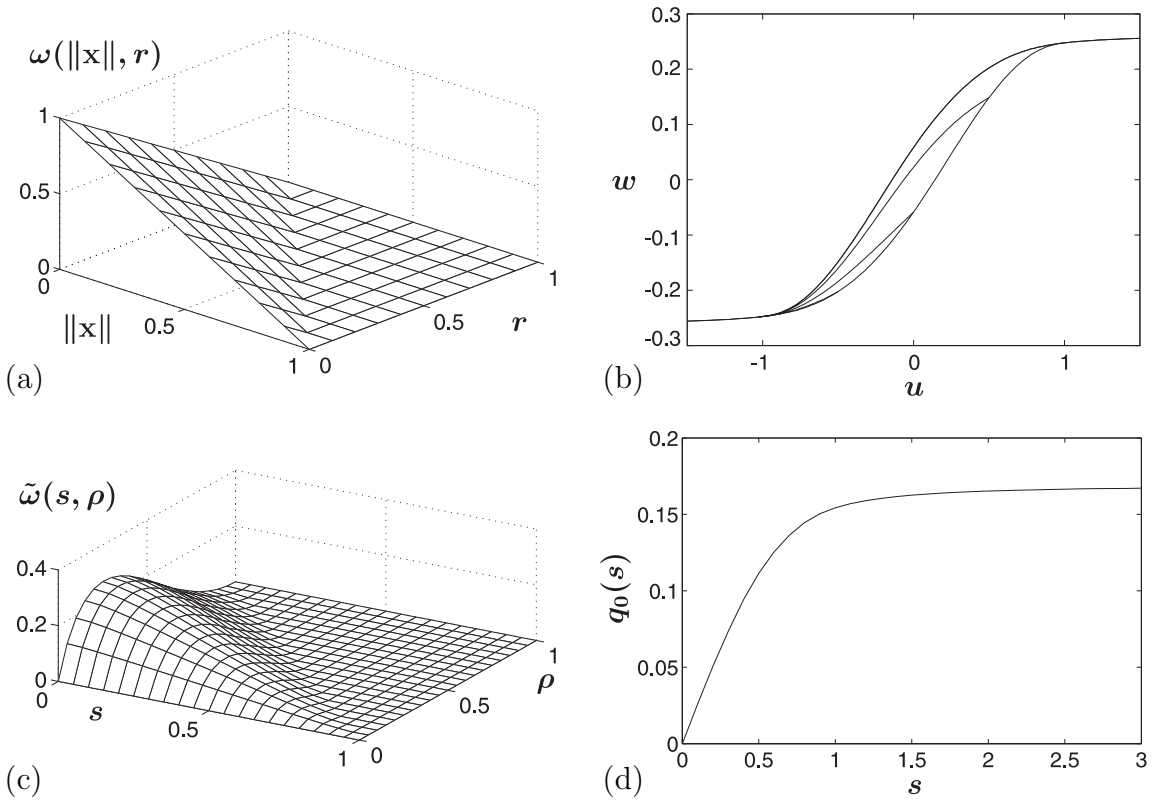

FIGURE 2.11. Example for the reduction from vector to scalar Preisach operator: (a) Preisach distribution $\omega(\|x\|, r)$, (b) scalar first order reversal curves of $\boldsymbol{\mathcal{P}}$ and $\mathcal{P}$, (c) Preisach distribution $\tilde{\omega}(s, \rho)$, (d) reversible contribution $q_0(s)$.

and ω is bounded. The distribution $\tilde{\omega}$ and the reversible component $q_0(s)$ were evaluated numerically and are shown in Figure 2.11(c) and (d).

2.4.5. Uniaxial monotonicity condition. In the modeling of magnetic hysteresis, the monotonicity of the scalar hysteresis curves is of particular interest. From the preceeding results on the shape function, we can quickly deduce a sufficient condition for the scalar hysteresis operator $\mathcal{P}$ to be piecewise increasing in u. According to definition [**16**, Def. 2.2.14], $\mathcal{P}$ is *piecewise increasing* if its shape function $\ell(\cdot,\cdot)$ is piecewise increasing with respect to its second variable, cf. (2.53). In other words, $\mathcal{P}$ is piecewise increasing if and only if

$$\partial_{y_2}\ell(y_1, y_2) \geq 0.$$

The derivative was computed in Lemma 2.4.13. Since both $\partial_y f_{\text{out}}(\boldsymbol{x}; y)$ and f_{in} are nonnegative, the following sufficient condition for $\mathcal{P}$ to be piecewise increasing is an immediate conclusion:

PROPOSITION 2.4.20. *If $\omega \geq 0$, then $\mathcal{P}$ is piecewise increasing.*

2.5. Infinitesimal properties of the vector Preisach operator

In this section, we discuss some infinitesimal properties of the operator. In the first part we show that the operator output $\boldsymbol{w} = \boldsymbol{\mathcal{P}}[\boldsymbol{u}]$ is always continuous for arbitrary ω of bounded support and, in fact, inherits some of the continuity properties of $\boldsymbol{u}$. In the second part, we derive the right-hand derivative of $\boldsymbol{w}$. This gives insight into the output evolution at a given $\boldsymbol{u}(t)$ and $\partial_{t+}\boldsymbol{u}(t)$, as we will demonstrate on an example. The arguments deployed there will be again of use in the last part of this section, where we suggest a possible hysteresis potential for $\boldsymbol{\mathcal{P}}$.

2.5.1. Output continuity. Let $0 < \lambda \leq 1$. We say that function $\boldsymbol{v} : [0, T] \to \mathbb{R}^n$ is *locally λ-Hölder continuous* if there exist constants $\gamma, L > 0$ such that

$$|t_1 - t_2| < \gamma \quad \Rightarrow \quad \|\boldsymbol{v}(t_1) - \boldsymbol{v}(t_2)\| < L|t_1 - t_2|^\lambda.$$

In particular, if $\lambda = 1$, then we call $\boldsymbol{v}$ *locally Lipschitz continuous*. If $\gamma \geq T$, then $\boldsymbol{v}$ is called *λ-Hölder continuous* or *Lipschitz continuous*, respectively.

THEOREM 2.5.1. *Assume ω is of bounded support $\mathcal{K}$. Then $\boldsymbol{w} = \boldsymbol{\mathcal{P}}[\boldsymbol{u}, \boldsymbol{\xi}]$ is a continuous function. In particular, if ω is absolutely bounded and $\boldsymbol{u}$ is Lipschitz continuous or λ-Hölder continuous, then $\boldsymbol{w}$ is Lipschitz continuous or locally λ-Hölder continuous, respectively.*

PROOF. To obtain Lipschitz and Hölder continuity, we will lead a computational proof. For just continuity, methods similar to those in Section 2.5.2 using the theory from Section 1.2.1 could also be applied.

Let $t_0 \in [0, T]$. By the continuity of $\boldsymbol{u}$, for all ε there exists a δ such that $|t - t_0| < \delta$ implies

$$\|\boldsymbol{u}(t) - \boldsymbol{u}(t_0)\| < \varepsilon. \tag{2.63}$$

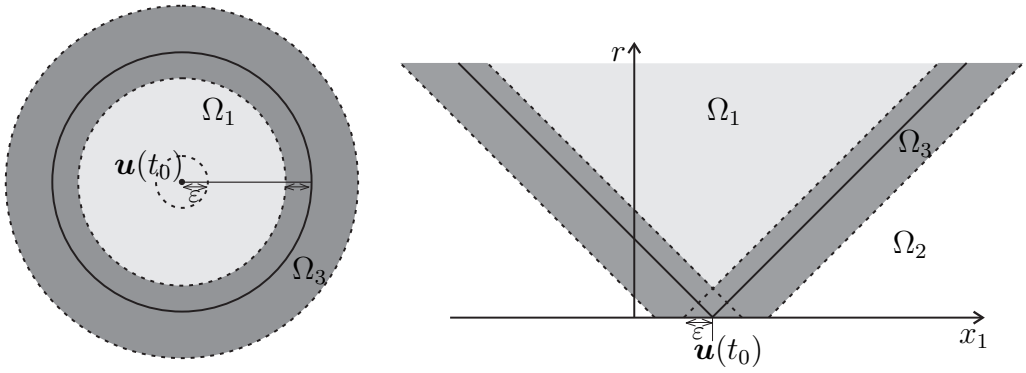

FIGURE 2.12. Possible variation of the freeze cone on $(t_0 - \delta, t_0 + \delta)$.

Assuming (2.63), we will derive an estimate on the variation of $\boldsymbol{w}$ in a δ-neighbourhood of t_0. As $\mathcal{K}$ is bounded, there exist constants R_1 and R_2 such that $\mathcal{K} \subseteq \{(\boldsymbol{x}, r) \in \mathbb{R}^n \times \mathbb{R}_+ \mid r < R_1,\ \|\boldsymbol{x}\| < R_2\}$. If ω is absolutely bounded, set $\overline{\omega} = \max|\omega(\boldsymbol{x}, r)|$.

Based on Equation (2.63), in $(t_0 - \delta, t_0 + \delta)$, the boundary of the freeze cone varies inside a ε-neighbourhood of $\partial B_{\boldsymbol{x},r}$, as sketched in Figure 2.12. We consider the relays separately on the following three subdomains of $\mathcal{K}$:

$$\begin{aligned}
\Omega_1 &:= \{(\boldsymbol{x}, r) \in [0, R_1] \times \mathbb{R}^n \mid \|\boldsymbol{x} - \boldsymbol{u}(t_0)\| < r - \varepsilon\},\\
\Omega_2 &:= \{(\boldsymbol{x}, r) \in [0, R_1] \times \mathbb{R}^n \mid \|\boldsymbol{x} - \boldsymbol{u}(t_0)\| > r + 2\varepsilon\},\\
\Omega_3 &:= \{(\boldsymbol{x}, r) \in [0, R_1] \times \mathbb{R}^n \mid r - \varepsilon \le \|\boldsymbol{x} - \boldsymbol{u}(t_0)\| \le r + 2\varepsilon\}.
\end{aligned}$$

Set

$$Q_i(\varepsilon) := \left\| \int_{\Omega_i} \omega(\boldsymbol{x}, r)(\boldsymbol{h}_{(\boldsymbol{x},r)}[\boldsymbol{u}, \boldsymbol{\xi}_{(\boldsymbol{x},r)}](t) - \boldsymbol{h}_{(\boldsymbol{x},r)}[\boldsymbol{u}, \boldsymbol{\xi}_{(\boldsymbol{x},r)}](t_0))\, \mathrm{d}\boldsymbol{x}\, \mathrm{d}r \right\|.$$

In Ω_1, for any $t \in (t_0 - \delta, t_0 + \delta)$ the relays are inside $\mathcal{C}_{\boldsymbol{u}(t)}$, so $\boldsymbol{h}_{(\boldsymbol{x},r)}[\boldsymbol{u}, \boldsymbol{\xi}_{(\boldsymbol{x},r)}](t)$ is constant. Therefore

$$Q_1(\varepsilon) = 0. \tag{2.64}$$

In Ω_3, the relays can take any state. Therefore, for all $t \in (t_0 - \delta, t_0 + \delta)$,

$$Q_3(\varepsilon) \le 2 \int_{\Omega_3} \|\omega(\boldsymbol{x}, r)\|\, \mathrm{d}\boldsymbol{x}\, \mathrm{d}r,$$

which goes to 0 with $\varepsilon \to 0$ because Ω_3 has measure 0 in the limit. In view of Lipschitz/Hölder continuity, for absolutely bounded ω we can bound this expression by

$$Q_3(\varepsilon) \le 2\overline{\omega} \frac{\pi^{\frac{n}{2}}}{(n+1)\Gamma(\frac{n}{2}+1)} \left((R_1 + 2\varepsilon)^{n+1} - (R_1 - \varepsilon)^{n+1} \right). \tag{2.65}$$

Here, we have estimated the volume of the domain by the volume difference of the two cones of heights $R_1 + 2\varepsilon$ and $R_1 - \varepsilon$, see Equations (1.1) and (1.2). We can now bound (2.65) by assuming without loss of generality that $\varepsilon < R_1$ and using

$$a^{n+1} - b^{n+1} = (a - b)(a^n + a^{n-1}b + \cdots + b) \le (n + 1)(a - b)a^n \tag{2.66}$$

for $0 \leq b \leq a$, which gives

$$Q_3(\varepsilon) \leq 6\overline{\omega}\frac{\pi^{\frac{n}{2}}}{\Gamma(\frac{n}{2}+1)}(R_1+2\varepsilon)^n\varepsilon. \tag{2.67}$$

In Ω_2, continuity is a consequence of Lemma 2.5.2 proved later. To derive a Lipschitz/Hölder constant, assume that ω is absolutely bounded. Note that the relays remain outside the freeze cone at any t, so for all $t \in (t_0-\delta, t_0+\delta)$

$$Q_2(\varepsilon) \leq \overline{\omega}\int_{\Omega_2}\left\|\frac{\boldsymbol{u}(t)-\boldsymbol{x}}{\|\boldsymbol{u}(t)-\boldsymbol{x}\|}-\frac{\boldsymbol{u}(t_0)-\boldsymbol{x}}{\|\boldsymbol{u}(t_0)-\boldsymbol{x}\|}\right\|\mathrm{d}\boldsymbol{x}\,\mathrm{d}r.$$

By Lemma 1.4.1, with $\min(\|\boldsymbol{u}(t)-\boldsymbol{x}\|, \|\boldsymbol{u}(t_0)-\boldsymbol{x}\|) \geq \|\boldsymbol{u}(t_0)-\boldsymbol{x}\|-\varepsilon$, we have that

$$0 \leq \left\|\frac{\boldsymbol{u}(t)-\boldsymbol{x}}{\|\boldsymbol{u}(t)-\boldsymbol{x}\|}-\frac{\boldsymbol{u}(t_0)-\boldsymbol{x}}{\|\boldsymbol{u}(t_0)-\boldsymbol{x}\|}\right\| \leq \frac{\varepsilon}{\|\boldsymbol{u}(t_0)-\boldsymbol{x}\|-\varepsilon} \leq 1 \tag{2.68}$$

in Ω_2. Therefore,

$$Q_2(\varepsilon) \leq \overline{\omega}\int_0^{R_1}\int_{\{\boldsymbol{x}\,|\,\|\boldsymbol{u}(t_0)-\boldsymbol{x}\|>2\varepsilon,\|\boldsymbol{x}\|<R_2\}}\frac{\varepsilon}{\|\boldsymbol{u}(t_0)-\boldsymbol{x}\|-\varepsilon}\,\mathrm{d}\boldsymbol{x}\,\mathrm{d}r.$$

If $\|\boldsymbol{u}(t_0)\| \leq R_2$, then

$$B_{\mathbf{0},R_2} \subseteq B_{\boldsymbol{u}(t_0),2R_2}.$$

Changing coordinates along Theorem 1.2.9 such that $\boldsymbol{y} := \boldsymbol{x}-\boldsymbol{u}(t_0)$, we obtain

$$\begin{aligned}&\int_0^{R_1}\int_{\{\boldsymbol{x}\,|\,\|\boldsymbol{u}(t_0)-\boldsymbol{x}\|>2\varepsilon,\|\boldsymbol{x}\|<R_2\}}\frac{\varepsilon}{\|\boldsymbol{u}(t_0)-\boldsymbol{x}\|-\varepsilon}\,\mathrm{d}\boldsymbol{x}\,\mathrm{d}r\\ &=\int_0^{R_1}\int_{\{\boldsymbol{y}\,|\,2\varepsilon\leq\|\boldsymbol{y}\|<2R_2\}}\frac{\varepsilon}{\|\boldsymbol{y}\|-\varepsilon}\,\mathrm{d}\boldsymbol{y}\,\mathrm{d}r.\end{aligned} \tag{2.69}$$

If, on the other hand, $\|\boldsymbol{u}(t_0)\| > R_2$, then

$$B_{\mathbf{0},R_2} \subseteq B_{\frac{R_2}{\|\boldsymbol{u}(t_0)\|}\boldsymbol{u}(t_0),2R_2}$$

and, by Lemma 1.4.2,

$$\frac{\varepsilon}{\|\boldsymbol{u}(t_0)-\boldsymbol{x}\|-\varepsilon} \leq \frac{\varepsilon}{\left\|\frac{R_2}{\|\boldsymbol{u}(t_0)\|}\boldsymbol{u}(t_0)-\boldsymbol{x}\right\|-\varepsilon}$$

for all $\boldsymbol{x}$ such that $\|\boldsymbol{x}\| < R_2$. Thus, changing coordinates such that $\boldsymbol{y} := \boldsymbol{x}-\frac{R_2}{\|\boldsymbol{u}(t_0)\|}\boldsymbol{u}(t_0)$, we again obtain (2.69).

To compute a bound for integral (2.69), we evaluate it by transformation into hyperspherical coordinates, resulting in

$$\begin{aligned}\varepsilon\int_0^{R_1}\int_{2\varepsilon}^{2R_2}\int_0^{2\pi}\int_0^{\pi}\cdots\int_0^{\pi}\frac{\rho^{n-1}}{\rho-\varepsilon}\sin\theta_1\sin^2\theta_2\cdots\sin^{n-2}\theta_{n-2}\,\mathrm{d}\theta_{n-2}\cdots\mathrm{d}\theta_1\,\mathrm{d}\theta_0\,\mathrm{d}\rho\,\mathrm{d}r\\ = 2\pi\varepsilon R_1\int_{2\varepsilon}^{2R_2}\frac{\rho^{n-1}}{\rho-\varepsilon}\,\mathrm{d}\rho\prod_{i=1}^{n-2}\int_0^{\pi}\sin^i\theta\,\mathrm{d}\theta.\end{aligned}$$

For the subintegral with respect to ρ, via (2.66), we get the following estimate:

$$\begin{aligned}
&\int_{2\varepsilon}^{2R_2} \frac{\rho^{n-1}}{\rho-\varepsilon}\,\mathrm{d}\rho \\
=&\int_{2\varepsilon}^{2R_2} \left(\frac{\rho^{n-1}-\varepsilon^{n-1}}{\rho-\varepsilon}+\frac{\varepsilon^{n-1}}{\rho-\varepsilon}\right)\mathrm{d}\rho \\
\leq&\int_{2\varepsilon}^{2R_2} (n-1)\rho^{n-2}\,\mathrm{d}\rho+\varepsilon^{n-1}\int_{2\varepsilon}^{2R_2}\frac{1}{\rho-\varepsilon}\,\mathrm{d}\rho \\
=&((2R_2)^{n-1}-(2\varepsilon)^{n-1})+\varepsilon^{n-1}(\log(2R_2-\varepsilon)-\log\varepsilon).
\end{aligned}$$

Note that

$$\lim_{\varepsilon\to 0}\varepsilon\log\varepsilon=0.$$

Because

$$\int_0^\pi \sin^i\theta\,\mathrm{d}\theta=\sqrt{\pi}\frac{\Gamma(i/2+1/2)}{\Gamma(i/2+1)},$$

evaluating the rest of the full integral exactly, on Ω_2 we get the upper bound

$$2\varpi R_1\frac{\pi^{n/2}}{\Gamma(n/2)}\left[(2R_2)^{n-1}-(2\varepsilon)^{n-1}+\varepsilon^{n-1}\log(2R_2-\varepsilon)-\varepsilon^{n-1}\log\varepsilon\right]\varepsilon. \tag{2.70}$$

This finishes the argument for Ω_2.

In summary, we have shown that

$$\|\boldsymbol{u}(t)-\boldsymbol{u}(t_0)\|<\varepsilon \qquad \Rightarrow \qquad \|\boldsymbol{w}(t)-\boldsymbol{w}(t_0)\|<C(\varepsilon)\varepsilon,$$

where $C(\varepsilon)\varepsilon$ is obtained from adding up the terms (2.67) and (2.70). $C(\varepsilon)$ is non-negative and bounded for $\varepsilon\in[0,R_2]$. Say $C(\varepsilon)\leq\tilde{C}$. Therefore, in particular, from Lipschitz/Hölder continuity of $\boldsymbol{u}$ we can conclude local Lipschitz-continuity or Hölder-continuity for $\boldsymbol{w}$ and $|t-t_0|<(R_2/L)^{\frac{1}{\lambda}}$:

$$\|\boldsymbol{u}(t)-\boldsymbol{u}(t_0)\|<L|t-t_0|^\lambda \qquad \Rightarrow \qquad \|\boldsymbol{w}(t)-\boldsymbol{w}(t_0)\|<L\tilde{C}|t-t_0|^\lambda.$$

With the subsequent remark, we moreover obtain global Lipschitz-continuity. □

Remark. Local Lipschitz-continuity is equivalent to global Lipschitz-continuity. Assume a function $\boldsymbol{w}$ is locally Lipschitz-continuous, i.e. $|t_2-t_1|<\varepsilon$ implies $\|\boldsymbol{w}(t_2)-\boldsymbol{w}(t_1)\|<L|t_2-t_1|$ with Lipschitz-constant L independent of t. Then if $|t_2-t_1|\geq\varepsilon$, pick intermediate values $t_1=\bar{t}_1<\bar{t}_2<\cdots<\bar{t}_k=t_2$ such that $|\bar{t}_{i-1}-\bar{t}_i|<\varepsilon$, so

$$\begin{aligned}
\|\boldsymbol{w}(t_2)-\boldsymbol{w}(t_1)\|&\leq\|\boldsymbol{w}(\bar{t}_k)-\boldsymbol{w}(\bar{t}_{k-1})\|+\cdots+\|\boldsymbol{w}(\bar{t}_2)-\boldsymbol{w}(\bar{t}_1)\| \\
&\leq L\left(|\bar{t}_k-\bar{t}_{k-1}|+\cdots+|\bar{t}_2-\bar{t}_1|\right) \\
&=L|t_2-t_1|.
\end{aligned}$$

2.5.2. Output derivative. In Section 2.4 on the reduction of the vectorial operator to a scalar Preisach operator, we have already differentiated the operator output $\boldsymbol{w}$ as a scalar function with respect to uniaxial input $\boldsymbol{u}$. Now, to obtain further insight into the infinitesimal properties, we will compute the right-hand derivative $\partial_{t+}\boldsymbol{w}(t)$ of $\boldsymbol{w}$ in dependence of the right-hand derivative of $\boldsymbol{u}$ at a given $t \in [0,T]$ in the general vector setting. The results will be applied to investigate the output behaviour of $\boldsymbol{\mathcal{P}}$ for piecewise linear inputs and in the subsequent discussion of hysteresis potentials.

So far, we have assumed $\boldsymbol{u}$ to be a continuous function. There were no assumptions on the differential properties of $\boldsymbol{u}$. Now, we assume that $\boldsymbol{u}$ is piecewise C^2, that is, there is a partition of $[0,T]$ such that $\boldsymbol{u}'(t)$ and $\boldsymbol{u}''(t)$ exist and are continuous on each subinterval of the partition, and the right-hand derivative $\partial_{t+}\boldsymbol{u}(t)$ exists everywhere in $[0,T)$. Then $\partial_{t+}\boldsymbol{w}(t)$ will depend on $\boldsymbol{u}$ in the interval $[0,t]$ and on $\partial_{t+}\boldsymbol{u}(t)$.

Throughout this subsection, suppose that ω has bounded support $\mathcal{K}$ and is continuous. Like in Section 2.4, we split the integral defining the operator $\boldsymbol{\mathcal{P}}$ into integrals on the freeze cone and its outside to satisfy the conditions of the theorems about differentiation under the integral sign in Section 1.2.1. Using the rotational properties of $\boldsymbol{\mathcal{P}}$, Lemma 2.3.3, it will suffice to compute Gâteaux derivates with respect to $\partial_{t+}\boldsymbol{u}(t) = (1,0,\dots,0)$.

The first lemma deals with the derivative obtained from the subdomain outside the freeze cone. Since the relay states on this domain depend only on the current input $\boldsymbol{u}(t)$, we can express this component of $\boldsymbol{\mathcal{P}}$ in terms of a function $\boldsymbol{F}(\boldsymbol{u}(t))$. To parametrize the freeze cone at $\boldsymbol{u}(t) \in \mathbb{R}^n$, we generalize some of the definitions from Section 2.4.4. For $\boldsymbol{y} = (y_1,\dots,y_n) \in \mathbb{R}^n$, the boundary of $\mathcal{C}_{\boldsymbol{y}}$ can be parametrized with respect to the x_1-direction in terms of the functions (Fig. 2.13)

$$\varphi_-(\Pi_1\boldsymbol{x}, r; \boldsymbol{y}) := \begin{cases} y_1 - (r^2 - \sum_{i=2}^n (x_i - y_i)^2)^{\frac{1}{2}}\,, & \text{if } \sum_{i=2}^n (x_i-y_i)^2 < r^2, \\ y_1 & \text{otherwise,} \end{cases}$$

$$\varphi_+(\Pi_1\boldsymbol{x}, r; \boldsymbol{y}) := \begin{cases} y_1 + (r^2 - \sum_{i=2}^n (x_i - y_i)^2)^{\frac{1}{2}}\,, & \text{if } \sum_{i=2}^n (x_i-y_i)^2 < r^2, \\ y_1 & \text{otherwise.} \end{cases}$$

Then the two half-shells of the cone are given by

$$\partial_-\mathcal{C}_{\boldsymbol{y}} := \left\{ (x_1,\dots,x_n,r) \;\middle|\; \sum_{i=2}^n (x_i-y_i)^2 < r^2,\ x_1 = \varphi_-(\Pi_1\boldsymbol{x}, r; \boldsymbol{y}) \right\},$$

$$\partial_+\mathcal{C}_{\boldsymbol{y}} := \left\{ (x_1,\dots,x_n,r) \;\middle|\; \sum_{i=2}^n (x_i-y_i)^2 < r^2,\ x_1 = \varphi_+(\Pi_1\boldsymbol{x}, r; \boldsymbol{y}) \right\}.$$

Define the function $\boldsymbol{f}_{\text{out}} = (f_{\text{out},1},\dots,f_{\text{out},n}) : \mathbb{R}^n \times \mathbb{R}^n \to \mathbb{R}^n$,

$$\boldsymbol{f}_{\text{out}}(\boldsymbol{x},\boldsymbol{y}) := \frac{\boldsymbol{y}-\boldsymbol{x}}{\|\boldsymbol{y}-\boldsymbol{x}\|},$$

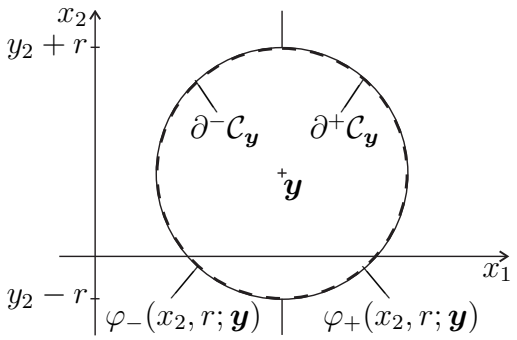

FIGURE 2.13. Illustration of φ_-, φ_+, $\partial^- C_{\boldsymbol{y}}$ and $\partial^+ C_{\boldsymbol{y}}$ for $n = 2$ and $\boldsymbol{y} = (y_1, y_2)$.

representing the relay states outside the freeze cone $\mathcal{C}_{\boldsymbol{y}}$, with

$$\partial_{y_1} f_{\text{out},1} = \frac{(y_2 - x_2)^2 + \cdots + (y_n - x_n)^2}{\|\boldsymbol{y} - \boldsymbol{x}\|^3},$$
$$\partial_{y_1} f_{\text{out},i} = \frac{(y_1 - x_1)(y_i - x_i)}{\|\boldsymbol{y} - \boldsymbol{x}\|^3}, \qquad i = 2, \ldots, n.$$

Let the integral over the outside of $\mathcal{C}_{\boldsymbol{y}}$ be given by $\boldsymbol{F} = (F_1, \ldots, F_n) : \mathbb{R}^n \to \mathbb{R}^n$,

$$\boldsymbol{F}(\boldsymbol{y}) := \int_{\mathcal{K} \setminus \mathcal{C}_{\boldsymbol{y}}} \omega(\boldsymbol{x}, r) \boldsymbol{f}_{\text{out}}(\boldsymbol{x}, \boldsymbol{y}) \, \mathrm{d}(\boldsymbol{x}, r). \tag{2.71}$$

The *Gâteaux derivative* of $\boldsymbol{F}$ in the direction $\boldsymbol{z} \in \mathbb{R}^n$ is defined by

$$d_{\boldsymbol{z}} \boldsymbol{F}(\boldsymbol{y}) = \lim_{\lambda \to 0+} \frac{\boldsymbol{F}(\boldsymbol{y} + \lambda \boldsymbol{z}) - \boldsymbol{F}(\boldsymbol{y})}{\lambda}.$$

LEMMA 2.5.2. *$\boldsymbol{F}$ is continuous. The derivative $d_{\boldsymbol{z}} \boldsymbol{F}(\boldsymbol{y})$ is continuous in both $\boldsymbol{y}$ and $\boldsymbol{z}$, and*

$$\begin{aligned} d_{(1,0,\ldots,0)} \boldsymbol{F}(\boldsymbol{y}) = & \int_{\mathcal{K} \setminus \mathcal{C}_{\boldsymbol{y}}} \omega(\boldsymbol{x}, r) \partial_{y_1} \boldsymbol{f}_{\text{out}}(\boldsymbol{x}, \boldsymbol{y}) \, \mathrm{d}(\boldsymbol{x}, r) \\ & + \int_{\Pi_1 \mathcal{C}_{\boldsymbol{y}}} \big(\omega(\boldsymbol{x}, r) \boldsymbol{f}_{\text{out}}(\boldsymbol{x}, \boldsymbol{y}) \mid_{x_1 = \varphi_-(\Pi_1 \boldsymbol{x}, r; \boldsymbol{y})} - \\ & \qquad \omega(\boldsymbol{x}, r) \boldsymbol{f}_{\text{out}}(\boldsymbol{x}, \boldsymbol{y}) \mid_{x_1 = \varphi_+(\Pi_1 \boldsymbol{x}, r; \boldsymbol{y})} \big) \, \mathrm{d}(\Pi_1 \boldsymbol{x}, r). \end{aligned} \tag{2.72}$$

PROOF. We will show that $\partial_{y_1} F_i$ exists and is continuous. Then the Gâteaux derivative with respect to $\boldsymbol{z} = (1, 0, \ldots, 0)$ is equal to the partial derivative $\partial_{y_1} \boldsymbol{F}$. We have

$$F_i(y_1, \ldots, y_n) = \int_{\mathcal{K} \setminus \mathcal{C}_{\boldsymbol{y}}} \omega(\boldsymbol{x}, r) f_{\text{out},i}(\boldsymbol{x}, \boldsymbol{y}) \, \mathrm{d}(\boldsymbol{x}, r)$$

with

$$f_{\text{out},i}(\boldsymbol{x}, \boldsymbol{y}) := \frac{y_i - x_i}{\|\boldsymbol{y} - \boldsymbol{x}\|}.$$

The existence and continuity of $\partial_{y_1} F_1$ follows directly from the proof of Lemma 2.4.15 after a change of variables $\tilde{\boldsymbol{x}} := (x_1, \dots, x_n) - (0, y_2, \dots, y_n)$.

For $\partial_{y_1} F_i$, $i \neq 1$, we apply the same line of argument as in the proof of Lemma 2.4.15. Assume $\omega \geq 0$ and fix a point $\boldsymbol{y}_0 \in \mathbb{R}^n$. Chose $R \in \mathbb{R}_+$ such that $\mathcal{K}$ is fully contained in the box $[-R, R]^n \times [0, R]$. We can parametrize F_i as

$$F_i(\boldsymbol{y}) = \int_0^R \int_{-R}^R \cdots \int_{-R}^R \left[\int_{-R}^{\varphi_-(x_2,\dots,x_n,r,\boldsymbol{y})} + \int_{\varphi_+(x_2,\dots,x_n,r,\boldsymbol{y})}^R \right] \omega(\boldsymbol{x}, r) f_{\mathrm{out},i}(\boldsymbol{x}, r, \boldsymbol{y}) \,\mathrm{d}x_1 \,\mathrm{d}x_2 \cdots \mathrm{d}x_n \,\mathrm{d}r.$$

Splitting the integral up over the inner sum of integrals into $F_i(\boldsymbol{y}) = F_-(\boldsymbol{y}) + F_+(\boldsymbol{y})$ and defining a corresponding function sequence $F_{-,m}(\boldsymbol{y})$, the respective formulas for F_-, F_+, $F_{-,m}$ and U_- carry over from Lemma 2.4.15 with y replaced by $\boldsymbol{y}$.

The function $f_{\mathrm{out},i}$ satisfies the assumptions of Theorem 1.2.6 on $U_m(\boldsymbol{y}_0) \times \{\boldsymbol{y} \mid \|\boldsymbol{y} - \boldsymbol{y}_0\| \leq \frac{1}{4m}\}$, so $F_{-,m}(\boldsymbol{y})$ is continuous in $\boldsymbol{y}_0$. Fixing some $a \in \mathbb{R}$, $a > 0$, by the same argument, $F_{-,m}(\boldsymbol{y})$ is continuous for all $\boldsymbol{y}$ such that $\|\boldsymbol{y} - \boldsymbol{y}_0\| \leq a$, so F_m converges uniformly. Thus $F_i(\boldsymbol{y})$ and subsequently $\boldsymbol{F}(\boldsymbol{y})$ are continuous.

Treating $y_2, \dots, y_n$ as fixed parameters, $f_{\mathrm{out},i}$ satisfies the assumptions of Corollary 1.2.3 as a function of $(\boldsymbol{x}, r, y_1)$ on $U \times ((\boldsymbol{y}_0)_1 - \frac{1}{4m}, (\boldsymbol{y}_0)_1 + \frac{1}{4m})$ where $(\boldsymbol{y}_0)_1$ denotes the first component of $\boldsymbol{y}_0$. Thus, $\partial_{y_1} F_{-,m}(\boldsymbol{y})$ exists at $\boldsymbol{y}_0$ and is given by

$$\partial_{y_1} F_{-,m}(\boldsymbol{y}) := \int_{\frac{1}{m}}^R \int_{-R}^R \cdots \int_{-R}^R \Bigg[\int_{-R}^{\varphi_-(x_2,\dots,x_n,r,\boldsymbol{y})} \omega(\boldsymbol{x}, r) \partial_{y_1} f_{\mathrm{out},i}(\boldsymbol{x}, \boldsymbol{y}) \,\mathrm{d}x_1 + \left[\omega(\boldsymbol{x}, r) f_{\mathrm{out},i}(\boldsymbol{x}, \boldsymbol{y})\right] \big|_{x_1 = \varphi_-(\Pi_1 \boldsymbol{x}, r, \boldsymbol{y})} \Bigg] \mathrm{d}x_2 \cdots \mathrm{d}x_n \,\mathrm{d}r$$

evaluated at $\boldsymbol{y} = \boldsymbol{y}_0$.

The existence of

$$D(\boldsymbol{y}) := \lim_{m \to \infty} \partial_{y_1} F_{-,m}(\boldsymbol{y})$$

is clear for the second integrand, and the limit for the first integrand exists because Lemma 1.2.17 implies that $\partial_{y_1} f_{\mathrm{out},i}(\boldsymbol{x}, r, \boldsymbol{y})$ is integrable on bounded domains in spite of its singularity. Further, as both integrands are continuous in $U_m(\boldsymbol{y}_0) \times \{\boldsymbol{y} \mid \|\boldsymbol{y} - \boldsymbol{y}_0\| \leq \frac{1}{4m}\}$, the derivative $\partial_{y_1} F_{-,m}(\boldsymbol{y})$ is continuous by Corollary 1.2.3. As above, this gives uniform convergence $\partial_{y_1} F_{-,m}(\boldsymbol{y}) \to D(\boldsymbol{y})$, so by Lemma 1.2.7 we have

$$\partial_{y_1} F_-(\boldsymbol{y}_0) = D(\boldsymbol{y}_0).$$

We can conclude that $\partial_{y_1} F_i(\boldsymbol{y})$ exists and is continuous for all $\boldsymbol{y} \in \mathbb{R}^n$.

By the symmetry of $\boldsymbol{F}(\boldsymbol{y})$ with respect to the components y_i of $\boldsymbol{y}$, continuity of $\boldsymbol{F}$ and $\partial_{y_i} F_j(\boldsymbol{y})$ follow in general. □

Note that by the chain rule, we obtain the derivative with respect to t from the derivative $\partial_{\boldsymbol{y}} \boldsymbol{F}(\boldsymbol{y})$ of (2.71) as

$$\partial_t F(\boldsymbol{u}(t)) = \partial_{\boldsymbol{y}} F(\boldsymbol{y})\big|_{\boldsymbol{y} = \boldsymbol{u}(t)} \, \partial_t \boldsymbol{u}(t). \tag{2.73}$$

For the integral over the inside of the freeze cone, the situation is more difficult, because the relay states do not depend on $\boldsymbol{u}(t)$ only, but on the history of $\boldsymbol{u}$ in $[0, t]$.

Also, in $\mathcal{C}_{\boldsymbol{u}(t)}$ the relay state $\boldsymbol{h}_{(\boldsymbol{x},r)}$ does not need to be a continuous function in $(\boldsymbol{x}, r)$. It is, in fact, easy to find input functions for which it is not continuous: Take for example the increasing and decreasing uniaxial inputs investigated in Section 2.4.

Denote the operator representing the integral over the freeze cone by

$$G[\boldsymbol{u}](t) := \int_{\mathcal{C}_{\boldsymbol{u}(t)}} \omega(\boldsymbol{x}, r)\boldsymbol{h}_{(\boldsymbol{x},r)}[\boldsymbol{u}](t)\,\mathrm{d}(\boldsymbol{x}, r). \tag{2.74}$$

Given $\boldsymbol{u}$, as first step we show in Lemmas 2.5.3 and 2.5.4 that if $\boldsymbol{u}$ is twice continuously differentiable from the right in t_0, then we can compute $\partial_{t+}G[\boldsymbol{u}](t_0)$ from the right-hand linearization of $\boldsymbol{u}$ in t_0. The derivative is computed in Lemma 2.5.5.

LEMMA 2.5.3. *Let a linear function* $\boldsymbol{v} : [0, T] \to \mathbb{R}^n$,

$$\boldsymbol{v}(t) = \boldsymbol{v}_0 + t\boldsymbol{v}_d, \quad \boldsymbol{v}_0, \boldsymbol{v}_d \in \mathbb{R}^n,$$

be given. Suppose there exists an interval $[t_0, t_1] \subseteq [0, T]$ *such that the function* $\boldsymbol{u} : [0, T] \to \mathbb{R}^n$ *satisfies*

$$\|\boldsymbol{u}(t) - \boldsymbol{v}(t)\| < \varepsilon \quad \forall t \in [t_0, t_1]. \tag{2.75}$$

Then there exists a function $K_1(\varepsilon) = \mathcal{O}(1)$ *as* $\varepsilon \to 0$ *and a constant* $K_2 \in \mathbb{R}_+$ *such that for all* $t \in [t_0, t_1]$,

$$\|G[\boldsymbol{u}](t) - G[\boldsymbol{v}](t)\| \le \|G[\boldsymbol{u}](t_0) - G[\boldsymbol{v}](t_0)\| + K_1(\varepsilon)\varepsilon + K_2\varepsilon^{1/2}(t - t_0). \tag{2.76}$$

PROOF. Choose $t \in [t_0, t_1]$. Set $\overline{\omega} = \max|\omega(\boldsymbol{x}, r)|$ and

$$\Omega := \{(\boldsymbol{x}, r) \mid \|\boldsymbol{x} - \boldsymbol{u}(t)\| < r + \varepsilon\},$$

so $\mathcal{C}_{\boldsymbol{v}(t)}, \mathcal{C}_{\boldsymbol{u}(t)} \subset \Omega$. Partition Ω into three subdomains, $\Omega = \Omega_1 \cup \Omega_2 \cup \Omega_3$, given by

$$\begin{aligned}
\Omega_1 =& \{(\boldsymbol{x}, r) \mid \|\boldsymbol{x} - \boldsymbol{v}(t)\| < r - \varepsilon,\ \|\boldsymbol{x} - \boldsymbol{v}(0)\| < r - \varepsilon\},\\
\Omega_2 =& \{(\boldsymbol{x}, r) \mid \|\boldsymbol{x} - \boldsymbol{v}(t)\| < r - \varepsilon,\ \|\boldsymbol{x} - \boldsymbol{v}(0)\| > r + \varepsilon\},\\
\Omega_3 =& \{(\boldsymbol{x}, r) \mid r - \varepsilon < \|\boldsymbol{x} - \boldsymbol{v}(t)\| < r + \varepsilon\} \cup\\
& \{(\boldsymbol{x}, r) \mid \|\boldsymbol{x} - \boldsymbol{v}(t)\| < r + \varepsilon,\ r - \varepsilon < \|\boldsymbol{x} - \boldsymbol{v}(0)\| < r + \varepsilon\},
\end{aligned}$$

as shown in Fig. 2.14. As a first estimate, we immediately obtain

$$\begin{aligned}
&\|G[\boldsymbol{u}](t) - G[\boldsymbol{v}](t)\|\\
&= \left\| \int_{\mathcal{C}_{\boldsymbol{u}(t)}} \omega(\boldsymbol{x}, r)\boldsymbol{h}_{(\boldsymbol{x},r)}[\boldsymbol{u}](t)\,\mathrm{d}(\boldsymbol{x}, r) - \int_{\mathcal{C}_{\boldsymbol{v}(t)}} \omega(\boldsymbol{x}, r)\boldsymbol{h}_{(\boldsymbol{x},r)}[\boldsymbol{v}](t)\,\mathrm{d}(\boldsymbol{x}, r) \right\|\\
&\le \sum_{i=1}^{3} \left\| \int_{\Omega_i} \omega(\boldsymbol{x}, r)\left(\boldsymbol{h}_{(\boldsymbol{x},r)}[\boldsymbol{u}](t) - \boldsymbol{h}_{(\boldsymbol{x},r)}[\boldsymbol{v}](t)\right)\,\mathrm{d}(\boldsymbol{x}, r) \right\|. \qquad (2.77)
\end{aligned}$$

We will compute bounds separately on these domains.

Obviously, since the relays in Ω_1 remain fixed at all $t \in [t_0, t_1]$, the error on Ω_1 is bounded by the error at t_0,

$$\left\| \int_{\Omega_1} \boldsymbol{h}_{(\boldsymbol{x},r)}[\boldsymbol{u}](t) - \boldsymbol{h}_{(\boldsymbol{x},r)}[\boldsymbol{v}](t) \right\| \mathrm{d}(\boldsymbol{x}, r) \le \|G[\boldsymbol{u}](t_0) - G[\boldsymbol{v}](t_0)\|,$$

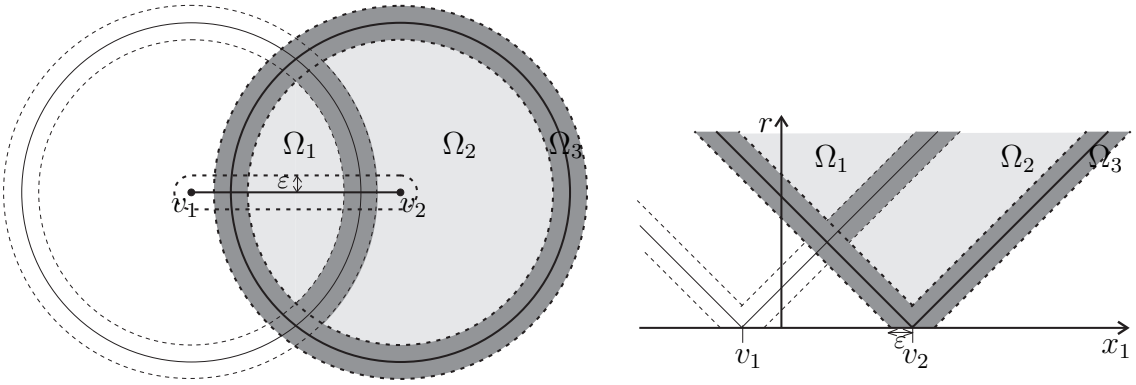

FIGURE 2.14. Partition of D into the subdomains Ω_1, Ω_2, and Ω_3 for $n = 2$ in a plane $r = \text{const}$ (left) and $\boldsymbol{x}_2 = \text{const}$ (right).

and gives the first term in (2.76).

For $i = 2, 3$, we make use of

$$\begin{aligned}&\left\| \int_{\Omega_i} \omega(\boldsymbol{x}, r) \left(\boldsymbol{h}_{(\boldsymbol{x},r)}[\boldsymbol{u}](t) - \boldsymbol{h}_{(\boldsymbol{x},r)}[\boldsymbol{v}](t) \right) \mathrm{d}(\boldsymbol{x}, r) \right\| \\ \leq & \overline{\omega} \int_{\Omega_i} \left\| \left(\boldsymbol{h}_{(\boldsymbol{x},r)}[\boldsymbol{u}](t) - \boldsymbol{h}_{(\boldsymbol{x},r)}[\boldsymbol{v}](t) \right) \right\| \mathrm{d}(\boldsymbol{x}, r)\end{aligned}$$

and compute a bound on the second integral.

For Ω_3, duplicating the derivation for Ω_3 in the proof of Lemma 2.5.1 with the correct radii, for the full and the half cone shell making up Ω_3 we obtain the estimate

$$\int_{\Omega_3} \left\| \left(\boldsymbol{h}_{(\boldsymbol{x},r)}[\boldsymbol{u}](t) - \boldsymbol{h}_{(\boldsymbol{x},r)}[\boldsymbol{v}](t) \right) \right\| \mathrm{d}(\boldsymbol{x}, r) \leq (4+2) \frac{\pi^{\frac{n}{2}}}{\Gamma(\frac{n}{2}+1)} (R + 2\varepsilon)^n \varepsilon.$$

This is the origin of the second term in (2.76).

Denote the term representing Ω_2 in (2.77) by Q. By the same line of argument applied to show Lemmas 2.3.3 and 2.3.4, without loss of generality, we can assume $\boldsymbol{v}_0 = 0$ and $\boldsymbol{v}_d = (\lambda, 0, \ldots, 0)$, $\lambda \geq 0$. Any relay $(\boldsymbol{x}, r) \in \Omega_2$ satisfies $(\boldsymbol{x}, r) \notin \mathcal{C}_{\boldsymbol{v}(t_0)}, \mathcal{C}_{\boldsymbol{u}(t_0)}$. Consequently, there exists a $\tau_1 \in [t_0, t_1]$ such that $\boldsymbol{v}(\tau_1)$ is on the relay boundary and remains inside the relay thereafter, i.e.

$$r = \|\boldsymbol{v}(\tau_1) - \boldsymbol{x}\| = \left\| ((\tau_1 - t_0)\lambda, 0, \ldots, 0)^T - \boldsymbol{x} \right\|,$$

and

$$\begin{aligned}\boldsymbol{h}_{(\boldsymbol{x},r)}[\boldsymbol{v}](t) &= \frac{1}{r} \left[((\tau_1 - t_0)\lambda, 0, \ldots, 0)^T - \boldsymbol{x} \right] \\ &= \frac{1}{r} \left(-\sqrt{r^2 - \|(x_2, \ldots, x_n)\|^2}, -x_2, \ldots, -x_n \right)^T.\end{aligned}$$

Similarly, there exists a $\tau_2 \in [0, t]$ such that

$$r = \|\boldsymbol{u}(\tau_2) - \boldsymbol{x}\|$$

and

$$\begin{aligned}\boldsymbol{h}_{(\boldsymbol{x},r)}[\boldsymbol{u}](t) &= \frac{1}{r}\left[\boldsymbol{u}(\tau_2) - \boldsymbol{x}\right] \\ &= \frac{1}{r}\left(-\sqrt{r^2 - (x_2 - u_2(\tau_2))^2 - \cdots - (x_n - u_n(\tau_2))^2}, u_2(\tau_2) - x_2, \ldots, u_n(\tau_2) - x_n\right)^T.\end{aligned}$$

Assumption (2.75) gives

$$\|(u_2(\tau_2), \ldots, u_n(\tau_2))\| \leq \|\boldsymbol{u}(\tau_2) - \boldsymbol{v}(\tau_2)\| < \varepsilon$$

and results in

$$(x_2 - u_2(t_1))^2 + \cdots + (x_n - u_n(t_1))^2 < (\|(x_2, \ldots, x_n)\| + \varepsilon)^2.$$

Substituting in the relay states and applying the bounds, we obtain

$$\begin{aligned}Q \leq& \overline{\omega} \int_{\Omega_2} \left\|(\boldsymbol{h}_{(\boldsymbol{x},r)}[\boldsymbol{v}](t) - \boldsymbol{h}_{(\boldsymbol{x},r)}[\boldsymbol{u}](t))\right\| \,\mathrm{d}(\boldsymbol{x}, r) \\ \leq& \overline{\omega} \int_{\Omega_2} \frac{1}{r}\left[\left(\sqrt{r^2 - \|(x_2, \ldots, x_n)\|^2} - \sqrt{r^2 - (\|(x_2, \ldots, x_n)\| + \varepsilon)^2}\right)^2 + \varepsilon^2\right]^{\frac{1}{2}} \mathrm{d}(\boldsymbol{x}, r)\end{aligned}$$

For any given r, the integrand is monotonically increasing in $\|(x_2, \ldots, x_n)\|$. On Ω_2, $\|(x_2, \ldots, x_n)\|$ takes the maximum $r - \varepsilon$. The substitution results in

$$Q \leq \int_{\Omega_2} \frac{1}{r}\left[2r\varepsilon\right]^{\frac{1}{2}} \mathrm{d}(\boldsymbol{x}, r)$$

Parametrizing the integration domain and subsequently evaluating and approximating the inner integral gives

$$\begin{aligned}Q \leq& \int_{\varepsilon}^{R} \int_{-(r-\varepsilon)}^{r-\varepsilon} \frac{1}{r}\left[2r\varepsilon\right]^{\frac{1}{2}} \int_{-\sqrt{(r-\varepsilon)^2 - x_n^2}}^{\sqrt{(r-\varepsilon)^2 - x_n^2}} \cdots \int_{-\sqrt{(r-\varepsilon)^2 - x_n^2 - \cdots - x_3^2}}^{\sqrt{(r-\varepsilon)^2 - x_n^2 - \cdots - x_3^2}} \\ & \int_{\max\left(v_1(t) - \sqrt{(r-\varepsilon)^2 - x_n^2 - \cdots - x_2^2}, v_1(t_0) + \sqrt{(r+\varepsilon)^2 - x_n^2 - \cdots - x_2^2}\right)}^{v_1(t) + \sqrt{(r-\varepsilon)^2 - x_n^2 - \cdots - x_3^2}} \mathrm{d}x_1 \,\mathrm{d}x_2 \cdots \mathrm{d}x_{n-1} \,\mathrm{d}x_n \,\mathrm{d}r \\ \leq& \lambda(t - t_0) \int_{\varepsilon}^{R} \frac{1}{r}\left[2r\varepsilon\right]^{\frac{1}{2}} \\ & \int_{-(r-\varepsilon)}^{r-\varepsilon} \int_{-\sqrt{(r-\varepsilon)^2 - x_n^2}}^{\sqrt{(r-\varepsilon)^2 - x_n^2}} \cdots \int_{-\sqrt{(r-\varepsilon)^2 - x_n^2 - \cdots - x_3^2}}^{\sqrt{(r-\varepsilon)^2 - x_n^2 - \cdots - x_3^2}} \mathrm{d}x_2 \cdots \mathrm{d}x_{n-1} \,\mathrm{d}x_n \,\mathrm{d}r.\end{aligned}$$

The inner integrals compute the volume of an $(n-1)$-dimensional ball of radius $r - \varepsilon$, which is bounded by $V_B^{(n-1)}(r)$, resulting in the third term of (2.76). □

Define the right hand linearization of $\boldsymbol{u}$ at time t_0 by

$$\tilde{\boldsymbol{u}}(t) = \begin{cases} \boldsymbol{u}(t) & \text{if } t \in [0, t_0], \\ \boldsymbol{u}(t_0) + (t - t_0)\partial_{t+}\boldsymbol{u}(t) \mid_{t=t_0} & \text{if } t > t_0. \end{cases}$$

LEMMA 2.5.4. *Suppose* $\boldsymbol{u}$ *is twice continuously differentiable on an interval* $[t_0, t_1]$, $t_0 < t_1$. *Then*

$$\partial_{t+} G[\boldsymbol{u}](t) \mid_{t=t_0} = \partial_{t+} G[\tilde{\boldsymbol{u}}](t) \mid_{t=t_0} .$$

PROOF. Since

$$\begin{aligned} \partial_{t+} G[\boldsymbol{u}](t) \mid_{t=t_0} &= \lim_{t \to t_0+} \frac{G[\boldsymbol{u}](t) - G[\boldsymbol{u}](t_0)}{t - t_0} \\ &= \lim_{t \to t_0+} \left[\frac{G[\boldsymbol{u}](t) - G[\tilde{\boldsymbol{u}}](t)}{t - t_0} + \frac{G[\tilde{\boldsymbol{u}}](t) - G[\boldsymbol{u}](t_0)}{t - t_0} \right], \end{aligned}$$

where the limit of the second term equals $\partial_{t+} G[\tilde{\boldsymbol{u}}](t) \mid_{t=t_0}$, we will show that

$$\lim_{t \to t_0+} \frac{\|G[\boldsymbol{u}](t) - G[\tilde{\boldsymbol{u}}](t)\|}{t - t_0} = 0.$$

As $\boldsymbol{u}$ is $C^2[t_0, t_1]$, Taylor's theorem gives

$$\boldsymbol{u}(t) = \boldsymbol{u}(t_0) + \partial_{t+} \boldsymbol{u}(t) \mid_{t=t_0} (t - t_0) + R_1(t), \quad t \in [t_0, t_1],$$

with the remainder

$$R_1(t) = \int_{t_0}^{t} \boldsymbol{u}''(\tau)(\tau - t_0) \, \mathrm{d}\tau.$$

Therefore, with $M := \max_{[t_0,t_1]} \|\boldsymbol{u}''(\tau)\|$, for any $t \in [t_0, t_1]$ we have

$$\|\boldsymbol{u}(\tau) - \tilde{\boldsymbol{u}}(\tau)\| = \|R_1(\tau)\| \leq M \int_{t_0}^{t} (\tau - t_0) \, \mathrm{d}\tau = \frac{M}{2}(t - t_0)^2 =: \tilde{R}_1(t) \quad \forall \tau \in [t_0, t].$$

As $\|G[\boldsymbol{u}](t_0) - G[\tilde{\boldsymbol{u}}](t_0)\| = 0$, applying Lemma 2.5.3 with $\varepsilon = \tilde{R}_1(t)$ results in

$$\lim_{t \to t_0+} \frac{\|G[\boldsymbol{u}](t) - G[\tilde{\boldsymbol{u}}](t)\|}{t - t_0} \leq \lim_{t \to t_0+} \left(K_1(\varepsilon) \frac{\tilde{R}_1(t)}{t - t_0} + K_2 \left(\tilde{R}_1(t) \right)^{1/2} \right) = 0. \qquad \square$$

The preceding lemma allows us to compute $\partial_{t+} G[\boldsymbol{u}](t) \mid_{t=t_0}$ from the right hand linearization $\tilde{\boldsymbol{u}}$ of $\boldsymbol{u}$ in t_0. This makes life easier because the relay states for $\partial_{t+} G[\tilde{\boldsymbol{u}}]$ are explicitly known. We will derive a formula for $\partial_{t+} G[u](t) \mid_{t=t_0}$ under the assumption that $\partial_{t+} \boldsymbol{u}(t) \mid_{t=t_0} = (\lambda, 0, \ldots, 0)^T$. For the general setting, we can then use an argument similar to Lemma 2.3.3 on the rotation of $\boldsymbol{\mathcal{P}}$.

LEMMA 2.5.5. *Assume* $\partial_{t+} \boldsymbol{u}(t) \mid_{t=t_0} = (\lambda, 0, \ldots, 0)^T$, $\lambda \in \mathbb{R}$, $\lambda \geq 0$. *Then*

$$\begin{aligned} \partial_{t+} G[\boldsymbol{u}](t) \mid_{t=t_0} = \lambda \int_{\Pi_1 \mathcal{C}_{\boldsymbol{u}(t_0)}} \omega(\boldsymbol{x}, r) \frac{\boldsymbol{u}(t_0) - \boldsymbol{x}}{\|\boldsymbol{u}(t_0) - \boldsymbol{x}\|} \mid_{x_1 = \varphi_+(\Pi_1 \boldsymbol{x}, r; \boldsymbol{u}(t_0))} \mathrm{d}(\Pi_1 \boldsymbol{x}, r) \\ - \lambda \lim_{t \to t_0+} \int_{\Pi_1 \left(\mathcal{C}_{\boldsymbol{u}(t_0)} \cap \mathcal{C}_{\tilde{\boldsymbol{u}}(t)} \right)} \omega(\boldsymbol{x}, r) \boldsymbol{h}_{(\boldsymbol{x}, r)}[\boldsymbol{u}](t_0) \mid_{x_1 = \varphi_-(\Pi_1 \boldsymbol{x}, r; \tilde{\boldsymbol{u}}(t))} \mathrm{d}(\Pi_1 \boldsymbol{x}, r) \end{aligned}$$

if these integrals exist and if the second integral is a continuous function of t *in some right-hand neighbourhood of* t_0 *for which the limit at* t_0 *exists.*

PROOF. We proceed in two steps: (a) We make use of the fact that for $t \geq t_0$, the cone $\mathcal{C}_{\tilde{\boldsymbol{u}}(t)}$ forms a convex set moving along a line, so any relay takes exactly one unambiguous state while inside $\mathcal{C}_{\tilde{\boldsymbol{u}}(t)}$. Therefore, we can replace $\boldsymbol{h}_{(\boldsymbol{x},r)}[\tilde{\boldsymbol{u}}]$ by a function $\tilde{\boldsymbol{h}}(\boldsymbol{x}, r)$ defined on the relevant domain $\bigcup_{t\geq t_0} \mathcal{C}_{\tilde{\boldsymbol{u}}(t)}$,

$$\tilde{\boldsymbol{h}}(\boldsymbol{x}, r) = \begin{cases} \boldsymbol{h}_{(\boldsymbol{x},r)}[\tilde{\boldsymbol{u}}](t_0) & \text{if } (\boldsymbol{x}, r) \in \mathcal{C}_{\tilde{\boldsymbol{u}}(t_0)} \\ \frac{1}{r}\big(-\sqrt{r^2 - (x_2 - \tilde{u}_2(t_0))^2 - \cdots - (x_n - \tilde{u}_n(t_0))^2}, & \\ \quad x_2 - \tilde{u}_2(t_0), \ldots, x_n - \tilde{u}_n(t_0)\big)^T & \text{otherwise.} \end{cases}$$

Then we can apply the theorems on differentiation under the integral sign from Section 1.2.1 and obtain the first term of $\partial_{t+} G[\boldsymbol{u}](t) \mid_{t=t_0}$ and an intermediate formulation of the second term. (b) We go from $\tilde{\boldsymbol{h}}(\boldsymbol{x}, r)$ to $\boldsymbol{h}_{(\boldsymbol{x},r)}[\tilde{\boldsymbol{u}}](t_0)$ by showing the error is 0 in the limit to obtain the second term of $\partial_{t+} G[\boldsymbol{u}](t) \mid_{t=t_0}$.

Step (a): Note that $\tilde{\boldsymbol{h}}(\boldsymbol{x}, r)$ is continuous in $\big(\bigcup_{t\geq t_0} \mathcal{C}_{\tilde{\boldsymbol{u}}(t)}\big) \setminus \mathcal{C}_{\tilde{\boldsymbol{u}}(t_0)}$, and that by the choice of $\partial_{t+}\boldsymbol{u}(t) \mid_{t=t_0}$, the function $\tilde{\boldsymbol{u}}$ satisfies $\tilde{\boldsymbol{u}}(t) = (\tilde{u}_1(t), \tilde{u}_2(t_0), \ldots, \tilde{u}_n(t_0))$. For the derivative we get

$$\begin{aligned} \partial_{t+} G[\boldsymbol{u}](t) \mid_{t=t_0} &= \lim_{t\to t_0+} \frac{G[\tilde{\boldsymbol{u}}](t) - G[\tilde{\boldsymbol{u}}](t_0)}{t - t_0} \\ &= \lim_{t\to t_0+} \frac{1}{t - t_0} \int_{\Pi_1 \mathcal{C}_{\boldsymbol{u}(t_0)}} \left[\int_{\varphi_+(x_2,\ldots,x_n,r;\tilde{u}(t_0))}^{\varphi_+(x_2,\ldots,x_n,r;\tilde{u}(t))} - \int_{\varphi_-(x_2,\ldots,x_n,r;\tilde{u}(t_0))}^{\varphi_-(x_2,\ldots,x_n,r;\tilde{u}(t))} \right] \\ &\qquad \omega(\boldsymbol{x}, r)\tilde{\boldsymbol{h}}(\boldsymbol{x}, r)\, \mathrm{d}x_1\, \mathrm{d}(\Pi_1 \boldsymbol{x}, r). \end{aligned} \tag{2.78}$$

To the first integral, by Theorem 1.2.9, on the open set $\mathbb{R} \times \Pi_1 \mathcal{C}_{\boldsymbol{u}(t_0)}$ we can apply the change of variables

$$x_1 = \varphi_+(x_2, \ldots, x_n, r; y, \tilde{u}_2(t_0), \ldots, \tilde{u}_n(t_0))$$

with Jacobian determinant 1. This gives

$$\begin{aligned} &\lim_{t\to t_0+} \frac{1}{t - t_0} \int_{\Pi_1 \mathcal{C}_{\boldsymbol{u}(t_0)}} \int_{\varphi_+(x_2,\ldots,x_n,r;\tilde{u}(t_0))}^{\varphi_+(x_2,\ldots,x_n,r;\tilde{u}(t))} \omega(\boldsymbol{x}, r)\tilde{\boldsymbol{h}}(\boldsymbol{x}, r)\, \mathrm{d}x_1\, \mathrm{d}(\Pi_1 \boldsymbol{x}, r) \\ &= \lim_{t\to t_0+} \frac{1}{t - t_0} \int_{\Pi_1 \mathcal{C}_{\boldsymbol{u}(t_0)}} \int_{\tilde{u}_1(t_0)}^{\tilde{u}_1(t)} \omega(\boldsymbol{x}, r)\tilde{\boldsymbol{h}}(\boldsymbol{x}, r) \mid_{x_1=\varphi_+(x_2,\ldots,x_n,r;y,\tilde{u}_2(t_0),\ldots,\tilde{u}_n(t_0))} \mathrm{d}y\, \mathrm{d}(\Pi_1 \boldsymbol{x}, r) \\ &= \lim_{t\to t_0+} \frac{1}{t - t_0} \int_{\tilde{u}_1(t_0)}^{\tilde{u}_1(t)} \tilde{\boldsymbol{g}}(y)\, \mathrm{d}y \end{aligned}$$

with

$$\tilde{\boldsymbol{g}}(y) := \int_{\Pi_1 \mathcal{C}_{\boldsymbol{u}(t_0)}} \omega(\boldsymbol{x}, r)\tilde{\boldsymbol{h}}(\boldsymbol{x}, r) \mid_{x_1=\varphi_+(x_2,\ldots,x_n,r;y,\tilde{u}_2(t_0),\ldots,\tilde{u}_n(t_0))} \mathrm{d}(\Pi_1 \boldsymbol{x}, r).$$

The function $\tilde{\boldsymbol{g}}$ is continuous for $y \geq \tilde{u}_1(t_0)$ by Theorem 1.2.6 because all the functions involved are continuous. In particular, $\tilde{\boldsymbol{h}}$ is continuous on the hypersurface $x_1 = \varphi_+(x_2, \ldots, x_n, r; y, \tilde{u}_2(t_0), \ldots, \tilde{u}_n(t_0))$, since the points lie completely in

$\big(\bigcup_{t\geq t_0}\mathcal{C}_{\tilde{\boldsymbol{u}}(t)}\big)\setminus\mathcal{C}_{\tilde{\boldsymbol{u}}(t_0)}$. Therefore, by the mean value theorem,

$$\lim_{t\to t_0+}\frac{1}{t-t_0}\int_{\tilde{u}_1(t_0)}^{\tilde{u}_1(t)}\tilde{\boldsymbol{g}}(y)\,\mathrm{d}y=\tilde{\boldsymbol{g}}(\tilde{u}_1(t_0))\tilde{u}_1'(t_0),$$

which accounts for the first term in $\partial_{t+}G[\boldsymbol{u}](t)\mid_{t=t_0}$.

For the second term in (2.78), follow the same line of argument with coordinate transformation

$$x_1=\varphi_-(x_2,\dots,x_n,r;y,\tilde{u}_2(t_0),\dots,\tilde{u}_n(t_0)),$$

obtaining

$$\begin{aligned}&\lim_{t\to t_0+}\frac{1}{t-t_0}\int_{\Pi_1\mathcal{C}_{\boldsymbol{u}(t_0)}}\int_{\varphi_+(x_2,\dots,x_n,r;\tilde{u}(t_0))}^{\varphi_+(x_2,\dots,x_n,r;\tilde{u}(t))}\omega(\boldsymbol{x},r)\tilde{\boldsymbol{h}}(\boldsymbol{x},r)\,\mathrm{d}x_1\,\mathrm{d}(\Pi_1\boldsymbol{x},r)\\ &=\lim_{t\to t_0+}\frac{1}{t-t_0}\int_{\tilde{u}_1(t_0)}^{\tilde{u}_1(t)}\int_{\Pi_1\mathcal{C}_{\boldsymbol{u}(t_0)}}\omega(\boldsymbol{x},r)\tilde{\boldsymbol{h}}(\boldsymbol{x},r)\mid_{x_1=\varphi_-(x_2,\dots,x_n,r;y,\tilde{u}_2(t_0),\dots,\tilde{u}_n(t_0))}\\ &\qquad\qquad\mathrm{d}(\Pi_1\boldsymbol{x},r)\,\mathrm{d}y\end{aligned}\tag{2.79}$$

Because the freeze cone is open, now the function represented by the inner integral will in general not be continuous at $\tilde{u}(t_0)$, preventing us from finishing the argument like for the first term. However, for

$$\lim_{t\to t_0+}\frac{1}{t-t_0}\int_{\tilde{u}_1(t_0)}^{\tilde{u}_1(t)}\int_{\Pi_1\left(\mathcal{C}_{\boldsymbol{u}(t_0)}\cap\mathcal{C}_{\tilde{\boldsymbol{u}}(t)}\right)}\omega(\boldsymbol{x},r)\boldsymbol{h}_{(\boldsymbol{x},r)}[\boldsymbol{u}](t_0)\mid_{x_1=\varphi_-(\Pi_1\boldsymbol{x},r;\tilde{\boldsymbol{u}}(t)]}\mathrm{d}(\Pi_1\boldsymbol{x},r)\,\mathrm{d}y\tag{2.80}$$

the function in y defined by the inner integral can be continuously extended from $y>\tilde{u}_1(t_0)$ to $\tilde{u}_1(t_0)$ by the assumptions and thus the mean value theorem can be applied in the same way as above, giving the second term of $\partial_{t+}G[\boldsymbol{u}](t)\mid_{t=t_0}$.

Step (b): To complete the proof, we will show that (2.80) is equal to (2.79). For this, note that for $t>t_0$

$$\begin{aligned}&\int_{\Pi_1\mathcal{C}_{\boldsymbol{u}(t_0)}}\omega(\boldsymbol{x},r)\tilde{\boldsymbol{h}}(\boldsymbol{x},r)\mid_{x_1=\varphi_-(\Pi_1\boldsymbol{x},r;\tilde{\boldsymbol{u}}(t)]}\mathrm{d}(\Pi_1\boldsymbol{x},r)\\ =&\int_{\Pi_1\left(\mathcal{C}_{\boldsymbol{u}(t_0)}\cap\mathcal{C}_{\tilde{\boldsymbol{u}}(t)}\right)}\omega(\boldsymbol{x},r)\boldsymbol{h}_{(\boldsymbol{x},r)}[\boldsymbol{u}](t_0)\mid_{x_1=\varphi_-(\Pi_1\boldsymbol{x},r;\tilde{\boldsymbol{u}}(t)]}\mathrm{d}(\Pi_1\boldsymbol{x},r)\\ &+\int_{\Pi_1\mathcal{C}_{\boldsymbol{u}(t_0)}\setminus\Pi_1\left(\mathcal{C}_{\boldsymbol{u}(t_0)}\cap\mathcal{C}_{\tilde{\boldsymbol{u}}(t)}\right)}\omega(\boldsymbol{x},r)\tilde{\boldsymbol{h}}(\boldsymbol{x},r)\mid_{x_1=\varphi_-(\Pi_1\boldsymbol{x},r;\tilde{\boldsymbol{u}}(t)]}\mathrm{d}(\Pi_1\boldsymbol{x},r)\end{aligned}$$

by the definition of $\tilde{\boldsymbol{h}}(\boldsymbol{x},r)$. The integral

$$\int_{\Pi_1\mathcal{C}_{\boldsymbol{u}(t_0)}\setminus\Pi_1\left(\mathcal{C}_{\boldsymbol{u}(t_0)}\cap\mathcal{C}_{\tilde{\boldsymbol{u}}(t)}\right)}\omega(\boldsymbol{x},r)\tilde{\boldsymbol{h}}(\boldsymbol{x},r)\mid_{x_1=\varphi_-(\Pi_1\boldsymbol{x},r;\tilde{\boldsymbol{u}}(t)]}\mathrm{d}(\Pi_1\boldsymbol{x},r)$$

is a continuous function in t. Its limit as $t\to t_0$ is 0 by the dominated convergence theorem, because $\|\omega\tilde{\boldsymbol{h}}\|$ is bounded and $\lim_{t\to t_0+}\Pi_1\mathcal{C}_{\boldsymbol{u}(t_0)}\setminus\Pi_1\left(\mathcal{C}_{\boldsymbol{u}(t_0)}\cap\mathcal{C}_{\tilde{\boldsymbol{u}}(t)}\right)=\varnothing$.

Therefore,

$$\lim_{t\to t_0+}\frac{1}{t-t_0}\int_{\tilde{u}_1(t_0)}^{\tilde{u}_1(t)}\int_{\Pi_1\mathcal{C}_{\boldsymbol{u}(t_0)}\setminus\Pi_1\left(\mathcal{C}_{\boldsymbol{u}(t_0)}\cap\mathcal{C}_{\tilde{\boldsymbol{u}}(t)}\right)}\omega(\boldsymbol{x},r)\tilde{\boldsymbol{h}}(\boldsymbol{x},r)\mid_{x_1=\varphi_-(\Pi_1\boldsymbol{x},r;\tilde{\boldsymbol{u}}(t)]}\mathrm{d}(\Pi_1\boldsymbol{x},r) = 0$$

by the mean value theorem, and equality follows. □

From the derivatives of $\boldsymbol{F}$ and $\boldsymbol{G}$, we can now conclude the right-hand derivative of $\boldsymbol{w}=\boldsymbol{\mathcal{P}}[\boldsymbol{u}]$, which results from the relay variation outside the freeze cone and the accumulated switches of relays leaving the freeze cone. In view of the theorem, for a function $\boldsymbol{f}:\mathbb{R}^n\times\mathbb{R}_+\to\mathbb{R}^n$ we define the jump $\lfloor\boldsymbol{f}\rfloor_{x_1=a}:\mathbb{R}^{n-1}\times\mathbb{R}_+\to\mathbb{R}^n$ at $x_1=a$ by

$$\lfloor\boldsymbol{f}\rfloor_{x_1=a}=\lim_{x_1\to a-}\boldsymbol{f}(\boldsymbol{x},r)-\lim_{x_1\to a+}\boldsymbol{f}(\boldsymbol{x},r).$$

THEOREM 2.5.6. *Assume $\boldsymbol{u}$ is twice continuously differentiable on some interval $[t_0,t_1]$, $t_0<t_1$.*

(a) *Let $\partial_{t+}\boldsymbol{u}(t)\mid_{t=t_0}=(\lambda,0,\dots,0)$, $\lambda\geq 0$. Then*

$$\partial_{t+}\boldsymbol{w}(t)\mid_{t=t_0}=\lambda\left[\int_{\mathcal{K}\setminus\mathcal{C}_{\boldsymbol{u}(t_0)}}\omega(\boldsymbol{x},r)\partial_{y_1}\left(\frac{\boldsymbol{y}-\boldsymbol{x}}{\|\boldsymbol{y}-\boldsymbol{x}\|}\right)\Big|_{\boldsymbol{y}=\boldsymbol{u}(t_0)}\mathrm{d}(\boldsymbol{x},r)\right.$$
$$\left.+\int_{\Pi_1\mathcal{C}_{\boldsymbol{u}(t_0)}}\omega(\boldsymbol{x},r)\left\lfloor\boldsymbol{h}_{(\boldsymbol{x},r)}[\boldsymbol{u}](t_0)\right\rfloor_{x_1=\varphi_-(\Pi_1\boldsymbol{x},r;\boldsymbol{u}(t_0))}\mathrm{d}(\Pi_1\boldsymbol{x},r)\right]$$

if the second term satisfies the assumption in Lemma 2.5.5.

(b) *The Gâteaux derivative with respect to arbitrary $\partial_{t+}\boldsymbol{u}(t)$ can be computed from the rotational formula*

$$\partial_{t+}\boldsymbol{w}(t)\mid_{t=t_0}=Q^{-1}\partial_{t+}\boldsymbol{\mathcal{P}}_{Q\omega}[Q\boldsymbol{u},Q\boldsymbol{\xi}](t)\mid_{t=t_0},$$

where $Q\in O(n)$ is chosen such that $Q\partial_{t+}\boldsymbol{u}(t)\mid_{t=t_0}=(\lambda,0,\dots,0)^T$.

PROOF. (a) With $\partial_{t+}\boldsymbol{w}(t)\mid_{t=t_0}=\partial_{t+}\boldsymbol{F}(\boldsymbol{u}(t))\mid_{t=t_0}+\partial_{t+}\boldsymbol{G}[\boldsymbol{u}](t)\mid_{t=t_0}$, the formula accumulates Lemma 2.5.2, Equation (2.73) and Lemma 2.5.5 together with an argument similar to that applied in Part (b) of the proof of Lemma 2.5.5 to show that the second integral term on $\Pi_1\mathcal{C}_{\boldsymbol{u}(t)}$ cancels out.

(b) Applying Lemma 2.3.3 gives

$$\partial_{t+}\boldsymbol{\mathcal{P}}_\omega[\boldsymbol{u}](t)\mid_{t=t_0}=\lim_{t\to t_0+}\frac{\boldsymbol{\mathcal{P}}_\omega[\boldsymbol{u},\boldsymbol{\xi}](t)-\boldsymbol{\mathcal{P}}_\omega[\boldsymbol{u},\boldsymbol{\xi}](t_0)}{t-t_0}$$
$$=Q^{-1}\lim_{t\to t_0+}\frac{\boldsymbol{\mathcal{P}}_{Q\omega}[Q\boldsymbol{u},Q\boldsymbol{\xi}](t)-\boldsymbol{\mathcal{P}}_{Q\omega}[Q\boldsymbol{u},Q\boldsymbol{\xi}](t_0)}{t-t_0}$$

and thus the result. □

REMARK (Derivative and rate-independence). The notion of rate-independence is represented in $\partial_{t+}\boldsymbol{w}$ via the factor λ. For two input functions $\boldsymbol{u}_1$ and $\boldsymbol{u}_2$ to be equivalent up to an admissible time transformation means that they are two different parametrizations of the same input curve. Then their right-hand derivatives $\partial_{t+}\boldsymbol{u}_1$

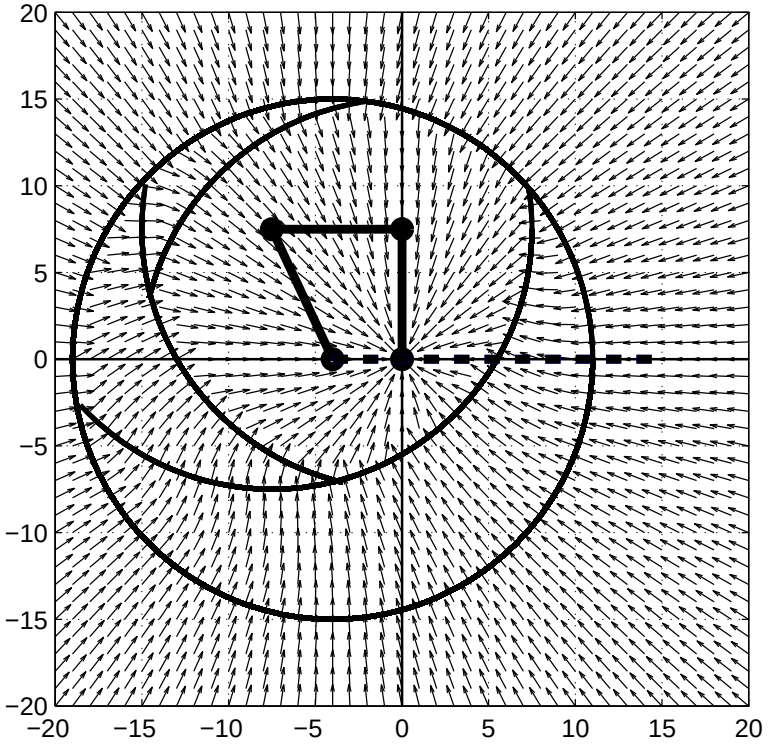

FIGURE 2.15. Memory state at $\boldsymbol{u}(t_3) = (-4, 0)$ in the plane $r = 15$ for initial state $\boldsymbol{\xi}^0$ and piecewice linear input interpolating $(0, 0)$, $(0, 7.5)$, $(-7.5, 7.5)$, $(-4, 0)$.

and $\partial_{t+}\boldsymbol{u}_2$ at corresponding curve points are two vectors equal up to a scalar factor, which reappears in the corresponding λ's in $\partial_{t+}\boldsymbol{w}_1$ and $\partial_{t+}\boldsymbol{w}_2$.

As an application of Theorem 2.5.6, we investigate the output behaviour for a piecewise linear input function and $n = 2$. This is a situation of practical interest because in real life applications, the input to a vectorial hysteresis operator usually consists of a sequence of discrete vectors, which are naturally extended to a continuous input function by linear interpolation.

EXAMPLE 2.5.7. As an example, assume $\boldsymbol{u}$ on $[0, t_3]$, $0 \leq t_3 < T$, is the piecewice linear function interpolating $\boldsymbol{u}(t_0) = (0, 0)$, $\boldsymbol{u}(t_1) = (0, 7.5)$, $\boldsymbol{u}(t_2) = (-7.5, 7.5)$ and $\boldsymbol{u}(t_3) = (-4, 0)$. Figure 2.15 shows the resulting memory state of $\boldsymbol{\mathcal{P}}[\boldsymbol{u}](t_3)$ in the plane $r = 15$, with each vector representing the state of the relay at its base point. As result of a linear step from one point to the next, $\boldsymbol{u}(t_i)$ to $\boldsymbol{u}(t_{i+1})$, the relay states $\boldsymbol{h}_{(\boldsymbol{x},r)}$ form a continuous function of $(\boldsymbol{x}, r)$ in $\mathcal{C}_{\boldsymbol{u}(t_{i+1})} \setminus \mathcal{C}_{\boldsymbol{u}(t_i)}$ at t_{i+1}. Discontinuities of $\boldsymbol{h}_{(\boldsymbol{x},r)}$ can only occur on the boundaries of previous freezecones, $\partial\mathcal{C}_{\boldsymbol{u}(t_j)}$, $j \leq i$, as far as they have not been erased from the memory. In Figure 2.15, these remaining boundaries are drawn at t_3.

Now suppose the input on $[t_3, T]$ is the line segment drawn dashed, so $\partial_{t+}\boldsymbol{u}(t) = (1, 0, \ldots, 0)$. Theorem 2.5.6(a) states that the derivative $\partial_{t+}\boldsymbol{w}(t)$ results from the variations of the relays outside $\mathcal{C}_{\boldsymbol{u}(t)}$, which form a continuous component of $\partial_{t+}\boldsymbol{w}(t)$, and the integral of the jump across $\partial^-\mathcal{C}_{\boldsymbol{u}(t)}$. Geometrically, we see that this second component will vary continuously, unless a discontinuity occurs in $\partial_{t+}\boldsymbol{u}(t)$ and thus in the set $\partial^-\mathcal{C}_{\boldsymbol{u}(t)}$, like at t_3, or $\partial^-\mathcal{C}_{\boldsymbol{u}(t)}$ coincides with $\partial\mathcal{C}_{\boldsymbol{u}(t_j)}$, $j \leq 4$, in a set $S \subset \mathbb{R}^2 \times \mathbb{R}_+$ whose projection $\Pi_1 S$ has non-zero measure in $\mathbb{R}^2$. This happens at most if $\boldsymbol{u}(t) = \boldsymbol{u}(t_j)$, that is, in our particular example, if $\boldsymbol{u}(t) = (0, 0)$. Using further Theorem 2.5.6(b), we conclude that in our example, $\partial_{t+}\boldsymbol{w}(t)$ is continuous everywhere but in t_i, $i = 1, 2, 3$, where $\partial^-\mathcal{C}_{\boldsymbol{u}(t)}$ is discontinuous, and in $t > t_3$ such that $\boldsymbol{u}(t) = (0, 0)$.

Using the same ideas as in the preceeding example, one can deduce the following result:

PROPOSITION 2.5.8. *Assume ω is continuous and of bounded support. For piecewise linear input $\boldsymbol{u}$, the output derivative $\partial_{t+}\boldsymbol{w}$ is discontinuous at most in the discontinuities $t_1, \ldots, t_k$ of $\partial_{t+}\boldsymbol{u}(t)$ and in t such that $\boldsymbol{u}(t) = \boldsymbol{u}(t_i)$ for some $t_i < t$.*

2.5.3. Energy dissipation. A much discussed issue in magnetic modeling is that of hysteresis losses. In order to obey the laws of thermodynamics, the hysteretic process must be dissipative. In Section 2.3.6, we have already discussed magnetic dissipation for closed cycles. To extend this notion to general inputs, we need to know the internal energy density, or hysteresis potential, associated with a hysteretic constitutive law. In [**16**, Chapter 2.5], this question is explored for scalar hysteresis, and hysteresis potentials are suggested for a number of scalar hysteresis operators. Here, we want to address the topic in our vectorial setting and propose a hysteresis potential for $\boldsymbol{\mathcal{P}}$.

As stated in [**16**], it is natural to expect the hysteresis potential to be a hysteresis operator itself, because it should be rate-independent like $\boldsymbol{\mathcal{W}}$ and obviously satisfy the Volterra property. That leads to the natural vector valued extension of Definition 2.5.1 for hysteresis potentials in [**16**].*

DEFINITION 2.5.9 (Hysteresis potentials). Let $\boldsymbol{\mathcal{W}}$ and $\mathcal{U}$ be respectively a vectorial and a scalar hysteresis operator. We call $\mathcal{U}$ a *hysteresis potential* for $\boldsymbol{\mathcal{W}}$, if and only if for all $\boldsymbol{u}$ in the appropriate input set for $\boldsymbol{\mathcal{W}}$ it holds that

$$\partial_t \left(\int_0^t \boldsymbol{u} \cdot \mathrm{d}\boldsymbol{\mathcal{W}}[\boldsymbol{u}] \right) - \partial_t \mathcal{U}[\boldsymbol{u}](t) \geq 0 \qquad \text{a.e. in } (0, T). \tag{2.81}$$

REMARK (Application to magnetic hysteresis losses). The above discussion reflects the situation in magnetism in the following way: The constitutive law

$$\boldsymbol{M} = \boldsymbol{\mathcal{W}}[\boldsymbol{H}]$$

gives

$$\boldsymbol{B} = \mu_0 \boldsymbol{H} + \boldsymbol{\mathcal{W}}[\boldsymbol{H}]. \tag{2.82}$$

*As we are concerned with magnetic hysteresis, we will restrict ourselves to what is called a *counterclockwise hysteresis potential* in [**16**].

As mentioned earlier, see Equation (2.37), the magnetic energy injected into a magnetization process in the interval $[0,t]$ is given by

$$\int_0^t \boldsymbol{H} \cdot \mathrm{d}\boldsymbol{B}.$$

With (2.82), the integral can be partially evaluated to give

$$\int_0^t \boldsymbol{H} \cdot \mathrm{d}\boldsymbol{B} = \frac{\mu_0}{2}(\|\boldsymbol{H}(t)\|^2 - \|\boldsymbol{H}(0)\|^2) + \int_0^t \boldsymbol{H} \cdot \mathrm{d}\boldsymbol{\mathcal{W}}[\boldsymbol{H}].$$

Treating both terms of this sum separately, the first terms contributes immediately to the internal energy. This is in accordance with the general practice of computing the internal energy of a linear magnetization process $\boldsymbol{H} = \mu\boldsymbol{B}$, $\mu = \text{const}$, by (see e.g. [**34**])

$$\int_0^t \boldsymbol{H} \cdot \mathrm{d}\boldsymbol{B} = \frac{\mu}{2}(\|\boldsymbol{H}(t)\|^2 - \|\boldsymbol{H}(0)\|^2).$$

This leaves the hysteresis potential for $\boldsymbol{\mathcal{W}}$ contributed by the second term to be determined.

PROPOSITION 2.5.10. *Consider $\boldsymbol{\mathcal{W}} = \boldsymbol{\mathcal{P}}$ with $\omega \geq 0$ of bounded support $\mathcal{K}$. Assume $\boldsymbol{u}$ is piecewise twice continuously differentiable, and that $\boldsymbol{w}'(t)$ exists and $\partial_{t+}\boldsymbol{w}(t)$ can be computed via Theorem 2.5.6 a.e. in $[0,T]$. Then*

$$\mathcal{U}[\boldsymbol{u}](t) = \int_0^\infty \int_{\mathbb{R}^n} \omega(\boldsymbol{x},r)\, \boldsymbol{x} \cdot \boldsymbol{h}_{(\boldsymbol{x},r)}[\boldsymbol{u}](t)\, \mathrm{d}\boldsymbol{x}\, \mathrm{d}r$$

satisfies (2.81).

PROOF. Where $\boldsymbol{w}'$ exists, it is equal to $\partial_{t+}\boldsymbol{w}$ given by Theorem 2.5.6. Due to the rotational symmetries of $\boldsymbol{\mathcal{P}}$ and accordingly $\mathcal{U}$, which we have worked out in detail earlier, we can suppose without loss of generality that $\boldsymbol{u}' = (\lambda, 0, \ldots, 0)$, $\lambda \geq 0$. Then $\partial_t\mathcal{U}[\boldsymbol{u}](t)$ can be derived in complete analogy to $\partial_{t+}\boldsymbol{w}$ by noting that

$$\mathcal{U}[\boldsymbol{u}](t) = \sum_{i=1}^n \int_0^\infty \int_{\mathbb{R}^n} x_i\, \omega(\boldsymbol{x},r) \left(\boldsymbol{h}_{(\boldsymbol{x},r)}[\boldsymbol{u}](t)\right)_i \mathrm{d}\boldsymbol{x}\, \mathrm{d}r$$

with $\left(\boldsymbol{h}_{(\boldsymbol{x},r)}[\boldsymbol{u}](t)\right)_i$ the ith component of $\boldsymbol{h}_{(\boldsymbol{x},r)}[\boldsymbol{u}](t)$, and carrying the derivatives over componentwise from the previous section. We obtain

$$\begin{aligned}\partial_t\mathcal{U}[\boldsymbol{u}](t) =& \lambda \left[\int_{\mathcal{K}\setminus\mathcal{C}_{\boldsymbol{u}(t)}} \omega(\boldsymbol{x},r)\, \boldsymbol{x} \cdot \partial_{y_1} \left(\frac{\boldsymbol{y}-\boldsymbol{x}}{\|\boldsymbol{y}-\boldsymbol{x}\|} \right) \Big|_{\boldsymbol{y}=\boldsymbol{u}(t)} \mathrm{d}(\boldsymbol{x},r) \right. \\ &\left. + \int_{\Pi_1\mathcal{C}_{\boldsymbol{u}(t)}} \omega(\boldsymbol{x},r)\, \boldsymbol{x} \cdot \left[\boldsymbol{h}_{(\boldsymbol{x},r)}[\boldsymbol{u}](t)\right]_{x_1=\varphi_-(\Pi_1\boldsymbol{x},r;\boldsymbol{u}(t))} \mathrm{d}(\Pi_1\boldsymbol{x},r) \right].\end{aligned}$$

The existence of $\boldsymbol{w}'$ by Theorem 1.2.16 gives

$$\partial_t \left(\int_0^t \boldsymbol{u} \cdot \mathrm{d}\boldsymbol{\mathcal{W}}[\boldsymbol{u}] \right) = \boldsymbol{u}(t) \cdot \boldsymbol{w}'(t).$$

Therewith, the left hand side of (2.81) is equal to

$$\begin{aligned}
&\boldsymbol{u}(t)\cdot\boldsymbol{w}'(t) - \partial_t\mathcal{U}[\boldsymbol{u}](t)\\
&\quad=\lambda\left[\int_{\mathcal{K}\setminus\mathcal{C}_{\boldsymbol{u}}(t)} \omega(\boldsymbol{x},r)\,(\boldsymbol{u}(t)-\boldsymbol{x})\cdot\partial_{y_1}\left[\frac{\boldsymbol{y}-\boldsymbol{x}}{\|\boldsymbol{y}-\boldsymbol{x}\|}\right]\Big|_{\boldsymbol{y}=\boldsymbol{u}(t)}\mathrm{d}(\boldsymbol{x},r)\right.\\
&\qquad\left.+\int_{\Pi_1\mathcal{C}_{\boldsymbol{u}}(t)} \omega(\boldsymbol{x},r)\,(\boldsymbol{u}(t)-\boldsymbol{x})\cdot\left\lfloor\boldsymbol{h}_{(\boldsymbol{x},r)}[\boldsymbol{u}](t)\right\rfloor_{x_1=\varphi_-(\Pi_1\boldsymbol{x},r;\boldsymbol{u}(t))}\mathrm{d}(\Pi_1\boldsymbol{x},r)\right].
\end{aligned}$$

To see that this is nonnegative, the integrand of the first integral can be explicitly evaluated to be equal to 0 by computing the derivative. The second integrand is nonnegative because for any $(\boldsymbol{x},r)$,

$$(\boldsymbol{u}(t)-\boldsymbol{x})\cdot\left\lfloor\boldsymbol{h}_{(\boldsymbol{x},r)}[\boldsymbol{u}](t)\right\rfloor_{x_1=\varphi_-(\Pi_1\boldsymbol{x},r;\boldsymbol{u}(t))} = (\boldsymbol{u}(t)-\boldsymbol{x})\cdot\left(\frac{\boldsymbol{u}(t)-\boldsymbol{x}}{\|\boldsymbol{u}(t)-\boldsymbol{x}\|}-\boldsymbol{e}\right)\geq 0$$

for some unit vector $\boldsymbol{e}$. □

Proposition 2.5.10 thus presents us with a possible hysteresis potential for $\boldsymbol{\mathcal{P}}$. In fact, for the scalar Preisach operator arising from $\boldsymbol{\mathcal{P}}$ for $n=1$, this $\mathcal{U}$ corresponds to the one suggested in [**16**, Proposition 2.5.4].

CHAPTER 3

Electromagnetic field simulation with hysteresis

In this Chapter, we present electromagnetic field simulations with hysteresis. The vector Preisach operator $\boldsymbol{\mathcal{P}}$ was computer implemented and coupled with an existing simulation software to numerically solve two-dimensional electromagnetic field problems.

The implementation of $\boldsymbol{\mathcal{P}}$ is done by discretization of its memory. As the electromagnetic simulation algorithm is based on the common vector potential formulation and therefore requires an inversion of the hysteresis relationship $\boldsymbol{B}[\boldsymbol{H}]$, an ad hoc method was developed to address these issues and provide an inverse solution.

In the first section of this chapter, we give a short introduction to Maxwell's equations and set up the relevant problem with hysteresis. The second section addresses the numerical algorithm used in the simulations. Then, we present numerical solutions for three electromagnetic field problems. The first is that of a hysteretic ring core and aims at analytical verification of the numerical results. The second problem considers a simple magnetic sensor and reproduces in simulations a hysteresis effect observed in measurements. The third model investigates hysteresis effects in a magnetic valve.

3.1. Maxwell's equations and hysteresis

The fundamental laws governing electromagnetism are Maxwell's equations [**40, 48**]. They describe the physical relationship between the magnetic and the electric field quantities, namely magnetic induction $\boldsymbol{B}$ [Vs/m^2], magnetic field $\boldsymbol{H}$ [A/m], electric induction $\boldsymbol{D}$ [V/m] and electric field $\boldsymbol{E}$ [As/m^2]. In differential form, Maxwell's equations are given by

$$\operatorname{curl} \boldsymbol{H} = \boldsymbol{g} + \partial_t \boldsymbol{D}, \tag{3.1}$$

$$\operatorname{curl} \boldsymbol{E} = -\partial_t \boldsymbol{B}, \tag{3.2}$$

$$\operatorname{div} \boldsymbol{B} = 0, \tag{3.3}$$

$$\operatorname{div} \boldsymbol{D} = \rho. \tag{3.4}$$

Here, $\boldsymbol{g}$ [A/m^2] is the free current density and ρ [As/m^2] the electric charge density. The quantities $\boldsymbol{B}$, $\boldsymbol{H}$, $\boldsymbol{E}$, $\boldsymbol{D}$ and $\boldsymbol{g}$ are vector valued functions and ρ is a scalar valued function in space $\boldsymbol{x} \in \mathbb{R}^3$ and time $t \in [0, T]$. The symbols s, m, A, and V denote the usual SI units.

To fully describe the involved quantities $(\boldsymbol{H}, \boldsymbol{B}, \boldsymbol{D}, \boldsymbol{E}, \boldsymbol{g}, \rho)$, the above system must be completed by additional equations representing the presence of matter and matter-field interaction [**40**]. They depend on the specific material properties. We

assume these constitutive laws to be of the general form [**46, 48**]

$$\boldsymbol{D} = \varepsilon_0 \boldsymbol{E} + \boldsymbol{P}, \tag{3.5}$$

$$\boldsymbol{B} = \mu_0 \boldsymbol{H} + \boldsymbol{M}, \tag{3.6}$$

$$\boldsymbol{g} = \boldsymbol{g}_s + \sigma \boldsymbol{E}. \tag{3.7}$$

Magnetic permeability of free space $\mu_0 = 4\pi \cdot 10^{-7}\mathrm{N/A}^2$, permittivity of free space $\varepsilon_0 = 1/(\mu_0 c^2)[\mathrm{As/(Vm)}]$ and speed of light c are universal constants. $\boldsymbol{M}$ $[\mathrm{Vs/m}^2]$ is the magnetization with which a material reacts to a magnetic field $\boldsymbol{H}$ that it is subjected to. Accordingly, $\boldsymbol{P}$ is the polarization resulting from the electric field $\boldsymbol{E}$ in the material. In Ohm's law (3.7), $\boldsymbol{g}_s$ is the impressed current density and σ $[\mathrm{A/(Vm)}]$ the material specific conductivity.

Remark. Note that Ohm's law (3.7) only holds true for stationary geometry. If moving bodies are involved, (3.7) must be replaced by [**40**]

$$\boldsymbol{g} = \boldsymbol{g}_s + \sigma(\boldsymbol{E} + \boldsymbol{v} \times \boldsymbol{B}).$$

The second term accounts for the currents induced by the Lorentz force resulting from the velocity $\boldsymbol{v}$ of a moving body. Quasi-stationary electromagnetic field problems with motion are discussed in detail in [**46**]. There, it is derived that for BEM-FEM coupling, which forms the numerical basis of our later simulations, $\boldsymbol{v}$ does not appear in the final formulation of the system but through moving domain boundaries. Therefore, we do not consider the additional term.

In fact, system (3.1)-(3.4) implicitly assumes the regularity of the fields at any point in space by differentiating them everywhere. This does not need to hold true at material interfaces, where the fields do not even need to be continuous. Maxwell's equations can be used to deduce transmission conditions arising at these interfaces [**40, 48**]. Assume two different media occupying domains Ω_1 and Ω_2 share a common surface Σ. Denote by $\boldsymbol{n}$ the normal field on Σ directed from Ω_1 to Ω_2, and by $\lfloor \boldsymbol{u} \rfloor_\Sigma$ the jump of a vector field $\boldsymbol{u}$ across Σ:

$$\lfloor \boldsymbol{u}(\boldsymbol{x}) \rfloor_\Sigma = \lim_{h \to 0+} \boldsymbol{u}(\boldsymbol{x} + h\boldsymbol{n}(\boldsymbol{x})) - \lim_{h \to 0-} \boldsymbol{u}(\boldsymbol{x} + h\boldsymbol{n}(\boldsymbol{x})).$$

Let ρ_Σ and $\boldsymbol{g}_\Sigma$ respectively be the charge and current densities concentrated on Σ. Then the transmission conditions at the interface Σ are given by

$$\boldsymbol{n} \times \lfloor \boldsymbol{H} \rfloor_\Sigma = \boldsymbol{g}_\Sigma, \tag{3.8}$$

$$\boldsymbol{n} \times \lfloor \boldsymbol{E} \rfloor_\Sigma = 0, \tag{3.9}$$

$$\boldsymbol{n} \cdot \lfloor \boldsymbol{B} \rfloor_\Sigma = 0, \tag{3.10}$$

$$\boldsymbol{n} \cdot \lfloor \boldsymbol{D} \rfloor_\Sigma = \rho_\Sigma. \tag{3.11}$$

We will only consider applications where $\boldsymbol{g}_\Sigma$ is negligible, and thus set

$$\boldsymbol{g}_\Sigma = 0.$$

The full system of Maxwell equations (3.1)-(3.4) together with the material equations (3.5)-(3.7) and initial conditions at $t = 0$ describes general time-dependent electromagnetic fields. The electromagnetic field problems considered in practice

often do not require the solution of Maxwell's equations in full generality. The applications in the context of this dissertation originate from low-frequency electromagnetic components like magnetic valves and sensors. Here the spatial distances involved are small relative to the speed at which field changes propagate in space. It suffices to consider the *quasi-stationary approximation* or *eddy current formulation* of Maxwell's equations [**7**], formally introduced by $\varepsilon_0 = 0$, $\boldsymbol{P} = 0$, and therefore $\boldsymbol{D} = 0$, $\rho = 0$ [**46**]. Maxwell's equations (3.1)-(3.4) reduce to

$$\operatorname{curl} \boldsymbol{H} = \boldsymbol{g}, \tag{3.12}$$

$$\operatorname{curl} \boldsymbol{E} = -\partial_t \boldsymbol{B}, \tag{3.13}$$

$$\operatorname{div} \boldsymbol{B} = 0, \tag{3.14}$$

together with the material equations (3.6) and (3.7).

If, moreover, the impressed currents vary very slowly, both time derivatives can be neglected, $\partial_t \boldsymbol{D} = \partial_t \boldsymbol{B} = 0$. Assuming further that $\boldsymbol{g} = \boldsymbol{g}_s$, we obtain the *magnetostatic formulation* of Maxwell's equations [**48**]

$$\operatorname{curl} \boldsymbol{H} = \boldsymbol{g}_s, \tag{3.15}$$

$$\operatorname{div} \boldsymbol{B} = 0, \tag{3.16}$$

together with

$$\boldsymbol{B} = \mu_0 \boldsymbol{H} + \boldsymbol{M}. \tag{3.17}$$

To complete the Maxwell system, we are still missing an equation relating the magnetization $\boldsymbol{M}$ to the other field quantities. Anhysteretic formulations assume either a linear dependence of $\boldsymbol{M}$ and thus $\boldsymbol{B}$ on $\boldsymbol{H}$,

$$\boldsymbol{B} = (\mu_0 + \mu)\boldsymbol{H} \tag{3.18}$$

with a constant $\mu \geq 0$, or a nonlinear relationship of the form

$$\boldsymbol{B} = (\mu_0 + \mu(\|\boldsymbol{H}\|))\boldsymbol{H} \tag{3.19}$$

with a bounded continuous function $\mu : \mathbb{R}_+ \to \mathbb{R}_+$ such that $\mu(\|\boldsymbol{H}\|)\|\boldsymbol{H}\|$ is monotonically increasing in $\|\boldsymbol{H}\|$.

We model the dependence of $\boldsymbol{M}$ on $\boldsymbol{H}$ in hysteretic model components by the constitutive relation $\boldsymbol{M} = \boldsymbol{\mathcal{P}}[\boldsymbol{H}]$, that is,

$$\boldsymbol{B} = \mu_0 \boldsymbol{H} + \boldsymbol{\mathcal{P}}[\boldsymbol{H}], \tag{3.20}$$

with a Preisach distribution $\omega \geq 0$ of bounded support. Together with Maxwell's equations, the result is a partial differential equation of vector-valued functions with hysteresis.

In view of the electromagnetic field simulations, the question of the existence and uniqueness of solutions immediately springs up. As hysteresis plays a role in many applications, partial differential equations with hysteresis form an active field of mathematical interest. In recent decades, much research has been done in the context of scalar-valued functions and hysteresis and many results have been established, see e.g. [**16, 44, 67**]. For the scalar-valued Maxwell's equations, an overview

of known existence and uniqueness results can be found in [**68**]. In summary, existence has been widely proven, whereas uniqueness remains an open problem in many cases.

The vectorial Maxwell's equations with hysteresis remain a mostly unresolved issue. The only known result is by Visintin [**69**], who has shown existence of the solution for hysteresis represented by a vectorial formulation of the scalar relay operator $h_{(x,r)}$ by the same projection method applied in the construction of Mayergoyz' vector Preisach operator (Example 2.1.9). His method of proof is approximation by time-discretization, derivation of energy-type estimates and passage to the limit. Uniqueness remains open, as well as the extension from scalar relay to scalar Preisach operator or other hysteresis operators.

For the hysteresis operator $\boldsymbol{\mathcal{P}}$ investigated in this dissertation, existence and uniqueness of solutions is also an open question. It would be interesting to see if Visintin's method of proof can be carried over in any way. The transition of the proof from his vector formulation of the scalar relay to the vector relay operator $\boldsymbol{h}_{(\boldsymbol{x},r)}$ is not immediate, because Visintin reformulates the relay variationally in terms of two conditions that he calls *confinement* and *dissipation condition*. Due to the only partially dissipative nature of $\boldsymbol{h}_{(\boldsymbol{x},r)}$ described in Lemma 2.2.8, we have only been able to carry over the confinement condition, see Lemma B.0.2.

However, given that $\boldsymbol{\mathcal{P}}$ is monotone in that setup, one can at least state the existence of a solution in each time step of the time discretized magnetostatic problem on an appropriate spatial domain Ω. To stay within the scope of this thesis, we will limit discussion to a brief outline of the argument. Time discretization $t_0, \ldots, t_L$ of the initial value problem associated with the system (3.15)-(3.17) removes hysteresis from the single time steps. This is because at each t_i, after defining the form of the step from $\boldsymbol{H}(t_{i-1})$ to $\boldsymbol{H}(t_i)$ to be e.g. linear (cf. the introductory remark on discontinuities and vectorial hysteresis in Section 2.1), $\boldsymbol{\mathcal{P}}$ corresponds to a function $\boldsymbol{P}_i : \mathbb{R}^n \to \mathbb{R}^n$. Define $\boldsymbol{a}_i : \Omega \times \mathbb{R}^n \to \mathbb{R}^n$ to be the function representing the respective constitutive law in each point of Ω, that is (3.18), (3.19) or (3.20) with $\boldsymbol{\mathcal{P}}$ replaced by $\boldsymbol{P}_i$. Then if $\boldsymbol{P}_i$ is monotonic, as defined in Section 1.1, $\boldsymbol{a}_i$ satisfies the following conditions in each $\boldsymbol{z} \in \Omega$:

- *pointwise continuity:* $\boldsymbol{a}_i(\boldsymbol{z}, \boldsymbol{H})$ is continuous with respect to $\boldsymbol{H}$ because $\boldsymbol{P}_i$ is continuous as a consequence of Lemma 2.5.3.
- *growth condition:* There exist constants c_0, c_1 such that

  $$\|\boldsymbol{a}_i(\boldsymbol{z}, \boldsymbol{H})\| \leq c_0 + c_1 \|\boldsymbol{H}\| \quad \text{for all } \boldsymbol{H} \in \mathbb{R}^n.$$

  For (3.18) and (3.19), this is clear. For $\boldsymbol{P}_i$, it follows from the observations on the saturation of $\boldsymbol{\mathcal{P}}$ in Section 2.3.4.
- *coercivity:*

  $$\lim_{\|\boldsymbol{H}\| \to \infty} \frac{\boldsymbol{a}_i(\boldsymbol{z}, \boldsymbol{H}) \cdot \boldsymbol{H}}{\|\boldsymbol{H}\|} = \infty.$$

  In each of the constitutive laws, this is guaranteed by the term $\mu_0 \boldsymbol{H}$.
- *monotonicity:*

  $$(\boldsymbol{a}_i(\boldsymbol{z}, \boldsymbol{H}_1) - \boldsymbol{a}_i(\boldsymbol{z}, \boldsymbol{H}_2)) \cdot (\boldsymbol{H}_1 - \boldsymbol{H}_2) \geq 0 \qquad \text{for all } \boldsymbol{H}_1, \boldsymbol{H}_2 \in \mathbb{R}^n.$$

This is quickly shown for (3.18) and (3.19), and follows from the monotonicity of $\boldsymbol{P}_i$ for hysteresis.

Based on these properties, the existence of a solution of the magnetostatic problem in each time step can now be shown using standard methods of convex analysis and, in particular, applying Browder's Theorem [**13, 37**].

It remains to be shown that $\boldsymbol{P}_i$ is monotone, or alternatively give monotonicity conditions for $\boldsymbol{P}_i$. The challenge here will be to characterize the attainable memory states of $\boldsymbol{\mathcal{P}}$, in order to make the investigation of monotonicity tangible. In any case, the reversible part of the memory, that is the relays outside $\mathcal{C}_{\boldsymbol{H}(t)}$, form a strictly monotone component. It dominates the behaviour of $\boldsymbol{P}_i$ with increasing distance from $\boldsymbol{H}(t_{i-1})$. Also, our computational tests have indicated that $\boldsymbol{P}_i$ is monotone, or at least very close to monotone, for the Preisach distributions used in the simulations presented later in this chapter.

Despite the open questions in the solution theory, it is nonetheless fruitful and desirable to investigate the electromagnetic field problems with hysteresis algorithmically. The results can be useful in solving industrial problems, and may provide some mathematical insight in the underlying theory. In some cases, it is possible to compute analytic solutions and validate the numerical results on these (e.g. [**65, 30, 45**]). Otherwise, one can compare the numerical solution to experimental measurements to see that reasonable results are obtained in the simulations and justify the approach.

3.2. Simulation

The vector Preisach operator $\boldsymbol{\mathcal{P}}$ was used to model isotropic magnetic hysteresis via the constitutive relation (3.20) in the framework of 2D electromagnetic field simulations. To this end, a discretized approximation of $\boldsymbol{\mathcal{P}}$ was computer implemented and coupled with an existing electromagnetic simulation software [**28, 46, 47, 61**]. The software combines finite elements method (FEM) and boundary elements method (BEM) to solve quasistationary electromagnetic field problems on the entire $\mathbb{R}^2$ or $\mathbb{R}^3$.* The unbounded domain is made possible because the BEM requires only a discretization of the domain boundary. The subdomains containing non-air materials are FEM discretized, and the remaining air space is discretized by the appropriate lower-dimensional BEM elements on the boundary of the FEM domains. Both methods are coupled on the common boundary via the respective transmission conditions.

The FEM-BEM method operates on a $\boldsymbol{B}$ based scheme, as it uses the magnetic vector potential formulation [**6**] to obtain a weak formulation of the partial differential equation. The simulation process consists of a sequence of discrete time steps $t_0, \ldots, t_L$. The vector Preisach operator is used to compute $\boldsymbol{M}$ in terms of $\boldsymbol{B}$ when setting up the right-hand side of the linear FEM equation system in each time step.

*The nodal Galerkin approach applied as finite elements method in the program has been demonstrated to be mathematically incorrect as in $\mathbb{R}^3$ it only discretizes a subspace of the solution space. The correct approach is that via edge elements (e.g. [**8**]). However, in $\mathbb{R}^2$ the solution is correctly discretized but on boundaries and the nodal method is appropriate [**19**].

Since the evaluation of $\boldsymbol{M}$ takes place in the Gauss points of the finite element mesh, we equip each Gauss point with its own vector Preisach operator. In each time step, the nonlinear system is solved applying $\boldsymbol{M}[\boldsymbol{B}]$-iteration [**28, 47**], a fixed point method. At t_0, we initialize the vector Preisach operator $\boldsymbol{\mathcal{P}}$ in the neutral initial state $\boldsymbol{\xi}^0$.

As discussed earlier, for $\boldsymbol{\mathcal{P}}$ it matters which path its input function $\boldsymbol{u}$ takes between two discrete inputs $\boldsymbol{u}(t_{i-1})$ and $\boldsymbol{u}(t_i)$. In the simulations, we assume the input step from $\boldsymbol{u}(t_{i-1})$ to $\boldsymbol{u}(t_i)$ to be linear. Define the prolongation operator π_A to map a string of vectors to the piecewise linear function

$$\boldsymbol{u} = \pi_A(\boldsymbol{u}_0, \dots, \boldsymbol{u}_L) \in C([0,T];\mathbb{R}^2)$$

interpolating the points $\boldsymbol{u}\left(\frac{i}{N}T\right) = \boldsymbol{u}_i$. With the above assumption, in each time step t_{i-1} to t_i, the operator $\boldsymbol{\mathcal{P}}$ reduces to a function $\boldsymbol{P}_i : \mathbb{R}^2 \to \mathbb{R}^2$,

$$\boldsymbol{P}_i(\tilde{\boldsymbol{u}}) = \boldsymbol{\mathcal{P}}[\pi_A(\boldsymbol{u}(t_1), \dots, \boldsymbol{u}(t_{i-1}), \tilde{\boldsymbol{u}})](t_i),$$

mapping the new input vector $\tilde{\boldsymbol{u}}$ to the corresponding output vector $\boldsymbol{P}_i(\tilde{\boldsymbol{u}})$. The function $\boldsymbol{P}_i$ is continuous in $\tilde{\boldsymbol{u}}$ as a consequence of Lemma 2.5.3. For later reference, set

$$\boldsymbol{w}(t_i) := \boldsymbol{P}_i(\boldsymbol{u}(t_i))$$

for the solution of the ith time step.

To computer implement $\boldsymbol{\mathcal{P}}$ for $n = 2$, the continuous Preisach memory is discretized by a finite number of relays $\boldsymbol{h}_{(\boldsymbol{x}^{i,j},r^k)}$ in the points $(\boldsymbol{x}^{i,j}, r^k) = (x_1^i, x_2^j, r^k) \in \mathbb{R}^2 \times (\mathbb{R}_+ \cup \{0\})$. A regular discretization grid

$$\left\{(x_1^i, x_2^j, r^k) \;\middle|\; x_1^i = i\frac{R}{N},\ x_2^j = j\frac{R}{N},\ r^k = k\frac{R}{N},\ i,j = -N,\dots,N,\ k = 0,\dots,N\right\}$$

is used. Here, N is the grid parameter, and R is chosen such that $\omega(\boldsymbol{x}, r) = 0$ for all $(\boldsymbol{x}, r)$ such that $\|\boldsymbol{x}\| + r > R$. The Preisach distribution $\omega(\boldsymbol{x}, r)$ is replaced by weights ω_{ijk},

$$\omega_{ijk} = \int_{\left(i-\frac{1}{2}\right)\frac{R}{N}}^{\left(i+\frac{1}{2}\right)\frac{R}{N}} \int_{\left(j-\frac{1}{2}\right)\frac{R}{N}}^{\left(j+\frac{1}{2}\right)\frac{R}{N}} \int_{\max\left\{0,\left(k-\frac{1}{2}\right)\frac{R}{N}\right\}}^{\left(k+\frac{1}{2}\right)\frac{R}{N}} \omega((x_1,x_2),r)\,\mathrm{d}x_1\,\mathrm{d}x_2\,\mathrm{d}r,$$

in the grid nodes.

We can now approximate $\boldsymbol{\mathcal{P}}$ by the discretized vector Preisach operator $\boldsymbol{\mathcal{P}}^{\mathrm{d}}$:

$$\boldsymbol{\mathcal{P}}[\boldsymbol{u}](t) \approx \boldsymbol{\mathcal{P}}^{\mathrm{d}}[\boldsymbol{u}](t) := \sum_{i=-N}^{N} \sum_{j=-N}^{N} \sum_{k=0}^{N} \omega_{ijk} \boldsymbol{h}_{(\boldsymbol{x}^{i,j},r^k)}[\boldsymbol{u}](t). \tag{3.21}$$

The definition of the corresponding function $\boldsymbol{P}_i^{\mathrm{d}}$ in analogy to $\boldsymbol{P}_i$ is clear.

In terms of our input and output variables, the material equation (3.17) in each time step turns into

$$\tilde{\boldsymbol{w}} = \mu_0 \tilde{\boldsymbol{u}} + \boldsymbol{P}_i(\tilde{\boldsymbol{u}}), \quad \tilde{\boldsymbol{u}}, \tilde{\boldsymbol{w}} \in \mathbb{R}^2.$$

Due to the method applied in the electromagnetic simulation software, we need to invert this equation to obtain $\boldsymbol{P}_i[\tilde{\boldsymbol{u}}]$, i.e. $\boldsymbol{M}(t_i)$, in dependence of a given $\tilde{\boldsymbol{w}}$, i.e. $\boldsymbol{B}(t_i)$. The function $\boldsymbol{P}_i^{\mathrm{d}}$ is not suitable for inversion because, unlike $\boldsymbol{P}_i$, it is

discontinuous: Each time t when one of the relays $\boldsymbol{h}_{(\boldsymbol{x}^{i,j},r^k)}$ leaves the freeze cone $\mathcal{C}_{\boldsymbol{u}(t)}$, it produces a jump of

$$\omega_{ijk}\left(\boldsymbol{h}_{(\boldsymbol{x}^{i,j},r^k)}[\boldsymbol{u}](t)-\lim_{\delta\to 0+}\boldsymbol{h}_{(\boldsymbol{x}^{i,j},r^k)}[\boldsymbol{u}](t-\delta)\right)$$

in $\boldsymbol{\mathcal{P}}^{\mathrm{d}}[\boldsymbol{u}]$, resulting in a discontinuity in $\boldsymbol{P}_i^{\mathrm{d}}$. We address this issue in a straightforward, rather crude, manner by replacing $\boldsymbol{P}_i^{\mathrm{d}}$ by a continuous piecewise linear approximation $\boldsymbol{P}_i^{\mathrm{dl}}$. For this, we evaluate $\boldsymbol{P}_i^{\mathrm{d}}$ exactly in the grid nodes,

$$\boldsymbol{P}_i^{\mathrm{dl}}(\boldsymbol{x}^{i,j})=\boldsymbol{P}_i^{\mathrm{d}}(\boldsymbol{x}^{i,j}).$$

Between the grid nodes $\boldsymbol{x}^{i,j}$, the funcion $\boldsymbol{P}_i^{\mathrm{dl}}$ is the piecewise linear interpolation of the grid nodes. Figure 3.1 shows the form of the interpolation grid. A fundamental property of rate-independent hysteresis is that the output function is constant in a time interval whenever the input function is. In the time-discretized setting this means that $\boldsymbol{P}_i^{\mathrm{dl}}$ must fix the solution from the previous time step,

$$\boldsymbol{P}_i^{\mathrm{dl}}(\boldsymbol{u}(t_{i-1}))=\boldsymbol{w}(t_{i-1}).$$

To guarantee this condition, the interpolation for $\boldsymbol{P}_i^{\mathrm{dl}}$ contains additionally the point $(\boldsymbol{u}(t_{i-1}),\boldsymbol{w}(t_{i-1}))$. Note that here lies a weakness of this approach: For lack of an interpolation method that depends continuously on $\boldsymbol{u}(t_{i-1})$, if this point is too close to a grid edge, the interpolation grid discontinuously switches to a different interpolation pattern, shown on the right-hand side of Figure 3.1. Another weakness of the grid approach is the lack of rotational symmetry of the grid.

It would be highly inefficient to pursue the grid interpolation method in saturation, that is, where $\|\tilde{\boldsymbol{u}}\|>R$ may be arbitrarily large and the output values are unambiguously known anyway. Here, we define a transitional ring on which the output value is the linear interpolation of $R\frac{\tilde{\boldsymbol{u}}}{\|\tilde{\boldsymbol{u}}\|}$ and $(R+\delta)\frac{\tilde{\boldsymbol{u}}}{\|\tilde{\boldsymbol{u}}\|}$. Outside the ring, the saturation curve

$$\tilde{\boldsymbol{w}}=\lambda(\|\tilde{\boldsymbol{u}}\|)\tilde{\boldsymbol{u}} \tag{3.22}$$

(cf. Equation (2.24)) is piecewise linearly interpolated to obtain a relationship of the form (3.19).

We now have a continuous map $\tilde{\boldsymbol{u}}\to\tilde{\boldsymbol{w}}=\mu_0\tilde{\boldsymbol{u}}+\boldsymbol{P}_i^{\mathrm{dl}}(\tilde{\boldsymbol{u}})$ which satisfies $\tilde{\boldsymbol{u}}\cdot\tilde{\boldsymbol{w}}=\mu(\|\tilde{\boldsymbol{u}}\|)\|\tilde{\boldsymbol{u}}\|^2\geq 0$ on any circle $\partial B_{\boldsymbol{0},\tilde{R}}$ for $\tilde{R}\geq R+\delta$ and is therefore surjective in $\overline{B_{\boldsymbol{0},\tilde{R}}}$ [**37**, Theorem 30.5]. As also the output can get arbitrarily large, an inverse exists for any $\tilde{\boldsymbol{w}}\in\mathbb{R}^2$. Uniqueness of the inverse cannot be ensured, because the applied interpolation does not guarantee monotonicity of $\boldsymbol{P}_i^{\mathrm{dl}}$, even if the provided nodal data were pairwise monotone (cf. Appendix C). However, to our knowledge, no $2D$ monotonicity preserving interpolation for this situation has been developed so far. In the test applications considered, the map appears to be close to monotone, so no further effort was invested into clearing that issue, which should rather be resolved later by means of a better implementation method of $\boldsymbol{\mathcal{P}}$. In saturation, the inverse is unique and easily computed from relationship (3.22). On the grid, an inverse is numerically computed by applying Newton's method with the local tangent matrices of the piecewise linear interpolation and stepwidth restriction combined

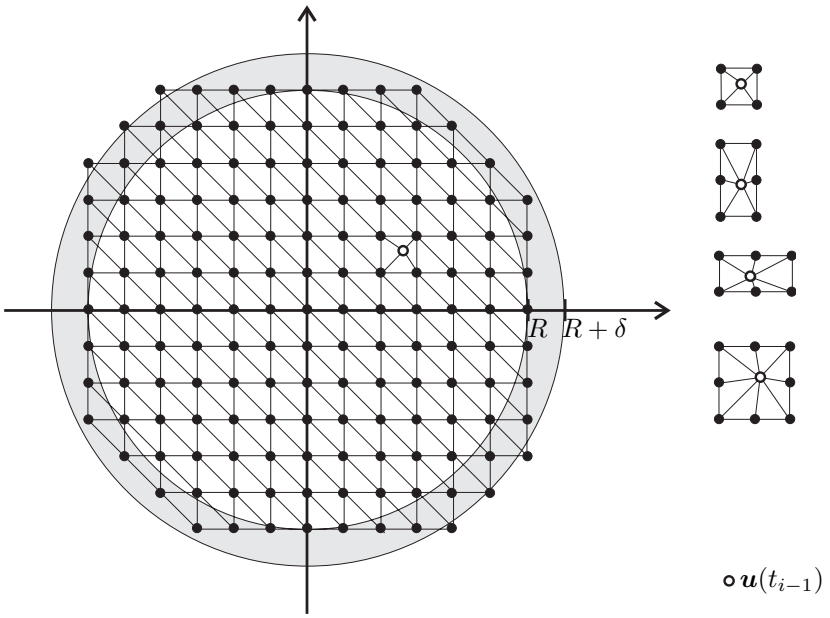

FIGURE 3.1. Linearization grid of $\boldsymbol{P}_i^{\mathrm{dl}}$: A special interpolation pattern is used on the square in the 1st quadrant containing $\boldsymbol{u}(t_{i-1})$. On the right, alternative special interpolation patterns are sketched for the case that $\boldsymbol{u}(t_{i-1})$ lies close to a grid edge or node. The shaded ring represents the transition from grid interpolation to saturation.

with a simple linesearch. To address the possible failure of this Newton's algorithm in view of non-monotonicity and resulting local minima around the reversal point $(\boldsymbol{u}(t_{i-1}), \boldsymbol{w}(t_{i-1}))$, initial values in different grid triangles in the neighbourhood of the previous time step solution $\boldsymbol{u}(t_{i-1})$ are tried until a solution is found.

$\boldsymbol{M}[\boldsymbol{B}]$-iteration requires a large number of evaluations of $\boldsymbol{P}_i^{\mathrm{dl}}$ in each time step. Storing the already computed nodal values of $\boldsymbol{P}_i^{\mathrm{dl}}$ in each time step cuts down significantly on the computational effort. The biggest computational involvement results from the large number of $\boldsymbol{M}[\boldsymbol{B}]$-iteration steps, as the fixed point iteration is very slow in finding a solution.

In the following, simulations with hysteresis in terms of $\boldsymbol{P}_i^{\mathrm{dl}}$ are presented.

3.3. Application 1: Ring core

In a first simulation, we want to verify the numerical results analytically. For this, we choose the model of a hysteretic core enclosing a conductor. The solution of this simple electromagnetic field problem can be determined analytically [**65, 45**]. Figure 3.2 shows the model as well as the finite element mesh used in the simulations. As remarked on before, due to BEM-FEM coupling we do not need to include the air space surrounding the model in the mesh.

The hysteresis data of the simulation is presented in Figures 3.3 and 3.4. The first figure shows the Preisach distribution $\omega(\|\boldsymbol{x}\|, r)$ used for the isotropic vector Preisach operator $\boldsymbol{\mathcal{P}}$, which is chosen piecewise linear on a grid as described in

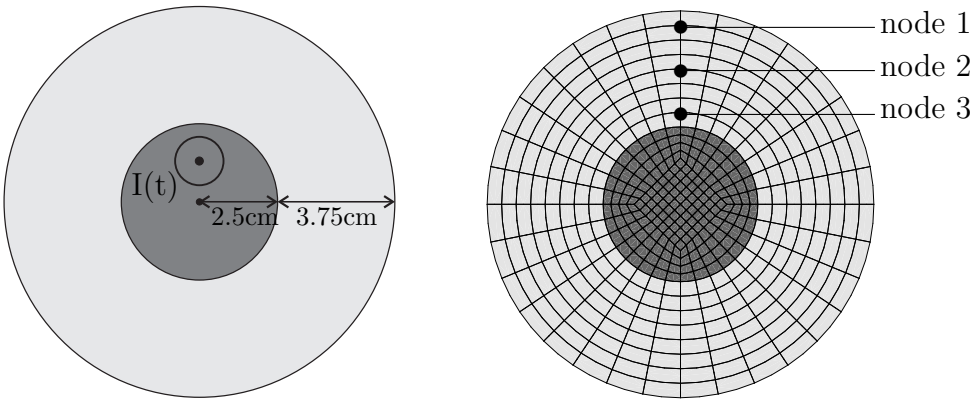

FIGURE 3.2. Ring core: Model geometry (left) and finite element mesh (right). The nodes marked are those for which a solution is extracted in Figure 3.8.

Appendix A with grid parameter $N = 3$. The second figure gives the resulting uniaxial hysteresis curves. Here, the constants are $\boldsymbol{H}_{\text{sat}} = 17.5$ kA/m, $\boldsymbol{M}_{\text{sat}} = 1.63$ T and $\omega_{\max} = 2.4 \cdot 10^{-12}$. For discretizing $\boldsymbol{\mathcal{P}}$, the parameter $N = 30$ was chosen.

For the excitation setup of our computations we chose $I_{\max} = 2$ kA. The excitation current $I(t)$ was linearly increased from 0 A to $I_{\max}$, lowered to $-I_{\max}$, and increased back to 0 A, see Figure 3.5.

The analytical solution can be derived from symmetry considerations, using Ampère's law, which states that the line integral of $\boldsymbol{H}(t)$ along a closed path is equal to the current $I(t)$ enclosed at time t [**48**],

$$\oint \boldsymbol{H}(t) \cdot \mathrm{d}s = I(t).$$

Choosing the path to be a concentric circle of radius ρ, we obtain that the azimuthal component of $\boldsymbol{H}$ is given by

$$H_{\text{az}}(\rho, t) = \frac{I(t)}{2\pi\rho}.$$

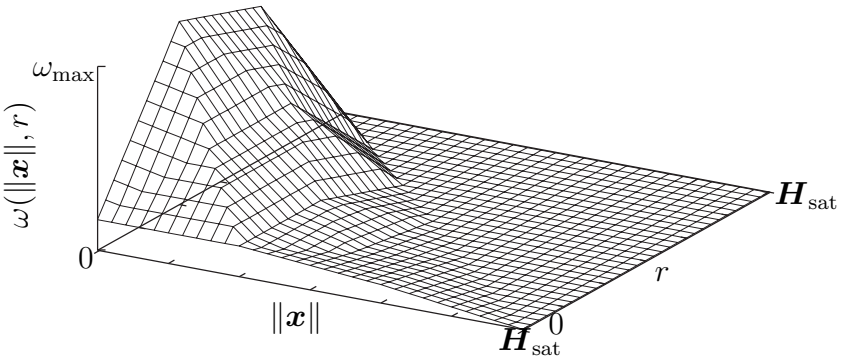

FIGURE 3.3. Ring core: Isotropic Preisach distribution $\omega(\|\boldsymbol{x}\|, r)$.

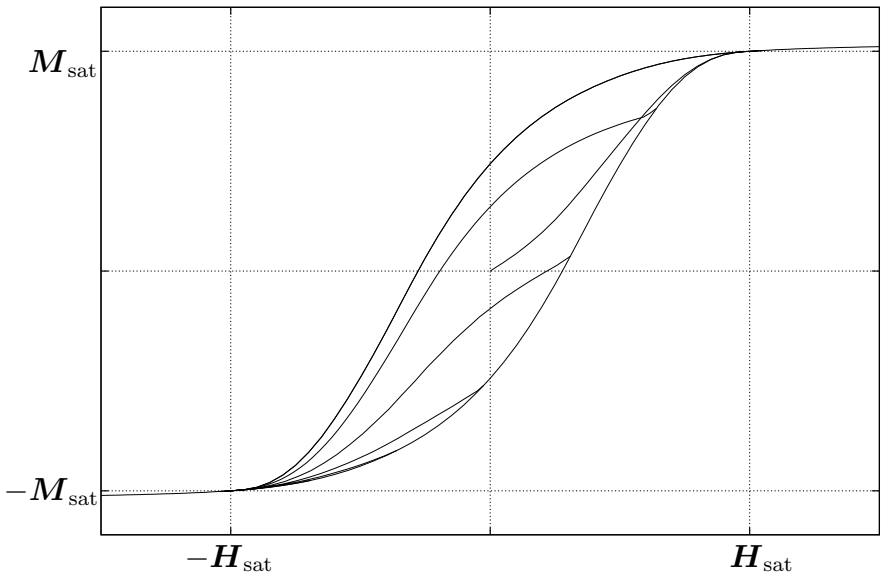

FIGURE 3.4. Ring core: Uniaxial hysteresis resulting from $\omega(\|\boldsymbol{x}\|, r)$ in Figure 3.3 with initial curve, outer loop, and first order reversal curves.

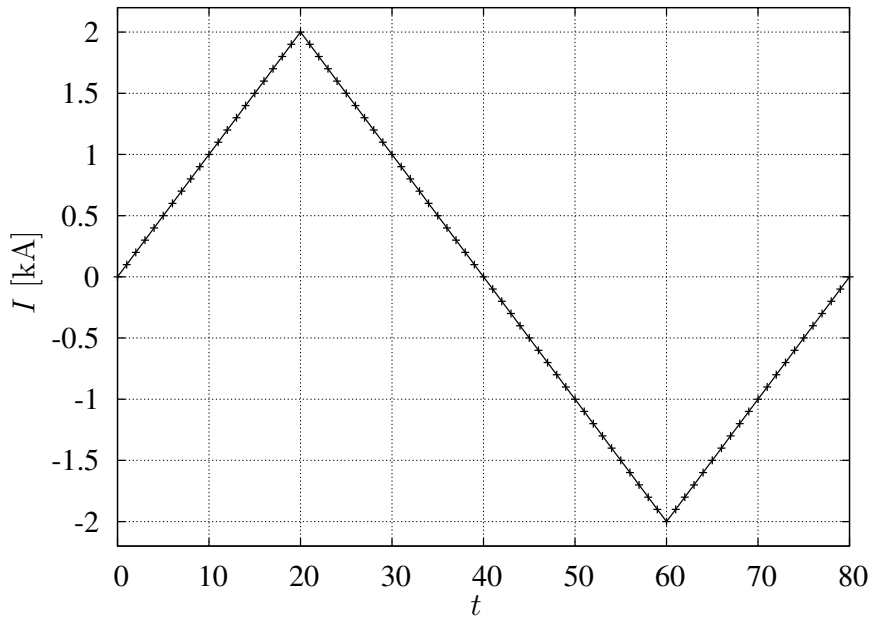

FIGURE 3.5. Ring core: Excitation current.

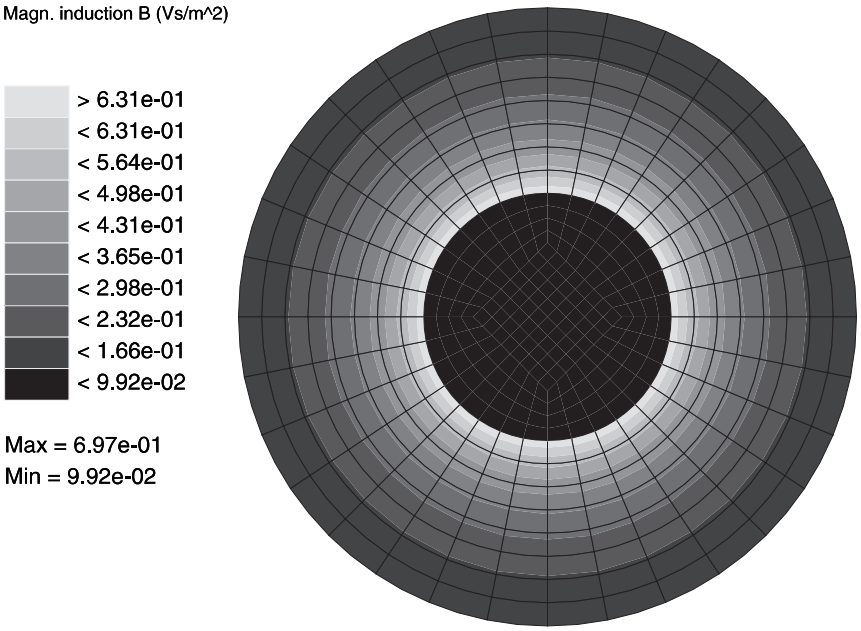

FIGURE 3.6. Ring core: Remanent $\boldsymbol{B}$ field at $t = 40$.

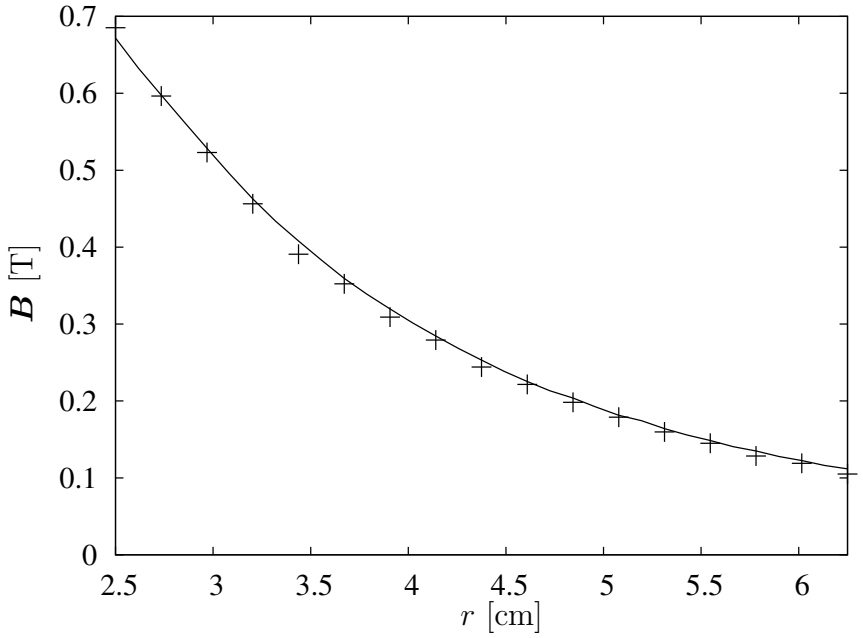

FIGURE 3.7. Ring core: Remanent $\boldsymbol{B}$ field at $t = 40$ in dependence of the radius r – analytical solution (solid line) vs. FE simulation result (+).

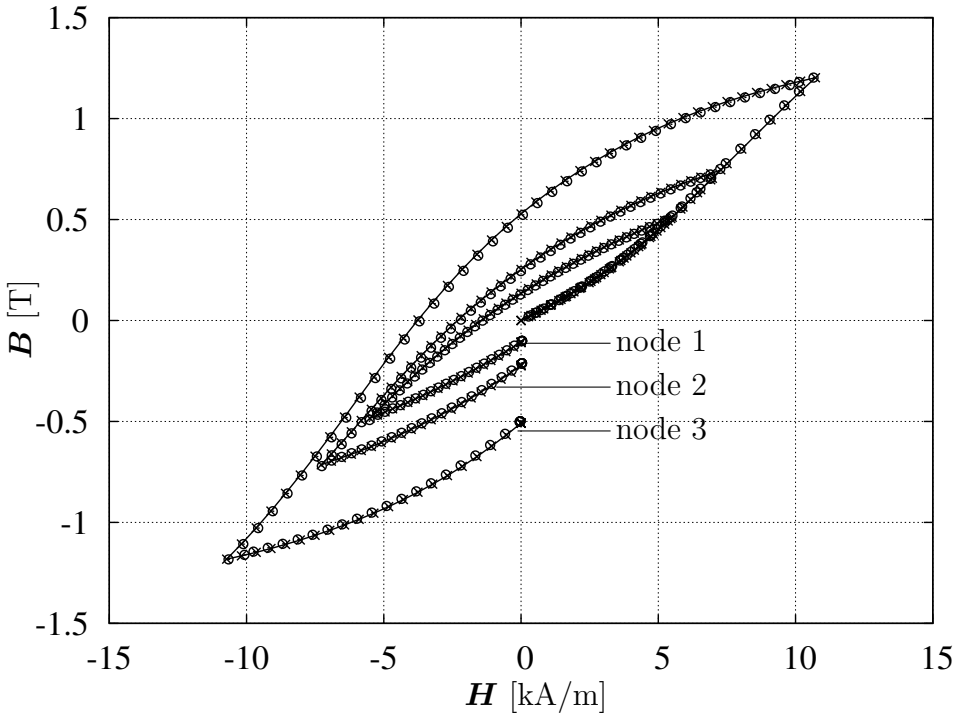

FIGURE 3.8. Ring core: Azimuthal component of analytical vs. simulated solution $(H_{\mathrm{az}}(\rho,t), B_{\mathrm{az}}(\rho,t))$ in nodes 1, 2, and 3 for the full simulation run.

The radial component of $\boldsymbol{H}$ is 0. The magnetic induction $\boldsymbol{B}$ can be computed from $\boldsymbol{H}$ by evaluating (3.20). For neutral initial state $\boldsymbol{\xi}^0$ of $\boldsymbol{\mathcal{P}}$, it also has only an azimuthal component, B_{az}. For the practical computation of $\boldsymbol{B}$ in the analytical solution, we used the discretized $\boldsymbol{\mathcal{P}}$ with very fine discretization $N = 80$.

The results of the numerical and analytical computations are shown in Figures 3.6 through 3.8. Figure 3.6 is a plot of the absolute $\boldsymbol{B}$ field values at $t = 40$. Because there is no excitation current, $I(40) = 0$, the entire $\boldsymbol{B}$ field is due to hysteresis. One can see well the radial symmetry. Figure 3.7 compares analytical and numerical solution along a radial line. A good correspondence with small deviations is seen. These deviations are due the coarse spatial discretization of the ring core model as well es the discretization error of $\boldsymbol{\mathcal{P}}$. Figure 3.8 displays the curves $(H_{\mathrm{az}}, B_{\mathrm{az}})$ at the three nodes marked in Figure 3.2 for analytical and simulated solution for the full excitation cycle. As expected, the solution in each node describes a different inner hysteresis curve, with amplitudes decreasing with increasing radius of the node position. The results exhibit a very good correspondence.

We have thus shown that the results obtained in our numerical simulations of the ring core with hysteresis in terms of $\boldsymbol{\mathcal{P}}$ agree well with the analytical solution.

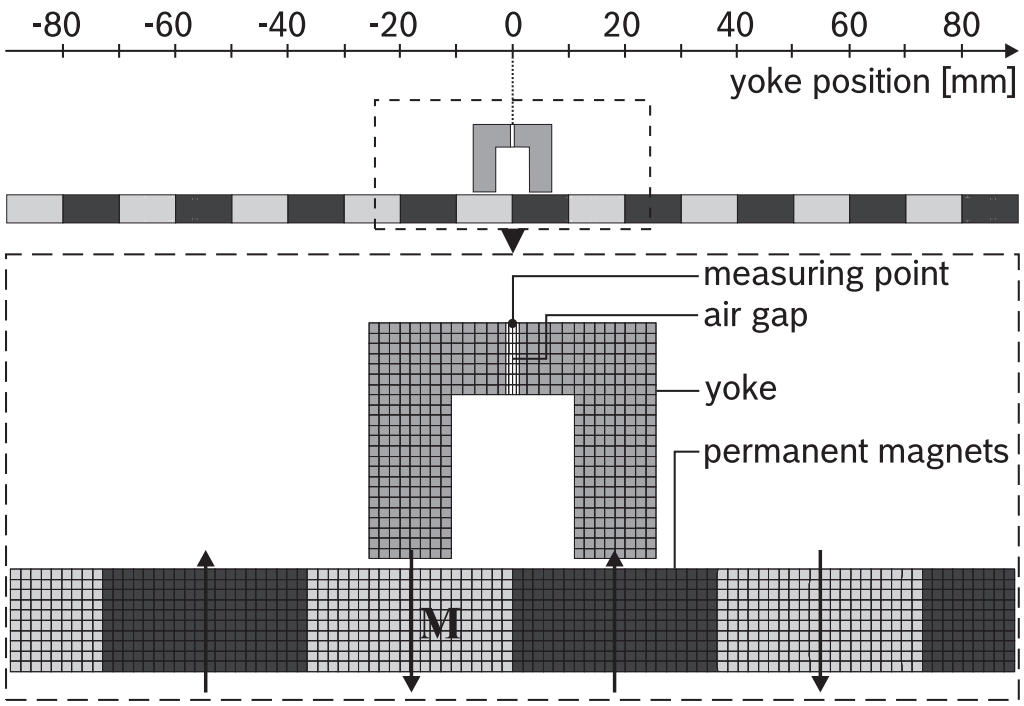

FIGURE 3.9. Position sensor: A hysteretic yoke is moved horizontally along a row of permanent magnets of alternating magnetization.

3.4. Application 2: Position sensor

We now investigate a more complicated, fully vectorial electromagnetic field problem. It represents a simple position sensor. The model and the finite element mesh are shown in Figure 3.9. The sensor consists of a hysteretic yoke made from soft magnetic material, which can be moved back and forth along a row of permanent magnets with alternating magnetization. In the air gap of the yoke, a Hall sensor measures the horizontal component B_h of the magnetic induction $\boldsymbol{B}$ in the measuring point. The sensor output B_h is periodically correlated with the position of the yoke. It takes maximum amplitudes when the legs of the yoke lie centered over the permanent magnets, as in Figure 3.9, and is 0 when the legs are centered over the borders of the permanent magnets.

In experiments, B_h was measured as the yoke was moved from left to right as well as from right to left. Depending on the direction of the movement, a lag was observed which is due to hysteresis in the yoke material. A pair of measured curves is displayed in Figure 3.10. The lag is small but was found consistently in all experiments with the yoke made of different hysteretic materials.

The aim was to reproduce this lag in simulations. Anhysteretic simulations, in which the initial hysteresis curve was used to represent the functional dependence of $\boldsymbol{B}$ on $\boldsymbol{H}$, show that the fields in both legs of the yoke rotate with varying absolute value as the yoke changes position (Figure 3.11). Thus, computations use the fully vectorial nature of the hysteresis model. Table 3.1 lists the model specifications

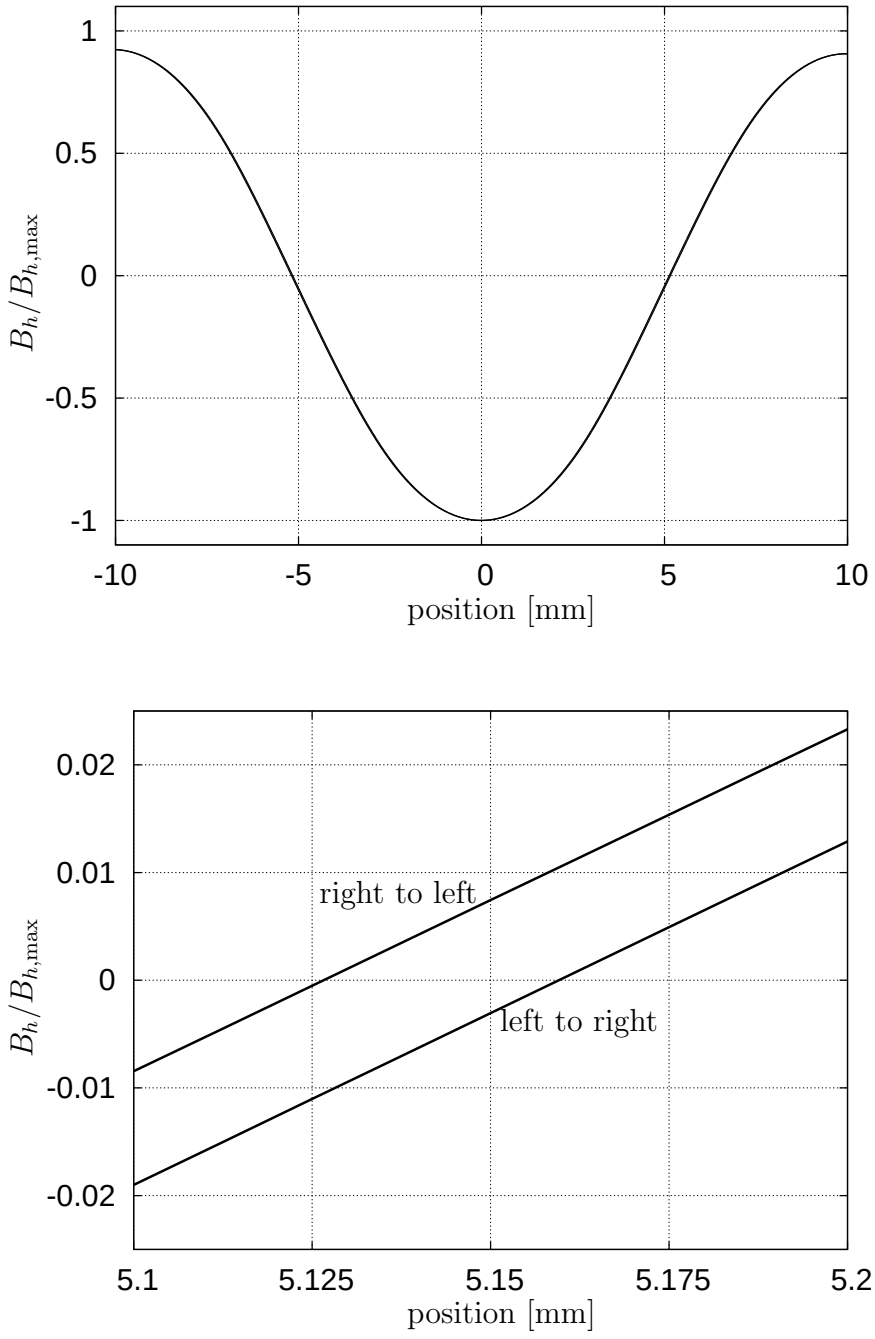

FIGURE 3.10. Position sensor: Normalized sensor output curves $B_h/B_{h,\max}$ versus yoke position obtained from measurements for the yoke moving from left to right and from right to left – (a) full curve, (b) curve enlarged at $B_h = 0$.

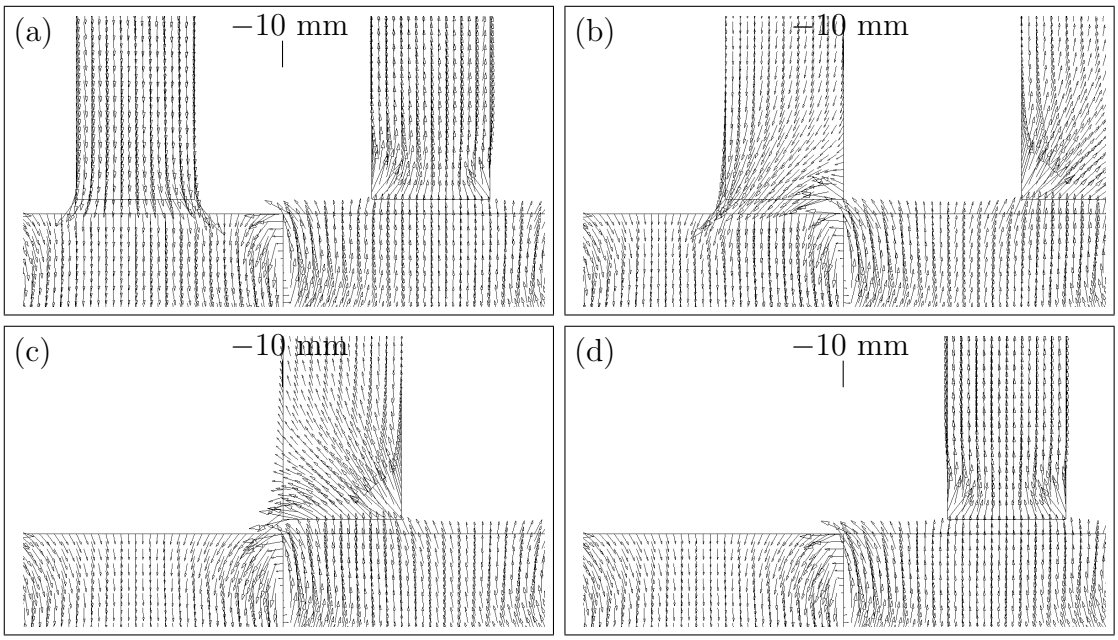

FIGURE 3.11. Position sensor: Magnetic induction $\boldsymbol{B}$ in the legs of the yoke, simulated without hysteresis, as the yoke position varies from −10 mm to 0 mm.

used in the simulation. The simulations were done with the same hysteresis data as for the ring core model, displayed in Figures 3.3 and 3.4, scaled to the values of $\boldsymbol{H}_{\text{sat}}$ and $\boldsymbol{M}_{\text{sat}}$ given in Table 3.1, and initial state $\boldsymbol{\xi}_0$ for the hysteresis. Since the movement of the yoke is slow, the simulations are magnetostatic.

Two simulations were performed: In the first, the yoke was moved left to right from position −30 mm to position 10 mm; in the second, the yoke was moved right to left from position 30 mm to position −10 mm. The additional hysteresis cycle

permanent magnets:	width = 10 mm, height = 5 mm, $\boldsymbol{M} = .75T$
yoke:	height = 12 mm, leg width = 4 mm, airgap width = .7 mm
distance permanent magnet - yoke:	.5 mm
yoke material hysteresis:	$\boldsymbol{H}_{\text{sat}} = 2$ kA/m, $\boldsymbol{M}_{\text{sat}} = 1.218$ T, $\omega_{\max} = 1.2 \cdot 10^{-9}$

TABLE 3.1. Position sensor: Data used in the simulation.

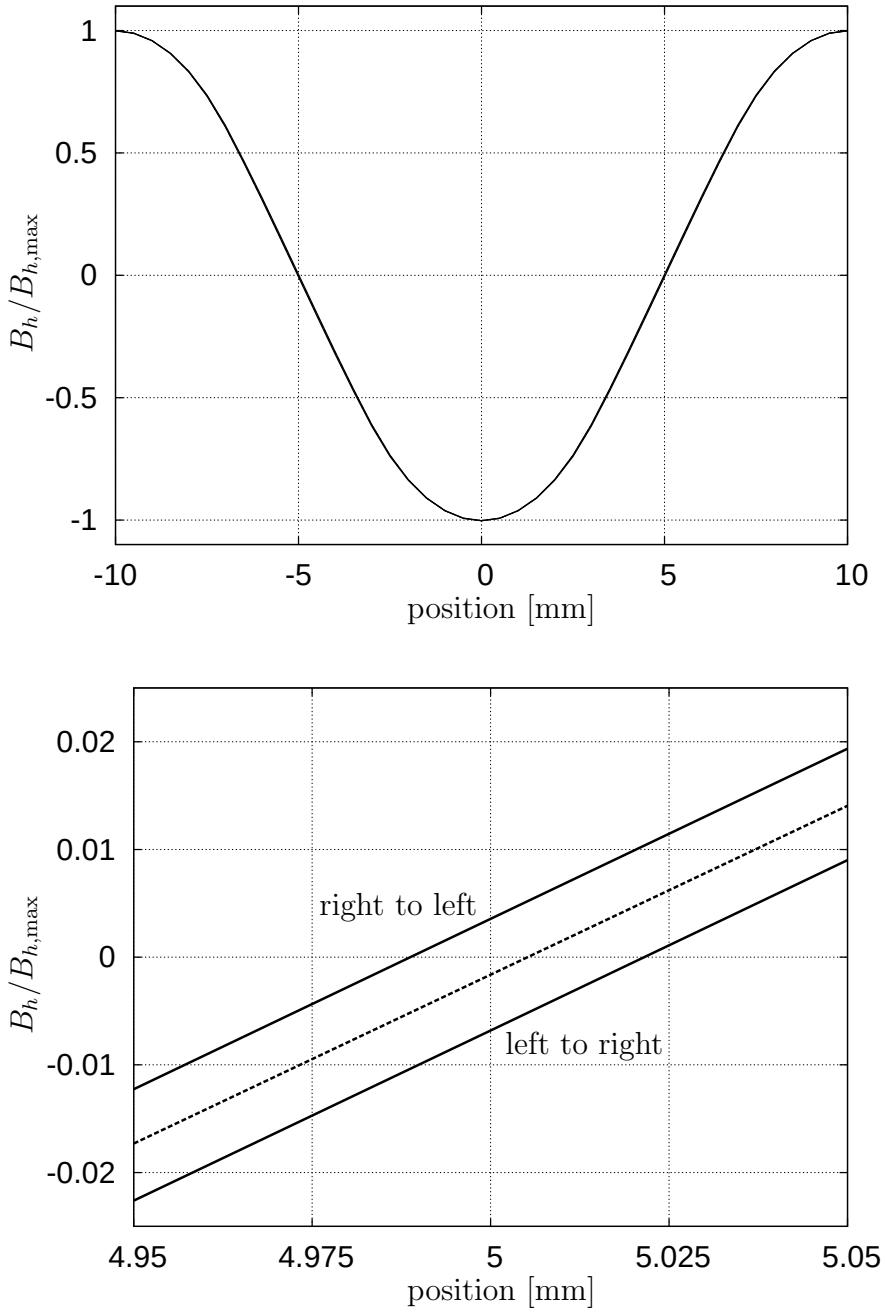

FIGURE 3.12. Position sensor: Normalized sensor output curves $B_h/B_{h,\max}$ versus yoke position obtained from simulation without hysteresis (dashed line) and with hysteresis (solid line) for the yoke moving from left to right and from right to left – (a) full curve, (b) curve enlarged at $B_h = 0$.

from -30 mm to -10 mm and from 30 mm to 10 mm, respectively, was added to erase initial state effects in $\boldsymbol{\mathcal{P}}$. The resulting B_h was extracted at the measuring point and is plotted in Figure 3.12. It can be seen that the curves reproduce the experimentally observed effect well, with the anhysteretic curve lying between the hysteretic ones.

Note that both measured and simulated curves do not have their zeros exactly at 5 mm and their maxima at -10 mm and 10 mm do not attain the full value. This is due to the finite lenght of the row of permanent magnets. In the measurements, it consisted only of six magnets, so the effect is more pronounced.

Figure 3.13 shows the $\boldsymbol{B}$ field for the yoke at position 0 mm, computed in the simulation with the yoke moving from left to right. One can clearly see that the field configuration is asymmetric. Without hysteresis, due to the symmetry of the model at this position, the fields must be distributed symmetrically in both legs of the yoke. The asymmetry is the result of hysteresis.

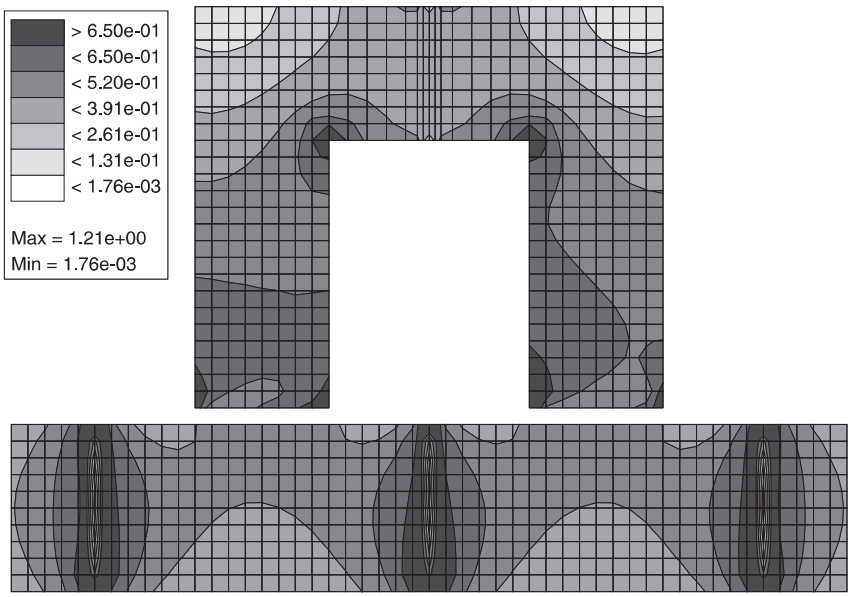

FIGURE 3.13. Position sensor: Absolute magnetic induction $\|\boldsymbol{B}\|$ [T] at yoke position 0 mm.

3.5. Application 3: Magnetic valve

As a third application, we have simulated a simple magnetic valve with the full eddy current approximation (3.12)-(3.14) with motion and a combination of different hysteretic and anhysteretic materials. The goal was to verify that reasonable results can also be obtained in this complex setting. Figure 3.14 shows a quarter section of the magnetic valve, consisting of a magnetic core surrounding a coil, armature and housing. When an electric current flows in the coil, a magnetic field builds up in the valve which results in an attractive magnetic force between core and armature.

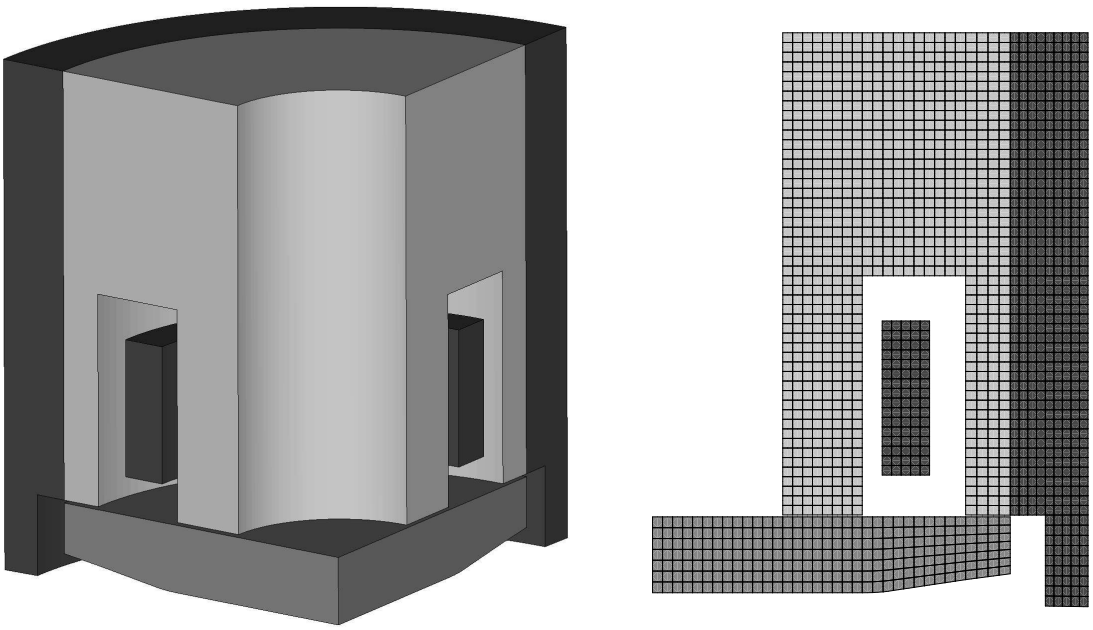

FIGURE 3.14. Magnetic valve: Quarter section of the rotationally symmetric 3D model (left), 2D mesh1 of 131 (right).

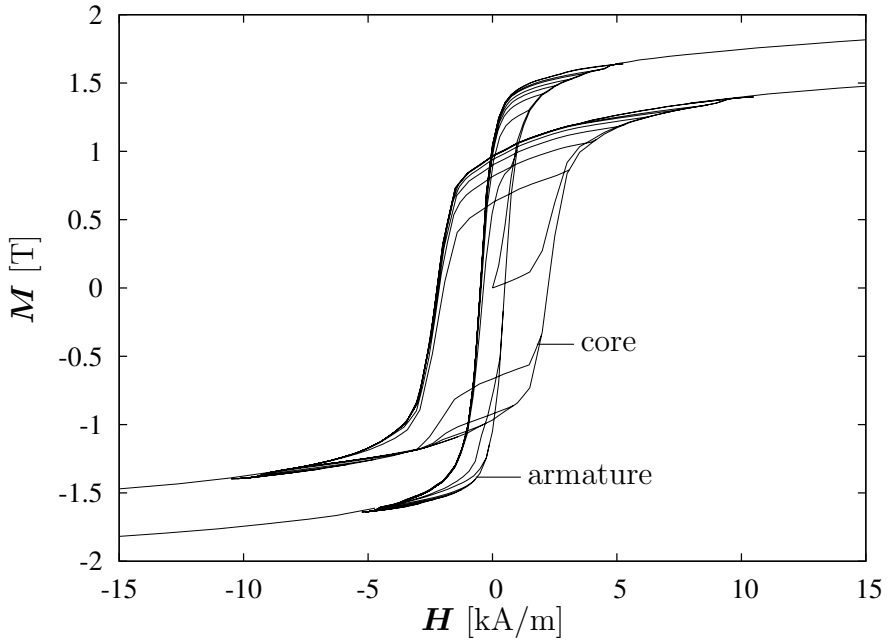

FIGURE 3.15. Magnetic valve: Uniaxial hysteresis curves consisting of initial, outer and first order reversal curves for core and armature.

The armature is pulled towards the core if the magnetic force exceeds a certain threshold, 78 N in our case, and moves back if the excitation is decreased and the force falls below the threshold. The problem is rotation-symmetric and can thus be modeled by means of a 2D model [**29**]. The corresponding 2D mesh for the rotation-symmetric simulations is shown on the right in Figure 3.14. The height of the valve is 15 mm, the radius 11.5 mm.

Both core and armature consist of hysteretic materials, whereas the housing is assumed anhysteretic. Figure 3.15 presents the hystereses assigned to core and armature. The first order reversal curves shown are computed with $\boldsymbol{\mathcal{P}}$. The respective Preisach distributions were fitted from measured material curves with the method described in Appendix A. As outlined there, the saturation curves resulting from $\boldsymbol{\mathcal{P}}$ are replaced by given curves, with the objective of saving hysteresis memory in fitting $\boldsymbol{\mathcal{P}}$. This has no theoretical implications on the simulations. For the dynamic simulations, the conductivities σ of core, armature and housing are set to $2.7 \cdot 10^6$A/Vm, $3 \cdot 10^6$A/Vm and $4.55 \cdot 10^6$A/Vm, respectively.

In a first sequence of simulations, we determine the $\boldsymbol{B}$ field in the valve for a magnetostatic process without motion. The excitation current is slowly increased to a maximum of 18 A and then decreased back to 0 A. In one simulation, the armature is fixed in its original position where the valve is open. In the second simulation, it is fixed in its final position where the valve is closed. Figure 3.16 shows vector plots of the resulting $\boldsymbol{B}$ field for the open valve at maximum excitation simulated without hysteresis and with hysteresis. For the anhysteretic simulation, the initial curves of the uniaxial hystereses were used as $\boldsymbol{B}(\boldsymbol{H})$-curves of the materials. We see that the results are almost identical, as expected. The remanent $\boldsymbol{B}$ fields of the two hysteretic computations are shown in Figure 3.17. There is no excitation current at this point, so the fields are entirely due to the hysteresis of the materials. It can be seen that for the open valve, as a result of the larger air gap between armature and core, part of the magnetic flux lines close inside the armature. The effect is a smaller remanent field than obtained for the closed valve, in particular in the core. This example demonstrates the large influence of small changes in air gap widths in the magnetic circuit.

In a second sequence of simulations, we carry out dynamic electromagnetic field computations with eddy currents. For this, the magnetic valve is subjected to a realistic excitation setup [**62**]. It consists of five phases: (1) The coil excitation is driven by a booster voltage U_1 until a given current I_2 has built up. (2) The current I_2 is kept constant until time t_1, at which point the armature has been pulled into its stopping position. (3) The excitation is kept constant at holding current I_3 until time t_2. (4) A deletion voltage U_4 is applied to lower the current to 0 A. (5) The excitation current remains at 0 A. In our simulations, we have chosen $U_1 = 47$ V, $I_2 = 18$ A, $I_3 = 3.5$ A, $U_4 = -33$ V, $t_1 = .8$ ms, and $t_2 = 1$ ms.

As the whole switching cycle takes place in less than 2 ms, eddy currents are induced and influence the evolution of the fields significantly. They counteract the field propagation in the material, and they outlast the excitation by quite some time, inducing a $\boldsymbol{B}$ field even after the excitation has been turned off.

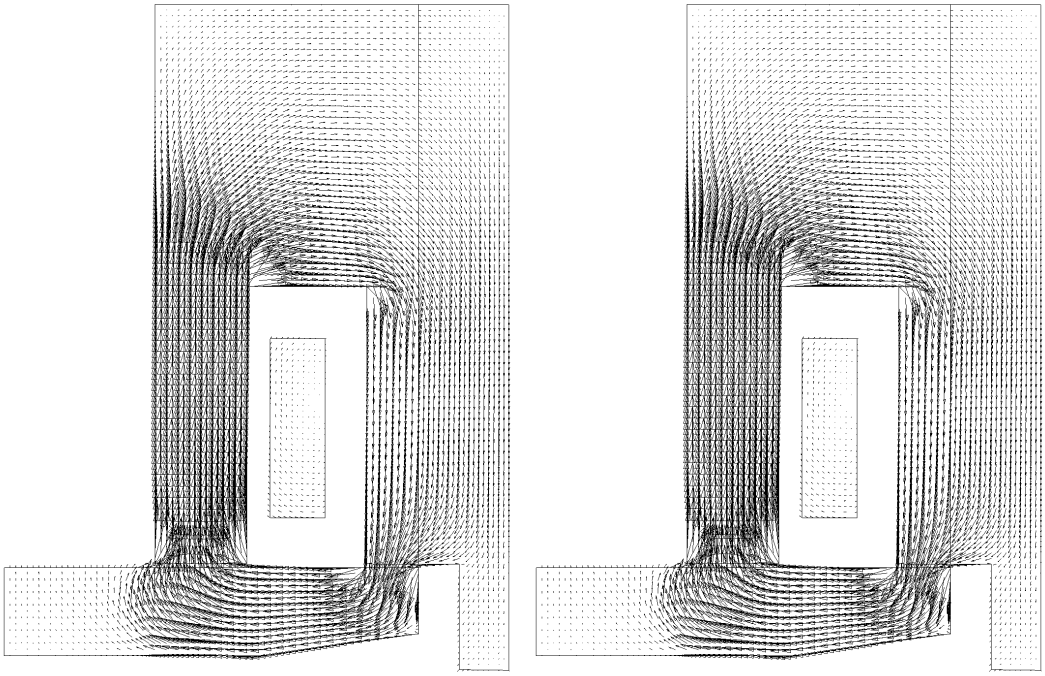

FIGURE 3.16. Magnetic valve: The $\boldsymbol{B}$ field at maximum excitation current for magnetostatic simulation of the open valve without (left) and with (right) hysteresis.

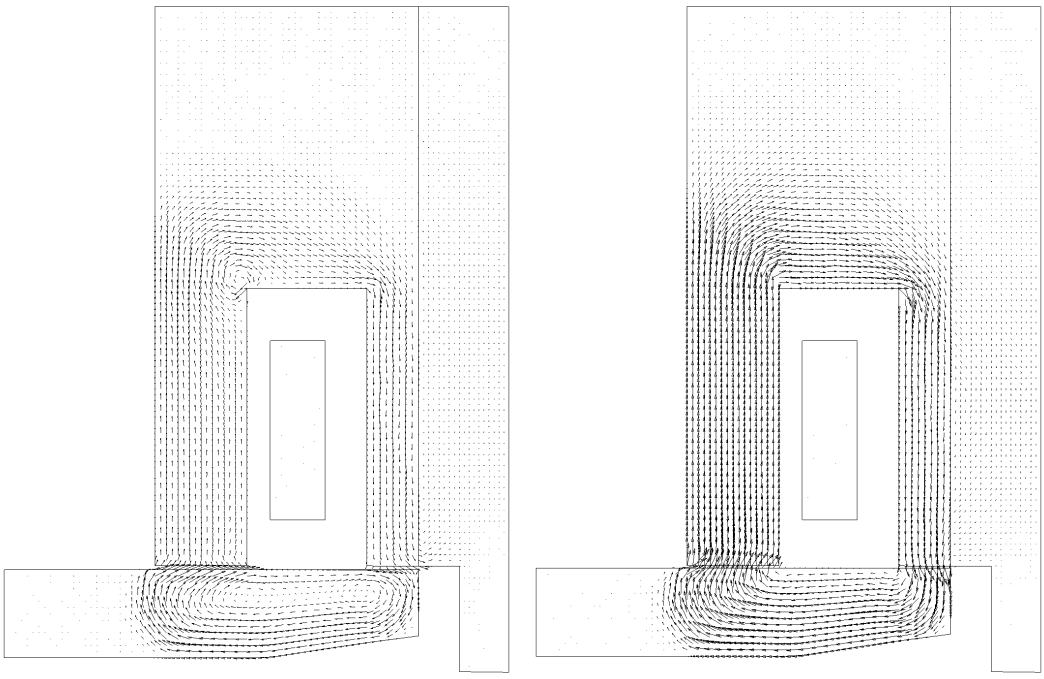

FIGURE 3.17. Magnetic valve: Remanent $\boldsymbol{B}$ field for magnetostatic simulation with hysteresis after turning off the excitation current – open valve (left) and closed valve (right).

Figure 3.18 shows the magnetic force between core and armature computed in simulation runs without and with hysteresis, normalized with the maximum force $F_{\max}$ attained in the anhysteretic case. The observed hysteresis effect satisfies well what would be expected to happen: Due to hysteresis in the field propagation, the maximum force obtained with hysteresis is lower than that without. When the excitation is lowered, hysteresis results in a lag in the decrease of the force and in larger remaining force. Figure 3.19 shows the corresponding $\boldsymbol{B}$ fields at $t = .8$ ms, when the fields attain their maximum. Again we can see a very good correspondence between the anhysteretic and the hysteretic result, as would be expected. Figure 3.20 presents the respective $\boldsymbol{B}$ fields at $t = 2$ ms. Note that $\boldsymbol{B}$ is not equal to 0 even in the anhysteretic case because the eddy currents have not yet died out. However, we clearly see that the hysteretic field is larger. In the armature, the remanent pattern observed in Figure 3.17 for the open valve has started to form.

From empirical evidence [**63**], it is known that introducing a larger airgap at some point in the magnetic circuit reduces the hysteretic lag at decreasing fields. In computations with modified armature design, we check if this effect is reproduced by the simulations. For this, we grade the armature to increase the air gap at the inner pole (Figure 3.21) and repeat the simulation runs done for the original design. The resulting force curves are shown in Figure 3.22 and the corresponding fields at $t = 2$ ms in Figure 3.23. As can be seen, the lag is indeed reduced, as well as the

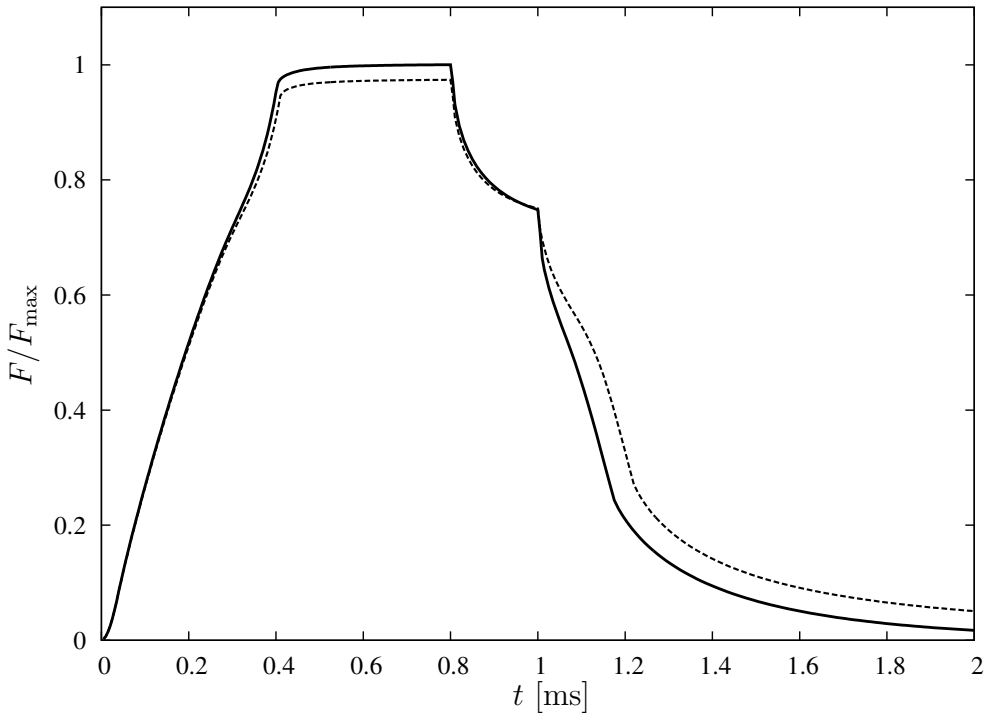

FIGURE 3.18. Magnetic valve: Magnetic force without hysteresis (solid line) and with hysteresis (dashed line).

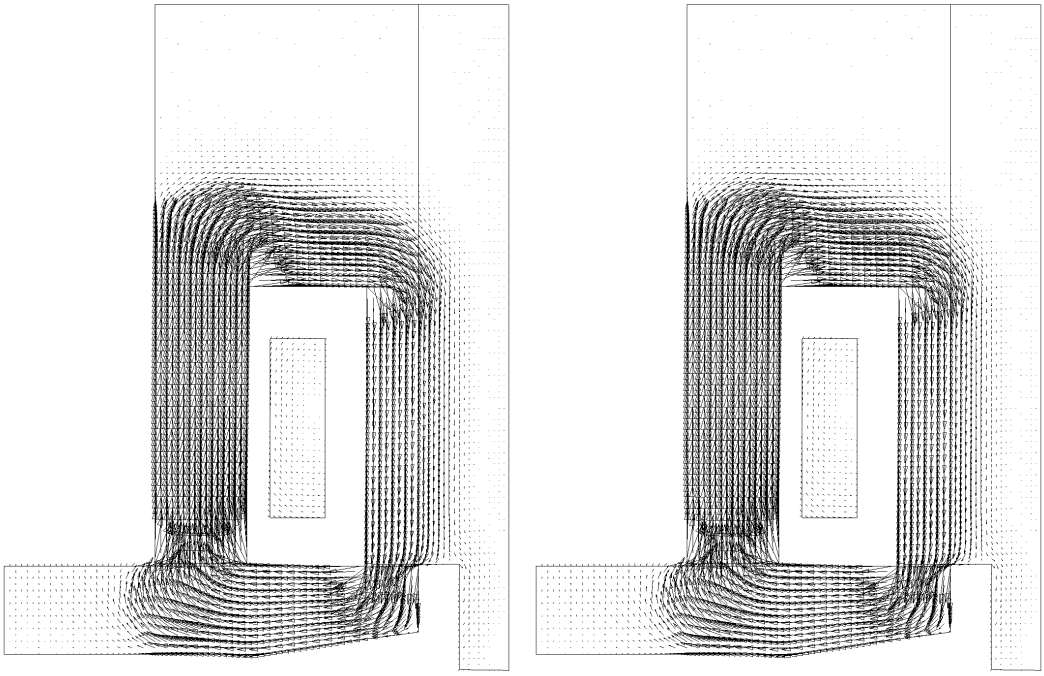

FIGURE 3.19. Magnetic valve: Maximum $\boldsymbol{B}$-field at $t = .8$ ms without (left) and with hysteresis (right).

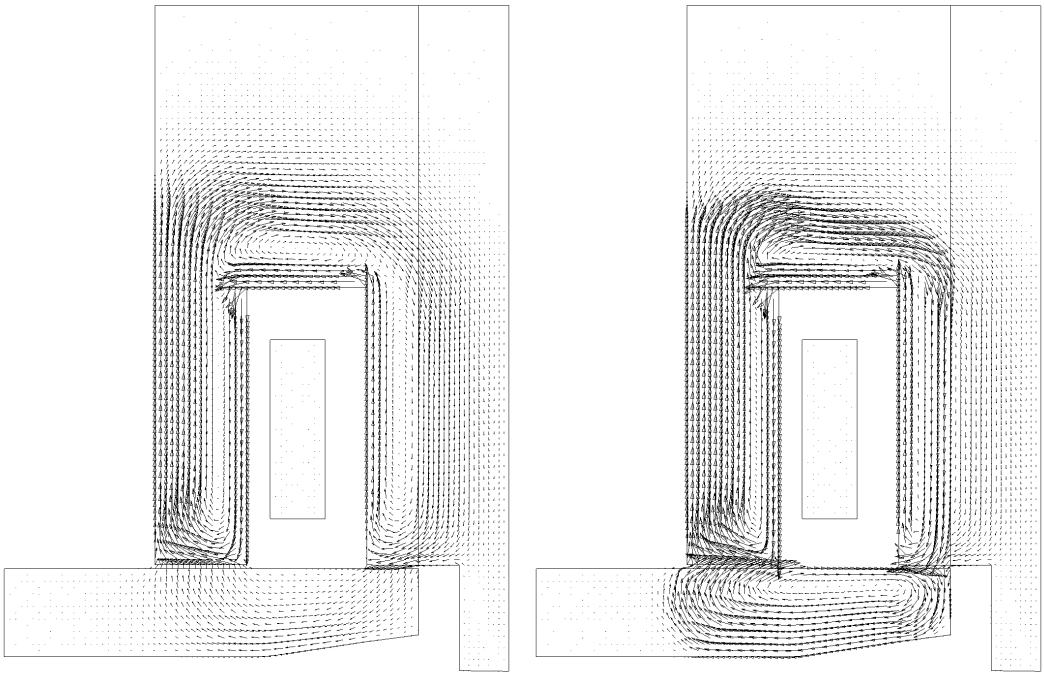

FIGURE 3.20. Magnetic valve: $\boldsymbol{B}$-field at $t = 2$ ms without (left) and with hysteresis (right).

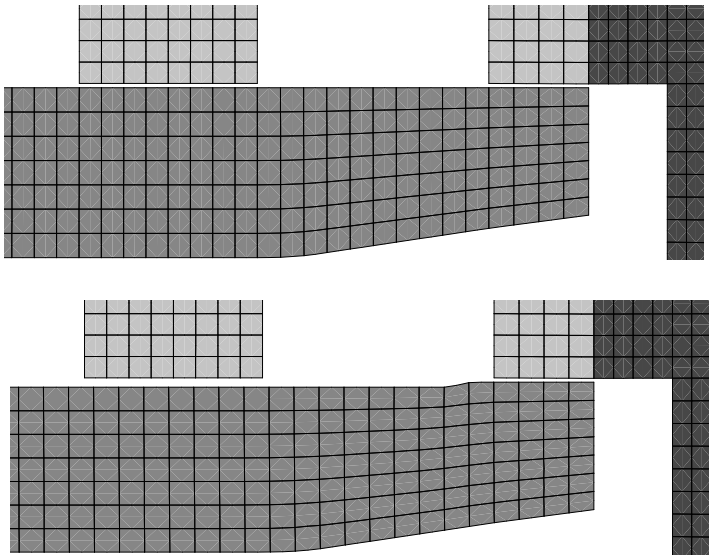

FIGURE 3.21. Magnetic valve: Original armature design (top), modified armature design (bottom).

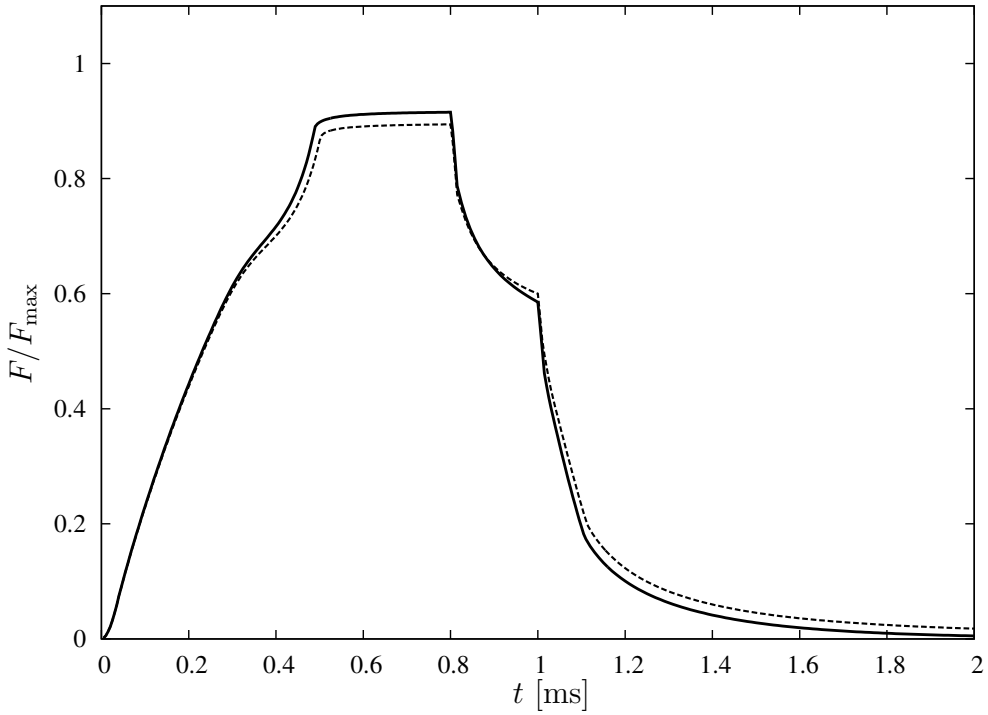

FIGURE 3.22. Magnetic valve: Magnetic force without hysteresis (solid line) and with hysteresis (dashed line) for the modified armature design.

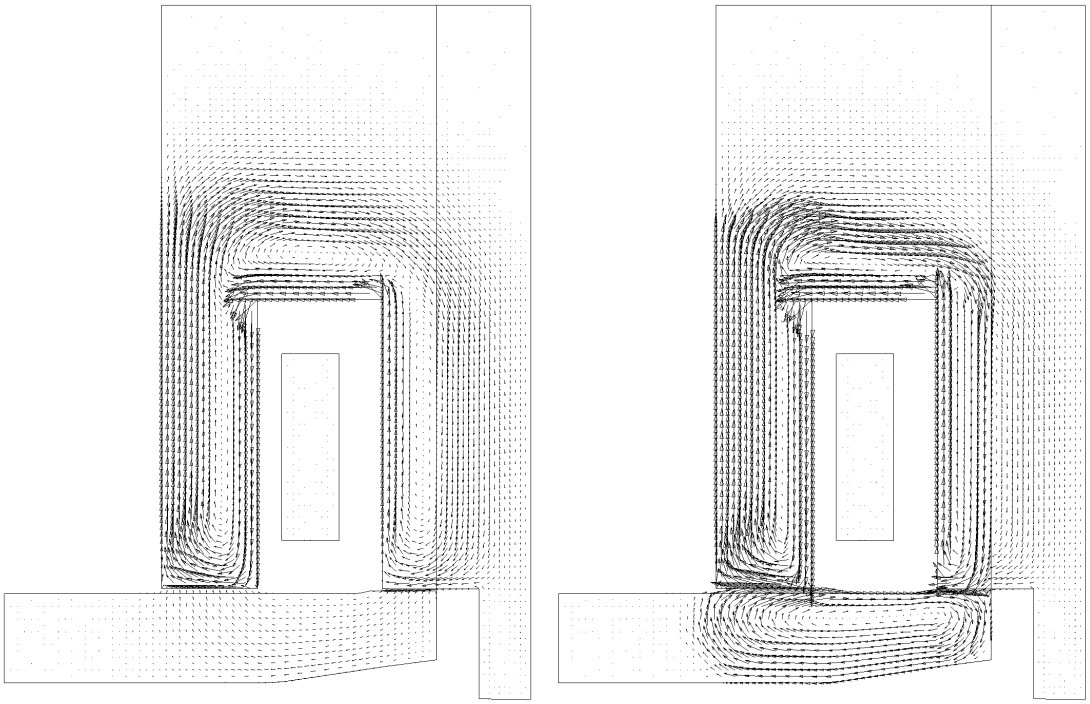

FIGURE 3.23. Magnetic valve: $\boldsymbol{B}$-field at $t = 2$ ms without (left) and with hysteresis (right) for the modified armature design.

remaining force at $t = 2$ ms. This effect seems to be a consequence of more field lines closing inside the armature rather than traversing the air gap to the core, as was previously seen in the magnetostatic case for differing airgap widths.

3.6. Summary

We have seen that our simulations have yielded good results, reproducing well the analytical solution in the case of the ring core and secondary hysteresis effects for the position sensor and the magnetic valve model. The simulations shed light on the internal field configurations forming in the presence of hysteresis. These are otherwise inaccessible, as measurements can only be taken of secondary effects but not of internal fields directly.

A quantitative validation of the hysteresis modeling with $\boldsymbol{\mathcal{P}}$ should be carried out to obtain better insight into the potential and limitations of this new model. This includes on one hand the comparison of measured and modeled hysteresis curves for a number of materials. In view of this, the parametrization question must be addressed more thoroughly. On the other hand, electromagnetic field simulations of model problems should be quantitatively verified with measurements. This poses the question of the quality of the hysteresis data used in the parametrization of $\boldsymbol{\mathcal{P}}$. The measuring of a material's specific hysteresis is challenging (see e.g. [**5**, Chapter 1] for a discussion of the arising problems) and requires specific toroidal or cylindrical probe geometries to guarantee the homogeneity of the ambient magnetic field in the

probe and thus generate accessible results [**10**],*. Any processing of the material has significant impact on the material hysteresis [**10**],*. It is thus uncertain to what degree the material specifications from standard hysteresis measurements assumed in the simulations are valid.

In any case, even if the exact quantitive performance of $\boldsymbol{\mathcal{P}}$ remains open for now, the simulations allow insight into the mechanisms underlying the secondary hysteresis effects observed in measurements.

Due to time restrictions and the predetermined numerical setup of the electromagnetic simulation software, a straightforward computer implementation of $\boldsymbol{\mathcal{P}}$ was chosen for the inclusion of hysteresis in the framework of electromagnetic field simulations. It leaves some potential numerical issues unaddressed and, in addition, is fairly inefficient with regard to storage and time requirements. It would be desirable to develop a more elegant and efficient implementation of the hysteresis memory of $\boldsymbol{\mathcal{P}}$ and to find a more satisfactory coupling with electromagnetic field methods.

*personal communication with Dr. H. Kleine, Magnettechnik Kleine, February 2006

Conclusion

In this dissertation, we have presented our results on the new vector Preisach operator recently introduced by Della Torre, Cardelli and Pinzaglia [**24, 25**]. Aside from giving a formal mathematical definition of the vector relay operator, we have proven a range of properties of the vector relay and Preisach operators regarding, for example, isotropy, saturation, dissipation, periodicity and output behaviour. We have shown that there is a good qualitative correspondence between some of the properties inherent to this vector Preisach operator and characteristic features of the hysteresis of magnetic materials observed in measurements, like the saturation behaviour or the typical shape of the loss curves. Further, we have presented electromagnetic field simulations with hysteresis in terms of the new operator and demonstrated that hysteresis effects observed in experiment are reproduced in the simulations. All this gives rise to the hope that it might offer an interesting new approach to the vectorial modeling of magnetic hysteresis.

Within the limits of this dissertation, it was possible to address no more than a small number of the issues arising with a new hysteresis operator. Some crucial questions remain open for further research. One is the continuity of the operator $\boldsymbol{\mathcal{P}}$, which forms the fundamental requirement for any sound numerical scheme. Investigations to this effect indicate that $\boldsymbol{\mathcal{P}}$ is continuous. However, a mathematical proof has not been found to date. Another question is that of a characterization of the operator, that is, to determine the defining properties of the input-output map, as presented by Mayergoyz [**49**] and Brokate [**12**] for the scalar Preisach operator, and by Friedman [**36**] for Mayergoyz' vector Preisach operator. Related to this is the development of a satisfactory parametrization method to identify the underlying Preisach distribution ω representing given hysteresis data, for which we have so far only suggested a perfunctory algorithm. Finally, the successful application of $\boldsymbol{\mathcal{P}}$ in the modeling of magnetic hysteresis will crucially depend on the question of whether it is possible to find an efficient numerical implementation of the operator. In the constraints of this dissertation, we have resigned to using an ad hoc implementation discretizing the relay memory of $\boldsymbol{\mathcal{P}}$. This results in large computational cost in storage and evaluation, which prohibits an application in the simulation of electromagnetic components requiring a mesh with a bigger number of finite elements or in three-dimensional simulations.

The vector modeling of magnetic hysteresis is a challenging subject. This dissertation hopefully contributes some interesting insight in the modeling approach via the new vector Preisach operator $\boldsymbol{\mathcal{P}}$.

APPENDIX A

A simple identification method

In order to be able to carry out 2-dimensional electromagnetic field simulations of real life problems, we need to identify the vector Preisach operator $\boldsymbol{\mathcal{P}}$ representing the measured hysteresis curves of a real material. For this, we present a simple fitting method. It computes an isotropic Preisach distribution ω such that the corresponding vector Preisach operator approximates the outer hysteresis loop obtained under uniaxial input. Figure A.1 shows example input data. The algorithm consists of making a nodal ansatz for ω, setting up a system of equations, completing this system with Tikhonov regularization and computing its nonnegativity constrained least squares solution.

We assume ω to be isotropic, nonnegative and continuous, and choose a piecewise linear ansatz for $\omega(\|\boldsymbol{x}\|, r)$ on a regular triangular grid of the form displayed in Figure A.1. Outside the grid and, to satisfy the continuity assumption, in the white nodes along the outer diagonal, ω is assumed to be 0. The discrete values $\omega_1, \ldots, \omega_L$ of ω in the black nodes must then be computed.

The input data provides two sorts of information that result in two types of equations for $\omega_1, \ldots, \omega_L$. Denote the upper hysteresis curve by $M_{\text{up}}(H)$, the lower hysteresis curve by $M_{\text{low}}(H)$. Let $\mathcal{K} := \{(\boldsymbol{x}, r) \mid ||\boldsymbol{x}|| + r \leq R\} \subset \mathbb{R}^2 \times \mathbb{R}_+$ be the volume covered by the ansatz grid, i.e. the volume where ω can differ from 0. Denote by N the grid parameter representing the number of black grid nodes along the $\|\boldsymbol{x}\|$-axis, so $L = N^2$. Because the curves originate in saturation, at any value

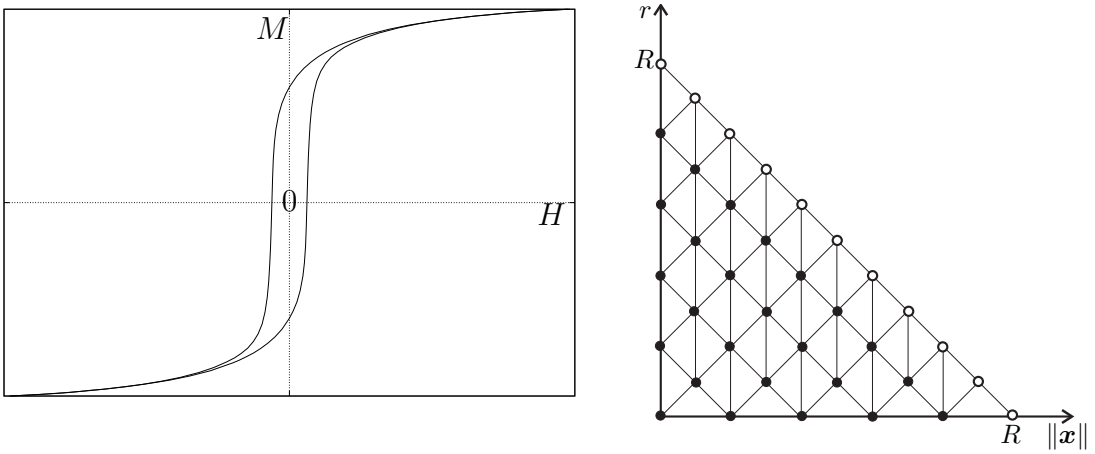

FIGURE A.1. Outer uniaxial hysteresis loop used in fitting (left), ansatz grid for $\omega(\|\boldsymbol{x}\|, r)$ with $N = 5$ (right).

of H, the memory states $\boldsymbol{h}_{(\boldsymbol{x},r)}$ for $M_{\text{up}}(H)$ and $M_{\text{low}}(H)$ are unambiguously known. Outside the freeze cone $\mathcal{C}_{(H,0)^T}$, for both curves they are equal to

$$\frac{(H,0)^T - \boldsymbol{x}}{\|(H,0)^T - \boldsymbol{x}\|}.$$

Inside the freeze cone, they are equal to

$$\pm\frac{1}{r}\begin{pmatrix}\sqrt{r^2 - x_2^2}\\ x_2\end{pmatrix}$$

with negative sign for M_{low} and positive sign for M_{up} (cf. Equation (2.48)). Therefore, adding up the corresponding curve values on lower and upper curve gives the integral over the outside of the freeze cone:

$$\frac{1}{2}\left(M_{\text{up}} + M_{\text{low}}\right) = \int_{\mathcal{K}\setminus\mathcal{C}_{(H,0)^T}} \omega(\|\boldsymbol{x}\|, r)\frac{H - x_1}{\|(H,0)^T - \boldsymbol{x}\|}\,\mathrm{d}(\boldsymbol{x}, r). \tag{A.1}$$

Subtracting the respective values gives the integral over the inside of the freeze cone:

$$\frac{1}{2}\left(M_{\text{up}} - M_{\text{low}}\right) = \int_{\mathcal{K}\cap\mathcal{C}_{(H,0)^T}} \omega(\|\boldsymbol{x}\|, r)\sqrt{1 - (x_2/r)^2}\,\mathrm{d}(\boldsymbol{x}, r). \tag{A.2}$$

The corresponding integrals for the x_2-components cancel out to 0 due to symmetry and thus do not need to be pursued. Plugging in the nodal ansatz for ω, Equations (A.1) and (A.2) can now be used to derive equations in $\omega_1, \ldots, \omega_L$ for any given set of points on the hysteresis curves.

In general, the resulting system will not determine $\omega_1, \ldots, \omega_L$ uniquely because the number of independent equations will not correspond to the number of variables. Even when it does, the solution might give perfect fit in the discrete points used for fitting but not satisfy the nonnegativity assumption on $\omega_1, \ldots, \omega_L$ and give undesirable hysteresis curves. Therefore, we subject the equation system to a simple Tikhonov regularization as suggested in [**59**]. For this, we set up a penalty term on the first derivative of $\omega(\|\boldsymbol{x}\|, r)$, represented by the first difference matrix of adjacent grid nodes.

The result is a nonnegativity constrained least squares problem of the form

$$\underset{(\omega_1,\ldots,\omega_L)}{\text{minimize}} \left\| \begin{pmatrix} A \\ \lambda T \end{pmatrix} \begin{pmatrix}\omega_1\\ \vdots \\ \omega_L\end{pmatrix} - \begin{pmatrix} b \\ 0 \end{pmatrix} \right\|^2 \quad \text{subject to } \omega_1, \ldots, \omega_L \geq 0 \tag{A.3}$$

with A the equation system matrix, b the corresponding right hand side, and $T(\omega_1, \ldots, \omega_L)^T$ the Tikhonov penalty term. The real number $\lambda \geq 0$ is the Tikhonov parameter weighting the penalty term. It can be varied to choose a solution vector $(\omega_1, \ldots, \omega_L)$ resulting in desirable hysteresis curves. Problem (A.3) can be solved by means of available software products, e.g. the DQED library [**26**].

As examples, we have fitted two measured hysteresis curves for the magnetic valve simulation in Section 3.5. Figures A.2 and A.4 show the input and the output of the fitting. Figures A.3 and A.5 show the corresponding Preisach distributions.

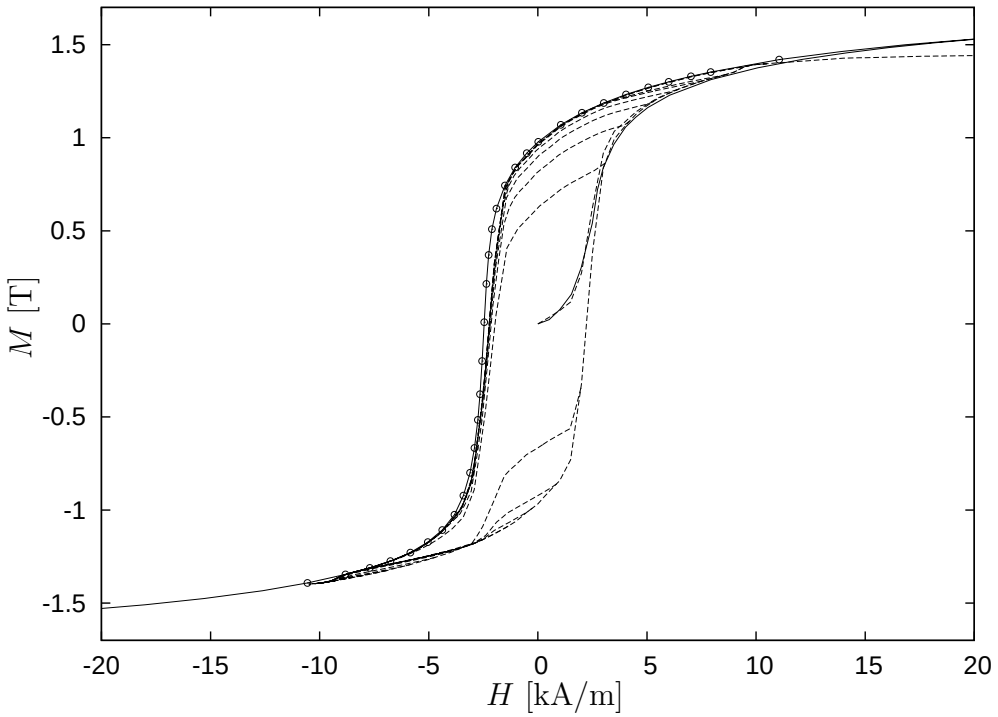

FIGURE A.2. **Fitting of ω for the armature of the magnetic valve in Section 3.5.** Measured initial and upper hysteresis curve (solid line), input data points ($\circ$) and initial, outer and first order reversal curves resulting from the fitted vector Preisach operator (dashed line). The fit was carried out with $N = 20$, $R = 10000$ and $\lambda = .01$.

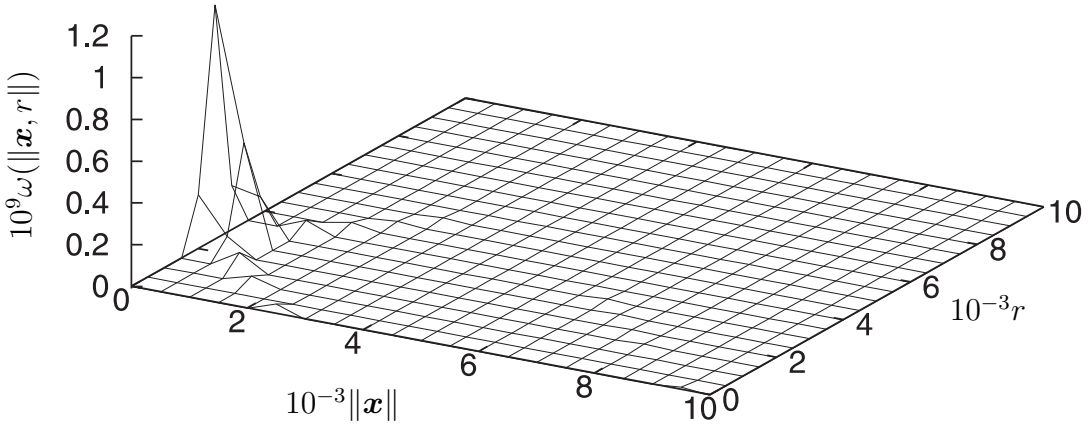

FIGURE A.3. Preisach distribution ω of the fit in Figure A.2.

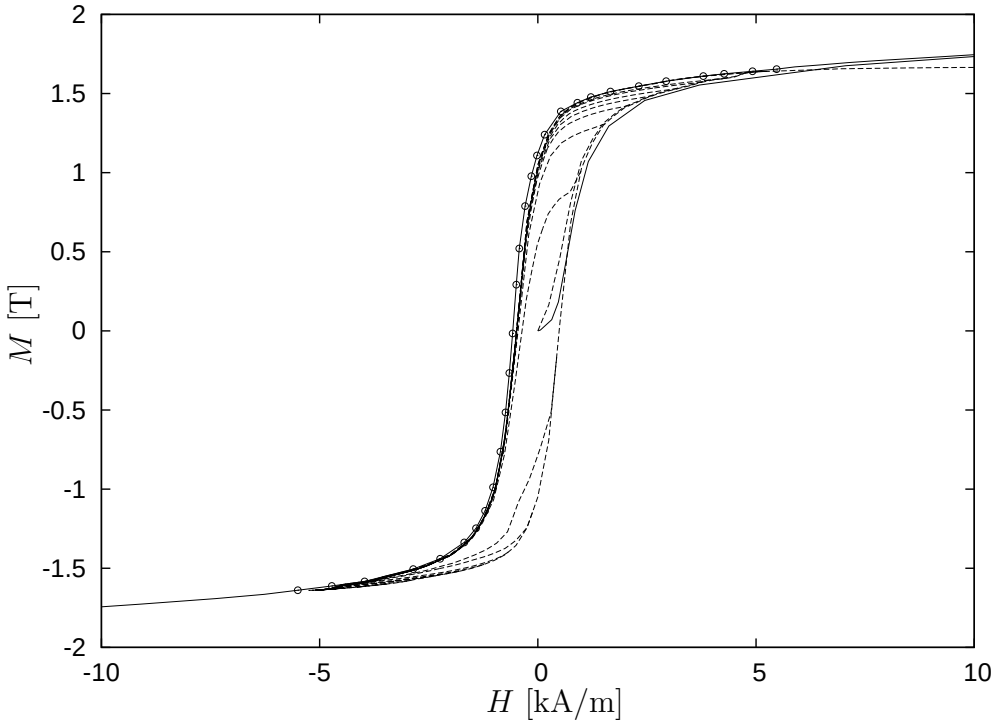

FIGURE A.4. **Fitting of ω for the core of the magnetic valve in Section 3.5.** Measured initial and upper hysteresis curve (solid line), input data points ($\circ$) and initial, outer and first order reversal curves resulting from the fitted vector Preisach operator (dashed line). The fit was carried out with $N = 50$, $R = 5000$ and $\lambda = .0075$.

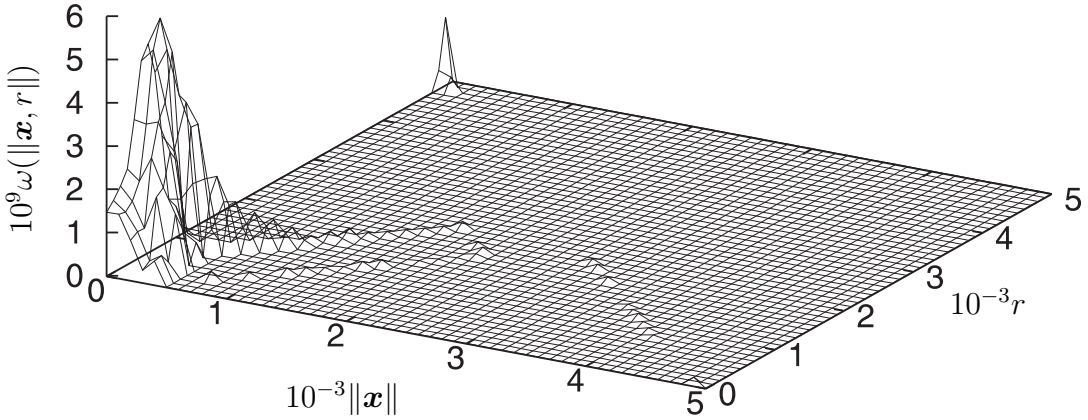

FIGURE A.5. Preisach distribution ω of the fit in Figure A.4.

We see that the fit is good but not perfect. It differs especially in the neighbourhood of the zeros of the outer curves, where the slope is steep. The reason for this is the lacking discretization of ω around this region of strong change in the hysteresis curve. It indicates that a better ansatz should be chosen in future approaches, e.g. a non-regular grid in a first attempt. In a straightforward manner, to increase the resolution without grid refinement, we resigned to only fitting the hysteretic part of the curves but not the saturation curves, and used a smaller R than the actual saturation of the curves would have required. Therefore, the saturation curves resulting from the fit are much less steep than the measured curves. This is compensated by replacing the saturation curves obtained from the vector Preisach operator by the measured ones in simulations.

In conclusion, the presented method is a straightforward way to obtain some ω representing a given hysteresis curve. However, the identification problem requires more extensive research and the development of more suitable approaches. As is the case with Mayergoyz' vector Preisach operator, for which identification is treated in [**53, 54, 51**], there will most likely not be a solution as straighforward as exists for the scalar Preisach operator, where the first order reversal curves provide directly the necessary information (Theorem 2.4.11,[**16, 51**]). In any case, it remains to be investigated what properties given hysteresis data must satisfy at all to allow perfect representation by the isotropic vector Preisach operator investigated in this thesis.

APPENDIX B

Variational results on the vector relay operator

In the following, a few statements on $\boldsymbol{h}_{(\boldsymbol{x},r)}$ are listed which may be of use in view of a variational formulation of the operator. They represent generalizations of results given by Visintin [**67**] for the scalar relay operator. The first part deals with what Visintin refers to as "laziness". The remainder presents a vectorial version of the confinement condition, which Visintin employes together with a dissipation condition to give a variational representation of the relay operator.

Define the set of right-continuous functions that agree with $\boldsymbol{w}$ while $\boldsymbol{u}$ is outside the relay $B_{\boldsymbol{x},r}$, and otherwise are equal to some arbitrary unit vector,

$$K_{(\boldsymbol{u},\boldsymbol{\xi})} := \{\boldsymbol{v} \in C_r([0,T];\partial B_{\boldsymbol{0},1}) \mid \boldsymbol{v}(0) = \boldsymbol{\xi} \text{ if } \boldsymbol{u}(0) \in B_{\boldsymbol{x},r},$$
$$\boldsymbol{v}(t) = \frac{\boldsymbol{u}(t) - \boldsymbol{x}}{\|\boldsymbol{u}(t) - \boldsymbol{x}\|} \quad \text{if } t \in [0,T] \text{ and } \boldsymbol{u}(t) \notin B_{\boldsymbol{x},r}\}.$$

Obviously, $\boldsymbol{w} \in K_{(\boldsymbol{u},\boldsymbol{\xi})}$. As $\boldsymbol{w}$ does not vary while $\boldsymbol{u}(t) \in B_{\boldsymbol{x},r}$, it satisfies

$$\operatorname*{Var}_{[0,t]}(\boldsymbol{w}) \leq \operatorname*{Var}_{[0,t]}(\boldsymbol{v}) \qquad \forall \boldsymbol{v} \in K_{(\boldsymbol{u},\boldsymbol{\xi})} \text{ and } \forall t \in [0,T]. \tag{B.1}$$

Visintin [**67**, Chapter IV], who discusses the analogous behaviour for the scalar relay, calls this behaviour *laziness*. In fact, the vectorial relay also satisfies a strict global minimization property:

LEMMA B.0.1 (Strict global minimization property). *For all $\boldsymbol{v} \in K_{(\boldsymbol{u},\boldsymbol{\xi})} \backslash \{\boldsymbol{w}\}$, there exists a $t \in (0,T]$ such that*

$$\operatorname*{Var}_{[0,t]}(\boldsymbol{w}) < \operatorname*{Var}_{[0,t]}(\boldsymbol{v}). \tag{B.2}$$

PROOF. Essentially, the argument is that even if $\boldsymbol{v}$ has the same total variation as $\boldsymbol{w}$ for any t such that $\boldsymbol{u}(t)$ is outside the relay, as it differs from $\boldsymbol{w}$, it must vary for some t such that $\boldsymbol{u}(t)$ is inside the relay, while $\boldsymbol{w}$ is constant. At that point, the strict inequality holds.

Formally, (B.2) can be shown as follows: For any $\boldsymbol{v} \neq \boldsymbol{w}$, there is a $\tau \in (0,T]$ such that $\boldsymbol{u}(\tau) \in B_{\boldsymbol{x},r}$ and $\boldsymbol{v}(\tau) \neq \boldsymbol{w}(\tau)$. One of two situation will be satisfied: Either there exists $\tilde{\tau} := \max\{t \in [0,\tau) \mid \boldsymbol{u}(t) \in \partial B_{\boldsymbol{x},r}\}$, or $\boldsymbol{u}(t) \mid_{[0,\tau]} \in B_{\boldsymbol{x},r}$, in which case we set $\tilde{\tau} := 0$. In both cases, $\boldsymbol{w}$ is constant on the entire interval $[\tilde{\tau},\tau]$, so $\boldsymbol{w}(\tau) = \boldsymbol{w}(\tilde{\tau})$, and by definition of $\tilde{\tau}$ function $\boldsymbol{v}$ satisfies $\boldsymbol{v}(\tau) \neq \boldsymbol{v}(\tilde{\tau}) = \boldsymbol{w}(\tilde{\tau})$. Thus, for $\tilde{\tau} := 0$,

$$\operatorname*{Var}_{[0,\tau]}(\boldsymbol{w}) = 0 < \operatorname*{Var}_{[0,\tau]}(\boldsymbol{v}).$$

For $\tilde{\tau} > 0$, by (B.1), $\operatorname*{Var}_{[0,\tilde{\tau}]}(\boldsymbol{w}) \leq \operatorname*{Var}_{[0,\tilde{\tau}]}(\boldsymbol{v})$, so $\operatorname*{Var}_{[0,\tau]}(\boldsymbol{w}) < \operatorname*{Var}_{[0,\tau]}(\boldsymbol{v})$. □

We want to present a vectorial version of what Visintin [**67**] calls *confinement condition*. For this, we define a new set of functions,

$$\tilde{K}_{(\boldsymbol{u},\boldsymbol{\xi})} := \{\boldsymbol{v} \in C_r([0,T];\partial B_{\mathbf{0},1}) \mid \boldsymbol{v}(0) = \boldsymbol{\xi} \text{ if } \boldsymbol{u}(0) \in B_{\boldsymbol{x},r},$$
$$\boldsymbol{v}(t) = \frac{\boldsymbol{u}(t)-\boldsymbol{x}}{\|\boldsymbol{u}(t)-\boldsymbol{x}\|} \quad \text{if } t \in [0,T] \text{ and } \boldsymbol{u}(t) \notin \overline{B_{\boldsymbol{x},r}}\},$$

which differs from $K_{(\boldsymbol{u},\boldsymbol{\xi})}$ only in that any $\boldsymbol{v} \in \tilde{K}_{(\boldsymbol{u},\boldsymbol{\xi})}$ can take arbitrary values on $\partial B_{\boldsymbol{x},r}$. The set $\tilde{K}_{(\boldsymbol{u},\boldsymbol{\xi})}$ will be relevant when attempting to close the image of $C([0,T];\mathbb{R}^n)$ under $\boldsymbol{h}_{(\boldsymbol{x},r)}$, as Visintin [**67**] does for the scalar relay. The following statement could be used in a variational formulation of the closed relay operator.

LEMMA B.0.2. *A function $\boldsymbol{v}$ is in $\tilde{K}_{(\boldsymbol{u},\boldsymbol{\xi})}$ if and only if $\boldsymbol{v} \in C_r([0,T];\mathbb{R}^n)$, $\boldsymbol{u}(0) \in B_{\boldsymbol{x},r}$ implies $\boldsymbol{v}(0) = \boldsymbol{\xi}$, and*

$$\begin{array}{rcll} \|\boldsymbol{v}(t)\| & = & 1, & \\ \left(\boldsymbol{v}(t) - \frac{\boldsymbol{u}(t)-\boldsymbol{x}}{\|\boldsymbol{u}(t)-\boldsymbol{x}\|}\right) \cdot \left(\boldsymbol{u}(t) - r\frac{\boldsymbol{u}(t)-\boldsymbol{x}}{\|\boldsymbol{u}(t)-\boldsymbol{x}\|}\right) & \geq & 0 & \forall t \in [0,T]. \end{array}$$

PROOF. Trivially, the equation is equivalent to $\boldsymbol{v} \in \partial B_{\mathbf{0},1}$. For showing the inequality, assume first that $\boldsymbol{u}(t) \notin \overline{B_{\boldsymbol{x},r}}$, i.e.

$$\boldsymbol{u}(t) - r\frac{\boldsymbol{u}(t)-\boldsymbol{x}}{\|\boldsymbol{u}(t)-\boldsymbol{x}\|} = \kappa\frac{\boldsymbol{u}(t)-\boldsymbol{x}}{\|\boldsymbol{u}(t)-\boldsymbol{x}\|} \tag{B.3}$$

holds with $\kappa > 0$. Therefore, the only unit vector for which the inequality in

$$\begin{aligned} &\left(\boldsymbol{v}(t) - \frac{\boldsymbol{u}(t)-\boldsymbol{x}}{\|\boldsymbol{u}(t)-\boldsymbol{x}\|}\right) \cdot \left(\boldsymbol{u}(t) - r\frac{\boldsymbol{u}(t)-\boldsymbol{x}}{\|\boldsymbol{u}(t)-\boldsymbol{x}\|}\right) \\ =&\kappa \left(\boldsymbol{v}(t) - \frac{\boldsymbol{u}(t)-\boldsymbol{x}}{\|\boldsymbol{u}(t)-\boldsymbol{x}\|}\right) \cdot \frac{\boldsymbol{u}(t)-\boldsymbol{x}}{\|\boldsymbol{u}(t)-\boldsymbol{x}\|} \\ \geq&0 \end{aligned}$$

holds true is $v(t) = \frac{\boldsymbol{u}(t)-\boldsymbol{x}}{\|\boldsymbol{u}(t)-\boldsymbol{x}\|}$. Now assume $\boldsymbol{u}(t) \in \overline{B_{\boldsymbol{x},r}}$, so Equation (B.3) holds with $\kappa \leq 0$. For this κ, $\boldsymbol{v}(t)$ can take on any unit vector to satisfy the inequality. □

Because the vectorial relay lacks the monotonicity property, we have not been able to derive a vectorial version of the *dissipation condition* presented by Visintin [**67**] for the scalar relay.

APPENDIX C

Piecewise linear monotone functions

In this appendix, a few facts on piecewise linear monotone functions are sketched.

LEMMA C.0.3 (Linear monotone functions). *Assume* $\boldsymbol{F}(\boldsymbol{x}) = \boldsymbol{A}\boldsymbol{x}$, $\boldsymbol{A} \in \mathbb{R}^{n\times n}$. *Then* $\boldsymbol{F}$ *is monotone if and only if* $\boldsymbol{A}$ *is positive semidefinite.*

PROOF.

$$(A\boldsymbol{x} - A\boldsymbol{y}) \cdot (\boldsymbol{x} - \boldsymbol{y}) = (\boldsymbol{x} - \boldsymbol{y})^T A(\boldsymbol{x} - \boldsymbol{y}) \geq 0. \qquad \square$$

Suppose $\Omega \subset \mathbb{R}^2$ is a polyhedral domain. A *triangulation* of Ω is a finite collection of open triangles $\{K_i\}$ such that [**11**]

(1) $K_i \cap K_j = \varnothing$ if $i \neq j$,
(2) $\bigcup \overline{K_i} = \overline{\Omega}$, and
(3) no vertex of any triangle lies in the interior of an edge of another triangle.

Obviously, the linearization grid in Figure 3.1 is a triangulation of the domain Ω arising as union of all triangles.

We will now show that the monotonicity property of a continuous function on each triangle extends to the whole domain.

LEMMA C.0.4. *Suppose* $\boldsymbol{F} : \Omega \to \mathbb{R}^2$ *is continuous, and monotone on each triangle. Then* $\boldsymbol{F}$ *is monotone on* Ω.

PROOF. Fix arbitrary $\boldsymbol{y}_1, \boldsymbol{y}_2 \in \Omega$. Then the line connecting $\boldsymbol{y}_1$ and $\boldsymbol{y}_2$ traverses finitely many triangles in Ω, cf. Figure C.1. Call the points where this line intersects with the triangle boundaries $\boldsymbol{z}_1, \ldots, \boldsymbol{z}_s$. Then the monotonicity of $\boldsymbol{F}$ on each triangle implies that there exist $\lambda_0, \ldots, \lambda_s \geq 0$ such that

$$\begin{aligned}
&(F(\boldsymbol{y}_1) - F(\boldsymbol{y}_2)) \cdot (\boldsymbol{y}_1 - \boldsymbol{y}_2) \\
=\ &(F(\boldsymbol{y}_1) - F(\boldsymbol{z}_1)) \cdot (\boldsymbol{y}_1 - \boldsymbol{y}_2) + (F(\boldsymbol{z}_1) - F(\boldsymbol{z}_2)) \cdot (\boldsymbol{y}_1 - \boldsymbol{y}_2) \\
&+ \cdots \\
&+ (F(\boldsymbol{z}_{s-1}) - F(\boldsymbol{z}_s)) \cdot (\boldsymbol{y}_1 - \boldsymbol{y}_2) + (F(\boldsymbol{z}_s) - F(\boldsymbol{y}_2)) \cdot (\boldsymbol{y}_1 - \boldsymbol{y}_2) \\
=\ &(F(\boldsymbol{y}_1) - F(\boldsymbol{z}_1)) \cdot \lambda_0(\boldsymbol{y}_1 - \boldsymbol{z}_1) + (F(\boldsymbol{z}_1) - F(\boldsymbol{z}_2)) \cdot \lambda_1(\boldsymbol{z}_1 - \boldsymbol{z}_2) \\
&+ \cdots \\
&+ (F(\boldsymbol{z}_{s-1}) - F(\boldsymbol{z}_s)) \cdot \lambda_{s-1}(\boldsymbol{z}_{s-1} - \boldsymbol{z}_s) + (F(\boldsymbol{z}_s) - F(\boldsymbol{y}_2)) \cdot \lambda_s(\boldsymbol{z}_s - \boldsymbol{y}_2) \\
\geq &0
\end{aligned}$$

$\square$

Note that for a piecewise linear interpolation function on a triangulation, it is not sufficient to require that the monotonicity condition is pairwise satisfied by the

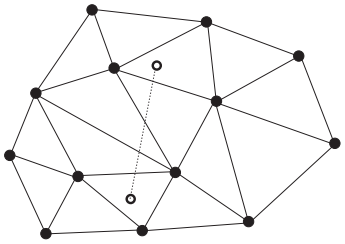

FIGURE C.1. Illustration for the proof of Lemma C.0.4.

vertices of each triangle,

$$(\boldsymbol{F}_i - \boldsymbol{F}_j) \cdot (\boldsymbol{x}_i - \boldsymbol{x}_j) \geq 0,$$

to guarantee that the linear interpolation on this triangle is monotone, cf. Lemma C.0.3. However, in practice, it is almost always sufficient.

Notation

$\mathbb{N}$	set of integers
$\mathbb{R}$	set of real numbers
$\mathbb{R}_+$	$= \{r \in \mathbb{R} \mid r > 0\}$
$\boldsymbol{x} \cdot \boldsymbol{y}$	scalar product in $\mathbb{R}^n$, p. 5
$\|\boldsymbol{x}\|$	$= (\boldsymbol{x} \cdot \boldsymbol{x})^{\frac{1}{2}}$, p. 5
$\boldsymbol{x}^T$, Q^T	transpose of a vector or a matrix
$\overline{X}$	closure of set X, p. 6
∂X	boundary of set X, p. 6
$\operatorname{sign}(x)$	sign function, p. 57
Γ	Gamma function [**35**]
a.e.	almost everywhere [**42**]
$B_{\boldsymbol{y},r}$	ball of radius r centered at $\boldsymbol{y}$, p. 5
$V_B^{(n)}(r)$	volume of the n-dimensional ball, p. 5
$\mathcal{C}_{\boldsymbol{y},R}$, $\mathcal{C}_{\boldsymbol{y}}$	cone, p. 5
$V_{\mathcal{C}}^{(n)}(R)$	volume of the cone in $\mathbb{R}^{n+1}$, p. 5
$Map(X;Y)$	set of maps from X to Y, p. 5
$C(X;Y)$	space of continuous functions from X to Y, p. 5
$C_r(X;Y)$	space of right-continuous functions from X to Y, p. 5
$\lim_{t\to\tau-} \boldsymbol{f}(t)$, $\lim_{t\to\tau+} \boldsymbol{f}(t)$	left-hand and right-hand limit, p. 5
$\boldsymbol{f}'(t)$	derivative, p. 6
$\partial_{t-}\boldsymbol{f}(t)$, $\partial_{t+}\boldsymbol{f}(t)$	left-hand and right-hand derivative, p. 6
$\partial_{y_i}\boldsymbol{\varphi}(y_1,\ldots,y_n)$, $\partial_{\boldsymbol{y}}\boldsymbol{\varphi}(\boldsymbol{y})$	partial derivative, Jacobian, p. 6
$d_{\boldsymbol{z}}\boldsymbol{f}(\boldsymbol{y})$	Gâteaux derivative of $\boldsymbol{f}$ in the direction $\boldsymbol{z}$, p. 72
$S(\boldsymbol{u};\Gamma)$	p. 12
$\operatorname{Var}_{[0,T]}(\boldsymbol{u})$	total variation of $\boldsymbol{u}$, p. 12
$R(u,w;\Gamma)$	Riemann-Stieltjes sum, p. 12
$\Gamma = \{t_0,\ldots,t_M\}$	partition, p. 12
$\|\Gamma\|$	p. 12

$\int_0^T u\,\mathrm{d}w$, $\int_0^T \boldsymbol{u}\cdot\,\mathrm{d}\boldsymbol{w}$	Riemann-Stieltjes integral, p. 12
$O(n)$, $SO(n)$	orthogonal group, special orthogonal group, p. 15
$\mathcal{I}d$	identity matrix
$\boldsymbol{u}_t$	truncation of $\boldsymbol{u}$ at t, p. 20
$\boldsymbol{u}^t$	shift of $\boldsymbol{u}$ by t, p. 25
$\boldsymbol{\mathcal{W}}_f$	generating functional, p. 20
$h_{(x,r)}$	scalar relay operator, p. 21
$\mathcal{F}_r$	scalar play operator, p. 22
$\mathcal{P}$	scalar Preisach operator, p. 22
Ψ_0	set of Preisach memory curves, p. 23
$\boldsymbol{h}_{(\boldsymbol{x},r)}$	vector relay operator, p. 24
$\boldsymbol{\gamma}_{(\boldsymbol{x},r)}$	p. 26
ξ^0, $\boldsymbol{\xi}^0$	neutral initial state, p. 34-36
$M_{pm}[0,T]$, $C_{pm}[0,T]$	piecewise monotone functions on $[0,T]$, p. 49
S, S_A	sets of finite (alternating) strings, p. 50
ρ_A, π_A	restriction/prolongation operator, p. 50
Π_i	projection, p. 57
$\lfloor\cdot\rfloor_{x_1=\cdot}$	jump, p. 80
$\lfloor\cdot\rfloor_{\Sigma}$	jump across a surface, p. 86
$\boldsymbol{H}$	magnetic field, p. 85
$\boldsymbol{B}$	magnetic induction, p. 85
$\boldsymbol{M}$	magnetization, p. 86
$\boldsymbol{D}$	electric induction, p. 85
$\boldsymbol{E}$	electric field, p. 85
$\boldsymbol{P}$	polarization, p. 86
$\boldsymbol{g}$	free current density, p. 85
$\boldsymbol{g}_s$	impressed current density, p. 86
ρ	electric charge density, p. 85
σ	conductivity, p. 86

Bibliography

1. A.A. Adly, I.D. Mayergoyz, R.D. Gomez, and E.R. Burke, *Computation of magnetic fields in hysteretic media*, IEEE Trans. Magn. **29** (1993), no. 6, 2380–2382.
2. M.A. Armstrong, *Groups and symmetry*, Springer-Verlag, New York, 1988.
3. F.G. Baily, *The hysteresis of iron and steel in a rotating magnetic field*, Phil. Trans. Roy. Soc. **107** (1896), 715–746.
4. A. Bergqvist, H. Tiberg, and G. Engdahl, *Application of a vector Preisach model in a magnetic circuit*, J. Appl. Phys. **73** (1993), no. 10, 5839–5841.
5. G. Bertotti, *Hysteresis in magnetism*, Academic Press, San Diego, 1998.
6. O. Bíró and K. Preis, *On the use of the magnetic vector potential in the finite element analysis of three-dimensional eddy currents*, IEEE Trans. Magn. **25** (1989), no. 4, 3145–3159.
7. A. Bossavit, *Électromagnetisme, en vue de la modélisation*, Springer-Verlag, Paris, 1993.
8. ———, *Computational electromagnetism*, Academic Press, Boston, 1998.
9. O. Bottauscio, D. Chiarabaglio, C. Ragusa, M. Chiampi, and M. Repetto, *Analysis of isotropic materials with vector hysteresis*, IEEE Trans. Magn. **34** (1998), no. 4, 1258–1260.
10. R.M. Bozorth, *Ferromagnetism*, D. van Nostrand Company, Inc., Princeton, 1951.
11. S.C. Brenner and L.R. Scott, *The mathematical theory of finite element methods*, Springer-Verlag, New York, 1994.
12. M. Brokate, *On a characterization of the Preisach model for hysteresis*, Rend. Sem. Mat. Padova **83** (1990), 153–163.
13. ———, *Konvexe Analysis*, lecture notes, Mathematisches Seminar, Christian-Albrechts-Universität Kiel, Germany, winter semester 1997/98.
14. M. Brokate, K. Dressler, and P. Krejčí, *On the Mròz model*, Eur. J. Appl. Math. **7** (1996), 473–497.
15. M. Brokate, P. Krejčí, and D. Rachinskii, *Some analytical properties of the multidimensional continuous Mròz model of plasticity*, Control & Cybernetics **27** (1998), 199–215.
16. M. Brokate and J. Sprekels, *Hysteresis and phase transitions*, Applied Mathematical Sciences, vol. 121, Springer-Verlag, New York, 1996.
17. E. Cardelli, E. Della Torre, and E. Pinzaglia, *Magnetic energy and radial vector model of hysteresis*, J. Appl. Phys. **99** (2006).
18. ———, *Numerical implementation of the radial vector hysteresis model*, IEEE Trans. Magn. **24** (2006), no. 4, 527–530.
19. M. Costabel and M. Dauge, *Singularities of electromagnetic fields in polyhedral domains*, Arch. Ration. Mech. Anal. **151** (2000), no. 3, 221–276.
20. C.B. Craus, *Magnetic properties of nanocrystalline materials for high frequency applications*, Ph.D. thesis, Faculty of Mathematics and Natural Sciences, University of Groningen, 2003.
21. A. Damlamian and A. Visintin, *Une généralisation vectorielle du modèle de Preisach pour l'hystéresis*, C. R. Acad. Sc. Paris **297** (1983), 437–440.
22. E. Della Torre, *Magnetic hysteresis*, John Wiley & Sons, 2000.
23. E. Della Torre, J. Oti, and G. Kádár, *Preisach modeling and reversible magnetization*, IEEE Trans. Magn. **26** (1990), no. 6, 3052–3058.
24. E. Della Torre, E. Pinzaglia, and E. Cardelli, *Vector modeling – Part I: Generalized hysteresis model*, Physica B **372** (2006), no. 1–2, 111–114.

25. ———, *Vector modeling – Part II: Ellipsoidal vector hysteresis model. Numerical application to a 2D case*, Physica B **372** (2006), no. 1–2, 115–119.
26. *DQED – Bounded Constrained Least Squares/Nonlinear Equations*, FORTRAN90 library, available at `http://people.scs.fsu.edu/~burkardt/f_src/dqed/dqed.html`.
27. L.R. Dupré, R. van Keer, and J.A.A. Melkebeek, *A 2d finite element procedure for magnetic field analysis taking into account a vector Preisach model*, Mathem. Probl. Engin. **3** (1997), no. 3, 267–286.
28. J. Fetzer, *Die Lösung statischer und quasistationärer elektromagnetischer Feldprobleme mit Hilfe der Kopplung der Methode der finiten Elemente und der Randelementmethode*, Ph.D. thesis, Faculty of Computer Science, Electrical Engineering and Information Technology, Universität Stuttgart, 1995.
29. J. Fetzer, M. Haas, and S. Kurz, *Numerische Berechnung elektromagnetischer Felder*, Kontakt & Studium, vol. 627, expert-Verlag, Renningen-Malmsheim, 2002.
30. J. Fetzer, S. Kurz, G. Lehner, and W.M. Rucker, *Application of BEM-FEM coupling and the vector Preisach model for the calculation of 3D magnetic fields in media with hysteresis*, IEEE Trans. Magn. **36** (2000), no. 4, 1258–1262.
31. G.M. Fichtenholz, *Differential- und Integralrechnung II*, Hochschulbücher für Mathematik, vol. 62, VEB Deutscher Verlag der Wissenschaften, Berlin, 1966.
32. J. Fidler and T. Schrefl, *Micromagnetic modelling – the current state of the art*, J. Phys. D: Appl. Phys. **33** (2000), 135–156.
33. G. Fischer, *Lineare Algebra*, Vieweg, Braunschweig/Wiesbaden, 1997.
34. J. Fischer, *Elektrodynamik*, Springer Verlag, Berlin/Heidelberg, 1976.
35. O. Forster, *Analysis 3*, Vieweg, Braunschweig/Wiesbaden, 1981.
36. G. Friedman, *Conditions for the representation of vector hysteresis by the vector Preisach model*, J. Appl. Phys. **85** (1999), no. 8, 4379–4381.
37. S. Fučík and A. Kufner, *Nonlinear differential equations*, Studies in Applied Mechanics, vol. 2, Elsevier Scientific Publishing Company, Amsterdam, 1980.
38. S.A. Harrison, R. Street, J.R. Budge, and S.K. Jones, *Rotational hysteresis losses in isotropic media*, IEEE Trans. Magn. **35** (1999), no. 5, 3962–3964.
39. M. Hazewinkel (ed.), *Encyclopedia of mathematics*, Kluwer Academic Publishers, 2002.
40. J.D. Jackson, *Klassische Elektrodynamik*, 2nd ed., Walter de Gruyter, Berlin, 1983.
41. J.E. Katz, Q.A. Kerns, and B.R. Sandberg, *Digital measurement of ferrite hysteresis loops*, IEEE Trans. Nucl. Sci. **NS-16** (1969), 546–550.
42. A.N. Kolmogorov and S.V. Fomin, *Introductory real analysis*, Prentice-Hall, Englewood Cliffs, N.J., 1970, revised English edition, translated and edited by Richard A. Silverman.
43. M.A. Krasnosel'skiĭ and A.V. Pokrovskiĭ, *Systems with hysteresis*, Springer-Verlag, Heidelberg, 1989, translation of the Russian original edition from 1983.
44. P. Krejčí, *Hysteresis, convexity and dissipation in hyperbolic equations*, Gakuto International Series of Mathematical Sciences and Applications, vol. 8, Gakkotosho, Tokyo, 1996.
45. S. Kurz, *Anwendung der Methode der finiten Elemente und des Vektor-Preisach-Modells zur Berechnung magnetostatischer Felder in hysteresebehafteten Medien*, thesis (Diplomarbeit), Faculty of Computer Science, Electrical Engineering and Information Technology, Universität Stuttgart, 1992.
46. ———, *Die numerische Behandlung elektromechanischer Systeme mit Hilfe der Kopplung der Methode der finiten Elemente und der Randelementmethode*, Ph.D. thesis, Faculty of Computer Science, Electrical Engineering and Information Technology, Universität Stuttgart, 1998.
47. S. Kurz, J. Fetzer, and G. Lehner, *Comparison between different iterative methods for calculation of magnetostatic fields in nonlinear media*, Proceedings of the 6th International IGTE Symposium (Graz, Austria), 1994, pp. 77–82.
48. G. Lehner, *Elektromagnetische Feldtheorie für Ingenieure und Physiker*, Springer-Verlag, Heidelberg, 1990.
49. I.D. Mayergoyz, *Mathematical models of hysteresis*, Phys. Rev. Letters **56** (1985), 1518–1521.

50. ———, *Mathematical models of hysteresis*, IEEE Trans. Magn. **22** (1986), 603–608.
51. ———, *Mathematical models of hysteresis*, Springer-Verlag, New York, 1991.
52. I.D. Mayergoyz, A.A. Adly, M.W. Huang, and C. Krafft, *Experimental testing of vector Preisach models for superconducting hysteresis*, IEEE Trans. Magn. **36** (2000), no. 5, 3505–3507.
53. I.D. Mayergoyz and G. Friedman, *Isotropic vector Preisach model of hysteresis*, J. Appl. Phys. **61** (1987), no. 8, 4022–4024.
54. ———, *On the integral equation of the vector Preisach hysteresis model*, IEEE Trans. Magn. **23** (1987), no. 5, 2638–2640.
55. A.H. Morrish, *The physical principles of magnetism*, Krieger, Malabar, FL, 1983.
56. Z. Mròz, *On the description of anisotropic workhardening*, J. Mech. Phys. Solids **15** (1967), 163–175.
57. H. Pfützner, *Rotational magnetization and rotational losses of grain oriented silicon steel sheets – fundamental aspects and theory*, IEEE Trans. Magn. **30** (1994), no. 5, 2802–2807.
58. F. Preisach, *Über die magnetische Nachwirkung*, Z. Phys. **94** (1935), 277–302.
59. W.H. Press, S.A. Teukolsky, W.T. Vetterling, and B.P. Flannery, *Numerical recipes in C*, 2nd ed., Cambridge University Press, New York, 1992.
60. C. Ragusa and M. Repetto, *Anisotropic vector Preisach model and magnetic field solutions*, COMPEL **18** (1999), no. 3, 458–468.
61. V. Rischmüller, J. Fetzer, M. Haas, S. Kurz, and W.M. Rucker, *Computational efficient BEM-FEM coupled analysis of 3D nonlinear eddy current problems using domain decomposition*, Proceedings of the 8th International IGTE Symposium (Graz, Austria), 1998, pp. 391–396.
62. Robert Bosch GmbH, Plochingen, *Diesel-Speichereinspritzsystem Common Rail*, 2007, Fachwissen Kfz-Technik, Dieselmotor-Management.
63. I. Rookes, P.J. Smith, and D.C. Ward, *An electro-magnetically operated valve*, European Patent Application EP 0816671A1.
64. E.C. Stoner and E.P. Wohlfarth, *A mechanism of magnetic hysteresis in heterogeneous alloys*, Phil. Trans. Roy. Soc. **A240** (1948), 599–642.
65. H.L. Toms, R.G. Colclaser Jr., and M.P. Krefta, *Two-dimensional finite element magnetic modeling for scalar hysteresis effects*, IEEE Trans. Magn. **37** (2001), no. 2, 982–988.
66. H. v. Mangoldt and K. Knopp, *Einführung in die höhere Mathematik III*, S. Hirzel Verlag, Leipzig, 1965.
67. A. Visintin, *Differential models of hysteresis*, Applied Mathematical Sciences, vol. 111, Springer-Verlag, Berlin, 1994.
68. ———, *Vector ferromagnetic hysteresis and Maxwell's equations*, J. Mater. Process. Manuf. Sci. **9** (2000), 64–69.
69. ———, *Maxwell's equations with hysteresis*, Arch. Rational Mech. Anal. **175** (2005), 1–37.
70. B. Walsh, *Theory of functions of a real variable I (Math 501)*, lecture notes, 1999, available at `www.math.rutgers.edu/courses/501/501-f99`.
71. P. Weiss and V. Planer, *Hystérèse dans les champs tournants*, Journal de Physique (Théor. et Appl.) **4** (1908), no. 7, 5–27.
72. W.L. Wheeden and A. Zygmund, *Measure and integral – an introduction to real analysis*, Monographs and Textbooks in Pure and Applied Mathematics, vol. 43, Marcel Dekker Inc., New York, 1977.
73. J.G. Woodward and E. Della Torre, *Particle interaction in magnetic recording tapes*, J. Appl. Phys. **31** (1960), no. 1, 56–62.
74. O. Yamada, H. Maruyama, R. Pauthenet, and J.C. Picoche, *Symmetric hysteresis curves of rare earth-cobalt magnets measured by high magnetic fields*, IEEE Trans. Magn. **17** (1981), no. 6, 2645–2647.
75. A.C. Zaanen, *Integration*, North-Holland Publishing Company, Berlin, 1967.